Nonlinear Optical Eigenmodes; perturbative approach for classical fields and single photons.

Graeme Docherty-Walthew

University of
St Andrews

This thesis is submitted in partial fulfilment for the degree of

Doctor of Philosophy (PhD)

at the University of St Andrews

April 2020

Candidate's declaration

I, Graeme Docherty-Walthew, do hereby certify that this thesis, submitted for the degree of PhD, which is approximately 48,000 words in length, has been written by me, and that it is the record of work carried out by me, or principally by myself in collaboration with others as acknowledged, and that it has not been submitted in any previous application for any degree.

I was admitted as a research student at the University of St Andrews in September 2016.

I received funding from an organisation or institution and have acknowledged the funder(s) in the full text of my thesis.

Date 11/11/2020 Signature of candidate

Supervisor's declaration

I hereby certify that the candidate has fulfilled the conditions of the Resolution and Regulations appropriate for the degree of PhD in the University of St Andrews and that the candidate is qualified to submit this thesis in application for that degree.

Date 11/11/2020 Signature of supervisor

Permission for publication

In submitting this thesis to the University of St Andrews we understand that we are giving permission for it to be made available for use in accordance with the regulations of the University Library for the time being in force, subject to any copyright vested in the work not being affected thereby. We also understand, unless exempt by an award of an embargo as requested below, that the title and the abstract will be published, and that a copy of the work may be made and supplied to any bona fide library or research worker, that this thesis will be electronically accessible for personal or research use and that the library has the right to migrate this thesis into new electronic forms as required to ensure continued access to the thesis.

I, Graeme Docherty-Walthew, confirm that my thesis does not contain any third-party material that requires copyright clearance.

The following is an agreed request by candidate and supervisor regarding the publication of this thesis:

Printed copy

No embargo on print copy.

Electronic copy

No embargo on electronic copy.

Date 11/11/2020 Signature of candidate

Date 11/11/2020 Signature of supervisor

Underpinning Research Data or Digital Outputs

Candidate's declaration

I, Graeme Docherty-Walthew, understand that by declaring that I have original research data or digital outputs, I should make every effort in meeting the University's and research funders' requirements on the deposit and sharing of research data or research digital outputs.

Date 11/11/2020 Signature of candidate

Permission for publication of underpinning research data or digital outputs

We understand that for any original research data or digital outputs which are deposited, we are giving permission for them to be made available for use in accordance with the requirements of the University and research funders, for the time being in force.

We also understand that the title and the description will be published, and that the underpinning research data or digital outputs will be electronically accessible for use in accordance with the license specified at the point of deposit, unless exempt by award of an embargo as requested below.

The following is an agreed request by candidate and supervisor regarding the publication of underpinning research data or digital outputs:

No embargo on underpinning research data or digital outputs.

Date 11/11/2020 Signature of candidate

Date 11/11/20 Signature of supervisor

This work is dedicated to my grandfather,
William Walthew.

Acknowledgements

First, I would like to thank my supervisor Dr Michael Mazilu for his guidance and insight during my time at the University of St Andrews. Michael was always available to discuss any issues or ideas that I had and consistently challenged me to improve my understanding.

On a personal note, I would like to thank all of my family members who have helped me through the tough times and always been there to celebrate the good times. In particular, I would like to thank my Mum and sisters for all of their emotional support throughout the years and my Dad for helping me see the humorous side of life and consistently reminding what is, and is not, important. Also, I would like to thank my wife, Alison, for all of her help and support throughout my time as a research student and for all of the years we have been together. I would like to thank my son, James, who has brought joy and true purpose in my life.

Finally, I would like to acknowledge the funding provided by the Engineering and Physical Sciences Research Council (EPSRC), U.K.

List of Publications

The work presented in this thesis will appear in the following papers:

- Nonlinear optical eigenmodes: Perturbative approach,
  Volume 10935, Article number 109351K, 2019, Complex Light and Optical Forces XIII, San Francisco, United States
- Multiphoton propagation eigenmodes for sum-frequency generation,
  Optics Communications, Volume 466, 1 July 2020, Article number 125610.

The following paper was also published while affiliated with the University of St Andrews:

- Flow dynamics of the resonances of a two-dimensional circular quantum well, *Physical Review A, Volume 99, Issue 4, 29 April 2019, Article number 042126.*

List of Conferences

- 13^{th} International Conference on Mathematical and Numerical Aspects of Wave Propagation (WAVES), University of Minnesota, Twin Cities, May 2017.
- SPIE Photonics West, San Francisco, California, February 2019.
- Progress in Electromagnetics Research Symposium (PIERS), Rome, Italy, June 2019.

Abstract

In linear optics, the concept of a mode or eigenmode is well established. Often these modes correspond to a set of fields that are mutually orthogonal with intensity profiles that are invariant as they propagate through a given optical system. More generally, using an eigenmode decomposition, one can define a set of orthogonal modes with respect to an optical measure given that is linear in the intensity of the fields or Hermitian in the fields themselves. However, if the intensity of the light is sufficiently large, the dipole response of an optical medium includes nonlinear terms that cause the eigenmode decomposition to break down. In this work, we introduce the eigenmode decomposition in the presence of these nonlinear source terms by introducing small perturbation fields whose interaction is mediated by some high-intensity background field. Unlike the eigenmodes of linear optics, these novel modes correspond to a set of orthogonal fields that are, in general, distributed across multiple wavelengths. Here, we study the definition and interaction of these eigenmodes for classical electromagnetic fields and multiphoton fields. In the context of classical fields, with our eigenmodes established, we highlight the influence of the high-intensity background field on the symmetry of the eigenmodes. At the multiphoton level, we show that the description of multiphoton fields is simplified by using the propagation eigenmodes while remaining equivalent to the standard approach.

Contents

List of Figures

Chapter 1

Introduction and Motivation

1.1 Introduction

In the physical sciences, the concept and use of a mode (or eigenmode) decomposition is well established and has been used to solve many problems. In the domain of optics, decomposing fields into eigenmodes has been used to describe light propagating in laser cavities [1], photonic crystals [2], optical fibres and waveguides [3]. Often, these modes correspond to a set of fields with unique transverse profiles, are mutually orthogonal and propagate independently of one another as they evolve through the optical system. For example, the eigenmodes of a waveguide or optical fibre have an invariant field profile that is subject only to a change in phase while propagating. In a resonator or microdisk structure, however, the eigenmodes are reproduced after a full round trip of the cavity. More generally, going beyond the propagation properties of light, one can define a set of orthogonal eigenmodes with respect to any optical measure that is linear in field intensity or quadratic/Hermitian in the fields using the method of Optical Eigenmodes [4, 5, 6, 7]. Prominent examples of such measures include the energy density, optical angular momentum and intensity of the electromagnetic field. The optical eigenmodes can be thought of as a classical analogue to the states of quantum mechanics that correspond to the set of measurable configurations of a given system: each with a certain probability of being measured or occupied. Much like the propagation eigenmodes of free space and waveguides, the optical eigenmode method exploits the linearity of Maxwell's equations [8, 9, 10]. Thus, if the intensity of the incident light is large, the dipole response of a given optical medium includes higher-order nonlinearities. In this so-called nonlinear regime, the superposition of two solutions of the propagation equations is not itself a solution and, as a consequence, the method of eigenmode decomposition and optical eigenmodes breaks down.

In this work, we restore the principle of linear superposition to systems with second-order, intensity-dependent, nonlinearities by considering the interaction of perturbation fields that are small in comparison to a high-intensity background field. In the simplest cases, this is identical to that of the non-depleting pump approximation commonly used in nonlinear optics and quantum optics. By introducing these perturbation fields, one can reintroduce the concept of eigenmodes to intensity-dependent optical systems. Unlike the fields in linear optics, however, the perturbation fields will interact with one another via a high-intensity background field resulting in eigenmodes which have coupled components oscillating at different frequencies. These eigenmodes again correspond to a set of mutually orthogonal fields that do not interact with one another as they evolve - even though they have components that will, in general, interact. The introduction of these eigenmodes, along with their interaction and propagation properties, is the subject of the third chapter of this thesis and is the first result of the work herein.

In general, the propagation of light through linear optical systems is fully characterised by a scattering matrix [11]. This is also the case for our perturbation fields as they propagate through a nonlinear crystal. Indeed, the interaction of these fields can be thought of as a multiwavelength beamsplitter. In the context of quantum optics, the same scattering matrix defines the input-output relationship of creation and annihilation operators associated with the perturbation fields. In the quantum case, however, the field amplitudes are interpreted as probability amplitudes [12]. If the perturbation fields are at the multiphoton or single-photon level, then we can describe the evolution of the associated photon number states or Fock states. Indeed, by quantising the perturbation fields, they become operators which act on the Fock states depending on an effective Hamiltonian derived from the classical scattering matrix. This is the subject of Chapter 4 and is the second result of this work.

The purpose of the present chapter is two-fold. First, we introduce the basic propagation properties of light and all of the transverse structured fields that we use throughout the thesis before, in section 1.4, introducing the method of optical eigenmodes. Second, we briefly review the current state of research associated with the use of an eigenmode decomposition in nonlinear systems: discussed in section 1.4.3. Consequently, the present chapter acts as an introduction to the theoretical methods used throughout the thesis and as a motivation for the work herein. Finally, a detailed outline of the thesis is given at the end of the chapter.

1.2 Propagation of Light

In the context of classical physics, light is described as electromagnetic waves that are represented in three dimensions as vector fields, $\mathbf{F}(\mathbf{r}, t)$ where $\mathbf{r} = (x, y, z)$. In linear, dielectric, homogeneous, isotropic materials with no free currents or charges, these monochromatic fields are solutions of the wave equation

$$\left(\nabla^2 - \frac{1}{c^2}\frac{\partial^2}{\partial t^2}\right)\mathbf{F}(\mathbf{r}, t) = 0, \tag{1.1}$$

where c is the material-dependent phase velocity, and $\mathbf{F}(\mathbf{r}, t)$ may correspond to either the electric or magnetic component of the electromagnetic field. This wave equation is separable and has a solution which is written as the product of a space-dependent and time-dependent function as $\mathbf{F}(\mathbf{r}, t) = \mathbf{A}(\mathbf{r})T(t)$. Upon inputting this separable form into Eq. 1.1 we obtain an equation describing the spatial variation and an equation describing the temporal variation of the field as:

$$\left(\frac{d^2}{dt^2} + k^2c^2\right)T(t) = \left(\frac{d^2}{dt^2} + \omega^2\right)T(t) = 0, \tag{1.2}$$

$$\left(\nabla^2 + k^2\right)\mathbf{A}(\mathbf{r}) = 0, \tag{1.3}$$

where k is a separation variable called the wavevector defined as $k = \omega/c$, and ω is the angular frequency of the field related to the frequency as $\omega = 2\pi f$. The solution of the temporal equation, Eq. 1.2, is found to be $T(t) = \exp(\pm i\omega t)$.

For the spatial part of the solution, and throughout the thesis, we are concerned with the propagation of monochromatic, collimated laser light that does not significantly diverge from the optical axis. Fields that exhibit this kind of behaviour are said to be within the small-angle or paraxial approximation [13]. This approximation is valid here as we consider laser light propagating through optical systems with beam widths larger than the wavelength. Moreover, throughout the thesis, we utilise field profiles derived from a paraxial wave equation. We do not consider small apertures, lenses or large changes in refractive index that might cause these paraxial beams to significantly diverge from the optical axis [14, 15].

Within the paraxial approximation, where the direction of propagation is along the z-axis, the spatial dependence, with some polarisation vector $\hat{\mathbf{p}}$, is written

$$\mathbf{A}(\mathbf{r}) = u(\mathbf{r})e^{ikz}\hat{\mathbf{p}}, \tag{1.4}$$

where we assume that the scalar field amplitude $u(\mathbf{r})$ varies slowly as a function of z compared to its wavelength such that

$$|\frac{\partial^2}{\partial z^2}u(\mathbf{r})| \ll k|\frac{\partial}{\partial z}u(\mathbf{r})|, \tag{1.5}$$

and, as we are within the paraxial approximation

$$|\frac{\partial^2}{\partial z^2}u(\mathbf{r})| \ll |\nabla^2 u(\mathbf{r})|. \tag{1.6}$$

Substituting Eq. 1.4 into Eq 1.3 and accounting for the above approximations we arrive at the so-called paraxial equation [16] which for the original complex field amplitude is of the form

$$\left(\nabla_T^2 + 2ik\frac{\partial}{\partial z}\right)\mathbf{A}(\mathbf{r}) = 0. \tag{1.7}$$

As with the temporal equation, the paraxial equation permits plane wave solutions in which the field amplitude is uniformly distributed across an infinite plane. However, the paraxial equation has more interesting solutions with non-uniform transverse field shapes that will be introduced in the following sections. In deriving these solutions and throughout this work, we consider fields with constant polarisation and neglect the vector character of the electromagnetic fields by solving the scalar paraxial equation,

$$\left(\nabla_T^2 + 2ik\frac{\partial}{\partial z}\right)A(\mathbf{r}) = 0, \tag{1.8}$$

where ∇_T^2 is the scalar transverse Laplacian operator and $A(\mathbf{r})$ is a scalar field.

1.3 Structured Beam Shapes

In this section, we introduce the eigenmodes of free space within the paraxial approximation. Unlike finite systems with well-defined boundary conditions, the solutions of free space satisfy all possible symmetries - for example rectangular and circular symmetry. Therefore, we introduce both the Hermite-Gaussian and Laguerre-Gaussian representation of free space eigenmodes in sections 1.3.2 and 1.3.3, respectively. Throughout the thesis, we use these solutions to decompose our fields to define eigenmodes of systems in which multiple monochromatic fields interact with one another. Additionally, in section 1.3.4, we introduce the eigenmodes of a finite rectangular waveguide which allow us to better understand the propagation properties of the eigenmodes in such systems.

1.3.1 Fundamental Gaussian Beam

In free space or a homogeneous optical medium, the intensity profile of light will, in general, change in shape during propagation. However, there exist solutions of the scalar paraxial equation that exhibit consistency in their complex field profile as they propagate. These solutions are often called the modes or eigenmodes of an optical system and constitute a set of mutually orthogonal, non-interfering fields. Indeed, for a field decomposed into a set of such solutions, $E(\mathbf{r}) = \sum_j E_j(\mathbf{r}) = \sum_j E_j(x, y, z)$, we have, for all z, the following condition

$$\iint E_j^*(x, y, z) E_k(x, y, z)\, \mathrm{d}x\, \mathrm{d}y = \delta_{j,k}. \tag{1.9}$$

One set of solutions of the paraxial wave equation, satisfying the above condition, are plane waves with wavefronts that are infinite planes normal to the direction of propagation. These plane waves, however, do not resemble the transverse profile of a collimated beam of light in practice. Although not physical, the plane waves can act as a basis on which we can decompose any reasonable field distribution as [16]

$$E_0(x, y, z) = \int_{-\infty}^{\infty}\int_{-\infty}^{\infty}\int_{-\infty}^{\infty} \mathscr{E}(k_x, k_y, k_z) e^{i(k_x x + k_y y + k_z z)}\ \mathrm{d}k_x\, \mathrm{d}k_y\, \mathrm{d}k_z, \tag{1.10}$$

where $\mathscr{E}(k_x, k_y, k_z)$ is a complex field amplitude distributed across Fourier space [13]. To determine the form of the spatial field profile given by Eq. 1.10 we begin with a Gaussian ansatz of the form

$$E_0(x, y, z) = A_0\ e^{\frac{ik(x^2+y^2)}{2q(z)}} e^{ip(z)}, \tag{1.11}$$

which, when substituted into the paraxial equation, gives expressions for the functions $p(z)$ and $q(z)$. Indeed, for $q(z)$ we find

$$\frac{1}{q(z)} = \frac{1}{z + \frac{z_R^2}{z}} + \frac{i}{z_R + \frac{z^2}{z_R}}, \tag{1.12}$$

where z_R is the distance over which the width of the beam waist, w_0, increases by a factor of two. By introducing the wavefront curvature, $R(z) = z + \frac{z_R^2}{z^2}$, and beamwidth, $w(z) = w_0\sqrt{1 + \frac{z^2}{z_R^2}}$, we find

$$e^{ip(z)} = \frac{w_0}{w(z)} e^{-i\psi(z)}, \tag{1.13}$$

where $\psi(z) = \arctan\left(\frac{z}{z_R}\right)$ is known as the Gouy phase. Including the above functions, this field profile is known as the fundamental mode of the paraxial equation often denoted the Gaussian mode. Named after German mathematician and physicist Carl Friedrich Gauss.

1.3.2 Hermite Gaussian Beams

In deriving the fundamental Gaussian mode, we assumed that the field profile has the same symmetry along the x and y axes. In general, however, the field may have different symmetries with respect to x and y. Therefore, we introduce an ansatz of the form $A_0 h(x)g(y)$ in order to derive higher-order Gaussian modes with more interesting field profiles. Indeed, inputting this ansatz into the paraxial wave equation, we find

$$E_{n,m}(x,y,z) = A_0 \frac{w_0}{w(z)} H_n\left(\frac{\sqrt{2}x}{w(z)}\right) H_m\left(\frac{\sqrt{2}y}{w(z)}\right) e^{\frac{ik(x^2+y^2)}{2q(z)}} e^{ip(z)} e^{-i(n+m+1)\psi(z)}, \quad (1.14)$$

where the indices $n = 0, 1, \ldots, n_{max}$ and $m = 0, 1, \ldots, m_{max}$ determine the shape of the mode and $n + m = N$ is the order of the mode. The functions $H_k(\tau)$ are the so-called physicists Hermite polynomials [17] defined as

$$H_k(\tau) = (-1)^k e^{\tau^2} \frac{d^k}{d\tau^k} e^{-\tau^2}. \quad (1.15)$$

If the polynomial index k is even (odd) the polynomial itself is also even (odd) and in the case that $n = m = 0$ we find the fundamental mode defined in section 1.3.1. The intensity profiles of the first 20 Hermite-Gaussian modes are represented in figure 1.1 where the indices n and m correspond to the order of the Hermite polynomial, Eq. 1.15, along the x and y axes, respectively. In the figure, the indices start at $n = m = 0$ in the top left panel with n increasing from left to right and m increasing from top to bottom where $n = m = 3$ in the bottom right panel. Like the plane waves, these Hermite-Gaussian (HG) modes form a complete orthogonal basis such that any monochromatic field can be described as a superposition of these modes akin to the plane wave decomposition, Eq. 1.10, used to define them.

1.3.3 Laguerre-Gaussian Beams

If our optical waveguide or cavity is of circular symmetry, the Hermite-Gaussian modes will no longer be supported. However, by transforming Eq. 1.8 to cylindrical coordinates,

$$(x, y, z) \to (r, \phi, z)\,,$$

the solutions of the equation are found, by separation of variables, to take the following form

$$E_{\ell,p}(r,\phi,z) = A_0 \frac{w_0}{w(z)} \left(\frac{\sqrt{2}r}{w(z)}\right)^{\ell} L_p^{\ell}\left(\frac{2r^2}{w(z)^2}\right) e^{-\frac{r^2}{w(z)^2}} e^{\frac{ikr^2}{2R(z)^2}} e^{-i\psi(z)} e^{i\ell\phi}, \quad (1.16)$$

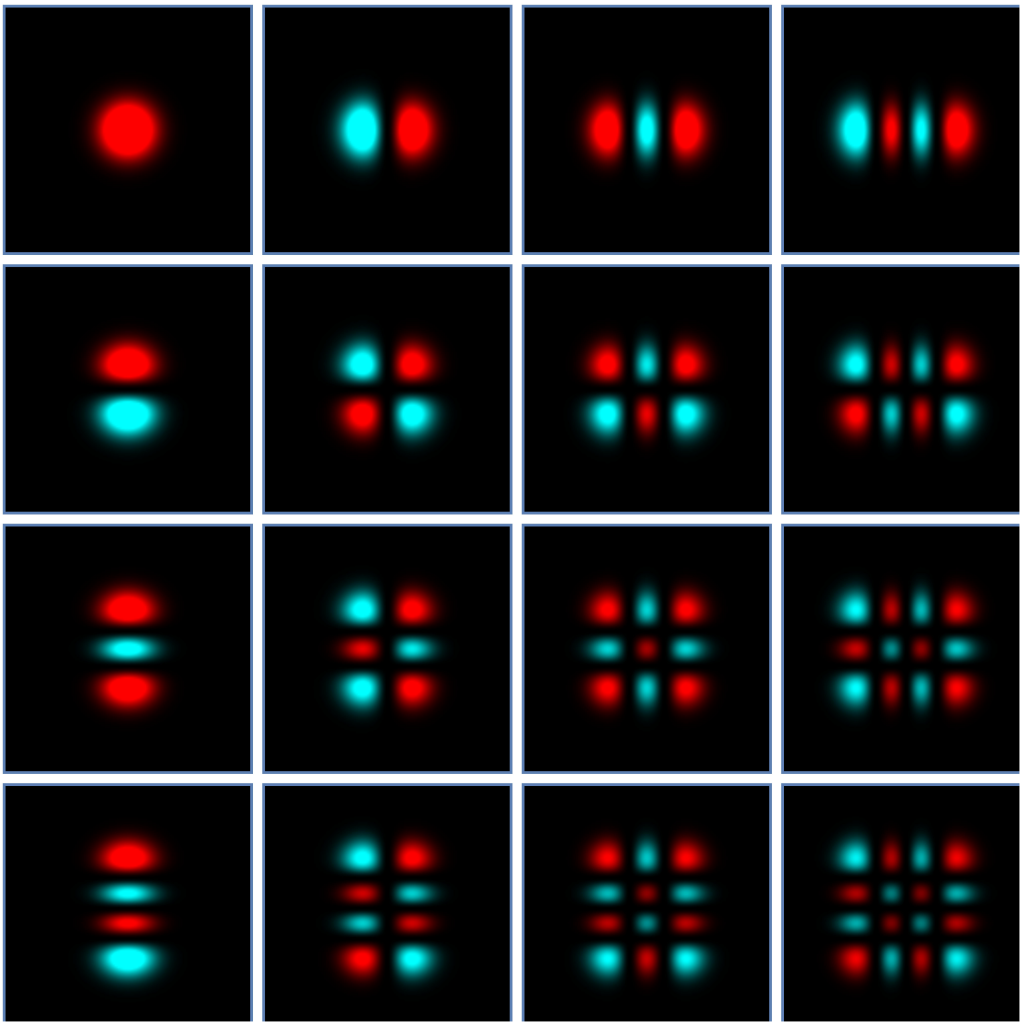

Figure 1.1: Intensity profiles of Hermite-Gaussian modes with hue representing intensity and colour representing phase. The false colour map is represented in figure 1.3. The indices (n, m) go from $(0, 0)$ top left to $(3, 3)$ bottom right where n increases from left to right and m from top to bottom.

where $\ell = -\ell_{max}, \ldots, -1, 0, 1, \ldots, \ell_{max}$ and $p = 0, 1, \ldots, p_{max}$; the order of the mode is $2p + |\ell| = N$. The functions $L_p^\ell(\tau)$ are the generalised Laguerre polynomials [17] which are defined using the Rodrigues formula [18] as

$$L_p^\ell(\tau) = \frac{\tau^{-\ell} e^\tau}{p!} \frac{d^p}{d\tau^p}(e^{-\tau}\tau^{\ell+p}). \tag{1.17}$$

The index ℓ corresponds to the number of helical wavefronts of the mode often called the orbital angular momentum [19] and the index p is the radial index corresponding to the order of the Laguerre polynomial. Indeed, like the indices n and m used to characterise the Hermite-Gaussian modes along the Cartesian axes, the indices ℓ and p characterise

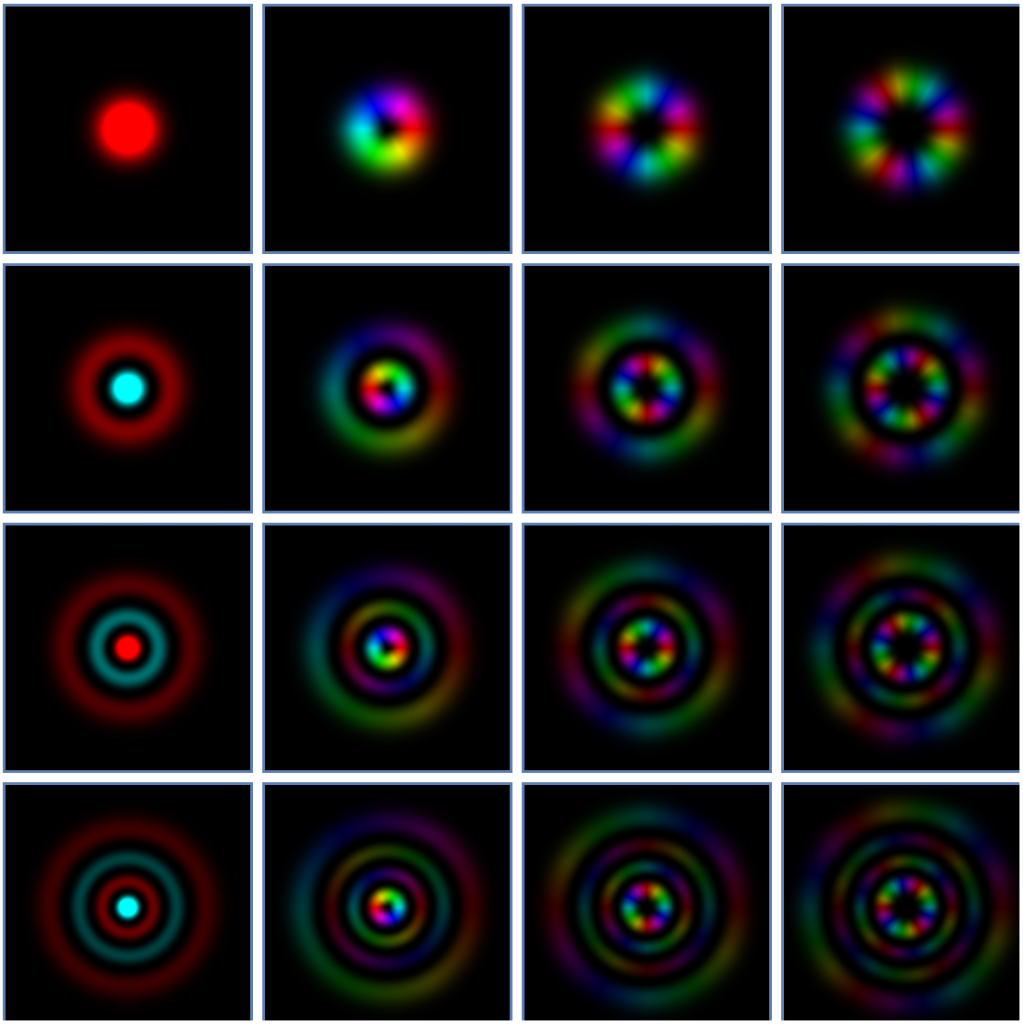

Figure 1.2: Intensity profiles of Laguerre-Gaussian modes represented on the phase map, figure 1.3. The indices (ℓ, p) go from $(0, 0)$ top left to $(3, 3)$ bottom right where ℓ increases from left to right and p from top to bottom.

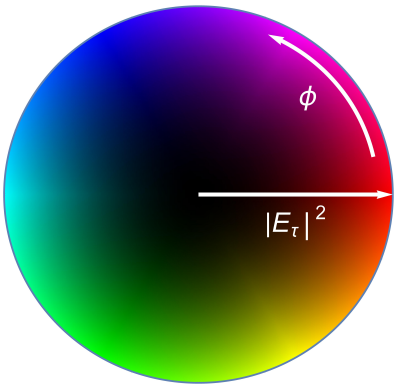

Figure 1.3: False colour map to represent complex field profiles with hue showing intensity, $|E_\tau|^2$, and colour showing phase, ϕ.

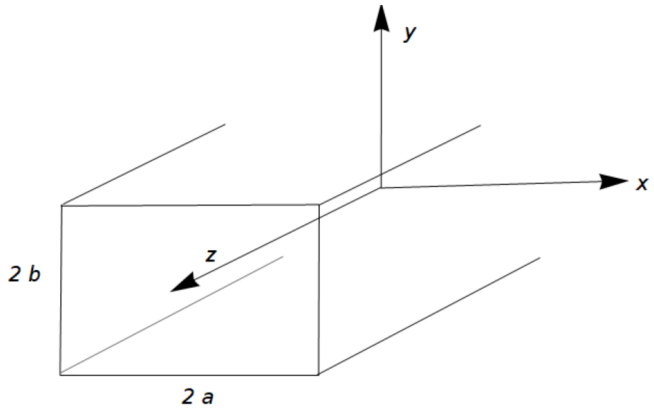

Figure 1.4: Schematic of a rectangular waveguide.

the angular and radial components of the Laguerre-Gaussian (LG) modes. Furthermore, these LG modes, shown in figure 1.2, form another complete orthogonal set similar to the Hermite-Gaussian modes. In both cases, one can write each basis set in terms of the other as:

$$\mathrm{LG}_{\ell,p} = \sum_{n=0}^{\infty}\sum_{m=0}^{\infty}\left(\mathrm{HG}_{n,m}\int_x\int_y \mathrm{HG}^*_{n,m}\mathrm{LG}_{\ell,p}\,\mathrm{d}x\,\mathrm{d}y\right), \tag{1.18}$$

$$\mathrm{HG}_{n,m} = \sum_{\ell=-\infty}^{\infty}\sum_{p=0}^{\infty}\left(\mathrm{LG}_{\ell,p}\int_x\int_y \mathrm{LG}^*_{\ell,p}\mathrm{HG}_{n,m}\,\mathrm{d}x\,\mathrm{d}y\right), \tag{1.19}$$

where $\mathrm{HG}_{n,m}$ and $\mathrm{LG}_{\ell,p}$ are of the form of Eq. 1.14 and 1.16 and the overlap integrals

$$\int_x\int_y \mathrm{HG}^*_{n,m}\mathrm{LG}_{\ell,p}\;\mathrm{d}x\,\mathrm{d}y = \int_x\int_y \left(\mathrm{LG}^*_{\ell,p}\mathrm{HG}_{n,m}\right)^*\;\mathrm{d}x\,\mathrm{d}y$$

take the values

$$\begin{cases} i^m g\left(\frac{N+\ell}{2}, \frac{N-\ell}{2}, m\right) : 2p+|\ell| = n+m \\ 0 \qquad\qquad\qquad\qquad\quad : 2p+|\ell| \neq n+m \end{cases}$$

with $N = n+m = 2p+|\ell|$ and

$$g(n',m',m) = \sqrt{\frac{(n'+m'-m)!m!}{2^{n'+m'}n'!m'!}}\frac{1}{m!}\frac{d^{m'}}{dt^{m'}}[(1-t)^{m'}(1+t)^{n'}]|_{t=0}. \tag{1.20}$$

Note, the indices of the HG and LG modes are related as $\ell(n,m) = n-m$ and $p(n,m) = \min(n,m)$. The linear transformations between these mode sets correspond to a rotation of the initial representation and thus defines the same Hilbert space.

1.3.4 Rectangular Waveguides

Within finite systems, such as waveguides or cavities, the Hermite-Gaussian and Laguerre-Gaussian modes lose their orthogonality. Here, we consider a rectangular waveguide with

perfectly reflecting walls and maintain the direction of propagation to be along the z-axis. The fields propagating in this waveguide are vector fields of the form

$$\mathbf{E} = \mathbf{E}(x, y)e^{\pm i\beta z}, \tag{1.21}$$

where β is the propagation wavenumber [20]. The fields in the waveguide evolve according to Maxwell's equations:

$$\nabla \cdot \mathbf{E} = 0, \tag{1.22}$$

$$\nabla \cdot \mathbf{B} = 0, \tag{1.23}$$

$$\nabla \times \mathbf{E} = -\partial_t \mathbf{B}, \tag{1.24}$$

$$\nabla \times \mathbf{B} = \tfrac{\varepsilon}{c^2}\partial_t \mathbf{E}, \tag{1.25}$$

where $\mathbf{E}$ and $\mathbf{B}$ represent electric and magnetic fields and ε is the relative permittivity of the dielectric material in the waveguide. If we are interested in the transverse magnetic (TM) modes where $\mathbf{E} = (E_x, E_y, E_z)$ and $\mathbf{B} = (B_x, B_y, 0)$ one can find, for the component of the electric field propagating along the waveguide, the following equation

$$\begin{aligned} &\partial_x^2 E_z(x, y) + \partial_y^2 E_z(x, y) + (k^2 n_1^2 - \beta^2) E_z(x, y) \\ &= \partial_x^2 E_z(x, y) + \partial_y^2 E_z(x, y) + k_c^2 E_z(x, y) = 0, \end{aligned} \tag{1.26}$$

where $k_c^2 = k^2 n_1^2 - \beta^2$ and $n_1 = \sqrt{\varepsilon}$ is the refractive index of the material. The solution of Eq. 1.26 is separable along the transverse coordinates as $E_z(x, y) = F(x)G(y)$ with:

$$F(x) = A\sin(k_x x - \phi), \tag{1.27}$$

$$G(y) = B\sin(k_y y - \psi), \tag{1.28}$$

where A and B are amplitudes of the field components. If we impose the boundary conditions $F(-a) = F(a) = 0$ and $G(-b) = G(b) = 0$, see figure 1.4, we find that the values of the wavevectors k_x and k_y are:

$$k_x = \frac{n\pi}{2a}, \quad k_y = \frac{m\pi}{2b}. \tag{1.29}$$

Similarly, for ϕ and ψ, we find:

$$\phi = \frac{n\pi}{2}, \quad \psi = \frac{m\pi}{2}, \tag{1.30}$$

where the indices n and m are introduced as the boundary conditions of the waveguide permit standing wave solutions with an integer number of oscillations n and m along the x and y axes, respectively. These indices are similar to those of the Hermite-Gaussian modes in section 1.3.2 except where the fundamental mode is defined for $n = m = 1$.

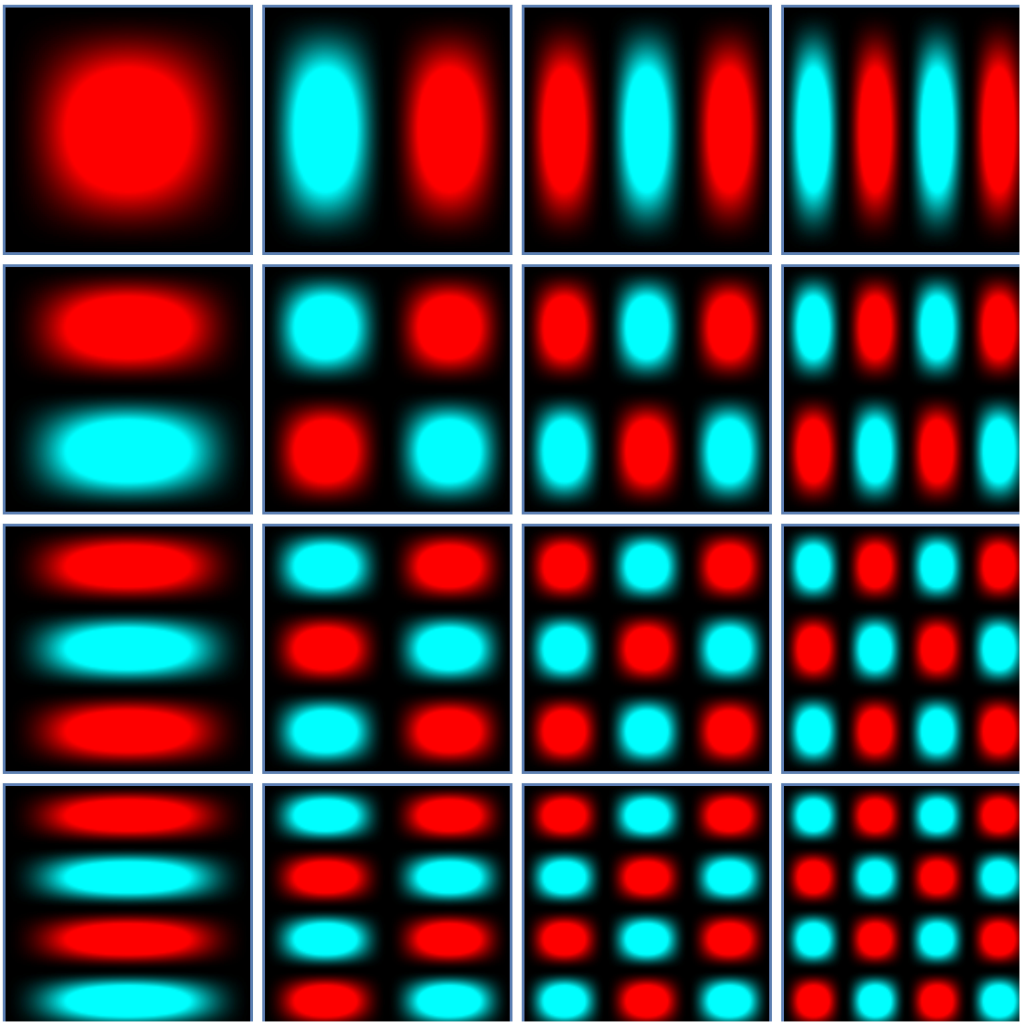

Figure 1.5: Intensity profiles of TM modes represented on the false colour map in figure 1.3. The indices (n, m) go from $(1, 1)$ top left to $(4, 4)$ bottom right where n increases from left to right and m from top to bottom.

Using the above coefficients, we define the cut-off wavevector for a given mode, TM_{nm}, propagating in the waveguide as

$$k_{c,nm} = \sqrt{k^2 n_1^2 - \beta^2} \tag{1.31}$$

$$= \sqrt{\left(\frac{n\pi}{2a}\right)^2 + \left(\frac{m\pi}{2b}\right)^2},$$

where the cut-off frequency is $f_{c,nm} = \omega_{c,nm}/2\pi$ with $\omega_{c,nm} = ck_{c,nm}$. This cut-off acts as a lower limit for propagation modes in the waveguide. Indeed, if the frequency, $f_{c,nm}$, of a given field is less than the operating frequency of the waveguide it corresponds to a propagating mode; otherwise, it is a non-propagating or evanescent field. If we recombine

our fields $F(x)$ and $G(y)$ the TM modes of the waveguide are defined as

$$E_{nm}(x,y) = E_0 \sin\left(\frac{n\pi}{2a}x - n\frac{\pi}{2}\right)\sin\left(\frac{m\pi}{2b}y - m\frac{\pi}{2}\right), \tag{1.32}$$

where E_0 is the amplitude at the input, and the fields form an orthogonal basis satisfying the condition

$$\int_{-a}^{a}\int_{-b}^{b} E^*_{nm}(x,y,z)E_{n'm'}(x,y,z)\,\mathrm{d}x\,\mathrm{d}y = \delta_{nn'}\delta_{mm'} \tag{1.33}$$

for all z, where the amplitude is normalised as $\int_{-a}^{a}\int_{-b}^{b}|E_0|^2\,\mathrm{d}x\,\mathrm{d}y = 1$. Note, as the evanescent fields cannot be normalised as described above, we only consider the propagating modes in this work. In doing so, we neglect any coupling between the evanescent fields that might generate modes that will propagate along the waveguide.

Unlike the derivation of the Hermite and Laguerre Gaussian modes introduced in the previous section, the TM modes are not derived as solutions of the paraxial equation. However, if we choose the propagation wavenumber as $\beta = k_{c,nm}/2$ then one can show that the TM_{nm} modes are solutions of

$$\left(\nabla_T^2 + 2ik_{c,nm}\frac{\partial}{\partial z}\right)E(x,y,z) = 0. \tag{1.34}$$

The intensity profiles for the first 20 TM propagating modes are represented in figure 1.5. These modes, along with the Hermite and Laguerre Gaussian modes, will be used throughout the thesis as bases on which we decompose our fields.

1.4 Theory of Optical Eigenmodes

The method of Optical Eigenmodes (OEi) allows one to find eigenmodes of any Hermitian optical measure in a mathematically rigorous manner. Much like the propagating modes introduced in section 1.3, the optical eigenmodes correspond to orthogonal solutions of Maxwell's equations. However, these eigenmodes are defined with respect to a physical observable and are thus characteristic of a particular measure of the electromagnetic field. In this section, we outline the fundamental theoretical considerations that lead one to the optical eigenmodes. In addition, we review the current state of affairs concerning the use of an eigenmode decomposition in nonlinear optics and note that if the intensity of the incident beam is large enough to induce nonlinear effects, the decomposition breaks down. Using a high-intensity background field, however, we can linearise these systems and define propagation and optical eigenmodes as described above. Unlike linear optics, the systems we consider here include terms that allow for the interaction of fields at different wavelengths. Introducing the optical eigenmodes to these systems is the first result of this thesis and,

therefore, this section acts as an introduction to optical eigenmodes and as motivation for the work presented.

1.4.1 Lorentz Reciprocity and Conservation of Interference

Following [7] it has been shown that for fields to be independent for a given optical measure, they must be eigenfunctions of an associated Hermitian operator. In this short section, we introduce these Hermitian operators from the perspective of reciprocity relations and Noether's theorem. We begin with Maxwell's equations in a linear, homogeneous dielectric material with no free currents or charges as:

$$\begin{aligned} \nabla \cdot \epsilon \mathbf{E} &= 0, \\ \nabla \cdot \mu \mathbf{H} &= 0, \\ \nabla \times \mathbf{E} &= -\mu \partial_t \mathbf{H}, \\ \nabla \times \mathbf{H} &= \varepsilon \partial_t \mathbf{E}, \end{aligned} \tag{1.35}$$

where $\mathbf{E}$ and $\mathbf{H} = \frac{1}{\mu}\mathbf{B}$ represent electric and magnetic fields, and μ and ε are the relative permeability and permittivity of the dielectric material. The energy density and momentum associated with the electromagnetic field $F = (\mathbf{E}, \mathbf{H})$ is expressed as:

$$\begin{aligned} E(F) &= \tfrac{1}{2}\left(\varepsilon \mathbf{E}^* \cdot \mathbf{E} + \mu \mathbf{H}^* \cdot \mathbf{H}\right), \\ \mathbf{S}(F) &= \tfrac{1}{2}\left(\mathbf{E}^* \times \mathbf{H} + \mathbf{E} \times \mathbf{H}^*\right), \end{aligned} \tag{1.36}$$

where $\mathbf{S}(F)$ is the energy flux of the electromagnetic field also denoted the Poynting vector. The local conservation of energy and momentum in free space is represented with the continuity equation

$$\nabla \cdot \mathbf{S}(F) + \partial_t E(F) = 0, \tag{1.37}$$

which simply states that the energy density of a region of dielectric material changes only if some energy has passed out with or entered the local region in question. This is analogous to the local conservation of charge where the energy density takes the role of the charge density and the Poynting vector of the current density [21].

Consider a superposition of fields $F = F_1 + F_2$ which are both solutions of Maxwell's equations, Eq. 1.35. Substituting this superposed field into the continuity relation results in four relations. One for F_1 and F_2 of the form of Eq. 1.37 and interference terms of the form:

$$\begin{aligned} E_{12}(F_1, F_2) &= \tfrac{1}{2}\left(\varepsilon \mathbf{E}_1^* \cdot \mathbf{E}_2 + \mu \mathbf{H}_1^* \cdot \mathbf{H}_2\right), \\ \mathbf{S}_{12}(F_1, F_2) &= \tfrac{1}{2}\left(\mathbf{E}_1^* \times \mathbf{H}_2 + \mathbf{E}_2 \times \mathbf{H}_1^*\right), \end{aligned} \tag{1.38}$$

where the fields $\mathbf{E}_i$ and $\mathbf{H}_i$ come from $F_i = (\mathbf{E}_i, \mathbf{H}_i)$ and the relations for $E_{21}(F_1, F_2)$ and $\mathbf{S}_{21}(F_1, F_2)$ are given by taking the complex conjugate of $E_{12}(F_1, F_2)$ and $\mathbf{S}_{12}(F_1, F_2)$, respectively. In order for the total local energy density to be conserved for all possible superpositions, $F = F_1 \pm F_2$ and $F = F_1 \pm iF_2$, the interference terms will satisfy the continuity relation,

$$\nabla \cdot \mathbf{S}_{12}(F_1, F_2) + \partial_t E_{12}(F_1, F_2) = 0, \tag{1.39}$$

which describes the conservation of interference between the two fields F_1 and F_2. If one now considers a linear transformation, $\mathscr{O}$, that leaves Maxwell's equations invariant then the transformed field, $\mathscr{O}F$, is also a solution of Eq. 1.35 with interference terms $E_{12}(F, \mathscr{O}F)$ and $\mathbf{S}_{12}(F, \mathscr{O}F)$. According to Noether's theorem [22], these continuous symmetries are associated with conserved quantities. These conserved quantities, for a given symmetry $\mathscr{O}$, are written:

$$\langle E_{12}(F)\rangle_{\mathscr{O}} = \int E_{12}(F, \mathscr{O}F)\ \mathrm{d}^3 r, \tag{1.40}$$

$$\langle \mathbf{S}_{12}(F)\rangle_{\mathscr{O}} = \int \mathbf{S}_{12}(F, \mathscr{O}F)\ \mathrm{d}^3 r. \tag{1.41}$$

The simplest example of a transformation that leaves Maxwell's equation invariant is the identity operator, $\mathbb{I}$, which is associated with the conservation of energy density, $\langle E_{12}(F)\rangle_{\mathbb{I}}$. For a field decomposition of the form, $F = \sum_j F_j$ the individual elements F_j are independent of one another only if the total energy density is the sum of individual energy densities. Consequently, for all linear transformations, $\mathscr{O}$, that leave Maxwell's equations invariant the fields F_j must satisfy the condition

$$\begin{aligned}\langle E_{12}(F)\rangle_{\mathscr{O}} &= \left\langle E_{12}\left(\sum_j F_j\right)\right\rangle_{\mathscr{O}} \\ &= \sum_j \langle E_{12}(F_j)\rangle_{\mathscr{O}},\end{aligned} \tag{1.42}$$

to be independent of the other fields in the decomposition. For the above condition to be satisfied the field is decomposed onto the eigenfunctions associated with the Hermitian operator $\mathscr{O}$. This is expressed mathematically as

$$\langle E_{12}(F)\rangle_{\mathscr{O}} = \sum_j \lambda_j \langle E_{12}(F_j)\rangle_{\mathscr{O}}, \tag{1.43}$$

where F_j is an eigenfunction of the Hermitian form given by Eq. 1.40 and λ_j are the associated eigenvalues. As already mentioned, the simplest transformation leaving Maxwell's equations invariant is the identity, $\mathscr{O} = \mathbb{I}$, corresponding to the energy density. Another example used in this work is the invariance of Maxwell's equations with respect to rotations

about a fixed point - generating the orbital angular momentum of the field. Indeed, in systems with circular or rotational symmetry as described in section 1.3.3 the fields are eigenfunctions of the operator $\mathscr{O} = i\partial_\phi$ where ϕ is the azimuthal angle. The energy density and momentum, in this case, are given as:

$$\begin{aligned} E_{12}(F, i\partial_\phi F) &= \tfrac{i}{2}\left(\varepsilon \mathbf{E}^* \cdot \partial_\phi \mathbf{E} + \mu \mathbf{H}^* \cdot \partial_\phi \mathbf{H}\right), \\ \mathbf{S}_{12}(F, i\partial_\phi F) &= \tfrac{i}{2}\left(\mathbf{E}^* \times \partial_\phi \mathbf{H} + \partial_\phi \mathbf{E} \times \mathbf{H}^*\right). \end{aligned} \tag{1.44}$$

In summary, by imposing the condition for independent fields, expressed in Eq. 1.42, one can introduce the time-dependent energy density operator and orbital angular momentum operator in the context of electromagnetic fields. Furthermore, given any symmetry that leaves Maxwell's equations invariant, one can introduce an associated Hermitian operator: the eigenvectors of which define the optical eigenmodes of the measure [4].

1.4.2 Optical Eigenmodes

Here, we consider an input scalar electric field $E(\mathbf{r}_1)$ that evolves through an optical system giving the field $F(\mathbf{r}_2)$ at the output plane as depicted in figure 1.6. Note, here we use $F(\mathbf{r}_2)$ to denote an electric field. This should not be confused with the electromagnetic fields used in the previous section. As we are concerned with finite optical systems, our fields are defined within some region defined by our detector. The fields that are incident on this region can be described by decomposing the field at the input plane as

$$E(\mathbf{r}_1) = \sum_{j=1}^{N} a_j E_j(\mathbf{r}_1), \tag{1.45}$$

where the fields $E_j(\mathbf{r}_1)$ form a basis with respect to our finite system and are orthogonal. That is, they satisfy the condition

$$\iint E_j^*(\mathbf{r}_1) E_k(\mathbf{r}_1)\, \mathrm{d}x_1\, \mathrm{d}y_1 = \delta_{j,k}. \tag{1.46}$$

Assuming the optical system is constructed with linear elements the corresponding output field is

$$F(\mathbf{r}_2) = \sum_{j=1}^{N} a_j F_j(\mathbf{r}_2), \tag{1.47}$$

where the complex coefficients a_j are the same as those in Eq. 1.45. Consider now a region of detection Ω in the output plane that measures some physical quantity $\mathbf{\Theta}$ represented by the operator $\mathscr{O}$. This measurement is expressed mathematically with the following Hermitian form

$$\mathbf{\Theta} = \int_\Omega F^*(\mathbf{r}_2) \mathscr{O} F(\mathbf{r}_2)\ d\Omega = \sum_{j,k}^{N} \left(\int_\Omega a_j^* F_j^*(\mathbf{r}_2) \mathscr{O} F_k(\mathbf{r}_2) a_k\ \mathrm{d}\Omega \right) = \mathbf{a}^\dagger \mathbf{M} \mathbf{a}, \tag{1.48}$$

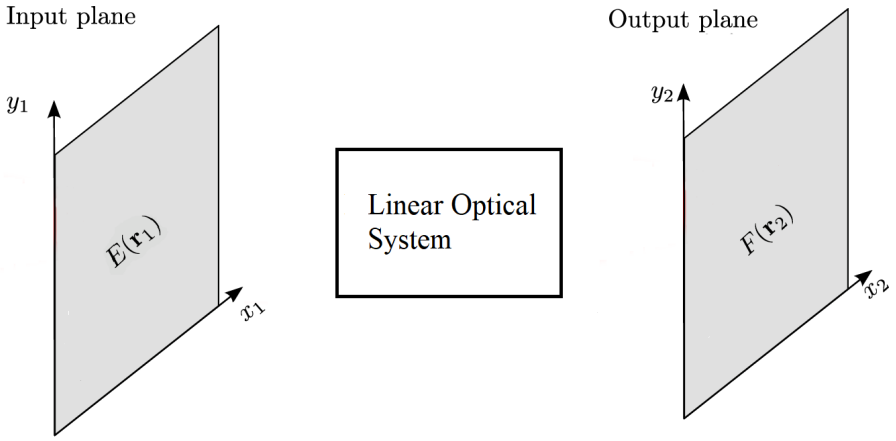

Figure 1.6: Linear optical system in which the field $F(\mathbf{r}_2)$ incident on the output plane is dependent on the input field $E(\mathbf{r}_1)$ and the optics of the set-up.

where the elements of the matrix $\mathbf{M}$ correspond to the cross interaction of all of the probe fields, $M_{jk} = \int_\Omega F_j^*(\mathbf{r}_2)\mathscr{O}F_k(\mathbf{r}_2)\ d\Omega$, and the vectors $\mathbf{a}$ contain the complex coefficients and their conjugates, $\mathbf{a} = (a_1, a_2 \dots a_N)^T$ and $\mathbf{a}^\dagger = (a_1^*, a_2^* \dots a_N^*)$. Diagonalising the cross-interaction matrix, we define the optical eigenmodes at the input and output plane as:

$$\mathbb{E}_k(\mathbf{r}_1) = \sum_{j=1}^{N} v_{kj} E_j(\mathbf{r}_1), \tag{1.49}$$

$$\mathbb{F}_k(\mathbf{r}_2) = \sum_{j=1}^{N} v_{kj} F_j(\mathbf{r}_2), \tag{1.50}$$

where v_{kj} are the elements of the k^{th} eigenvector, $\mathbf{v}_k$, of the matrix $\mathbf{M}$ and λ_k is the associated eigenvalue. Regardless of the physical quantity in question, the matrix $\mathbf{M}$ is Hermitian by definition. Consequently, it will have a spectrum of real eigenvalues with an associated set of orthogonal eigenvectors. These eigenvectors define the optical eigenmodes as in Eq. 1.49, and the corresponding eigenvalue is the magnitude of the physical quantity that would be measured for that eigenmode.

In summary, the Optical Eigenmodes allows one to find system-dependent eigenmodes in a mathematically precise manner. These eigenmodes generalise the concept of non-interacting fields to a broader scope of structured optical illuminations and light-matter interactions that go beyond the propagation properties of light. It is one of the main topics of this thesis to introduce this method in the context of nonlinear systems with the use of small perturbation fields. As a result, it is instructive to review the current state of affairs with respect to use of the eigenmode decomposition in nonlinear optics.

1.4.3 Eigenmode Decomposition in Nonlinear Systems

In the domain of nonlinear optics, the description of the propagation of electromagnetic fields is mathematically more involved than in the linear regime. Therefore, the tools for describing fields in nonlinear systems are not as well developed as in linear optics. This is due to the interaction of intense optical fields that generate light at frequencies different from that of the initial input field(s) [8]. Moreover, the fields generated by nonlinear interactions will interact with the input field(s), resulting in a non-trivial link between the input and output in which the principle of superposition is no longer applicable. As a consequence, the method of optical eigenmodes introduced in section 1.4.2 cannot be directly applied to nonlinear systems. Nevertheless, the eigenmode decomposition has been used in the context of nonlinear optics. Indeed, eigenmodes have been used to describe the nonlinear propagation of light in photonic crystals and have also been used to model the third-order nonlinear Kerr effect [23, 24] and second harmonic generation [25]. Similarly, Fourier modal methods, also known as rigorous coupled-wave theory, have been established for modelling second harmonic generation [26] and Kerr like nonlinearities [27] in layered periodic structures. In addition, boundary element methods have been used in this capacity. These methods are suited towards the modelling of nonlinear scattering effects of nanoparticles [28] and clusters of nanoparticles [29].

Another area of research in which the concept of eigenmodes and nonlinear effects are brought together is in the study and development of optical fibres for communication systems. The propagation of light in optical fibres is in practice a nonlinear process; however, much of the global communications systems involving optical fibres are designed with linearity as an approximation [20, 30]. Yet, chromatic dispersion and the fibre Kerr effect negatively impact the performance of modern fibre optic systems. Usually, these effects can be minimised by using compensation techniques, but, as the demand for information transmission increases, the capacity of fibre systems are approaching their theoretical limits [31, 32]. An alternative approach to linear transmission is to use the nonlinear effects to model and design fibre optic systems rather than compensating for them. This shift in paradigm requires a description of transmission from truly nonlinear channels and, consequently, requires knowledge of the nonlinear eigenmodes (usable degrees of freedom) on which information can be encoded. The existing methods concerned with nonlinear transmission employ the Nonlinear Fourier Transform (NFT) [33] which is an analogue of the standard Fourier transform. The NFT allows one to address dispersion and nonlinearities in a way similar to how the FT deals with chromatic dispersion in linear propagation, i.e., in Fourier space. However, in the case of the NFT, this is done in a nonlinear spectral domain

that is essentially an analogue of conventional Fourier space. Information can be encoded directly onto this nonlinear spectrum by using the associated nonlinear propagation modes. One approach used to find these modes is to use the discrete part of the nonlinear spectrum that contains eigenvalues that signify the existence of optical solitons [34]. Solitons have the propagation invariance required for encoding and transmission and are not disturbed by the Kerr effect. Using the solitonic eigenvalues in this way to transmit information in the discrete part of the spectra is known as 'eigenvalue communications' and is detailed in [35]. There also exist methods that exploit the continuous part of the nonlinear spectrum [36, 37]. The encoded information can be directly mapped on to the continuous part of the nonlinear spectrum using an inverse NFT. This method is called Nonlinear Inverse Synthesis and has received a lot of attention in nonlinear fibre systems [38].

All of the above methods introduce the concept of eigenmodes into the nonlinear regime but in most cases only maintain some of the advantages of the optical eigenmodes described in section 1.4.2 while others remain somewhat underdeveloped areas of research. It is, therefore, the first result of this thesis to introduce eigenmodes and optical eigenmodes to nonlinear systems. Similar to much of the research outlined above, we consider field propagation within the paraxial approximation and the non-depleting pump approximation. Our concern here, however, is not just with the propagation properties of the eigenmodes of fields coupled by a nonlinear crystal. We also consider the symmetry of the transverse field profiles that define these orthogonal eigenmodes and the symmetry of the eigenmodes with respect to the optical measures introduced in section 1.4.1. Furthermore, much of the research outlined above is concerned with the interaction and propagation of classical fields. In this thesis, we extend our discussion to fields at the single-photon and multiphoton level.

1.5 Outline of the Thesis

In this thesis, we introduce the method of optical eigenmodes to systems with intensity-dependent interaction terms. In particular, we consider the second-order nonlinear effects sum-frequency generation and parametric down-conversion. This is done by introducing perturbation fields to the nonlinear system such that one can restore the principle of linear superposition and, therefore, utilise an eigenmode decomposition. With these optical eigenmodes defined, we consider perturbation fields that are at the multiphoton level and analyse the quantum behaviour of the Fock states associated with these fields.

In Chapter 2, we outline all relevant theoretical considerations concerned with the field of nonlinear optics. In particular, we describe the basics of nonlinear light-matter interactions and, in section 2.2.2, derive the equations of evolution for fields propagating in a second-order nonlinear crystal. In section 2.2.3 and 2.2.4, we discuss the phase-matching conditions of the propagating fields and the symmetries of the second-order susceptibility tensor. Finally, in section 2.3, we introduce perturbation fields that propagate with each of the fields in three-wave mixing. From the resulting equations, we highlight two distinct effects which can be described in the context of the perturbation fields. Namely, sum-frequency generation and parametric down-conversion. This chapter concludes with a brief analysis of these two nonlinear effects.

In Chapter 3, the method of optical eigenmodes is introduced independently for both sum-frequency generation and parametric down-conversion. Indeed, in section 3.2.1, the mathematical formalism for optical eigenmodes in the context of sum-frequency generation is discussed in detail. In section 3.3.1, we discuss the computational set-up used in the thesis, followed by some numerical examples in sections 3.3.2 and 3.3.3. For the numerical examples, we first consider bulk nonlinear material that exhibits rectangular and circular symmetry. The symmetry and degeneracy associated with the optical eigenmodes for both rectangular and circular systems are also discussed in the respective sections. In section 3.4.1, we introduce optical eigenmodes for finite optical systems in the form of waveguides. Again, we consider systems with rectangular and circular geometry. The propagation eigenmodes in these waveguides are introduced and discussed in section 3.4.4. In section 3.5.1, we present the formalism of optical eigenmodes for the equations for parametric down-conversion and consider numerical examples. Finally, at the end of Chapter 3, in section 3.8, we outline the set of commuting operators that allow one to uniquely label optical eigenmodes for circular and rectangular systems for both sum-frequency generation and parametric down-conversion.

Chapter 4 is concerned with the quantum behaviour of single-photon or Fock states in the context of our three-wave mixing effects. In all of the previous chapters, we considered classical fields and their evolution. Consequently, this chapter begins with an introductory section where we discuss the basic principles of quantum optics that are pertinent in understanding the rest of the chapter. Indeed, in section 4.2, we introduce the equations of evolution for quantum states of light in both the Schrödinger and Heisenberg pictures. In the same section, we briefly discuss expanding the Optical Eigenmode (OEi) method to the domain of quantum optics via the second quantisation of the electromagnetic field. To

conclude this section, we introduce the creation and annihilation operators of the quantised fields and the photon number or Fock state representation of the associated quantum system. In section 4.3.1, we consider the behaviour of Fock states in sum-frequency generation. In particular, we outline the derivation of an effective Hamiltonian using results from group theory. Following this, we introduce the propagation eigenmodes defined in the previous chapter to simplify the quantum behaviour of the system, followed by some numerical examples. In section 4.4.1, we turn our attention to the case of parametric down-conversion.

Finally, in Chapter 5, we conclude the thesis with a summary and discussion of any conclusions thereof before outlining potential research avenues to expand upon the material herein.

Chapter 2

Introduction to Nonlinear Optics

2.1 Introduction

The field of nonlinear optics is relatively young when compared to the study of the linear effects of light. The origin of the field of nonlinear optics closely coincides with the invention of the laser in the 1960s [39]. Before this time, light sources used in experiments were not intense enough to induce nonlinear optical effects. Even with the coherent, focused light produced by lasers, the detection of nonlinear signals still proved a challenge in the early experimental work related to the subject. Indeed, in the paper that first reported the observation of the second harmonic [40], the signal was so small that the printing press mistook it for an ink blemish and omitted it from the published article. In the years proceeding this seminal paper much of the theoretical foundations of nonlinear optics was established in several articles that form the introductory chapters in many books on the subject [8, 9, 10, 41, 42, 43]. Although not observed in everyday life, nonlinear effects have proved very useful in many areas of science and engineering. Indeed, many tunable lasers make use of frequency mixing and harmonic generation to create coherent radiation across the electromagnetic spectrum. Furthermore, these tunable light sources and optical nonlinearities have been utilised in various spectroscopic scenarios [44, 45, 46, 47, 48]. From a more fundamental perspective, nonlinear effects remain the most useful source to generate entangled photon pairs [49, 50, 51].

In this work, we are concerned with eigenmodes in the context of nonlinear optical systems within the non-depleting pump approximation. In this chapter, we outline all of the theoretical considerations used throughout the thesis associated with nonlinear optics. Indeed, in section 2.2, we introduce the physical intuition and mathematical form of nonlinear interactions. In particular, we consider second-order nonlinearities giving rise to effects like second-harmonic generation and sum/difference-frequency generation and introduce the

coupled partial differential wave equations that describe how the fields in these effects evolve. In sections 2.2.3 and 2.2.4, we outline the phase matching of second-order nonlinear interactions and the crystal symmetry that allow the simplification of the third-rank tensor that links the Cartesian components of the fields. Also, in section 2.3, we introduce the concept of low-intensity perturbation fields that interact with one another via a non-depleting high-intensity background field. In this non-depleting pump approximation, we describe briefly the two effects that we are mainly concerned with here, namely, sum-frequency generation and parametric down-conversion.

In practice, sum-frequency generation has proved a very useful effect in the physical sciences. In the first instance, by combining two lower frequency signals, one can generate collimated beams at wavelengths not otherwise accessible with a single source [52, 53, 54, 55]. Further, the use of sum-frequency generation in spectroscopy has proved to be a powerful technique for probing material surfaces and interfaces between different materials [56, 57]. This technique has also found use in the field of atmospheric chemistry due to the importance of understanding chemical reactions at air-liquid interfaces [58]. Furthermore, sum-frequency generation has been used in various single-photon scenarios [59, 60, 61].

Parametric down-conversion is an important effect in the context of quantum optics and single-photon experiments. This is due to the potential for generating entangled photon pairs [62, 63, 64] and single photons [65, 66]. Consequently, parametric down-conversion has proved of great importance in the study of quantum information experiments [67], nanophotonics [68, 69], quantum cryptography [70] and experiments for testing Bell's inequalities [71, 72, 73]. Moreover, due to the high degree of spatial correlations between the photons generated by parametric down-conversion, these photon pairs can be utilised in the context of quantum imaging techniques [74, 75]. Due to the connection with quantum optics, the theoretical and experimental study of these effects still provides fertile ground for interesting scientific research.

2.2 Wave Description of Nonlinear Optics

2.2.1 Nonlinear Optical Interactions

To understand the interaction of light with matter, we consider the dipole response of the atoms in the material in which the field propagates. Indeed, consider a single atom in a dielectric material, the overall charge of which is neutral. If an electromagnetic field is incident on this atom, the electric component of the field will cause a small separation between the positively charged nucleus and negatively charged electron cloud generating an

oscillating dipole moment. The magnetic field will similarly disturb the positively charged particles in the atoms; however, this is negligible when compared to the influence of the electric component of the field. Therefore, we neglect the influence of the magnetic field: this is known as the electric dipole approximation [9]. After being excited, the oscillating dipole created by the electric field will radiate light in a characteristic dipole pattern at the frequency of the incident field [76, 77]: this is commonly denoted Rayleigh scattering. If the light incident on the dielectric material has sufficient intensity, it will induce a nonlinear response and stimulate the generation of frequency components different from that of the input field.

In classical optics, we are concerned with the evolution and interaction of electromagnetic fields in macroscopic materials made up of a large number of atoms. Consequently, we characterise the response of the material with respect to the density of dipole moments or polarisation, $P(\mathbf{r},t)$, of the material. If this bulk electric polarisation has nonlinear terms that are small compared to the linear term, it can be written as a series expansion with respect to a scalar electric field as [8]

$$\begin{aligned} P(\mathbf{r},t) &\approx \varepsilon_0 \left(\chi^{(1)}\ E(\mathbf{r},t) + \chi^{(2)}\ E(\mathbf{r},t)^2 + \chi^{(3)}\ E(\mathbf{r},t)^3 + ... + \chi^{(N)}\ E(\mathbf{r},t)^N\right) \\ &= P^{(1)}(\mathbf{r},t) + P^{(2)}(\mathbf{r},t) + P^{(3)}(\mathbf{r},t) + ... + P^{(N)}(\mathbf{r},t), \end{aligned} \tag{2.1}$$

where $\chi^{(1)}$ corresponds to the linear electric susceptibility, and the higher-order terms correspond to the second, third and N^{th} order susceptibility of the material. As the above expression indicates, the susceptibility is a dimensionless coefficient that describes the degree of polarisation of a given material in response to an incident electric field. Note, we have assumed that the nonlinear material is lossless and dispersionless such that susceptibility in the polarisation expansion depends on the instantaneous electric field strength. The first term in the above expansion encompasses all of the effects of linear optics. The higher-order terms describe various kinds of nonlinear effects. The first nonlinear term of interest, and the one we are concerned within this work, is the second-order nonlinearity characterised by the susceptibility tensor $\chi^{(2)}$.

The simplest example of a second-order nonlinear interaction is second harmonic generation. If we consider a monochromatic field of the form $E(\mathbf{r},t) = E_0(\mathbf{r})\ e^{-i\omega t} + \text{c.c.}$ with complex amplitude, $E_0(\mathbf{r})$, at the input, then the resulting second-order nonlinear polarisation is of the form

$$P^{(2)}(\mathbf{r},t) = 2\varepsilon_0\chi^{(2)}|E_0(\mathbf{r})|^2 + \varepsilon_0\chi^{(2)}(E_0(\mathbf{r})^2 e^{-2i\omega t} + \text{c.c}) \tag{2.2}$$

and is made up of a zero-frequency D.C. term and a contribution at twice the input frequency, 2ω. The generation of this second harmonic corresponds to a double excitation from the field at frequency ω resulting in a dipole oscillating at 2ω, which will emit electromagnetic radiation. In macroscopic materials, we have a large number of dipoles and, therefore, the interactions described above will occur a great number of times as the fields propagate through the crystal. Thus, the relative phases of the oscillating dipoles should be such that the emitting radiation interferes constructively creating a detectable signal. This point is discussed in more detail in section 2.2.1.

More generally, one can consider an input field made up of two distinct frequency components, i.e., $E(\mathbf{r},t) = E_1(\mathbf{r})\ e^{-i\omega_1 t} + E_2(\mathbf{r})\ e^{-i\omega_2 t} + \text{c.c.}$ The second-order polarisation in this instance is of the form

$$\begin{aligned} P^{(2)}(\mathbf{r},t) =& \varepsilon_0\chi^{(2)}\big(E_1(\mathbf{r})^2 e^{-2i\omega_1 t} + E_2(\mathbf{r})^2 e^{-2i\omega_2 t} + 2E_1(\mathbf{r})E_2(\mathbf{r})e^{-i(\omega_1+\omega_2)t} \\ &+ 2E_1(\mathbf{r})E_2^*(\mathbf{r})e^{-i(\omega_1-\omega_2)t} + \text{c.c}\big) + 2\varepsilon_0\chi^{(2)}\left(|E_1(\mathbf{r})|^2 + |E_2(\mathbf{r})|^2\right). \end{aligned} \tag{2.3}$$

Similar to the nonlinear polarisation waves for a single monochromatic field in Eq 2.2, we find a D.C. term and a contribution at the second harmonic. In addition to these terms, however, we find dipoles oscillating at the sum, $\omega_1+\omega_2$, and difference, $\omega_1-\omega_2$, of the two input frequencies. These components are denoted the sum and difference-frequency waves.

Another important process, especially in the context of quantum optics, occurs when we consider the annihilation of a photon at the sum $\omega_3\ (=\omega_1+\omega_2)$. In Eq. 2.3 we observed that if a photon at ω_1 and ω_2 are absorbed by a dipole then a photon at their sum, $\omega_3=\omega_1+\omega_2$, can be generated under suitable conditions. Thus, if we consider an input photon at ω_3, the reverse interaction is possible and results in the emission of two photons: one at ω_1 and one at ω_2. This process - known as parametric down-conversion - is prominent in quantum optics and is a powerful source of generating single photons and entangled photon pairs [78, 79, 80, 81]. This effect can be understood in the context of the energy-level diagrams in figure 2.1. Indeed, if we take a field of the form $E(\mathbf{r},t) = E_1(\mathbf{r})\ e^{-i\omega_1 t} + E_3(\mathbf{r})\ e^{-i\omega_3 t} + \text{c.c.}$ at the input of the nonlinear crystal then the difference term $\omega_3-\omega_1$ will stimulate the transition generating the field at ω_2. Similarly, the ω_3 and ω_2 fields have a difference-frequency term that will stimulate the generation of the ω_1 field. Thus, the ω_1 field acts to amplify the ω_2 field and vice versa. This process is discussed in more details in section 2.3.3.

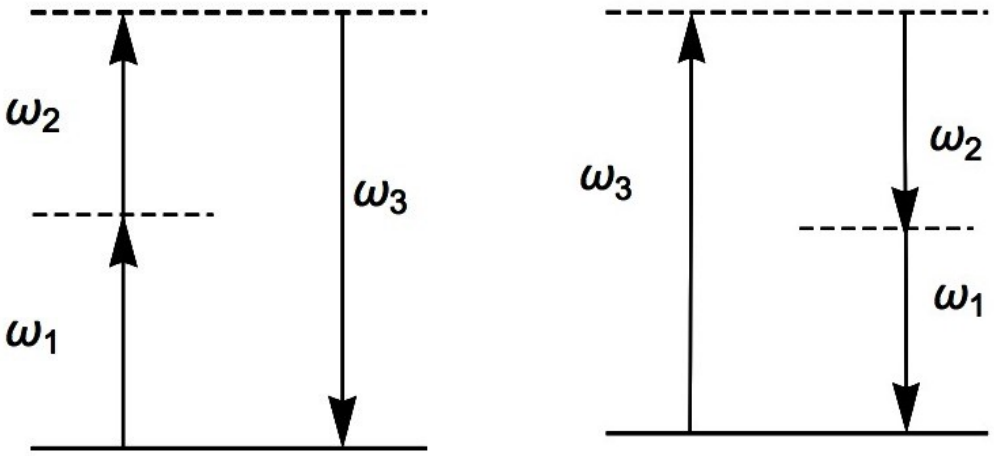

(a) (b)

Figure 2.1: Energy-level diagrams for (a) sum-frequency generation and (b) parametric down-conversion. As we are off-resonance, the horizontal lines correspond to unobservable, short-lived, virtual states.

Note, the classical description of the polarisation presented here permits a single resonant frequency for each atom and is only suitable for cases where all of the incident field components have a frequency smaller than the lowest electronic resonance of the nonlinear material. For a complete treatment, one must consider a quantum description of the polarisation that permits more than one resonant frequency for each atom. This introduces additional terms to the higher-order polarisation corresponding to cases in which the atoms can simultaneously exhibit single-photon and two-photon excitations [8, 9, 43].

2.2.2 Wave Equations of Nonlinear Optics

If the incident light is of sufficient intensity to induce nonlinear effects, this will change the form of the equations describing the evolution of the fields. As a consequence, the paraxial equation introduced in section 1.2 is no longer valid as it only describes propagation in the linear approximation. Consider an input field made up of frequency components of the form $E(\mathbf{r},t) = \sum_\tau E_\tau(\mathbf{r})e^{-i\omega_\tau t} + \text{c.c.}$ Each of the complex components $E_\tau(\mathbf{r})e^{-i\omega_\tau t}$ of this field exist in a different Hilbert space as

$$E^*_\tau(\mathbf{r})E_\sigma(\mathbf{r}) \int e^{i(\omega_\tau - \omega_\sigma)t}\ \mathrm{d}t = 2\pi\delta(\omega_\tau - \omega_\sigma)E^*_\tau(\mathbf{r})E_\sigma(\mathbf{r}), \tag{2.4}$$

where $\delta(\omega_\tau - \omega_\sigma)$ is the Dirac delta function. Therefore, each of these complex field components will satisfy a frequency-dependent wave equation. These wave equations are of the

form

$$\nabla^2 E_\tau(\mathbf{r}) + \frac{\omega_\tau^2}{c^2}\varepsilon^{(1)}(\omega_\tau)E_\tau(\mathbf{r}) = -\frac{\omega_\tau^2}{\epsilon_0 c^2}\mathrm{P}_\tau^{\mathrm{NL}}(\mathbf{r}), \tag{2.5}$$

where the relative permittivity $\varepsilon^{(1)}(\omega_\tau)$ is related to the refractive index as $\varepsilon^{(1)}(\omega_\tau) \approx n_\tau^2$ and $P_\tau^{\mathrm{NL}}(\mathbf{r}) = P_\tau^{(2)}(\mathbf{r}) + P_\tau^{(3)}(\mathbf{r}) + ... + P_\tau^{(\mathrm{N})}(\mathbf{r})$ is the nonlinear polarisation where $P_\tau^{\mathrm{NL}}(\mathbf{r},t) = P_\tau^{\mathrm{NL}}(\mathbf{r})e^{-i\omega_\tau t}$. If we consider a field with three components at the input, we have three equations; each of which describes the evolution of a field oscillating at one of the frequencies. Indeed, if we consider a field propagating along the positive z-axis, the field at the input is written

$$E(\mathbf{r},t) = E_1(\mathbf{r})e^{i(k_1 z-\omega_1 t)} + E_2(\mathbf{r})e^{i(k_2 z-\omega_2 t)} + E_3(\mathbf{r})e^{i(k_3 z-\omega_3 t)} + \text{c.c.}, \tag{2.6}$$

where $k_\tau = (n_\tau\omega_\tau)/c$ and we choose the frequencies such that $\omega_3 = \omega_2+\omega_1$ with $\omega_2 > \omega_1 > 0$. If we truncate the polarisation up to the second-order effects in which $P^{(N\geq 3)}(\mathbf{r}) \ll P^{(2)}(\mathbf{r})$ then the terms in $P^{\mathrm{NL}}(\mathbf{r})$ will be those $\propto E(\mathbf{r})^2$. Indeed, if we consider first the polarisation waves that will contribute to the field at ω_3, we are left with a single contribution of the form $P_3^{\mathrm{NL}}(\mathbf{r}) = 2\varepsilon_0\chi^{(2)}E_1(\mathbf{r})E_2(\mathbf{r})e^{i(k_1+k_2)z}$. Hence, within the paraxial approximation discussed in section 1.2, we can write the equation of evolution for this field as

$$\left(\nabla_T^2 + 2ik_3\frac{\partial}{\partial z}\right)E_3(\mathbf{r}) = -\chi_3 E_1(\mathbf{r})E_2(\mathbf{r})e^{i\Delta k z}, \tag{2.7}$$

where $\chi_3 = (2\chi^{(2)}\omega_3)/(n_3 c)$ and $\Delta k = k_1 + k_2 - k_3$ is the phase mismatch. This is a paraxial wave equation in nonlinear optics and when compared to Eq. 1.8 is distinct due to the source term on the right-hand side. Consequently, if $E_1(\mathbf{r})$ and $E_2(\mathbf{r})$ are zero or we are in free space, i.e. $\chi^{(2)} = 0$, the equation describes a monochromatic field propagating according to the paraxial equation of section 1.2.

Following the same process as above, for the fields $E_1(\mathbf{r})$ and $E_2(\mathbf{r})$, we find a set of coupled equations describing three-wave mixing in second-order nonlinear materials:

$$\left(\nabla_T^2 + 2ik_2\frac{\partial}{\partial z}\right)E_2(\mathbf{r}) = -\chi_2 E_1^*(\mathbf{r})E_3(\mathbf{r})e^{-i\Delta k z}, \tag{2.8}$$

$$\left(\nabla_T^2 + 2ik_1\frac{\partial}{\partial z}\right)E_1(\mathbf{r}) = -\chi_1 E_2^*(\mathbf{r})E_3(\mathbf{r})e^{-i\Delta k z}, \tag{2.9}$$

in which $\chi_\tau = (\chi^{(2)}\omega_\tau)/(2n_\tau c)$. These three equations collectively describe all three-wave mixing processes in nonlinear materials and are the main equations used in work presented here. Equations for higher-order nonlinearities can be easily found in the same manner by including more terms in the polarisation expansion in Eq. 2.1. For this work, however, we assume that $P^{(3)}(\mathbf{r},t)$ to $P^{(N)}(\mathbf{r},t)$ are negligible compared to the second-order nonlinearities, $P^{(2)}(\mathbf{r},t)$.

(a) (b)

Figure 2.2: Condition for perfect phase matching for (a) collinear propagating and (b) non-collinear propagating field for $\mathbf{k}_1 < \mathbf{k}_2$.

2.2.3 Phase Matching

The phase mismatch in Eqs. 2.7 to 2.9 is an expression of the momentum conservation associated with the second-order nonlinear effects represented in figure 2.1. In a macroscopic material, we have many dipoles that may contribute to the propagating fields in the form of polarisation waves resulting from the terms in $P^{(2)}(\mathbf{r}, t)$. Each of these polarisation waves will have some phase that will determine if they interfere constructively with the propagating fields. The efficiency of this constructive interference is determined by the phase matching, Δk. In three-wave mixing, one could consider the following field incident on the material

$$E(\mathbf{r}, t) = E_1(\mathbf{r})e^{i(\mathbf{k}_1.\mathbf{r}-\omega_1 t)} + E_2(\mathbf{r})e^{i(\mathbf{k}_2.\mathbf{r}-\omega_2 t)} + \text{c.c.}, \tag{2.10}$$

where $\mathbf{k}_j = (k_{j,x}, k_{j,y}, k_{j,z})^\top$, $\mathbf{r} = (x, y, z)^\top$ and $\top$ denotes the transpose. Substituting this field into the second-order polarisation, we have the following elements

$$P^{(2)}(\mathbf{r}, t) = \varepsilon_0 \left(\cdots + 2\chi^{(2)} E_1(\mathbf{r}) E_2(\mathbf{r}) e^{-i\omega_3 t} e^{i(\mathbf{k}_1+\mathbf{k}_2).\mathbf{r}} + \ldots \right) \tag{2.11}$$

contributing to the propagating fields where we maintain the condition $\omega_3 = \omega_1 + \omega_2$. For the polarisation field to generate a useful signal the phase-matching condition

$$\mathbf{k}_1 + \mathbf{k}_2 = \mathbf{k}_3 \tag{2.12}$$

should be approximately satisfied such that the polarisation wave amplitude in Eq. 2.11 has a phase that allows it to constructively interfere with the field $E_3(\mathbf{r})e^{i(\mathbf{k}_3.\mathbf{r}-\omega_3 t)}$. This is equivalent to maximising the interaction term in Eq. 2.7, which generates the field at ω_3. The condition for phase matching is illustrated in figure 2.2 for non-collinear and collinear propagating fields.

In practice, this phase matching is achieved by taking advantage of the birefringence of a given material. Indeed, in birefringent materials, the refractive index experienced by a field is dependent on its polarisation with respect to particular crystal axes [82]. In uniaxial materials, light incident on the material is subject to either the ordinary refractive index, $n_o(\omega) = n_x(\omega) = n_y(\omega)$, or the extraordinary refractive index, $n_e(\omega) = n_z(\omega)$. For three-wave mixing the largest frequency - in this case, ω_3 - is often chosen to be polarised along the direction with the lowest refractive index. The crystal axis with the lowest refractive index depends if the material is positive uniaxial, $n_e(\omega) > n_o(\omega)$, or negative uniaxial, $n_o(\omega) > n_e(\omega)$. In both of these crystal types, there are two permutations for the polarisation of the lower frequency fields, denoted type I and type II phase matching. Indeed, for positive uniaxial crystals, these phase-matching conditions are:

$$\text{Type I}: \quad n_3^o\omega_3 = n_2^e\omega_2 + n_1^e\omega_1, \tag{2.13}$$

$$\text{Type II}: \quad n_3^o\omega_3 = n_2^e\omega_2 + n_1^o\omega_1, \tag{2.14}$$

and for negative uniaxial crystals we have:

$$\text{Type I}: \quad n_3^e\omega_3 = n_2^o\omega_2 + n_1^o\omega_1, \tag{2.15}$$

$$\text{Type II}: \quad n_3^e\omega_3 = n_2^o\omega_2 + n_1^e\omega_1, \tag{2.16}$$

where n_τ^e and n_τ^o are the refractive index for a field of frequency ω_τ along the extraordinary and ordinary axis, respectively. In order to phase match the crystal, Δk should be as close to zero as possible where $\Delta k = 0$ is known as perfect phase matching. In uniaxial crystals, this can be achieved by taking advantage of the angular dependence of birefringent materials using the relation

$$\frac{1}{n_e\left(\phi\right)^2} = \frac{\sin^2\left(\phi\right)}{n_e^2} + \frac{\cos^2\left(\phi\right)}{n_o^2}, \tag{2.17}$$

where the angle ϕ is the angle between the wavevector, $\mathbf{k}$, and the optical axis with $n_e = n_e(\pi/2)$ and $n_o = n_e(0)$. This angle is adjusted to find the appropriate $n_e(\phi)$ to satisfy $\Delta k \approx 0$. However, this equation is not guaranteed to give a physically meaningful azimuthal angle in which case, if the material birefringence is temperature-dependent, one can fix the orientation of the beams incident on the crystal and vary the temperature to achieve phase matching [83, 84, 85]. Alternatively, one can achieve phase matching by using a material made up of multiple layers that periodically reverses the crystals optical axis. This technique is known as quasi-phase-matching [86, 87, 88, 89].

2.2.4 Permutation Symmetry

In deriving the coupled wave equations in section 2.2.2, we introduced the susceptibility, $\chi^{(2)}$, for second-order nonlinear effects. However, these nonlinear equations were introduced in the context of scalar fields, and we thus neglected the tensor character of the susceptibility. In this section, we briefly describe how we reduce the second-order susceptibility tensor to a matrix which can then be reduced to a single coefficient, as described in section 3.3.1. Each of the vector fields in three-wave mixing has three Cartesian components $E_i(\omega_\tau), E_j(\omega_\tau)$ and $E_k(\omega_\tau)$; the susceptibility tensor describes all possible interactions between these field components. Indeed, if we consider the polarisation wave $P_i(\omega_n + \omega_m)$ generated by the interaction of the fields $\mathbf{E}(\omega_n)$ and $\mathbf{E}(\omega_m)$, we have

$$P_i(\omega_n + \omega_m) = \varepsilon_0 \sum_{j,k} \sum_{n,m} \chi^{(2)}_{ijk}(\omega_n + \omega_m, \omega_n, \omega_m) E_j(\omega_n) E_k(\omega_m), \tag{2.18}$$

where the sum over n, m is taken such that each frequency can vary but their sum, $\omega_n + \omega_m$, is fixed. Note, we initially consider a nonlinear material with dispersion; therefore, the polarisation and nonlinear susceptibility take an explicit frequency dependence. If we consider a general three-wave mixing process with fields at frequencies, ω_1, ω_2 and $\omega_3 = \omega_1 + \omega_2$ then to describe the polarisation we require the following six tensors:

$$\begin{aligned} &\chi^{(2)}_{ijk}(\omega_3, \omega_1, \omega_2), \quad \chi^{(2)}_{ijk}(\omega_3, \omega_2, \omega_1), \quad \chi^{(2)}_{ijk}(\omega_2, \omega_3, -\omega_1), \\ &\chi^{(2)}_{ijk}(\omega_3, -\omega_1, \omega_2), \quad \chi^{(2)}_{ijk}(\omega_1, \omega_3, -\omega_2), \quad \chi^{(2)}_{ijk}(\omega_1, -\omega_2, \omega_3) \end{aligned} \tag{2.19}$$

and their conjugates in which all of the frequencies are exchanged with their negative. Each of these susceptibility tensors are of dimensions $3 \times 3 \times 3$ and are made up of 27 components. Fortunately, there are several symmetries associated with nonlinear crystals that reduce the number of non-zero terms and simplify the analysis of the interactions. Indeed, we can reduce the number of terms since any a measured field is real and, therefore, the positive and negative frequency components are related as:

$$\begin{aligned} E_i(\omega_\tau) &= E_i^*(-\omega_\tau), \\ E_j(\omega_\tau) &= E_j^*(-\omega_\tau), \\ E_k(\omega_\tau) &= E_k^*(-\omega_\tau). \end{aligned} \tag{2.20}$$

Consequently, the polarisation has the following properties:

$$\begin{aligned} P_i(\omega_3 = \omega_1 + \omega_2) &= P_i^*(-\omega_3 = -\omega_2 - \omega_1), \\ P_j(\omega_3 = \omega_1 + \omega_2) &= P_j^*(-\omega_3 = -\omega_2 - \omega_1), \\ P_k(\omega_3 = \omega_1 + \omega_2) &= P_k^*(-\omega_3 = -\omega_2 - \omega_1) \end{aligned} \tag{2.21}$$

and we only need to consider the six tensors in Eq. 2.19 or their complex conjugates to describe the nonlinear interaction. We can further simplify due to the commutative nature of the product $E_j(\omega_1)E_k(\omega_2)$. Indeed, if an atom is first excited by a field oscillating at ω_1 and then by a field at ω_2 the resulting dipole is no different from an oscillating dipole created by the excitation of a field at ω_2 preceding a field at ω_1. This is known as intrinsic permutation symmetry and is written in terms of the susceptibility tensors as

$$\chi^{(2)}_{ijk}(\omega_3, \omega_2, \omega_1) = \chi^{(2)}_{ikj}(\omega_3, \omega_1, \omega_2). \tag{2.22}$$

Intrinsic permutation symmetry can be extended such that any of the indices, (i, j, k), can be freely permuted given the corresponding frequency components are appropriately interchanged as

$$\chi^{(2)}_{ijk}(\omega_3, \omega_2, \omega_1) = \chi^{(2)}_{kij}(\omega_1, \omega_3, -\omega_2) = \chi^{(2)}_{jki}(\omega_2, -\omega_1, \omega_3). \tag{2.23}$$

This is known as full-permutation or Kleinmann symmetry [42] and reduces the number of coefficients required to describe an interaction to a 3×6 matrix with 18 terms. This symmetry can be understood as an assumption that the response of the nonlinear material is instantaneous and independent of the order of the frequency components; allowing the indices to be freely permuted. In practice, depending on the crystal symmetry group, many of these coefficients are zero: simplifying the analysis further [8, 41, 42]. Combining all permutation symmetries and assuming a lossless media the polarisation $\mathbf{P}(\omega_3)$ is

$$\begin{pmatrix} P_i(\omega_3) \\ P_j(\omega_3) \\ P_k(\omega_3) \end{pmatrix} = 2\varepsilon_0 \begin{pmatrix} \chi_{11} & \chi_{12} & \chi_{13} & \chi_{14} & \chi_{15} & \chi_{16} \\ \chi_{21} & \chi_{22} & \chi_{23} & \chi_{24} & \chi_{25} & \chi_{26} \\ \chi_{31} & \chi_{32} & \chi_{33} & \chi_{34} & \chi_{35} & \chi_{36} \end{pmatrix} \begin{pmatrix} E_i(\omega_1)E_i(\omega_2) \\ E_j(\omega_1)E_j(\omega_2) \\ E_k(\omega_1)E_k(\omega_2) \\ E_j(\omega_1)E_k(\omega_2) + E_k(\omega_1)E_j(\omega_2) \\ E_k(\omega_1)E_i(\omega_2) + E_i(\omega_1)E_k(\omega_2) \\ E_i(\omega_1)E_j(\omega_2) + E_j(\omega_1)E_i(\omega_2) \end{pmatrix}, \tag{2.24}$$

where we have introduced contracted suffix notation for the elements $\chi_{ijk} = \chi_{ip}$ according to table 2.1.

jk:	11	22	33	23,32	31,13	21,12
p:	1	2	3	4	5	6

Table 2.1: Contacted suffix notation for uniaxial media [41]

2.2.5 Manley-Rowe Relations

Systems that exhibit full permutation symmetry are lossless, and in an optical system with no loss, the total intensity or energy density will be conserved. In three-wave mixing the

total intensity is defined as the sum of intensities of the fields propagating in the system as

$$I = \sum_{\tau} \frac{1}{2} n_\tau \epsilon_0 c \iint_{-\infty}^{\infty} E_\tau^*(\mathbf{r}) E_\tau(\mathbf{r}) \, \mathrm{d}x \, \mathrm{d}y. \tag{2.25}$$

The variation of this intensity along the direction of propagation is

$$\frac{d}{dz} I = \sum_{\tau} \frac{1}{2} n_\tau \varepsilon_0 c \iint_{-\infty}^{\infty} \frac{d}{dz} \left(E_\tau^*(\mathbf{r}) E_\tau(\mathbf{r}) \right) \, \mathrm{d}x \, \mathrm{d}y$$

$$= \sum_{\tau} \frac{1}{2} n_\tau \varepsilon_0 c \iint_{-\infty}^{\infty} \left(E_\tau^*(\mathbf{r}) \frac{d}{dz} E_\tau(\mathbf{r}) + E_\tau(\mathbf{r}) \frac{d}{dz} E_\tau^*(\mathbf{r}) \right) \, \mathrm{d}x \, \mathrm{d}y. \tag{2.26}$$

With the equations of propagation defined in section 2.2.2, we find for the field $E_1(\mathbf{r})$ the following variation in intensity

$$\frac{d}{dz} I_1 = \frac{1}{2} n_1 \varepsilon_0 c \iint_{-\infty}^{\infty} \left(E_1^*(\mathbf{r}) \frac{d}{dz} E_1(\mathbf{r}) + E_1(\mathbf{r}) \frac{d}{dz} E_1^*(\mathbf{r}) \right) \, \mathrm{d}x \, \mathrm{d}y \tag{2.27}$$

$$= i \epsilon_0 \chi^{(2)} \omega_1 \iint_{-\infty}^{\infty} \left(E_1^*(\mathbf{r}) E_2^*(\mathbf{r}) E_3(\mathbf{r}) e^{-i\Delta k z} - E_1(\mathbf{r}) E_2(\mathbf{r}) E_3^*(\mathbf{r}) e^{i\Delta k z} \right) \, \mathrm{d}x \, \mathrm{d}y,$$

where

$$\iint_{-\infty}^{\infty} E_\tau^*(\mathbf{r}) \nabla_T^2 E_\tau(\mathbf{r}) \, \mathrm{d}x \, \mathrm{d}y = \iint_{-\infty}^{\infty} E_\tau(\mathbf{r}) \nabla_T^2 E_\tau^*(\mathbf{r}) \, \mathrm{d}x \, \mathrm{d}y. \tag{2.28}$$

Similarly, for the fields $E_2(\mathbf{r})$ and $E_3(\mathbf{r})$, we have

$$\frac{d}{dz} I_2 = \frac{1}{2} n_2 \varepsilon_0 c \iint_{-\infty}^{\infty} \left(E_2^*(\mathbf{r}) \frac{d}{dz} E_2(\mathbf{r}) + E_2(\mathbf{r}) \frac{d}{dz} E_2^*(\mathbf{r}) \right) \, \mathrm{d}x \, \mathrm{d}y \tag{2.29}$$

$$= i \epsilon_0 \chi^{(2)} \omega_2 \iint_{-\infty}^{\infty} \left(E_1^*(\mathbf{r}) E_2^*(\mathbf{r}) E_3(\mathbf{r}) e^{-i\Delta k z} - E_1(\mathbf{r}) E_2(\mathbf{r}) E_3^*(\mathbf{r}) e^{i\Delta k z} \right) \, \mathrm{d}x \, \mathrm{d}y,$$

and

$$\frac{d}{dz} I_3 = \frac{1}{2} n_3 \varepsilon_0 c \iint_{-\infty}^{\infty} \left(E_3^*(\mathbf{r}) \frac{d}{dz} E_3(\mathbf{r}) + E_3(\mathbf{r}) \frac{d}{dz} E_3^*(\mathbf{r}) \right) \, \mathrm{d}x \, \mathrm{d}y \tag{2.30}$$

$$= i \epsilon_0 \chi^{(2)} \omega_3 \iint_{-\infty}^{\infty} \left(E_1(\mathbf{r}) E_2(\mathbf{r}) E_3^*(\mathbf{r}) e^{i\Delta k z} - E_1^*(\mathbf{r}) E_2^*(\mathbf{r}) E_3(\mathbf{r}) e^{-i\Delta k z} \right) \, \mathrm{d}x \, \mathrm{d}y.$$

Using the above equations, we can show that the variation of the total intensity with respect to the direction of propagation is conserved as

$$\frac{d}{dz}I = i\varepsilon_0\chi^{(2)}\left(\omega_3-\omega_2-\omega_1\right)\iint_{-\infty}^{\infty}\Big(E_1(\mathbf{r})E_2(\mathbf{r})E_3^*(\mathbf{r})e^{-i\Delta kz}-\text{c.c.}\Big)\,\mathrm{d}x\,\mathrm{d}y=0, \tag{2.31}$$

when we have the relation $\omega_3=\omega_1+\omega_2$. Using Eq. 2.27, 2.29 and 2.30, the conservation of intensity can be restated in the following way

$$\frac{d}{dz}\left(\frac{I_1}{\omega_1}\right)=\frac{d}{dz}\left(\frac{I_2}{\omega_2}\right)=-\frac{d}{dz}\left(\frac{I_3}{\omega_3}\right), \tag{2.32}$$

which are known as the Manley-Rowe relations [8, 41]. These relations show that the creation rate of photons with energy $\hbar\omega_1$ and $\hbar\omega_2$ is equal to the rate of the annihilation of photons at energy $\hbar\omega_3$ in a lossless medium. Thus, although the derivation presented here is purely classical, it offers insight into the quantum interpretation of nonlinear interactions [9].

2.3 Small Perturbation Fields

Owing to the nonlinear polarisation waves in three-wave mixing the method of optical eigenmodes introduced in section 1.4 is no longer valid. In this section, we introduce small perturbation fields to the nonlinear equations to restore the principle of superposition and reintroduce the concept of eigenmode decomposition to intensity-dependent optical systems. We begin with the full nonlinear equations for three-wave mixing:

$$-i\frac{\partial}{\partial z}E_1(\mathbf{r})=\frac{1}{2k_1}\,\nabla_T^2E_1(\mathbf{r})+\chi_1E_2^*(\mathbf{r})E_3(\mathbf{r})e^{-i\Delta kz}, \tag{2.33}$$

$$-i\frac{\partial}{\partial z}E_2(\mathbf{r})=\frac{1}{2k_2}\,\nabla_T^2E_2(\mathbf{r})+\chi_2E_1^*(\mathbf{r})E_3(\mathbf{r})e^{-i\Delta kz}, \tag{2.34}$$

$$-i\frac{\partial}{\partial z}E_3(\mathbf{r})=\frac{1}{2k_3}\,\nabla_T^2E_3(\mathbf{r})+\chi_3E_1(\mathbf{r})E_2(\mathbf{r})e^{i\Delta kz}, \tag{2.35}$$

where $\chi_\tau=\frac{\chi^{(2)}\omega_\tau}{2n_\tau c}$ and $\Delta k=k_1+k_2-k_3$ is the phase mismatch, as discussed in section 2.2.3. In a linear system if we have two fields which we label $E_{\tau,p}(\mathbf{r})$ and $E_{\tau,b}(\mathbf{r})$ that both satisfy the equations of propagation and have the same wavevectors and frequency then their superposition, $E_{\tau,p}(\mathbf{r})+E_{\tau,b}(\mathbf{r})$, is also a solution. If we input the superposition into the nonlinear equations we find:

$$\begin{aligned}-i\frac{\partial}{\partial z}\left(E_{1,b}(\mathbf{r})+E_{1,p}(\mathbf{r})\right)&=\frac{1}{2k_1}\,\nabla_T^2\left(E_{1,b}(\mathbf{r})+E_{1,p}(\mathbf{r})\right)\\&+\chi_1\big(E_{2,b}^*(\mathbf{r})E_{3,b}(\mathbf{r})+E_{2,b}^*(\mathbf{r})E_{3,p}(\mathbf{r})+E_{2,p}^*(\mathbf{r})E_{3,b}(\mathbf{r})+E_{2,p}^*(\mathbf{r})E_{3,p}(\mathbf{r})\big)e^{-i\Delta kz},\end{aligned} \tag{2.36}$$

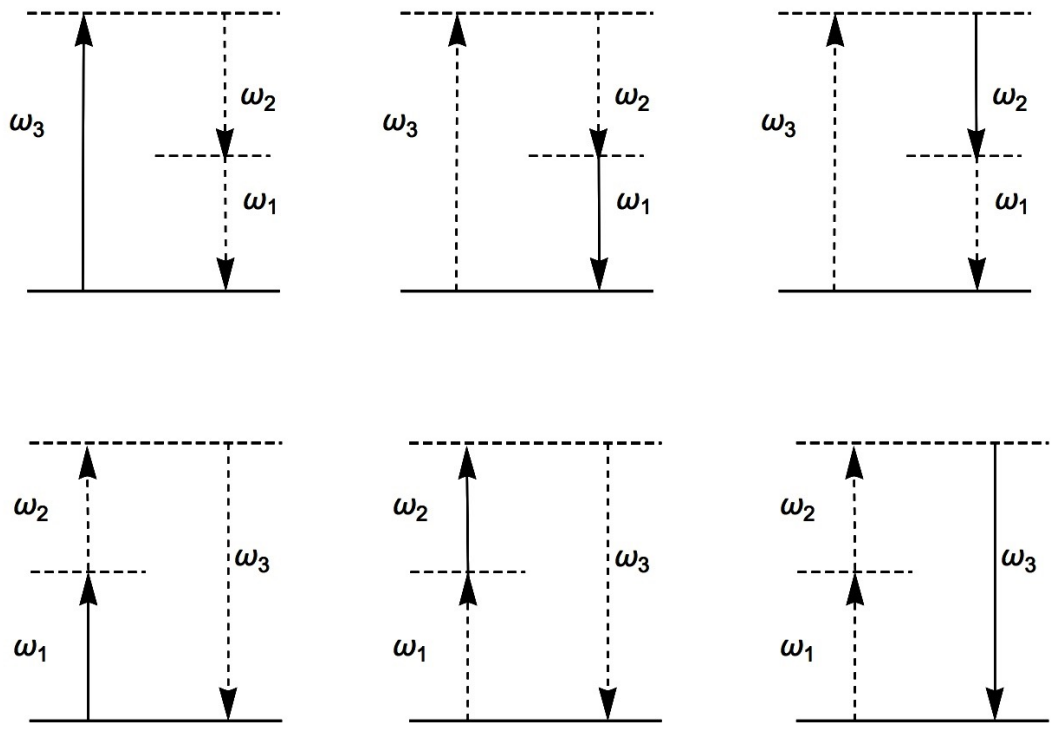

Figure 2.3: Energy-level diagram where vertical dashed lines correspond to small perturbation fields, $E_{\tau,p}(\mathbf{r})$, and the solid lines denote the background fields, $E_{\tau,b}(\mathbf{r})$. As we are off-resonance, the horizontal lines correspond to unobservable, short-lived, virtual states.

$$-i\frac{\partial}{\partial z}\left(E_{2,b}(\mathbf{r})+E_{2,p}(\mathbf{r})\right)=\frac{1}{2k_2}\,\nabla_T^2\left(E_{2,b}(\mathbf{r})+E_{2,p}(\mathbf{r})\right) \tag{2.37}$$
$$+\chi_3\big(E_{1,b}^*(\mathbf{r})E_{3,b}(\mathbf{r})+E_{1,b}^*(\mathbf{r})E_{3,p}(\mathbf{r})+E_{1,p}^*(\mathbf{r})E_{3,b}(\mathbf{r})+E_{1,p}^*(\mathbf{r})E_{3,p}(\mathbf{r})\big)e^{-i\Delta kz},$$

$$-i\frac{\partial}{\partial z}\left(E_{3,b}(\mathbf{r})+E_{3,p}(\mathbf{r})\right)=\frac{1}{2k_3}\,\nabla_T^2\left(E_{3,b}(\mathbf{r})+E_{3,p}(\mathbf{r})\right) \tag{2.38}$$
$$+\chi_3\big(E_{1,b}(\mathbf{r})E_{2,b}(\mathbf{r})+E_{1,b}(\mathbf{r})E_{2,p}(\mathbf{r})+E_{1,p}(\mathbf{r})E_{2,b}(\mathbf{r})+E_{1,p}(\mathbf{r})E_{2,p}(\mathbf{r})\big)e^{i\Delta kz}.$$

As expected, the superposition is not a solution of the nonlinear equations due to the mixing terms between the two fields. With this mixing, it is not clear how to separate the above equations for each of the fields in the superposition. In order to progress beyond this issue, we change the physical meaning of the solutions in the superposition. Indeed, we assume that the fields $E_{\tau,b}(\mathbf{r})$ are high-intensity background fields and that the fields $E_{\tau,p}(\mathbf{r})$ correspond to low-intensity "perturbation" fields. Furthermore, we assume that these perturbation fields are sufficiently small with respect to the background fields such

that $|E_{\tau,p}(\mathbf{r})| \ll |E_{\tau,b}(\mathbf{r})|$ and, consequently, the terms that are quadratic in $E_{\tau,p}(\mathbf{r})$ are neglected. In this approximation Eq. 2.36, for example, is

$$\begin{aligned} -i\frac{\partial}{\partial z}\left(E_{1,b}(\mathbf{r})+E_{1,p}(\mathbf{r})\right) &= \frac{1}{2k_1}\,\nabla_T^2\left(E_{1,b}(\mathbf{r})+E_{1,p}(\mathbf{r})\right) \\ &+\chi_1\left(E_{2,b}^*(\mathbf{r})E_{3,b}(\mathbf{r})+E_{2,p}^*(\mathbf{r})E_{3,b}(\mathbf{r})+E_{2,b}^*(\mathbf{r})E_{3,p}(\mathbf{r})\right)e^{-i\Delta kz}, \end{aligned} \tag{2.39}$$

which, for a thin slice of material, is written in terms of finite differences as

$$\begin{aligned} &E_{1,b}(x,y,\Delta z)+E_{1,p}(x,y,\Delta z) \\ &=E_{1,b}(x,y,0)+E_{1,p}(x,y,0)+\frac{i\Delta z}{2k_1}\nabla_T^2\big(E_{1,b}(x,y,0)+E_{1,p}(x,y,0)\big) \\ &+i\chi_1\left(E_{2,b}^*(x,y,0)E_{3,b}(x,y,0)+E_{2,p}^*(x,y,0)E_{3,b}(x,y,0)+E_{2,b}^*(x,y,0)E_{3,p}(x,y,0)\right)\Delta z, \end{aligned} \tag{2.40}$$

where Δz is the thickness of the slice of the nonlinear material. As we assume that the background field is large in field strength compared to the perturbation fields, we have

$$\iint |E_{1,b}(x,y,0)|\,\mathrm{d}x\mathrm{d}y \gg \iint |E_{1,p}(x,y,0)|\,\mathrm{d}x\mathrm{d}y,$$

and

$$\iint |E_{1,b}(x,y,\Delta z)|\,\mathrm{d}x\mathrm{d}y \gg \iint |E_{1,p}(x,y,\Delta z)|\,\mathrm{d}x\mathrm{d}y,$$

from which the conditions:

$$\iint |\chi_1 E_{2,b}^*(x,y,0)E_{3,b}(x,y,0)\Delta z|\,\mathrm{d}x\mathrm{d}y \gg \iint |\chi_1 E_{2,p}^*(x,y,0)E_{3,b}(x,y,0)\Delta z|\,\mathrm{d}x\mathrm{d}y,$$

$$\iint |\chi_1 E_{2,b}^*(x,y,0)E_{3,b}(x,y,0)\Delta z|\,\mathrm{d}x\mathrm{d}y \gg \iint |\chi_1 E_{2,b}^*(x,y,0)E_{3,p}(x,y,0)\Delta z|\,\mathrm{d}x\mathrm{d}y,$$

follow. A consequence of the above inequalities is that any interaction between the high-intensity background fields and the perturbation fields will disturb the small perturbations significantly but will influence the background fields a negligible amount. Hence, any interaction between the background and perturbation fields creates photons only in the fields $E_{\tau,p}(\mathbf{r})$. If the above conditions are satisfied for each slice of a bulk nonlinear crystal, then we can factor Eqs. 2.36 to 2.38 into the following set of equations:

$$-i\frac{\partial}{\partial z}E_{1,b}(\mathbf{r}) = \frac{1}{2k_1}\nabla_T^2 E_{1,b}(\mathbf{r}) + \chi_1 E_{2,b}^*(\mathbf{r})E_{3,b}(\mathbf{r})e^{-i\Delta kz}, \tag{2.41}$$

$$-i\frac{\partial}{\partial z}E_{2,b}(\mathbf{r}) = \frac{1}{2k_2}\nabla_T^2 E_{2,b}(\mathbf{r}) + \chi_2 E_{1,b}^*(\mathbf{r})E_{3,b}(\mathbf{r})e^{-i\Delta kz}, \tag{2.42}$$

$$-i\frac{\partial}{\partial z}E_{3,b}(\mathbf{r}) = \frac{1}{2k_3}\nabla_T^2 E_{3,b}(\mathbf{r}) + \chi_3 E_{1,b}(\mathbf{r})E_{2,b}(\mathbf{r})e^{i\Delta kz}, \tag{2.43}$$

$$-i\frac{\partial}{\partial z}E_{1,p}(\mathbf{r}) = \frac{1}{2k_1}\nabla_T^2 E_{1,p}(\mathbf{r}) + \chi_1\left(E_{2,b}^*(\mathbf{r})E_{3,p}(\mathbf{r})+E_{2,p}^*(\mathbf{r})E_{3,b}(\mathbf{r})\right)e^{-i\Delta kz}, \tag{2.44}$$

$$-i\frac{\partial}{\partial z}E_{2,p}(\mathbf{r}) = \frac{1}{2k_2}\nabla_T^2 E_{2,p}(\mathbf{r}) + \chi_2\left(E_{1,b}^*(\mathbf{r})E_{3,p}(\mathbf{r})+E_{1,p}^*(\mathbf{r})E_{3,b}(\mathbf{r})\right)e^{-i\Delta kz}, \tag{2.45}$$

$$-i\frac{\partial}{\partial z}E_{3,p}(\mathbf{r}) = \frac{1}{2k_3}\nabla_T^2 E_{3,p}(\mathbf{r}) + \chi_3\left(E_{1,b}(\mathbf{r})E_{2,p}(\mathbf{r})+E_{1,p}(\mathbf{r})E_{2,b}(\mathbf{r})\right)e^{i\Delta kz}. \tag{2.46}$$

The first three of these equations are identical to the three-wave mixing equations described in section 2.2.2. The latter three equations, however, describe the evolution of the low-intensity perturbation fields that, although linear, depend on background fields whose evolution is nonlinear. Vitally, due to the linearity of these equations, we can reintroduce the method of optical eigenmodes to the perturbation fields. The energy-level diagrams of all of the interactions associated with these fields are illustrated in figure 2.3.

2.3.1 Energy Conservation of Perturbation Fields

In section 2.2.5, we outlined the Manley-Rowe relations that expressed the conservation of intensity for three-wave mixing processes. In a similar manner, it is instructive to check the conservation of intensity of the system with the low-intensity perturbation fields. In this case, the total system intensity is defined as

$$I = \sum_{\tau} \frac{1}{2} n_\tau \varepsilon_0 c \iint_{-\infty}^{\infty} (E^*_{\tau,b}(\mathbf{r})E_{\tau,b}(\mathbf{r}) + E^*_{\tau,b}(\mathbf{r})E_{\tau,p}(\mathbf{r}) + E^*_{\tau,p}(\mathbf{r})E_{\tau,b}(\mathbf{r}) + E^*_{\tau,p}(\mathbf{r})E_{\tau,p}(\mathbf{r}))\,\mathrm{d}x\,\mathrm{d}y. \tag{2.47}$$

As mentioned in section 2.3, we assume the perturbations are sufficiently small such that $|E_{\tau,p}(\mathbf{r})| \ll |E_{\tau,b}(\mathbf{r})|$ and the terms that are quadratic in $E_{\tau,p}(\mathbf{r})$ are negligible. The first term in the total intensity, Eq. 2.47, involves only the background fields and corresponds to three-wave mixing with conserved intensity as described in section 2.2.5. The variation of the total intensity can hence be written as

$$\begin{aligned}\frac{d}{dz} I = \sum_{\tau} \frac{1}{2} n_\tau \varepsilon_0 c \iint_{-\infty}^{\infty} \big(&E^*_{\tau,b}(\mathbf{r})\frac{d}{dz}E_{\tau,p}(\mathbf{r}) + E_{\tau,p}(\mathbf{r})\frac{d}{dz}E^*_{\tau,b}(\mathbf{r}) \\ &+ E^*_{\tau,p}(\mathbf{r})\frac{d}{dz}E_{\tau,b}(\mathbf{r}) + E_{\tau,b}(\mathbf{r})\frac{d}{dz}E^*_{\tau,p}(\mathbf{r})\big)\,\mathrm{d}x\,\mathrm{d}y.\end{aligned} \tag{2.48}$$

Using Eqs. 2.41 to 2.46 and their conjugates we find:

$$\begin{aligned}\frac{d}{dz} I_1 = \frac{1}{2} i\varepsilon_0 \chi^{(2)} \omega_1 \iint_{-\infty}^{\infty} &(E^*_{1,b}(\mathbf{r})E^*_{2,b}(\mathbf{r})E_{3,p}(\mathbf{r})e^{-i\Delta kz} + E^*_{1,b}(\mathbf{r})E^*_{2,p}(\mathbf{r})E_{3,b}(\mathbf{r})e^{-i\Delta kz} \\ &+ E^*_{1,p}(\mathbf{r})E^*_{2,b}(\mathbf{r})E_{3,b}(\mathbf{r})e^{-i\Delta kz} - \text{c.c.})\,\mathrm{d}x\,\mathrm{d}y,\end{aligned} \tag{2.49}$$

$$\begin{aligned}\frac{d}{dz} I_2 = \frac{1}{2} i\varepsilon_0 \chi^{(2)} \omega_2 \iint_{-\infty}^{\infty} &(E^*_{1,b}(\mathbf{r})E^*_{2,b}(\mathbf{r})E_{3,p}(\mathbf{r})e^{-i\Delta kz} + E^*_{1,b}(\mathbf{r})E^*_{2,p}(\mathbf{r})E_{3,b}(\mathbf{r})e^{-i\Delta kz} \\ &+ E^*_{1,p}(\mathbf{r})E^*_{2,b}(\mathbf{r})E_{3,b}(\mathbf{r})e^{-i\Delta kz} - \text{c.c.})\,\mathrm{d}x\,\mathrm{d}y,\end{aligned} \tag{2.50}$$

$$\frac{d}{dz}I_3 = \frac{1}{2}i\varepsilon_0\chi^{(2)}\omega_3 \iint_{-\infty}^{\infty} (E_{1,b}(\mathbf{r})E_{2,b}(\mathbf{r})E^*_{3,p}(\mathbf{r})e^{i\Delta kz} + E_{1,b}(\mathbf{r})E_{2,p}(\mathbf{r})E^*_{3,b}(\mathbf{r})e^{i\Delta kz} \\ + E_{1,p}(\mathbf{r})E_{2,b}(\mathbf{r})E^*_{3,b}(\mathbf{r})e^{i\Delta kz} - \text{c.c.})\,\mathrm{d}x\,\mathrm{d}y. \tag{2.51}$$

As the Laplacian operator is Hermitian upon integration over infinite bounds, as in Eq. 2.28, these terms cancel out in the above expressions. With these relations, we can show that the total intensity is conserved as

$$\frac{d}{dz}I = \frac{1}{2}i\varepsilon_0\chi^{(2)}(\omega_3 - \omega_2 - \omega_1) \iint_{-\infty}^{\infty} (E^*_{1,b}(\mathbf{r})E^*_{2,b}(\mathbf{r})E_{3,p}(\mathbf{r})e^{-i\Delta kz} \\ + E^*_{1,p}(\mathbf{r})E^*_{2,b}(\mathbf{r})E_{3,b}(\mathbf{r})e^{-i\Delta kz} + E^*_{1,b}(\mathbf{r})E^*_{2,p}(\mathbf{r})E_{3,b}(\mathbf{r})e^{-i\Delta kz} - \text{c.c.})\,\mathrm{d}x\,\mathrm{d}y = 0, \tag{2.52}$$

where we have assumed full permutation symmetry, see section 2.2.4, such that $\chi^{(2)}$ is the same for all three equations and that $\omega_3 = \omega_1 + \omega_2$. From a physical perspective, this is a reasonable result as we are in a lossless system, and thus there is no mechanism for the system to lose or gain energy.

2.3.2 Sum-Frequency Generation

In section 2.3, we described the evolution of fields that are dependent on some nonlinear interacting background fields. As illustrated in figure 2.3, these equations give rise to a number of interactions between low-intensity perturbation fields and the background. If we assume now that our input is a high-intensity field of frequency ω_1 with a weaker input at ω_2, then these fields will interact to generate a polarisation wave at ω_3. Indeed, if we have $E_{2,b}(\mathbf{r}) = E_{3,b}(\mathbf{r}) = 0$ then Eqs. 2.41 to 2.46 simplify to the following set of equations:

$$-i\frac{\partial}{\partial z}E_{1,b}(\mathbf{r}) = \frac{1}{2k_1}\nabla_T^2 E_{1,b}(\mathbf{r}), \tag{2.53}$$

$$-i\frac{\partial}{\partial z}E_{2,p}(\mathbf{r}) = \frac{1}{2k_2}\nabla_T^2 E_{2,p}(\mathbf{r}) + \chi_2 E^*_{1,b}(\mathbf{r})E_{3,p}(\mathbf{r}), \tag{2.54}$$

$$-i\frac{\partial}{\partial z}E_{3,p}(\mathbf{r}) = \frac{1}{2k_3}\nabla_T^2 E_{3,p}(\mathbf{r}) + \chi_3 E_{1,b}(\mathbf{r})E_{2,p}(\mathbf{r}), \tag{2.55}$$

which describe the interaction of two fields mediated by a high-intensity background field which we denote $E_{1,b}(\mathbf{r})$ and, for simplicity, we have assumed perfect phase matching in which $\Delta k = k_1 + k_2 - k_3 = 0$. If we had at the input no signal on the field $E_{3,p}(\mathbf{r})$ the interaction between $E_{1,b}(\mathbf{r})$ and $E_{2,p}(\mathbf{r})$ would generate a signal at the sum-frequency, ω_3. Hence, throughout the rest of the thesis, we refer to this set of equations as those describing sum-frequency generation.

In their current form the equations for sum-frequency generation, Eqs. 2.53 to 2.55, are difficult to solve analytically. However, if we are only interested in the variation of intensity associated with each field and not the transverse field profiles, then one can describe the evolution of the fields in 1D as:

$$\frac{d}{dz}E_{2,p}(z) = i\chi_2 E^*_{1,b}E_{3,p}(z), \tag{2.56}$$

$$\frac{d}{dz}E_{3,p}(z) = i\chi_3 E_{1,b}E_{2,p}(z), \tag{2.57}$$

where the background field is constant with respect to the propagation direction. If we take the second derivative of Eqs. 2.56 and 2.57 we find:

$$\frac{d^2}{dz^2}E_{2,p}(z) = i\chi_2 E^*_{1,b}\frac{d}{dz}E_{3,p}(z) = -\kappa^2 E_{2,p}(z), \tag{2.58}$$

$$\frac{d^2}{dz^2}E_{3,p}(z) = i\chi_3 E_{1,b}\frac{d}{dz}E_{2,p}(z) = -\kappa^2 E_{3,p}(z), \tag{2.59}$$

where $\kappa^2 = \chi_2\chi_3|E_{1,b}|^2$. The general solution for $E_{2,p}(z)$ is

$$E_{2,p}(z) = C_1\sin(\kappa z) + C_2\cos(\kappa z). \tag{2.60}$$

Inputting this solution into Eq. 2.56 we find

$$E_{3,p}(z) = -\frac{i}{\chi_2 E^*_{1,b}}\frac{d}{dz}E_{2,p}(z) = -\frac{i\kappa}{\chi_2 E^*_{1,b}}\left[C_1\cos(\kappa z) - C_2\sin(\kappa z)\right]. \tag{2.61}$$

If we assume that we have no signal at ω_3 at the input then $C_1 = 0$ and $C_2 = E_{2,p}(0)$ giving the following:

$$E_{2,p}(z) = E_{2,p}(0)\cos(\kappa z), \tag{2.62}$$

$$E_{3,p}(z) = \frac{i\kappa}{\chi_2 E^*_{1,b}}E_{2,p}(0)\sin(\kappa z) = \frac{i\sqrt{\chi_3}|E_{1,b}|}{\sqrt{\chi_2}E^*_{1,b}}E_{2,p}(0)\sin(\kappa z). \tag{2.63}$$

In general, $E_{1,b}$ is complex and in polar form is written $E^*_{1,b} = |E_{1,b}|e^{-i\phi_1}$ such that $|E_{1,b}|/E^*_{1,b} = e^{i\phi_1}$ and

$$E_{3,p}(z) = \frac{i\sqrt{\chi_3}}{\sqrt{\chi_2}}E_{2,p}(0)\sin(\kappa z)e^{i\phi_1}. \tag{2.64}$$

Figure 2.4 gives an example of how these solutions evolve through a nonlinear material. It is clear from the figure that the total intensity with respect to the small perturbation fields $E_{3,p}(z)$ and $E_{2,p}(z)$ is not conserved. Indeed, if at some moment we have more energy in the field $E_{3,p}(z)$ than in $E_{2,p}(z)$ then the intensity is more than if we had $E_{2,p}(z)$ with more energy than $E_{3,p}(z)$ as $\hbar\omega_3 > \hbar\omega_2$. We can check this analytically as

$$\begin{aligned} I &= E^*_{2,p}(z)E_{2,p}(z) + E^*_{3,p}(z)E_{3,p}(z) \\ &= |E_{2,p}(0)|^2\cos(\kappa z)^2 + \frac{\chi_3}{\chi_2}|E_{2,p}(0)|^2\sin(\kappa z)^2 \\ &= |E_{2,p}(0)|^2\left(\cos(\kappa z)^2 + \frac{\omega_3 n_2}{\omega_2 n_3}\sin(\kappa z)^2\right). \end{aligned} \tag{2.65}$$

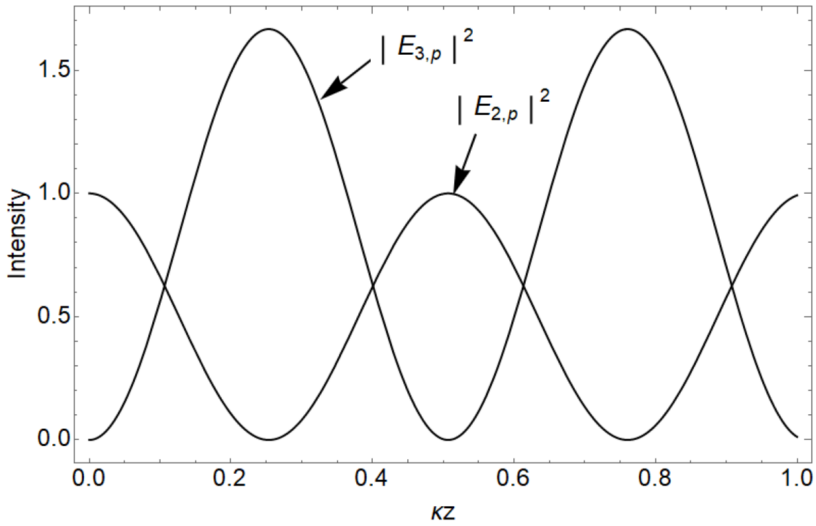

Figure 2.4: Variation of the intensity of fields $E_{3,p}(z)$ and $E_{2,p}(z)$ for sum-frequency generation in arb. units.

Evidently, the only condition in which the above intensity is conserved is if the two frequencies are degenerate, i.e. $\omega_2 = \omega_3$. In the context of sum-frequency generation, this is only possible in the trivial case where the non-depleted background field is a D.C. field with $\omega_1 = 0$.

2.3.3 Parametric Down-Conversion

If we assume now that the background field $E_{3,b}(\mathbf{r})$ is non-depleting with $E_{1,b}(\mathbf{r}) = E_{2,b}(\mathbf{r}) = 0$ and $\Delta k = 0$ then our set of propagation equations are:

$$-i\frac{\partial}{\partial z}E_{3,b}(\mathbf{r}) = \frac{1}{2k_3}\nabla_T^2 E_{3,b}(\mathbf{r}), \tag{2.66}$$

$$-i\frac{\partial}{\partial z}E_{1,p}(\mathbf{r}) = \frac{1}{2k_1}\nabla_T^2 E_{1,p}(\mathbf{r}) + \chi_1 E_{2,p}^*(\mathbf{r})E_{3,b}(\mathbf{r}), \tag{2.67}$$

$$-i\frac{\partial}{\partial z}E_{2,p}(\mathbf{r}) = \frac{1}{2k_2}\nabla_T^2 E_{2,p}(\mathbf{r}) + \chi_2 E_{1,p}^*(\mathbf{r})E_{3,b}(\mathbf{r}). \tag{2.68}$$

As with the previous section, one can develop insight into these equations by considering the intensity variation of the two fields $E_{1,p}(z)$ and $E_{2,p}(z)$. Again, we consider the 1D evolution of the complex amplitudes with a constant background giving the equations:

$$-i\frac{d}{dz}E_{1,p}(z) = \chi_1 E_{2,p}^*(z)E_{3,b}, \tag{2.69}$$

$$-i\frac{d}{dz}E_{2,p}(z) = \chi_2 E_{1,p}^*(z)E_{3,b}, \tag{2.70}$$

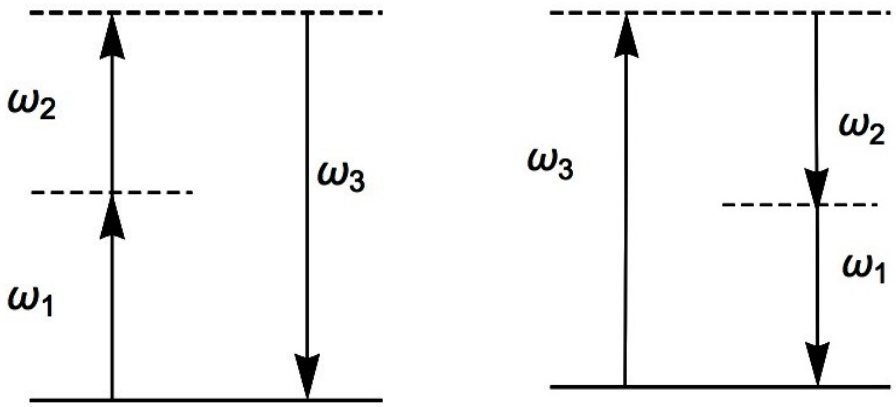

(a) (b)

Figure 2.5: Energy-level diagrams for (a) sum-frequency generation and (b) parametric down-conversion. As we are off-resonance, the horizontal lines correspond to unobservable, short-lived, virtual states.

which we refer to collectively as describing the effect of parametric down-conversion. Again, we take the second derivative of the equations and find:

$$\frac{d^2}{dz^2}E_{1,p}(z) = i\chi_1 E_{3,b}\frac{d}{dz}E^*_{2,p}(z) = \kappa^2 E_{1,p}(z), \tag{2.71}$$

$$\frac{d^2}{dz^2}E_{2,p}(z) = i\chi_2 E_{3,b}\frac{d}{dz}E^*_{1,p}(z) = \kappa^2 E_{2,p}(z), \tag{2.72}$$

with $\kappa^2 = \chi_1\chi_2|E_{3,b}|^2$. The general solution of the first of these equations is

$$E_{1,p}(z) = C_1\sinh(\kappa z) + C_2\cosh(\kappa z). \tag{2.73}$$

If we assume we have $E_{2,p}(0) = 0$ and $E_{1,p}(0)$ is arbitrary then we have for $E_{1,p}(z)$ a solution of the form

$$E_{1,p}(z) = E_{1,p}(0)\cosh(\kappa z). \tag{2.74}$$

Moreover, from Eq. 2.69, we can write $E_{2,p}(z)$ with respect to $E_{1,p}(z)$ as

$$E_{2,p}(z) = \frac{i\kappa}{\chi_1 E^*_{3,b}}E_{1,p}(0)\sinh(\kappa z) = i\frac{\sqrt{\chi_2}|E_{3,b}|}{\sqrt{\chi_1}E^*_{3,b}}E_{1,p}(0)\sinh(\kappa z). \tag{2.75}$$

The background field is, in general complex, and in polar form, is written $E^*_{3,b} = |E_{3,b}|e^{-i\phi_3}$ such that $|E_{3,b}|/E^*_{3,b} = e^{i\phi_3}$. Hence the solutions are now written as:

$$E_{1,p}(z) = E_{1,p}(0)\cosh(\kappa z), \qquad E_{2,p}(z) = i\frac{\sqrt{\chi_2}}{\sqrt{\chi_1}}E_{1,p}(0)\sinh(\kappa z)e^{i\phi_3}. \tag{2.76}$$

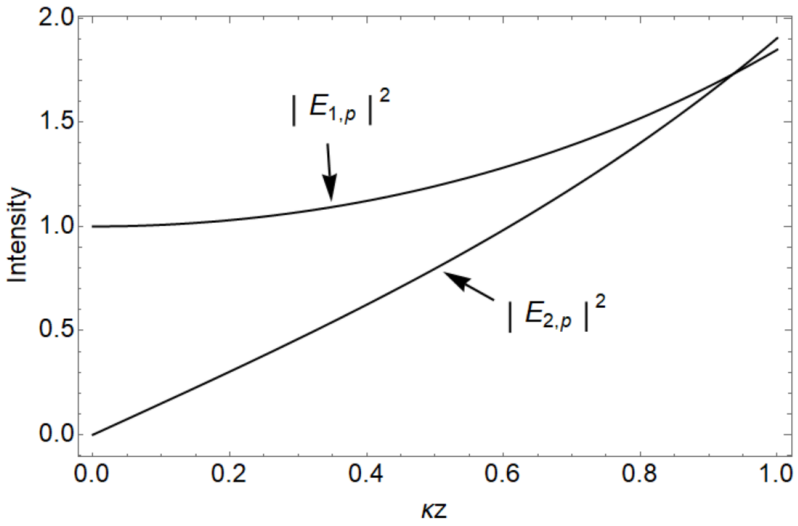

Figure 2.6: Variation of the intensity of the fields $E_{2,p}(z)$ and $E_{1,p}(z)$ in arb. units.

Figure 2.6 shows the behaviour of these solutions, which are not oscillatory like the solutions for sum-frequency generation shown in figure 2.4. Indeed, in parametric down-conversion, there is an exponential growth of the perturbation fields when $\kappa z \gg 1$. From a physical point of view, we can understand the distinction between the two effects with respect to the energy level diagrams in figure 2.5. In the case of sum-frequency generation, the polarisation wave oscillating at ω_3 is generated by an interaction with the field at ω_2 and the background field at ω_1. In the case of parametric down-conversion, however, the field at ω_3 decays into radiation that contributes to both of the low-intensity perturbation fields. This leads to exponential growth, as illustrated in figure 2.6. In this case, it is clear that the intensity is not conserved which can be seen mathematically as

$$\begin{aligned} I &= E^*_{1,p}(z)E_{1,p}(z) + E^*_{2,p}(z)E_{2,p}(z) \\ &= |E_{1,p}(0)|^2 \cosh(\kappa z)^2 + \frac{\chi_2}{\chi_1}|E_{1,p}(0)|^2 \sinh(\kappa z)^2 \\ &= |E_{1,p}(0)|^2 \left(\cosh(\kappa z)^2 + \frac{\omega_2 n_1}{\omega_1 n_2}\sinh(\kappa z)^2\right). \end{aligned} \tag{2.77}$$

The two sets of equations describing sum-frequency generation and parametric down-conversion correspond to the simplest cases of the evolution of the perturbation fields described by Eqs. 2.41 to 2.46. In these simplified cases, the number of interaction terms is minimised such that the symmetries associated with the interactions can be easily understood. Furthermore, by considering sum-frequency generation and parametric down-conversion, we are describing effects that are commonly used and well understood in the field of nonlinear optics [8, 9, 10].

2.4 Conclusions

In this chapter, we have introduced the background associated with nonlinear optics that is relevant to the work herein. We first outlined how high-intensity light can lead to optical nonlinearities in the context of oscillating dipoles. With these optical nonlinearities, we can derive a set of coupled partial differential equations that describe how fields with certain phase-matching conditions will evolve. In particular, we considered second-order nonlinear systems from which effects like sum-frequency generation and parametric down-conversion arise: known collectively as three-wave mixing. Due to the nonlinearity of the equations describing three-wave mixing, the eigenmode decomposition conventionally used in linear optics is no longer valid. However, as described in section 2.3, we can introduce low-intensity perturbation fields which, given the intensity is small enough, evolve according to a set of coupled partial differential equations that are linear. Therefore, we can reintroduce the principle of superposition with respect to these low-intensity fields and again utilise an eigendecomposition to describe the system. Unlike the linear systems discussed in the first chapter, however, the perturbation fields interact with each other resulting in a non-trivial relationship between fields at the input and output. Indeed, the equations we introduce for these fields, although linear, are characteristic of a nonlinear background interaction. In the simplest cases, where the initial conditions result in a single high-intensity background field, we recover the two well-known second-order nonlinear effects known as parametric down-conversion and sum-frequency generation.

Chapter 3

Eigenmodes of Interacting Fields in Three-Wave Mixing

3.1 Introduction

In the previous chapter, we saw how the introduction of low-intensity perturbation fields into nonlinear systems allows one to reestablish the principle of linear superposition and, consequently, the concept of eigenmodes. In particular, we highlighted two simplified cases of the mixing of two low-intensity fields corresponding to sum-frequency generation and parametric down-conversion. In this chapter, we introduce the method of eigenmode decomposition to both of these effects. Unlike the eigenmodes of linear optics, these novel modes correspond to a set of orthogonal beams distributed across multiple wavelengths. With these eigenmodes defined, we highlight the influence of the high-intensity background field on the form of the modes by considering various examples in systems with circular and rectangular symmetry. In these examples, we are primarily concerned with the optical eigenmodes with respect to the total intensity of the fields incident on some region of detection and the propagation eigenmodes of the systems. Finally, in the last section of the chapter, we discuss the symmetry and degeneracy associated with the optical eigenmodes for systems with circular and rectangular geometry.

As discussed in section 1.4.3, the use of an eigenmode decomposition has been utilised in various nonlinear systems. In all of these cases, however, the main concern of the research was with the propagation eigenmodes. As outlined in section 1.4, the optical eigenmodes allow one to define a set of mutually orthogonal fields with respect to any Hermitian optical measure. Consequently, by introducing the method of optical eigenmodes to the perturbation fields, defined in section 2.3, we are expanding the domain of light-matter interactions in which we have fields of different wavelengths interacting with one another - a behaviour not observed in conventional linear systems. Furthermore, due to the low intensity of the

perturbation fields, the systems we discuss in this chapter are well suited to going towards the single or multiphoton level.

3.2 Sum-Frequency Generation

In the previous chapter, in section 2.3, we introduced a set of equations describing the propagation of small perturbation fields in the presence of a non-depleting pump field. In the simplest case of a single background field, we observed two distinct nonlinear effects. In this section, we are concerned with sum-frequency generation [90]. Indeed, in section 3.2.1, we introduce the method of optical eigenmodes to this effect before highlighting the characteristic properties of these eigenmodes with numerical examples in sections 3.3.2 and 3.4.3. Later in the chapter, in section 3.4.4, we discuss the propagation eigenmodes of sum-frequency generation, which we subsequently utilise in the final chapter when considering the quantum behaviour of three-wave mixing systems.

3.2.1 Optical Eigenmodes in Sum-Frequency Generation

The equations for sum-frequency generation are, as shown in section 2.3, of the form:

$$-i\frac{\partial}{\partial z}E_b(\mathbf{r}) = \frac{1}{2k_1}\nabla_T^2 E_b(\mathbf{r}), \tag{3.1}$$

$$-i\frac{\partial}{\partial z}E_2(\mathbf{r}) = \frac{1}{2k_2}\nabla_T^2 E_2(\mathbf{r}) + \chi_2 E_b^*(\mathbf{r})E_3(\mathbf{r})e^{-i\Delta kz}, \tag{3.2}$$

$$-i\frac{\partial}{\partial z}E_3(\mathbf{r}) = \frac{1}{2k_3}\nabla_T^2 E_3(\mathbf{r}) + \chi_3 E_b(\mathbf{r})E_2(\mathbf{r})e^{i\Delta kz}, \tag{3.3}$$

where $E_{1,b}(\mathbf{r}) = E_b(\mathbf{r})$ is our high-intensity pump field and, for notational simplicity, we have dropped the p subscript for the perturbation fields. As discussed in section 2.3, we have the frequency relation $\omega_3 = \omega_1 + \omega_2$ with $\omega_2 > \omega_1 > 0$. We decompose the perturbation fields at the input plane as

$$E_\tau(\mathbf{r}_1) = \sum_{j=1}^{N} a_{\tau,j}E_{\tau,j}(\mathbf{r}_1), \tag{3.4}$$

where the basis elements, $E_{\tau,j}(\mathbf{r}_1)$, form an orthogonal basis at the input of the nonlinear material satisfying the following condition

$$\iiint E_{\tau,j}^*(\mathbf{r}_1)E_{\sigma,k}(\mathbf{r}_1)e^{-i(\omega_\sigma-\omega_\tau)t}\,\mathrm{d}x_1\mathrm{d}y_1\mathrm{d}t = 2\pi\delta(\omega_\tau-\omega_\sigma)\delta_{jk}. \tag{3.5}$$

We choose this as our condition for orthogonality as three-wave mixing conserves the total intensity and, thus, conserves the above inner product. As observed in section 2.3.2 and 2.3.3, the local intensity of the perturbation fields is not always conserved, however, this product is suitable for sum-frequency generation after a simple transformation of the field

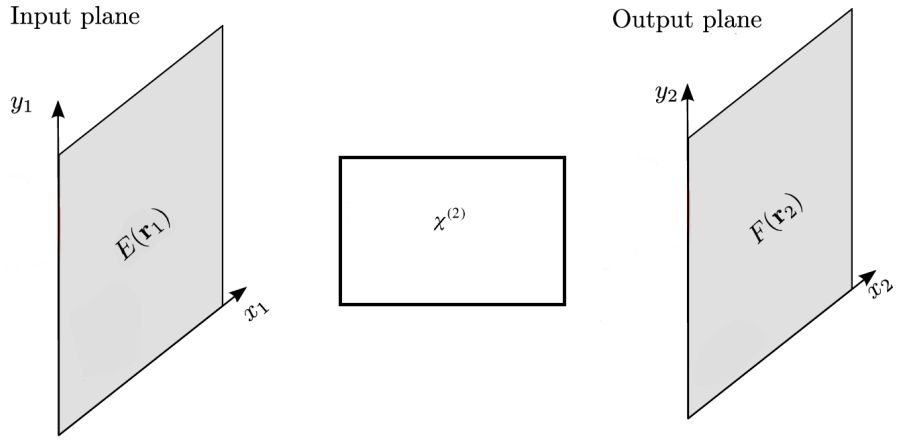

Figure 3.1: Optical system in which the field $F(\mathbf{r}_2)$ incident on the output plane is dependent on the input field $E(\mathbf{r}_1)$ and the $\chi^{(2)}$ nonlinear material.

variables; discussed in more detail in sections 3.4.1 and 4.3.1. Issues do arise when we consider parametric down-conversion as there is no simple transformation that conserves the above inner product, as shown in sections 3.6 and 4.4.1. In all cases, this condition for orthogonal fields is satisfied at the input of the nonlinear crystal. However, due to the interaction term in the equations of evolution, the modes will interact in a manner such that Eq. 3.5 is not satisfied for $z > 0$. Indeed, with the above basis decomposition, Eq. 3.4, acting as our initial conditions, the equations for sum-frequency generation are written:

$$-i\frac{\partial}{\partial z}E_{2,j}(\mathbf{r}) = \frac{1}{2k_2}\nabla_T^2 E_{2,j}(\mathbf{r}) + \sum_{k=1}^{N}\chi_2 E_b^*(\mathbf{r})E_{3,k}(\mathbf{r})e^{-i\Delta kz}, \tag{3.6}$$

$$-i\frac{\partial}{\partial z}E_{3,j}(\mathbf{r}) = \frac{1}{2k_3}\nabla_T^2 E_{3,j}(\mathbf{r}) + \sum_{k=1}^{N}\chi_3 E_b(\mathbf{r})E_{2,k}(\mathbf{r})e^{i\Delta kz}. \tag{3.7}$$

As we are not interested in the mode decomposition of the background field the interaction terms that would normally correspond to the tensor product $(E_{b,1}(\mathbf{r}) + \cdots + E_{b,N}(\mathbf{r}))\otimes (E_{\tau,1}(\mathbf{r}) + \cdots + E_{\tau,N}(\mathbf{r}))$ reduces to the product $E_b(\mathbf{r})\,(E_{\tau,1}(\mathbf{r}) + \cdots + E_{\tau,N}(\mathbf{r}))$. After propagating through the second-order nonlinear material, the field decomposition at the output plane is

$$F_\tau(\mathbf{r}_2) = \sum_{j=1}^{N} a_{\tau,j}F_{\tau,j}(\mathbf{r}_2), \tag{3.8}$$

where the coefficients $a_{\tau,j}$ are the same as those in the initial decomposition due to the linearity of the coupled wave equations. In the output plane, see figure 3.1, we define the

Hermitian form of some observable $\mathbf{\Theta}$ related to the operator $\mathscr{O}$ in a region of interest Ω as

$$\mathbf{\Theta} = \sum_{\tau} \sum_{j,k}^{N} a^*_{\tau,j} a_{\tau,k} \left(\int_{\Omega} F^*_{\tau,j}(\mathbf{r}_2) \mathscr{O} F_{\tau,k}(\mathbf{r}_2) \mathrm{d}\Omega \right) = \mathbf{a}^\dagger \mathbf{O} \mathbf{a}, \tag{3.9}$$

where the eigenvectors of the matrix $\mathbf{O}$ define the optical eigenmodes of the measure in question. A simple example of an optical measurement is the total intensity of the fields. In the context of sum-frequency generation the total intensity at the output plane for some region of detection, Ω, is defined as

$$I = \sum_{\tau} \sum_{j,k}^{N} a^*_{\tau,j} a_{\tau,k} \left(\int_{\Omega} \frac{1}{2} n_\tau \varepsilon_0 c \; F^*_{\tau,j}(\mathbf{r}_2) F_{\tau,k}(\mathbf{r}_2) \mathrm{d}\Omega \right) = \mathbf{a}^\dagger \mathbf{M} \mathbf{a}. \tag{3.10}$$

Similar to section 1.4.2, the elements of the Hermitian matrix $\mathbf{M}$ correspond to the cross-interaction of all of the probe fields. The vectors $\mathbf{a}$ and $\mathbf{a}^\dagger$ contain complex coefficients and their conjugates,

$$\mathbf{a} = \left(a_{\tau,1}, \ldots, a_{\tau,N}, a_{\sigma,1}, \ldots, a_{\sigma,N} \right)^\top \tag{3.11}$$

and

$$\mathbf{a}^\dagger = \left(a^*_{\tau,1}, \ldots, a^*_{\tau,N}, a^*_{\sigma,1}, \ldots, a^*_{\sigma,N} \right), \tag{3.12}$$

where N is the number of independent basis elements in the field decomposition given by Eq. 3.4. Unlike the intensity operator for linear optics, defined in section 1.4.2, here we have two fields contributing to the total intensity. With this, we can split the measure into two distinct contributions to the total intensity, each with its own Hermitian form,

$$\begin{aligned} I &= \sum_{j,k}^{N} \int_{\Omega} \left(\frac{1}{2} n_2 \varepsilon_0 c \; a^*_{2,j} a_{2,k} F^*_{2,j}(\mathbf{r}_2) F_{2,k}(\mathbf{r}_2) + \frac{1}{2} n_3 \varepsilon_0 c \; a^*_{3,j} a_{3,k} F^*_{3,j}(\mathbf{r}_2) F_{3,k}(\mathbf{r}_2) \right) \mathrm{d}\Omega \\ &= \mathbf{a}_2^\dagger \mathbf{M}_2 \mathbf{a}_2 + \mathbf{a}_3^\dagger \mathbf{M}_3 \mathbf{a}_3 \\ &= \mathbf{a}^\dagger \mathbf{M} \mathbf{a}. \end{aligned} \tag{3.13}$$

By writing the intensity in this way, we can consider the intensity of the fields at ω_2 or ω_3 independent of the other field. However, the interaction of the perturbation fields will influence these frequency-dependent measurements. Collectively, these Hermitian forms make up the total intensity which does not distinguish between the wavelengths. If we consider the total intensity, one can diagonalise the cross-interaction matrix and define the components of the optical eigenmodes at the output and input as:

$$\mathbb{F}_{\tau,k}(\mathbf{r}_2) = \sum_{j=1}^{N} v_{kj} F_{\tau,j}(\mathbf{r}_2), \tag{3.14}$$

$$\mathbb{E}_{\tau,k}(\mathbf{r}_1) = \sum_{j=1}^{N} v_{kj} E_{\tau,j}(\mathbf{r}_1), \tag{3.15}$$

where v_{kj} are the elements of the k^{th} eigenvector of $\mathbf{M}$ associated with the eigenvalue λ_k. For each of these optical eigenmodes, the total intensity in the region of detection is given by

$$\sum_{\tau} \int_{\Omega} \frac{1}{2} n_\tau \varepsilon_0 c \; \mathbb{F}^*_{\tau,j}(\mathbf{r}_2) \mathbb{F}_{\tau,k}(\mathbf{r}_2) \; \mathrm{d}\Omega = \delta_{jk} \lambda_j, \tag{3.16}$$

where $\mathbb{F}_{\tau,k}(\mathbf{r}_2)$ is the component of the k^{th} eigenmode, Eq. 3.89, oscillating at the frequency ω_τ.

Due to the interaction between the perturbation fields, the optical eigenmodes introduced here are, in general, distributed across both wavelengths. Consequently, as the eigenmodes propagate, there will be an interaction between the components that define them. Nevertheless, as the eigenmodes correspond to an orthogonal set, there will be no interaction between the eigenmodes themselves. Furthermore, as the interaction of the fields is mediated by the background field, $E_b(\mathbf{r})$, the symmetry and interaction of the eigenmodes will be characteristic of the symmetry of the background. It is these properties that distinguish our low-intensity perturbation eigenmodes from the eigenmodes of linear optics defined in section 1.4.2.

3.3 Numerical Examples

In this section, we outline various numerical examples of the intensity optical eigenmodes for sum-frequency generation. In all of the numerical examples here, we have used the computer software Mathematica [91], and all of the nonlinear crystal optics parameters were calculated using the free software SNLO and references therein [92]. We first consider the intensity eigenmodes of a bulk nonlinear material with the fields decomposed into a set of Hermite-Gaussian and Laguerre-Gaussian modes as introduced in sections 1.3.2 and 1.2, respectively.

3.3.1 System Set-up

As we are in the non-depleting pump regime, discussed in section 2.3, we must ensure that the field intensities associated with the perturbation and background fields satisfy the approximation from a numerical perspective. In the case of sum-frequency generation, this approximation is not as limiting as it is for parametric down-conversion as the sum-frequency solutions are oscillatory; therefore, there is no exponential gain or loss associated with the interacting fields. Nevertheless, the background should still be large in intensity compared

to the small perturbation fields to satisfy the non-depleting pump approximation. In the examples highlighted in this chapter, we will consider background fields that are 10^4 Vm^{-1} larger than the perturbation fields. As we define intensity as

$$I_\tau = \iint \frac{1}{2} n_\tau \varepsilon_0 c E_\tau^*(\mathbf{r}) E_\tau(\mathbf{r}) \, \mathrm{d}x \, \mathrm{d}y, \tag{3.17}$$

there will be an intensity difference of 10^{12} Wm^{-2} between the background and perturbation fields. In the case of sum-frequency generation, a couple of orders of magnitude in the difference in intensity between the pump and perturbation fields is sufficient to satisfy the non-depleted pump approximation due to the oscillatory nature of the solutions. The only additional constraint is that the background field must be of sufficient strength to induce optical nonlinearities in the crystal [8, 9].

In addition to the field intensity, we must consider the crystal optics of our numerical set-up. In the examples that follow, we consider the uniaxial crystal Potassium Dihydrogen Phosphate (KH_2PO_4) that is in the $2m$ symmetry point group. KH_2PO_4 or KDP is a non-centrosymmetric crystal that permits a non-zero $\chi^{(2)}$ and has a high damage threshold [93]. Vitally, this crystal is suitable for sum-frequency generation, as shown in [94, 95, 96]. A further benefit of using KDP is that there are only three non-zero elements in the susceptibility tensor, $\chi_{14} = \chi_{25}$ and χ_{36} [10]. Indeed, the expression given by Eq. 2.24 becomes

$$\begin{pmatrix} P_i(\omega_3) \\ P_j(\omega_3) \\ P_k(\omega_3) \end{pmatrix} = 2\varepsilon_0 \begin{pmatrix} 0 & 0 & 0 & \chi_{14} & 0 & 0 \\ 0 & 0 & 0 & 0 & \chi_{14} & 0 \\ 0 & 0 & 0 & 0 & 0 & \chi_{36} \end{pmatrix} \begin{pmatrix} E_i(\omega_1)E_i(\omega_2) \\ E_j(\omega_1)E_j(\omega_2) \\ E_k(\omega_1)E_k(\omega_2) \\ E_j(\omega_1)E_k(\omega_2) + E_k(\omega_1)E_j(\omega_2) \\ E_k(\omega_1)E_i(\omega_2) + E_i(\omega_1)E_k(\omega_2) \\ E_i(\omega_1)E_j(\omega_2) + E_j(\omega_1)E_i(\omega_2) \end{pmatrix}. \tag{3.18}$$

As outlined in section 2.2.3, in uniaxial crystals, it is common for the high-frequency field to be polarised along the axis with the highest refractive index. In the case of KDP, which is a negative uniaxial crystal, we assume the field at ω_3 is polarised along the extraordinary axis denoted e in figure 3.2. Moreover, if we assume we have type I phase matching, see section 2.2.3, then the fields at ω_1 and ω_2 are polarised along the ordinary axis which is denoted o in the figure. As the fields $\mathbf{E}(\omega_\tau)$ are polarised in the x-y plane, we have $E_k(\omega_\tau) = 0$, and the above matrix equation can be simplified to

$$P_k(\omega_3) = 2\varepsilon_0 \chi_{36} \left[E_i(\omega_1)E_j(\omega_2) + E_j(\omega_1)E_i(\omega_2) \right]. \tag{3.19}$$

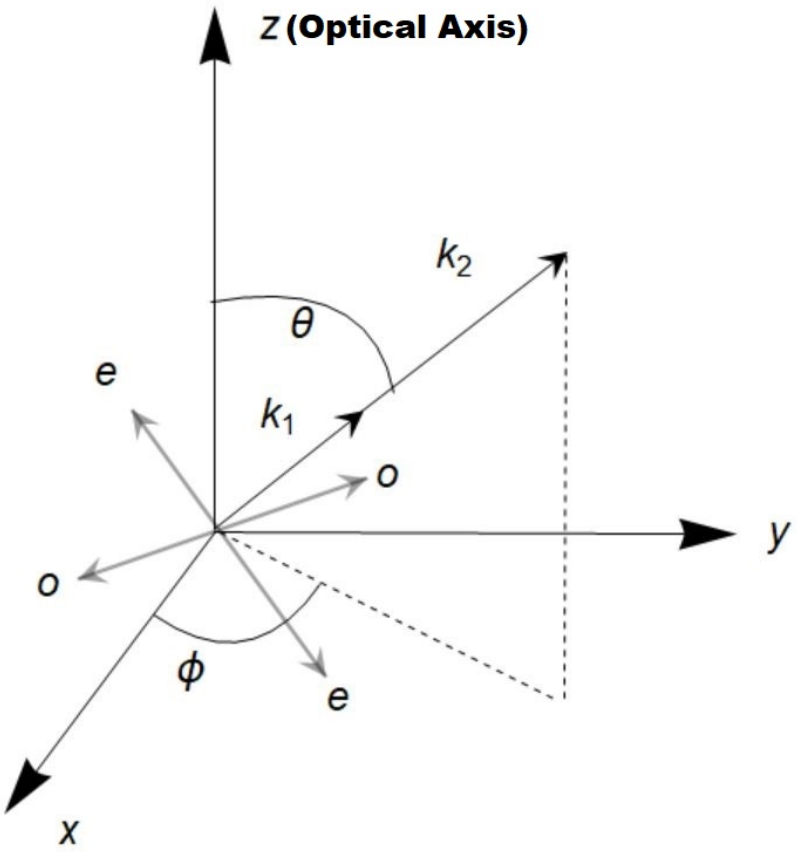

Figure 3.2: Type I phase matching for KDP crystal where k_1 and k_2 are the wavevectors of the fields $E_1(\mathbf{r})$ and $E_2(\mathbf{r})$, which are polarised along the ordinary axis in the x-y plane, denoted by o. The polarisation perpendicular to k_τ and o corresponds to the extraordinary axis and is denoted by e.

From the diagram, figure 3.2, one can see that the Cartesian components, $E_i(\omega_\tau)$ and $E_j(\omega_\tau)$, of the fields propagating in the direction of k_τ are:

$$E_i(\omega_\tau) = E_\tau(\mathbf{r}) \sin(\phi), \tag{3.20}$$

$$E_j(\omega_\tau) = E_\tau(\mathbf{r}) \cos(\phi), \tag{3.21}$$

where ϕ is the azimuthal angle between the k-vector and the x-axis and $E_\tau(\mathbf{r})$ is a transverse amplitude of the fields. The polarisation along the direction of the optical axis is therefore

$$P_k(\omega_3) = 4\varepsilon_0\chi_{36}E_1(\mathbf{r})E_2(\mathbf{r})\sin(\phi)\cos(\phi) = 2\varepsilon_0\chi_{36}E_1(\mathbf{r})E_2(\mathbf{r})\sin(2\phi). \tag{3.22}$$

If the angle between the direction of propagation and the optical axis is θ then the polarisation wave that contributes along $k_3(= k_1 + k_2)$ is $P(\omega_3) = P_k(\omega_3)\sin(\theta)$ such that

$$P(\omega_3) = 2\varepsilon_0\chi_{36}E_1(\mathbf{r})E_2(\mathbf{r})\sin(\theta), \tag{3.23}$$

where $\phi = \pi/4$. If we assume the crystal has full permutation symmetry, described in section 2.2.4, then the other polarisation waves are written:

$$P(\omega_2) = 2\varepsilon_0\chi_{36}E_1^*(\mathbf{r})E_3(\mathbf{r})\sin(\theta), \tag{3.24}$$

$$P(\omega_1) = 2\varepsilon_0\chi_{36}E_2^*(\mathbf{r})E_3(\mathbf{r})\sin(\theta), \tag{3.25}$$

with $\chi_{36} = 0.558$ pm/V and for the wavelengths, $\lambda_1 = 1064$, $\lambda_2 = 740$ and $\lambda_3 = 436.5$ nm we have the refractive indices $n_1^o = 1.525$, $n_2^o = 1.527$ and $n_3^e = 1.537$ which gives an angle $\theta = 41.9°$ at a temperature of 293 K [92].

3.3.2 Rectangular Symmetry

In this section, we decompose our fields into the Hermite-Gaussian modes of free space outlined in section 1.3.2. As discussed, these fields are orthogonal to each other as they propagate from the source to the input of the KDP crystal. As these fields propagate through the nonlinear material, they interact with one another and lose their orthogonality due to the coupling terms in the equations of propagation. Consequently, the orthogonal eigenmodes defined at the output of the nonlinear crystal are distinct from those of conventional linear systems that were discussed in section 1.4. In this section, we consider the intensity optical eigenmodes as an example to illustrate the difference between the eigenmodes of linear optics and the eigenmodes of our perturbation fields. In particular, by considering background fields with different symmetries, we observe how the background influences the eigenmodes.

To calculate the eigenmodes, we consider a basis set of 36 Hermite-Gaussian modes for all n and m truncated up to the maximal index $n + m \leq 7$. As we have two distinct fields, which we can decompose onto this basis, we have a total of 72 elements that are orthogonal to one another at the input of the nonlinear crystal. Additionally, we calculate the output fields using the split-step method, outlined in Appendix A, decomposed onto a discrete 42×42 grid. As a first example, we consider a HG_{00} background field, as shown in figure 3.3 (a). Figure 3.4 illustrates the field profiles of the first 20 intensity eigenmodes ordered with respect to their eigenvalues from top left to bottom right. In this example, the background field is rotationally symmetric about its origin and, consequently, the eigenmodes also exhibit this symmetry. Moreover, as this rotational symmetry is not broken by the intensity operator, we observe degeneracy in the eigenvalues shown in figure 3.7 (a).

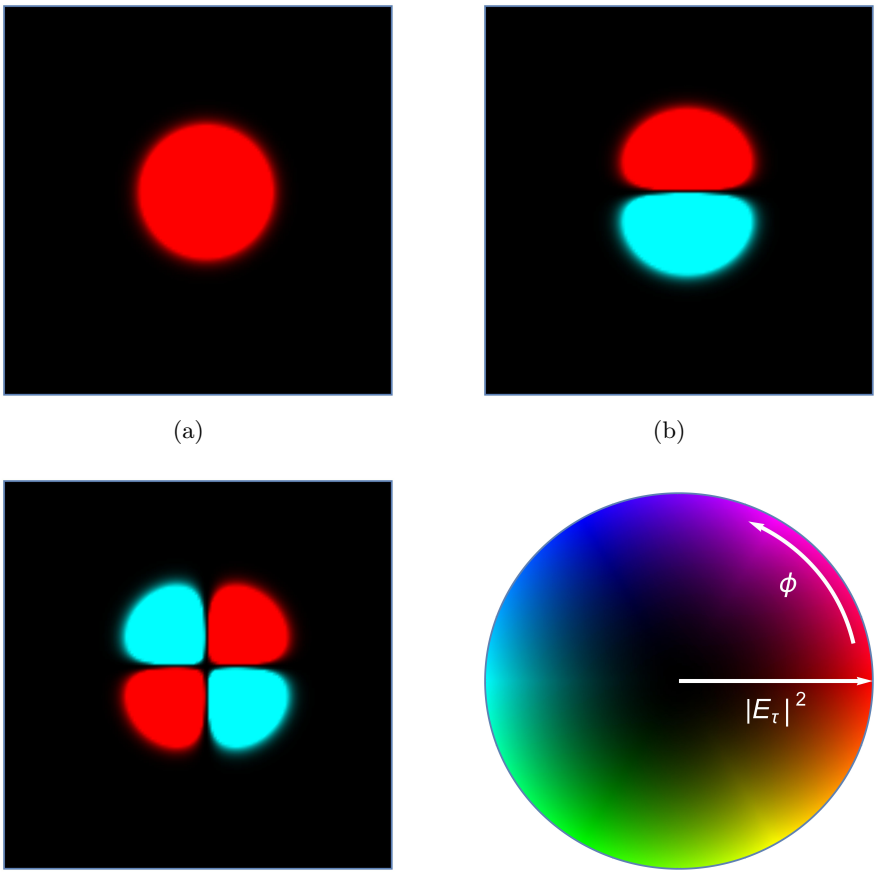

Figure 3.3: Hermite-Gaussian background fields with indices (a) $(n, m) = (0, 0)$, (b) $(n, m) = (0, 1)$ and (c) $(n, m) = (1, 1)$ represented on false colour map (d) where colour denotes phase and hue denotes intensity.

In general, the Hermite-Gaussian intensity profiles are invariant with respect to some spatial translation or reflection of the x-y plane, V_x or V_y, defined as:

$$V_x : \begin{pmatrix} x \\ y \\ z \end{pmatrix} \rightarrow \begin{pmatrix} -x \\ y \\ z \end{pmatrix}, \tag{3.26}$$

$$V_y : \begin{pmatrix} x \\ y \\ z \end{pmatrix} \rightarrow \begin{pmatrix} x \\ -y \\ z \end{pmatrix}. \tag{3.27}$$

If these symmetries are not probed, it will lead to degenerate eigenmodes as has been observed with the HG_{00} example. We can categorise all of the operations that leave the

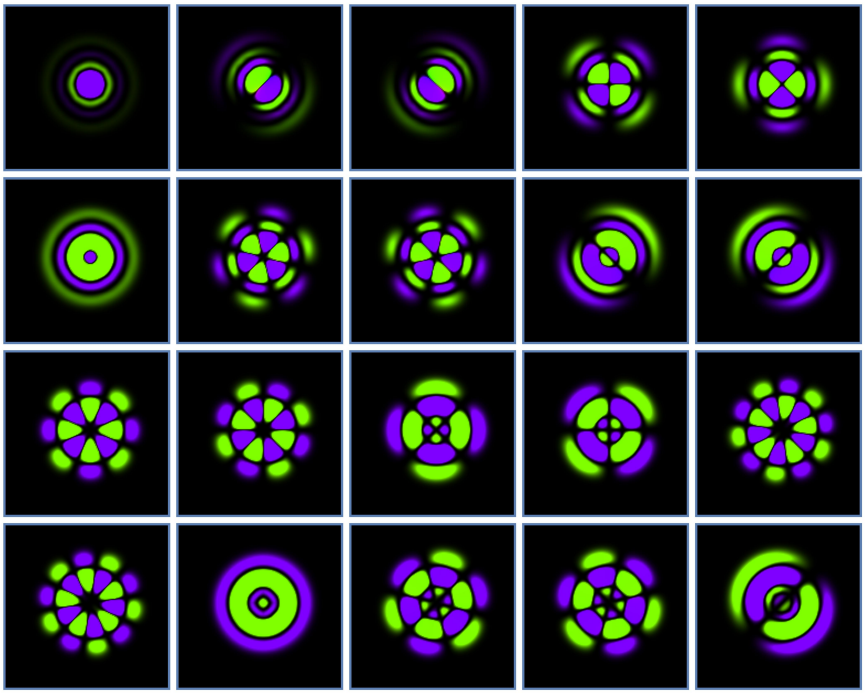

(a)

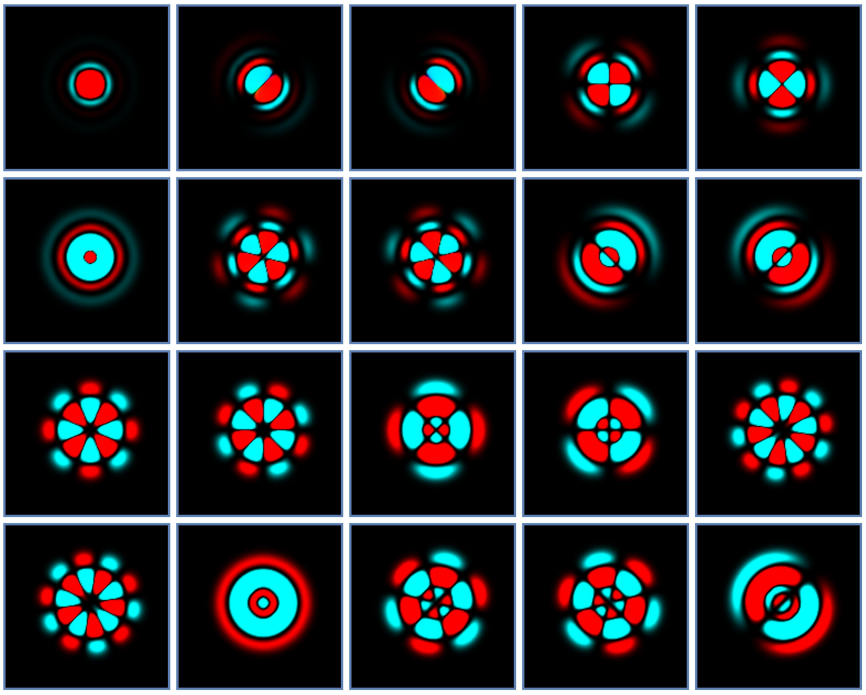

(b)

Figure 3.4: The first 20 intensity optical eigenmodes for an HG_{00} background with components (a) $\mathbb{F}_{2,k}(\mathbf{r}_2)$ and (b) $\mathbb{F}_{3,k}(\mathbf{r}_2)$. The eigenmodes are ordered from the top left to the bottom right in descending intensity. First row: Modes 1 to 5 and second row: Modes 6 to 10 etc. Note, corresponding components in (a) and (b) define a single optical eigenmode.

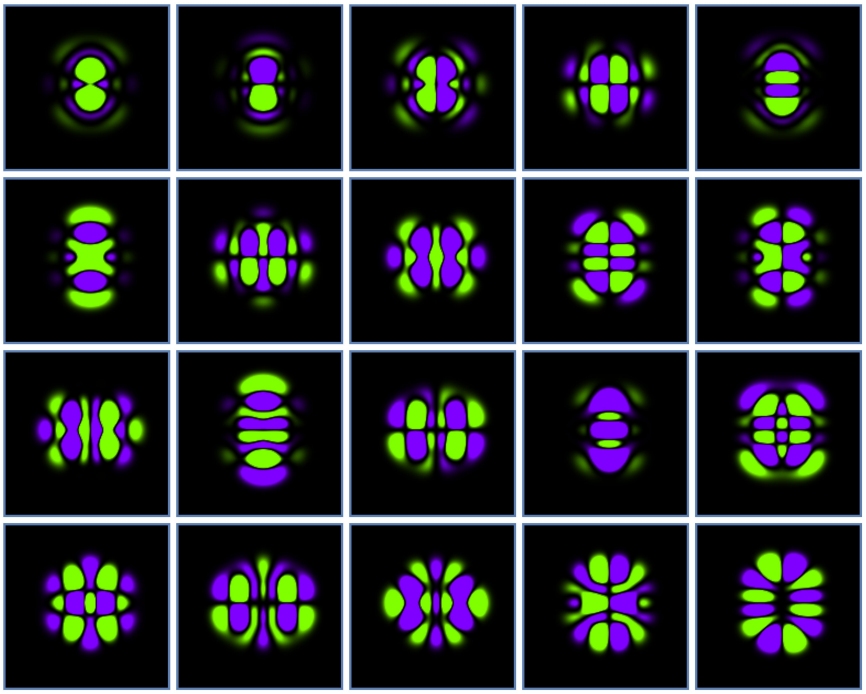

(a)

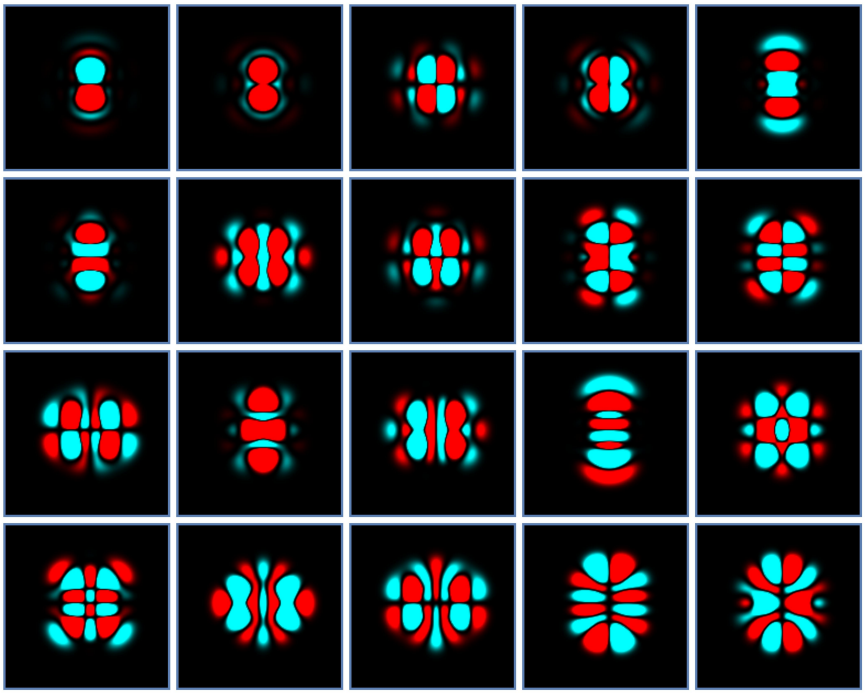

(b)

Figure 3.5: The first 20 intensity optical eigenmodes for a HG_{10} background with components (a) $\mathbb{F}_{2,k}(\mathbf{r}_2)$ and (b) $\mathbb{F}_{3,k}(\mathbf{r}_2)$. The eigenmodes are ordered from the top left to the bottom right in descending intensity represented on the false colour map in figure 3.3 (d).

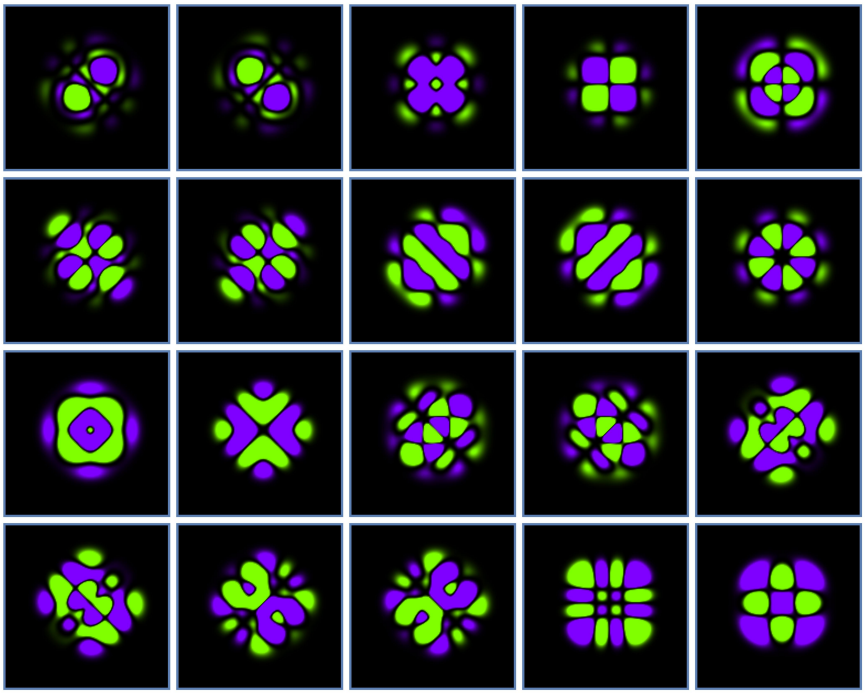

(a)

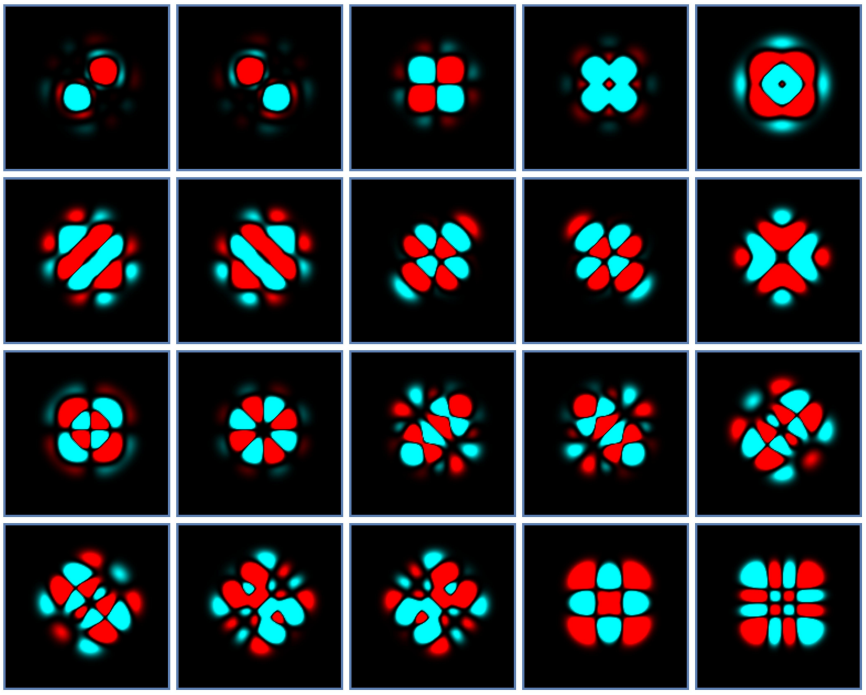

(b)

Figure 3.6: The first 20 intensity optical eigenmodes for a HG_{11} background with components (a) $\mathbb{F}_{2,k}(\mathbf{r}_2)$ and (b) $\mathbb{F}_{3,k}(\mathbf{r}_2)$ represented on the false colour map in figure 3.3 (d).

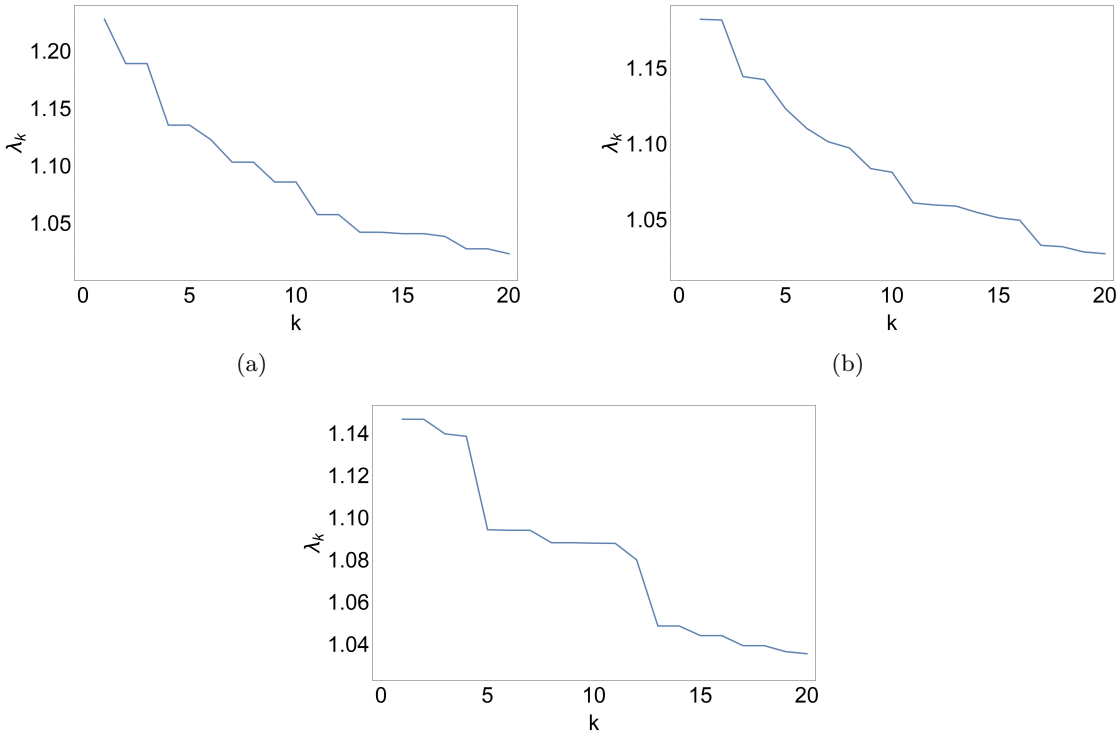

Figure 3.7: Eigenvalues for the first 20 intensity optical eigenmodes with (a) HG_{00}, (b) HG_{10} and (c) HG_{11} background field.

HG_{nm} modes invariant according to the indices n and m as:

$$\begin{cases} V_x V_y & : \text{for } n = m \\ V_x & : \text{for } n \neq m \text{ with odd } n \text{ and even } m \\ V_y & : \text{for } n \neq m \text{ with odd } m \text{ and even } n \end{cases}$$

As we are considering the optical eigenmodes of the intensity operator we are not breaking or probing any of the above symmetries and, therefore, we observe degenerate subspaces in which the associated eigenmodes transform into their degenerate counterparts with respect to a spatial reflection. Furthermore, we observe that all of the degenerate subspaces are two-fold degenerate, i.e., they consist of two eigenmodes with the same intensity eigenvalue. This can be attributed to using the same HG mode decomposition for both of the perturbation fields. Although each decomposition exists in a different frequency space, the field profiles that define them are the same and, thus, in the context of transverse field profiles, we have a two-fold degeneracy.

As a secondary example, we consider a HG_{10} background field that is symmetric for the operator V_y. Unlike the HG_{00} background field, HG_{10} is symmetric with respect to

discrete reflections as opposed to continuous rotations. This discrete symmetry, like the previous example, leads to a number of two-fold degenerate eigenspaces. This is observed in the eigenmodes shown in figure 3.5, where the corresponding eigenvalues are shown in figure 3.7 (b). Lastly, if we consider the background field HG_{11}, represented in figure 3.3 (c), we note that this field is symmetric about the spatial reflections V_x, V_y and V_xV_y. The first 20 intensity eigenmodes with this background field are illustrated in figure 3.6. As with the previous examples, we see the eigenmodes adopt the discrete symmetry associated with the background, and we observe some degeneracy in the intensity Hilbert space which is highlighted in the eigenvalues shown in figure 3.7 (c). Note, as described in section 2.3.2, the solutions of sum-frequency generation are oscillatory. Due to this behaviour, we may find accidental degeneracy in which two degenerate subspaces have the same intensity at certain points in the nonlinear crystal. This is most apparent in figure 3.7 (c)

3.3.3 Circular Symmetry

As described in the first chapter, the Laguerre-Gaussian (LG) modes correspond to a superposition of HG modes. Consequently, by truncating the Hilbert space with respect to the maximal index $2p + |\ell| \leq 7$, we can probe the same Hilbert space used in the previous section in terms of LG modes. We are interested in the LG modes as, unlike the HG basis set, these modes have helical wavefronts characterised by optical angular momentum, ℓ [19]. This orbital angular momentum represents a clear way to relate the symmetries of the eigenmodes to that of the background field.

(a) (b)

Figure 3.8: Discrete Laguerre-Gaussian background fields on 42×42 grid with indices (a) $(\ell, p) = (0, 0)$ and (b) $(\ell, p) = (1, 0)$ represented on false colour map figure 3.3 (d).

As with the previous section, we find a scattering matrix, as outlined in Appendix A, for each of the background fields and probe our system with 36 Laguerre-Gaussian modes on a discrete 42×42 grid. The LG modes at the input plane are of the form $E(\mathbf{r}_1) = \sum_j E_{\tau,j}(r_1) \exp(-i\ell_{\tau,j}\phi)$ where $E_{\tau,j}(r_1)$ are as shown in Eq. 1.16, less the angular dependence which we have accounted for explicitly here. The equations evolving these LG modes are:

$$-i\frac{\partial}{\partial z}E_b(r,z) = \frac{1}{2k_1}\left(\nabla_r^2 + \frac{1}{r}\nabla_r - \frac{\ell_b^2}{r^2}\right)E_b(r,z), \tag{3.28}$$

$$\begin{aligned}-i\frac{\partial}{\partial z}E_{2,j}(r,z) =& \frac{1}{2k_2}\left(\nabla_r^2 + \frac{1}{r}\nabla_r - \frac{\ell_{2,j}^2}{r^2}\right)E_{2,j}(r,z) \\ &+ \sum_{k=1}^{N}\chi_2 E_b^*(r,z)E_{3,k}(r,z)e^{-i\Delta kz}e^{i\left(\ell_b+\ell_{2,j}-\ell_{3,k}\right)\phi},\end{aligned} \tag{3.29}$$

$$\begin{aligned}-i\frac{\partial}{\partial z}E_{3,j}(r,z) =& \frac{1}{2k_3}\left(\nabla_r^2 + \frac{1}{r}\nabla_r - \frac{\ell_3^2}{r^2}\right)E_{3,j}(r,z) \\ &+ \sum_{k=1}^{N}\chi_3 E_b(r,z)E_{2,k}(r,z)e^{i\Delta kz}e^{i\left(\ell_{3,j}-\ell_{2,k}-\ell_b\right)\phi},\end{aligned} \tag{3.30}$$

giving the fields $F_\tau(\mathbf{r}_2) = \sum_j F_{\tau,j}(r_2)\exp(-i\ell_{\tau,j}\phi)$ at the output plane of the system. As a first example, we consider the background field shown in figure 3.8 (a) where $\ell_b = 0$. In this case, the conservation of OAM reduces to the simple relation $\ell_3 = \ell_2$. This conservation is observed in the intensity optical eigenmodes of the system - the first 20 of which are represented in figure 3.9. With no angular momentum on the background field, the eigenmodes take on the symmetry of the eigenmodes in figure 3.4. This is unsurprising as the background field in both cases is the same and, as shown in section 1.3.3, the Hermite-Gaussian and Laguerre-Gaussian basis span the same Hilbert subspace if truncated up to the same maximal index.

As a secondary example, we consider a background field with $\ell_b = +1$, as shown in figure 3.8 (b). In this case, the conservation rule for the OAM becomes $\ell_3 = \ell_2 + 1$. In the previous example, with $\ell_b = 0$, each element within the set ℓ_2 is transformed into an element in ℓ_3 by interacting with the background field. For a background field with non-zero OAM, however, this is not necessarily the case. Indeed, consider a background field with $\ell_b = +1$ interacting with a perturbation field at, for example, $\ell_{2,k} = 7$. The field from this interaction will have OAM $\ell_{3,j} = \ell_{2,k} + 1 = 8$ which is beyond the initially considered basis. Therefore,

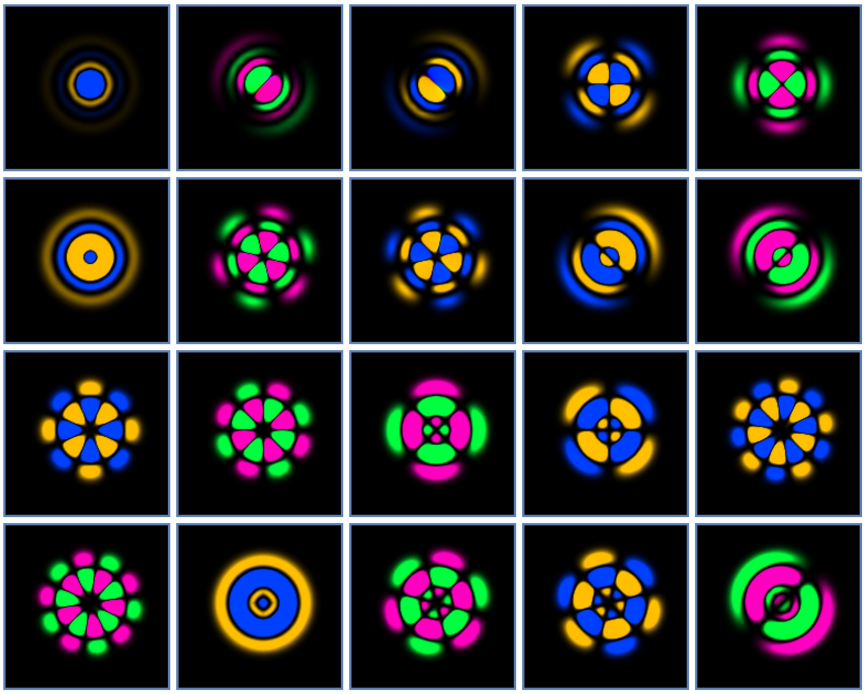

(a)

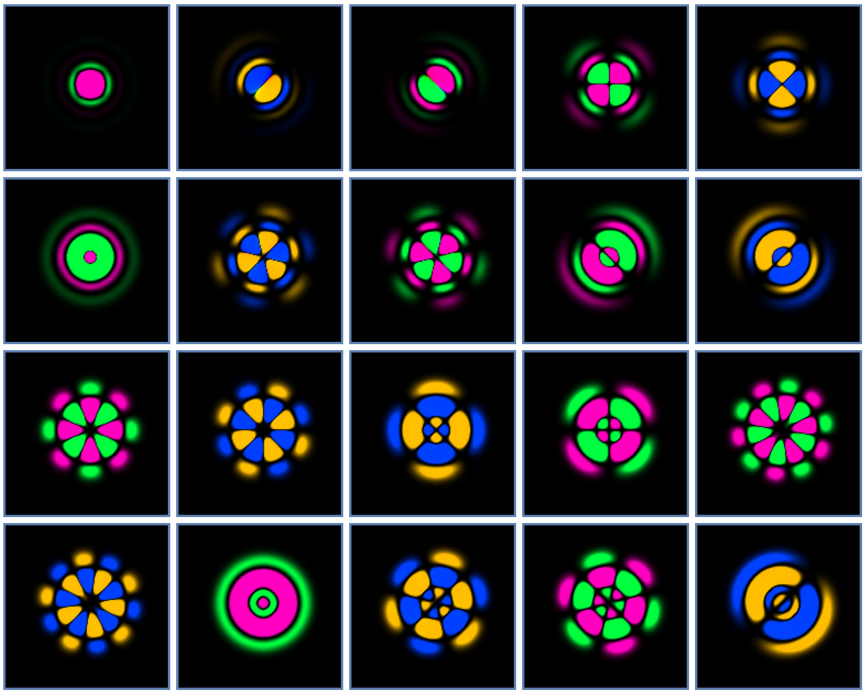

(b)

Figure 3.9: The first 20 intensity optical eigenmodes for a LG_{00} background with components (a) $\mathbb{F}_{2,k}(r_2)e^{-i\ell_{2,k}\phi}$ and (b) $\mathbb{F}_{3,k}(r_2)e^{-i\ell_{3,k}\phi}$ represented on the false colour map in figure 3.3 (d). The eigenmodes are ordered from the top left to the bottom right in descending intensity. First row: Modes 1 to 5 and second row: Modes 6 to 10 etc.

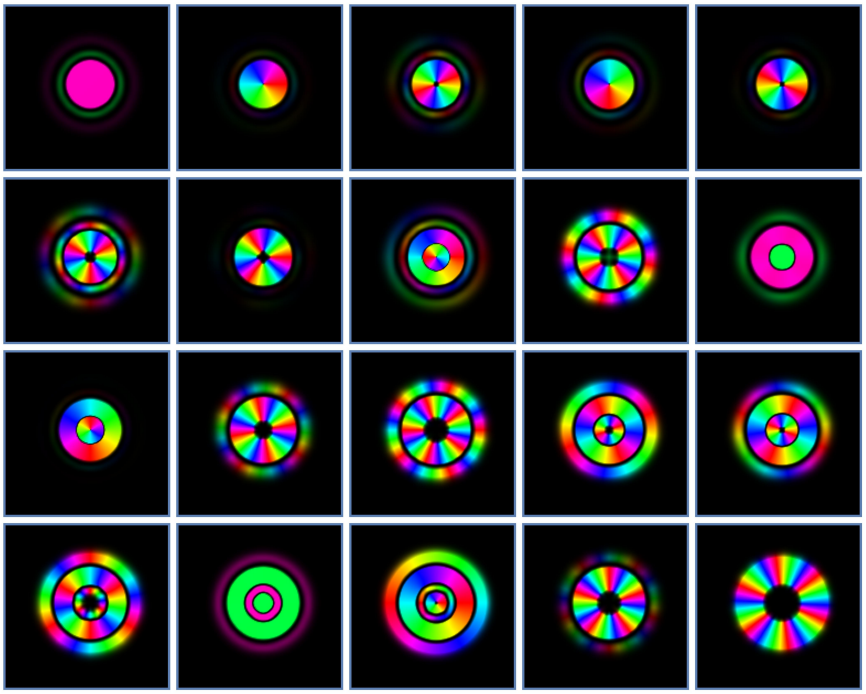

(a)

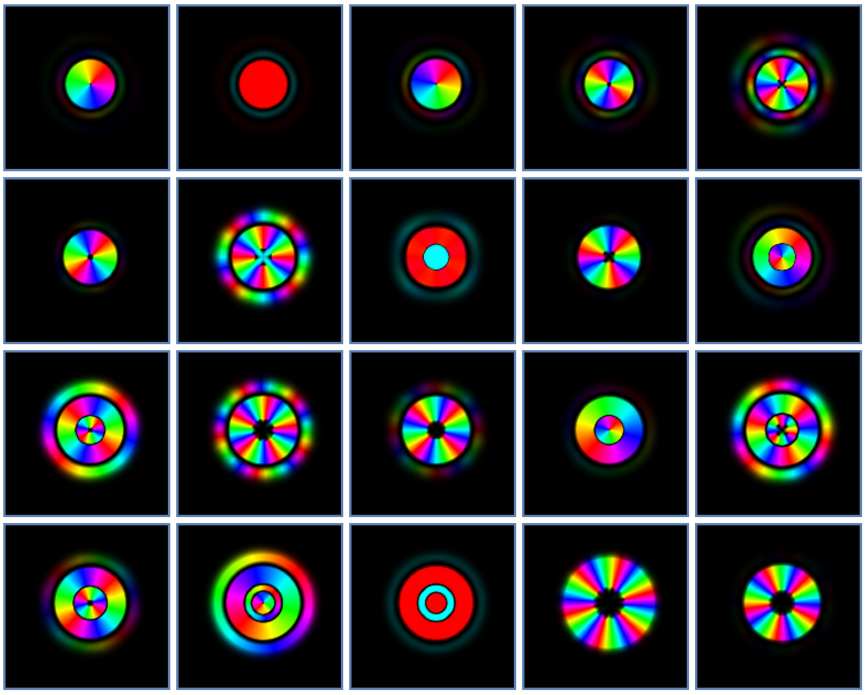

(b)

Figure 3.10: The first 20 intensity optical eigenmodes for a LG_{10} background with components (a) $\mathbb{F}_{2,k}(r_2)e^{-i\ell_{2,k}\phi}$ and (b) $\mathbb{F}_{3,k}(r_2)e^{-i\ell_{3,k}\phi}$ represented on the false colour map in figure 3.3 (d).

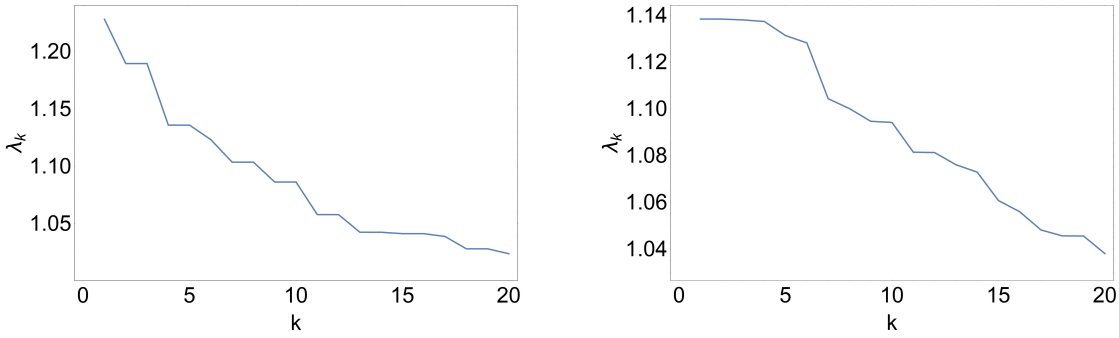

(a) (b)

Figure 3.11: Intensity eigenvalues for the first 20 optical eigenmodes with (a) LG_{00} and (b) LG_{10} background field shown in figures 3.9 and 3.10, respectively.

considering the two basis sets $\ell_2 = \{-7, \ldots, 0, \ldots, 7\}$ and $\ell_3 = \{-7, \ldots, 0, \ldots, 7\}$, we can use the relations $\ell_2 = \ell_3 - 1$ and $\ell_3 = \ell_2 + 1$ to find the following sets:

$$\ell_2' = \{-8, \ldots, 0, \ldots, 6\},$$

$$\ell_3' = \{-6, \ldots, 0, \ldots, 8\}.$$

These new basis pairs, ℓ_2, ℓ_3' and ℓ_2', ℓ_3, each corresponds to sets that are closed with respect to an interaction with the background field when $\ell_b = +1$. That is, all elements in ℓ_2 or ℓ_3 are mapped to a single component in the set ℓ_3' or ℓ_2' via an interaction with the background. Note, the choice of which basis to shift in the manner described above is somewhat arbitrary. Indeed, if we choose $\ell_2 = \{-7, \ldots, 0, \ldots, 7\}$ then we have for the other field the set ℓ_3' as defined above. If, however, we choose $\ell_3 = \{-7, \ldots, 0, \ldots, 7\}$ then for the other field we would have to use ℓ_2'. In the examples presented here, we choose the basis set ℓ_2 and ℓ_3'. If we now include the radial index p_τ, we have the following conditions for our sets:

$$2p_2 + |\ell_2| \leq 7, \tag{3.31}$$

$$2p_3 + |\ell_3'| \leq 8, \tag{3.32}$$

where $\ell_3' = \ell_2 + 1$, as shown above. More generally, for a background field with OAM, ℓ_b, we have:

$$2p_2 + |\ell_2| \leq 7, \tag{3.33}$$

$$2p_3 + |\ell_3'| \leq 7 + \ell_b, \tag{3.34}$$

where $\ell_3' = \ell_2 + \ell_b$; this is discussed further in section 3.8.

In the first example here, we observed symmetry similar to the eigenmodes found in the first example of section 3.3.2. In this example, we have $\ell_b = +1$, which can be written in terms of Hermite-Gaussian modes as

$$\mathrm{LG}_{10} = \frac{1}{\sqrt{2}} \left(\mathrm{HG}_{10} - i\, \mathrm{HG}_{01} \right).$$

Consequently, we observe different symmetries in the optical eigenmodes to that of section 3.3.2, even though the two are related. The first 20 intensity optical eigenmodes are represented for this example in figure 3.10, with their corresponding eigenvalues shown in figure 3.11 (b). In these modes, we observe that the OAM conservation rule is satisfied for all of the eigenmode components. Like the Hermite-Gaussian examples, we observe a number of two-fold degenerate subspaces. In the Laguerre-Gaussian basis, this degeneracy is due to rotational symmetry not probed by the intensity measure of the fields. Indeed, if we consider the intensity of output eigenmodes with components $\mathbb{F}_{\tau,k}(r_2)e^{-i\ell_{\tau,k}\phi}$ we have

$$\lambda_k = \sum_\tau \int \frac{1}{2} n_\tau \varepsilon_0 c\; \mathbb{F}^*_{\tau,k}(r_2)\mathbb{F}_{\tau,k}(r_2) e^{i\ell_{\tau,k}\phi} e^{-i\ell_{\tau,k}\phi}\, \mathrm{d}\phi\, \mathrm{d}r_2 \tag{3.35}$$

$$= \sum_\tau \int \frac{1}{2} n_\tau \varepsilon_0 c\; \mathbb{F}^*_{\tau,k}(r_2)\mathbb{F}_{\tau,k}(r_2)\, \mathrm{d}\phi\, \mathrm{d}r_2 \tag{3.36}$$

which is independent of the orbital angular momentum of the fields. Consequently, eigenmodes with the same total OAM, $\ell_{2,k} + \ell_{3,k}$, may result in degenerate intensity states. Indeed, if the eigenmode at the output has components $\mathbb{F}_{2,k}(r_2)e^{-i\ell_{2,k}\phi}$ and $\mathbb{F}_{3,k}(r_2)e^{-i\ell_{3,k}\phi}$ then the intensity is invariant with respect to the transformations $\ell_{2,k} \to \ell_{3,k}$ and $\ell_{3,k} \to \ell_{2,k}$ which leads to, in some cases, a two-fold degeneracy. The lifting of this degeneracy and the definition of the OAM operators for sum-frequency generation are discussed in more details in section 3.8.

3.4 Eigenmodes in Waveguides

In the previous sections, we showed some examples of intensity optical eigenmodes in bulk nonlinear material with basis sets constructed of Hermite-Gaussian and Laguerre-Gaussian modes. In this section, we will outline the definition of eigenmodes in optical waveguides with circular and rectangular symmetry. In particular, in section 3.4.1, we derive a 1D coefficient form of the equations of evolution that leads to a simple scattering matrix relation. Moreover, with this coefficient form, we have an analytical description of the interaction between the basis elements as they propagate. Indeed, in sections 3.4.2 and 3.4.3, we derive expressions that describe the coupling of the modes introduced in section 1.3.4 and 1.3.3, respectively. Lastly, in section 3.4.4, we utilise the scattering matrix in order to define the propagation eigenmodes of this system.

3.4.1 Coefficient Form

Again, we begin with the set of equations describing sum-frequency generation:

$$-i\frac{\partial}{\partial z}E_b(\mathbf{r}) = \frac{1}{2k_1}\nabla_T^2 E_b(\mathbf{r}), \tag{3.37}$$

$$-i\frac{\partial}{\partial z}E_2(\mathbf{r}) = \frac{1}{2k_2}\nabla_T^2 E_2(\mathbf{r}) + \chi_2 E_b^*(\mathbf{r})E_3(\mathbf{r})e^{-i\Delta kz}, \tag{3.38}$$

$$-i\frac{\partial}{\partial z}E_3(\mathbf{r}) = \frac{1}{2k_3}\nabla_T^2 E_3(\mathbf{r}) + \chi_3 E_b(\mathbf{r})E_2(\mathbf{r})e^{i\Delta kz}. \tag{3.39}$$

In the previous section, it was this set of equations that we used to evolve the fields and calculate the optical eigenmodes. In a waveguide, however, we can assume that the propagation modes defined in section 1.3.4 and 1.3.3 are stationary, non-diffracting solutions of the system such that we can expand the fields at the input plane as

$$E_\tau(\mathbf{r}_1) = \sum_{j=1}^{N} E_{\tau,j}(\mathbf{r}_1) = \sum_{j=1}^{N} a_{\tau,j}(0) f_{\tau,j}(x_1, y_1) = \sum_{j=1}^{N} a_{\tau,j}(0) f_{\tau,j}(x, y), \tag{3.40}$$

where the fields $f_{\tau,j}(x, y)$ are the propagating modes of the waveguide that describe a Hilbert space of orthogonal elements with

$$\iiint f_{\tau,j}^*(x, y) f_{\sigma,k}(x, y) e^{-i(\omega_\sigma - \omega_\tau)t}\,\mathrm{d}x\,\mathrm{d}y\,\mathrm{d}t = 2\pi\delta(\omega_\tau - \omega_\sigma)\delta_{jk}. \tag{3.41}$$

The coefficients in the above field expansion evolve according to the following set of equations:

$$-i\partial_z a_{2,j}(z) = \sum_{k=1}^{N} \upsilon_{2,jk} a_{2,k}(z) + \chi_2 g_{jk}(z) a_{3,k}(z), \tag{3.42}$$

$$-i\partial_z a_{3,j}(z) = \sum_{k=1}^{N} \upsilon_{3,jk} a_{3,k}(z) + \chi_3 g_{kj}^*(z) a_{2,k}(z), \tag{3.43}$$

with the matrices:

$$\upsilon_{\tau,jk} = \iint \frac{1}{2k_\tau}\ f_{\tau,j}^*(x, y)\nabla_T^2 f_{\tau,k}(x, y)\,\mathrm{d}x\,\mathrm{d}y, \tag{3.44}$$

$$g_{jk}(z) = \iint E_b^*(\mathbf{r}) f_{2,j}^*(x, y) f_{3,k}(x, y) e^{-i\Delta kz}\,\mathrm{d}x\,\mathrm{d}y, \tag{3.45}$$

where the field $E_b(\mathbf{r})$ is a solution of Eq. 3.37 and the matrices υ_{jk} and $g_{jk}(z)$ describe a linear phase term and background dependent interaction term. These equations give fields at the output plane of the form

$$F_\tau(\mathbf{r}_2) = \sum_{j=1}^{N} F_{\tau,j}(\mathbf{r}_2) = \sum_{j=1}^{N} a_{\tau,j}(z_2) f_{\tau,j}(x_2, y_2) = \sum_{j=1}^{N} a_{\tau,j}(z_2) f_{\tau,j}(x, y), \tag{3.46}$$

where z_2 is the distance between the input and output plane, see figure 3.1, which have the same transverse dimensions due to the fixed basis elements $f_{\tau,j}(x_1, y_1) = f_{\tau,j}(x_2, y_2) = f_{\tau,j}(x, y)$. Using the above set of equations, one can define the input-output relation with a scattering matrix as

$$\begin{pmatrix} a'_{2,k} \\ a'_{3,k} \end{pmatrix} = \mathbf{S} \begin{pmatrix} a_{2,k} \\ a_{3,k} \end{pmatrix}, \tag{3.47}$$

where

$$a_{\tau,k} = (a_{\tau,1}, \ldots, a_{\tau,k})^\top = (a_{\tau,1}(0), \ldots, a_{\tau,k}(0))^\top$$

are the field amplitudes of the modes at the input plane and

$$a'_{\tau,k} = \left(a'_{\tau,1}, \ldots, a'_{\tau,k}\right)^\top = (a_{\tau,1}(z_2), \ldots, a_{\tau,k}(z_2))^\top$$

are the amplitudes of the corresponding output modes and $\mathbf{S} = \exp\left(\int_z i\mathbf{P}(z)\mathrm{d}z\right)$ where

$$\mathbf{P}(z) = \begin{pmatrix} \upsilon_{2,jk} & \chi_2 g_{jk}(z) \\ \chi_3 g^*_{kj}(z) & \upsilon_{3,jk} \end{pmatrix}. \tag{3.48}$$

As the equations are now in 1D, the evolution of the coefficients does not require any involved computational methods like the split-step method outlined in Appendix A. Moreover, due to the simplicity of the coefficient form, we can gain some intuition with respect to the interaction of the fields and the propagation properties of the eigenmodes which we define at the output and input as:

$$\mathbb{F}_{\tau,k}(\mathbf{r}_2) = \sum_{j=1}^{N} v_{kj} F_{\tau,j}(\mathbf{r}_2) = \sum_{j=1}^{N} v_{kj} a'_{\tau,j} f_{\tau,j}(x, y), \tag{3.49}$$

$$\mathbb{E}_{\tau,k}(\mathbf{r}_1) = \sum_{j=1}^{N} v_{kj} E_{\tau,j}(\mathbf{r}_1) = \sum_{j=1}^{N} v_{kj} a_{\tau,j} f_{\tau,j}(x, y), \tag{3.50}$$

where v_{kj} are the elements of the k^{th} eigenvector of a Hermitian matrix associated with the eigenvalue λ_k.

3.4.2 Rectangular Waveguide

We take as a first example, a rectangular nonlinear waveguide with the same boundary conditions as described in section 1.3.4. The basis elements for this waveguide are of the form

$$f_{nm}(x, y) = \sin\left(\frac{n\pi}{2b}x - n\frac{\pi}{2}\right) \sin\left(\frac{m\pi}{2c}y - m\frac{\pi}{2}\right), \tag{3.51}$$

where b and c correspond to the transverse lengths of the waveguide shown in figure 3.12. If we assume our basis to be fixed, as in section 3.4.1, then we can describe the dynamics

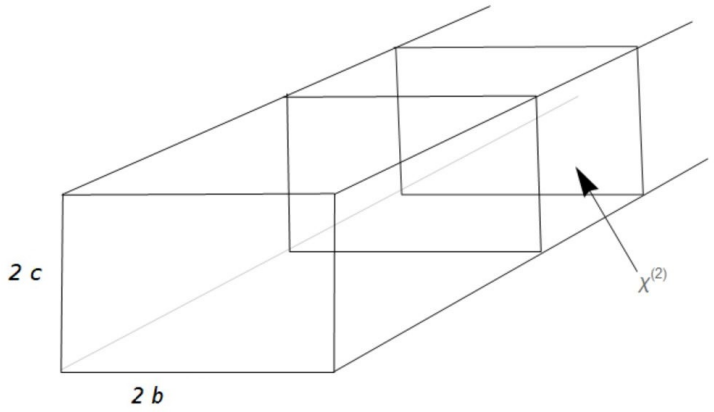

Figure 3.12: Schematic of a rectangular waveguide with a nonlinear, $\chi^{(2)}$, material embedded along its length.

of the system by evolving the coefficients $\alpha_{\tau,j}(z)$. The link between the coefficients and the fields is given by

$$E_\tau(\mathbf{r}) = \sum_{j=1}^{N} \alpha_{\tau,j}(z) f_{\tau,j}(x,y), \tag{3.52}$$

where we label the modes with index pair $\{n_i, m_i\}$ with a single index j for simplicity. In coefficient space, the equations of motion are of the form of Eq. 3.42 with matrices $\upsilon_{\tau,jk}$ and $g_{jk}(z)$ corresponding to a propagation or phase term and the mixing of the fields, respectively. A benefit of using a basis set of the form in Eq. 3.51 is that the elements of both of these matrices have a simple analytical form. Indeed, with fields that are normalised in intensity, $\frac{1}{2} n_\tau \varepsilon c \iint f^*_{\tau,j}(x,y) f_{\tau,k}(x,y) = \delta_{jk}$, we find the matrix elements of υ_{jk} as

$$\upsilon_{\tau,jk} = -\frac{(bm_j + cn_j)^2 \pi^2}{4bc}\, \delta_{n_j,n_k} \delta_{m_j,m_k}. \tag{3.53}$$

In the case of the interaction matrix, we can write the general form of its elements by assuming the background is also a mode of the form of Eq. 3.51. Indeed, we find

$$g_{jk}(z) = \frac{\zeta_n \left(1 \pm \cos\left(n_j\pi\right)\cos\left(n_k\pi\right)\right)}{(n_j^4 + (n_k^2 - n_b^2)^2 - 2n_j^2(n_k^2 + n_b^2))\pi^2} \frac{\zeta_m \left(1 \pm \cos\left(m_j\pi\right)\cos\left(m_k\pi\right)\right)}{(m_j^4 + (m_k^2 - m_b^2)^2 - 2m_j^2(m_k^2 + m_b^2))} e^{-i\Delta k z}, \tag{3.54}$$

in which $\zeta_n = 4bn_b n_j n_k$ and $\zeta_m = 4cm_b m_j m_k$. The numbers n_b and m_b corresponds to the background field indices, and when they are odd (even), the numerator takes on a positive (negative) sign. With this interaction matrix, we can explicitly see the interaction between the basis field elements. Indeed, if we take, for example, the fundamental background field with $n_b = m_b = 1$ then the terms

$$(1 + \cos(n_j\pi)\cos(n_k\pi))$$

and

$$(1 + \cos(m_j\pi)\cos(m_k\pi))$$

are non-zero only when the numbers n_j, n_k and m_j, m_k are both even or both odd. All of these symmetries are shown, for the background fields in figure 3.13, in the scattering matrices of figure 3.14.

To calculate the intensity optical eigenmodes, we again consider a basis set of 36 fields truncated with respect to $n+m \leq 7$. In addition, we use the same system set up as outlined in section 3.3.1 with the assumption that all wavelengths and fields in the decomposition are above the cut-off of the waveguide. As a first example, we take the background field to be of the form of the fundamental TM mode with $n_b = m_b = 1$. The first 20 optical eigenmodes for this background are shown in figure 3.15. Perhaps unsurprisingly, the symmetry of the eigenmodes follows that of the Hermite-Gaussian modes shown in section 3.3.2. Again, similar to the HG modes, we observe degeneracy in the eigenvalues, as illustrated in figure 3.17 (a). This is to be expected given the discrete symmetries of the TM modes is similar to the HG modes as described in section 3.3.2. This degeneracy is also observed for other TM background fields. Indeed, figure 3.16 shows the eigenmodes for a background field with $n_b = 2$ and $m_b = 1$ with the corresponding eigenvalues represented in figure 3.17 (b). Again, in both of these examples, we see the influence of the background field on the symmetry of the eigenmodes.

3.4.3 Circular Waveguide

If we consider a waveguide that exhibits circular symmetry, the system is solved using the Laguerre-Gaussian modes introduced in section 1.3.3. In a similar way to the rectangular waveguide, we can expand the fields as described in section 3.4.1 where we have the matrices:

$$\upsilon_{\tau,jk} = \iint \frac{1}{2k_\tau}\, f^*_{\tau,j}(r) \left(\nabla_r^2 + \frac{1}{r}\nabla_r - \frac{\ell^2_{\tau,k}}{r^2}\right) f_{\tau,k}(r)\; e^{-i\left(\ell_{\tau,j}-\ell_{\tau,k}\right)\phi}\, \mathrm{d}\phi\, \mathrm{d}r, \tag{3.55}$$

$$g_{jk}(z) = \iint E^*_b(r,z) f^*_{2,j}(r) f_{3,k}(r) e^{-i\left(\ell_{3,k}-\ell_{2,j}-\ell_b\right)\phi} e^{-i\Delta k z}\, \mathrm{d}\phi\, \mathrm{d}r, \tag{3.56}$$

where $\ell_{\tau,j}$ is the OAM of the j^{th} mode of frequency ω_τ. Unlike the rectangular waveguide, these matrices do not have simple analytical form, but the symmetry of the interactions can be understood from the perspective of the conservation of orbital angular momentum. As the Laguerre-Gaussian modes are separable in the variables (r, ϕ) we can take just the angular part of the interaction integral. Indeed, the integral along the azimuthal angle, ϕ, for arbitrary $\ell_{\tau,k}$ is

$$\int_0^{2\pi} e^{-i\left(\ell_{3,k}-\ell_{2,j}-\ell_b\right)\phi}\, \mathrm{d}\phi = 2\pi\delta_{\ell_{3,k},\ell_{2,k}+\ell_{1,k}}, \tag{3.57}$$

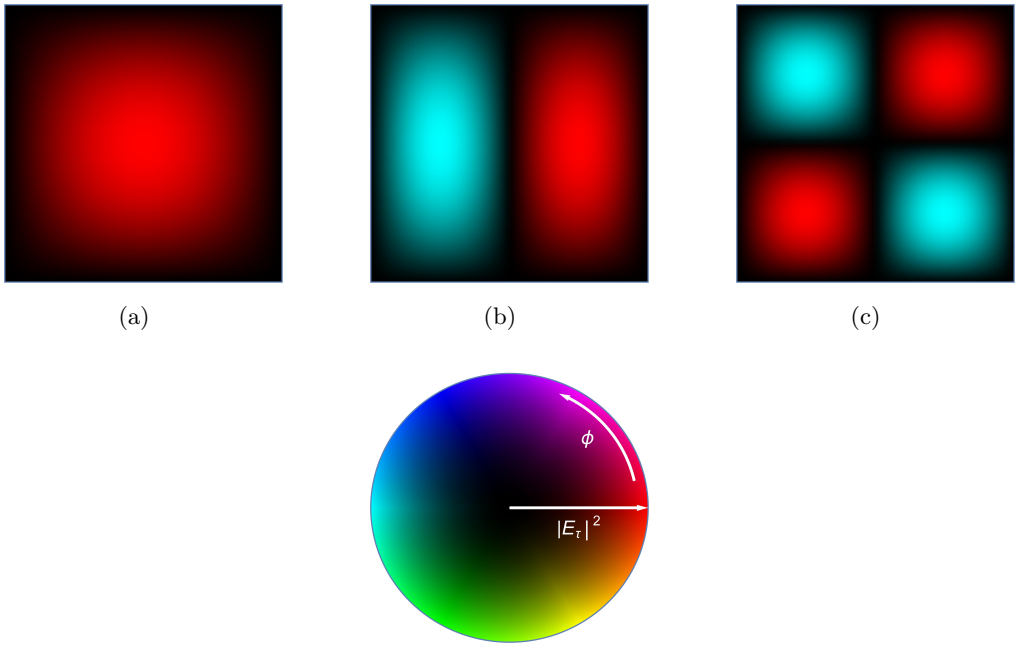

Figure 3.13: TM modes with indices (a) $(n, m) = (1, 1)$, (b) $(n, m) = (1, 2)$ and (c) $(n, m) = (2, 2)$ represented on false colour map (d) where colour denotes phase and hue denotes intensity.

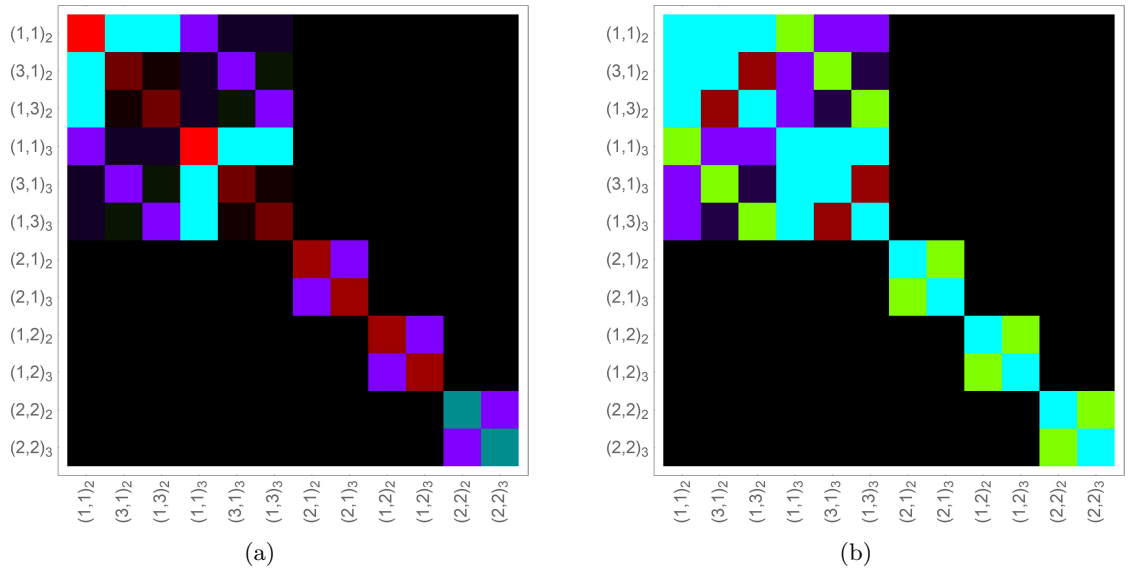

Figure 3.14: Scattering matrix, $\mathbf{S}$, for (a) TM_{11} and (b) TM_{22} background fields shown in figure 3.13 represented on the false colour map in figure 3.13 (d) where $(n, m)_\tau = (n_\tau, m_\tau)$.

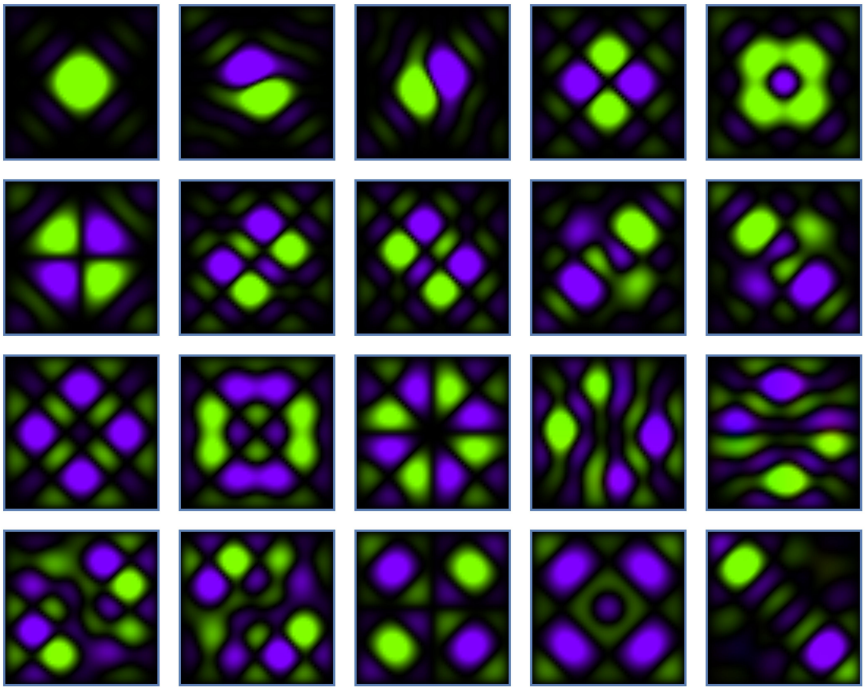

(a)

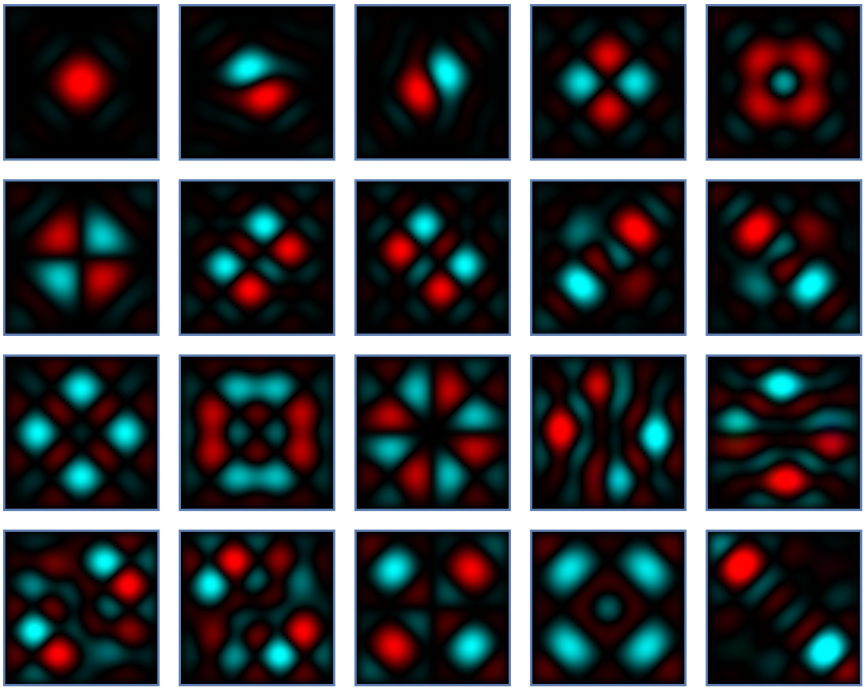

(b)

Figure 3.15: Intensity optical eigenmodes for a TM_{11} background with components (a) $\mathbb{F}_{2,k}(\mathbf{r}_2)$ and (b) $\mathbb{F}_{3,k}(\mathbf{r}_2)$ represented on the false colour map in figure 3.13 (d).

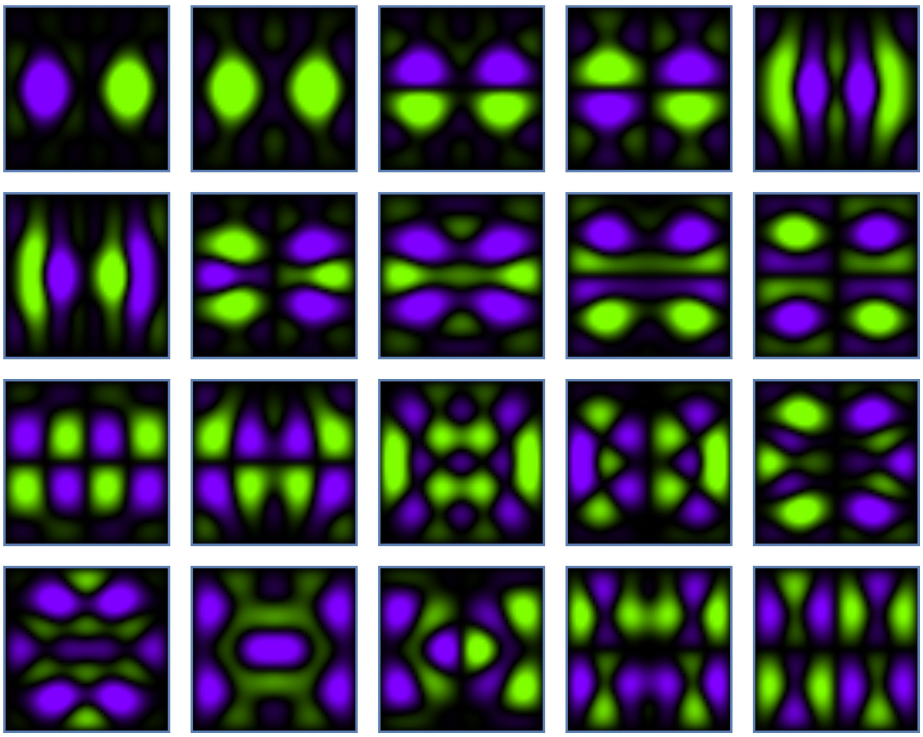

(a)

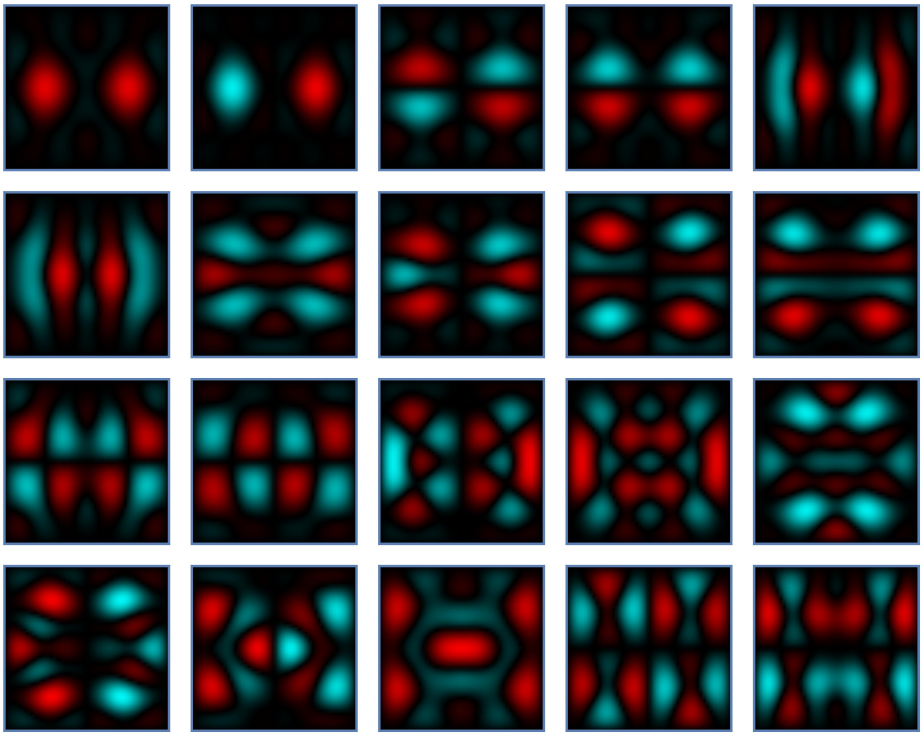

(b)

Figure 3.16: Intensity optical eigenmodes for a TM_{12} background with components (a) $\mathbb{F}_{2,k}(\mathbf{r}_2)$ and (b) $\mathbb{F}_{3,k}(\mathbf{r}_2)$ represented map in figure 3.13 (d).

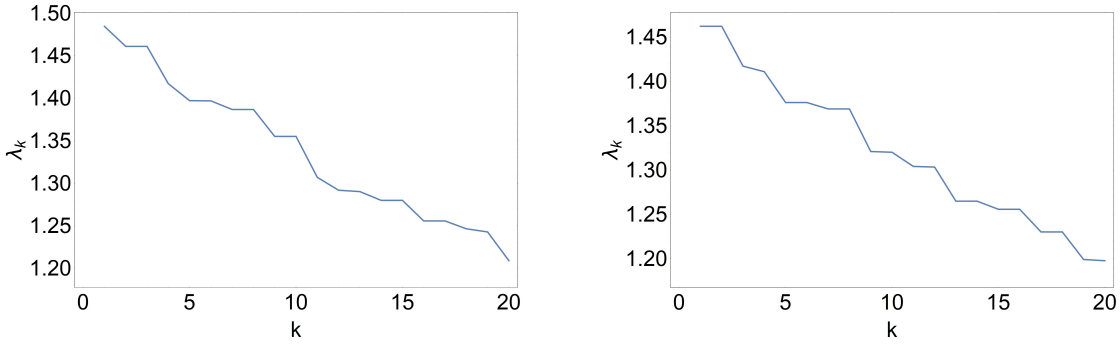

(a) (b)

Figure 3.17: Eigenvalues optical eigenmodes with (a) TM_{11} and (b) TM_{12} background field.

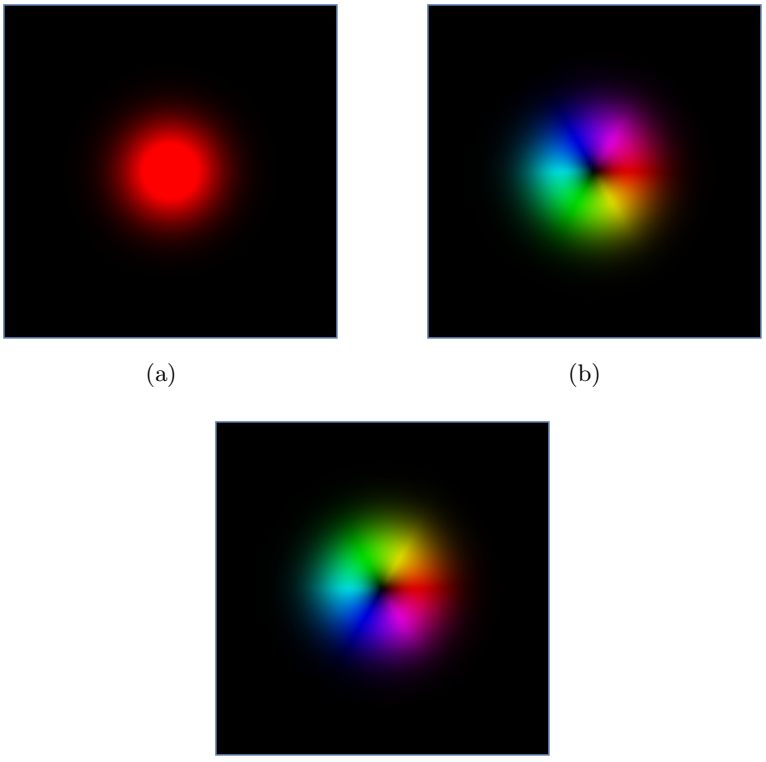

(a) (b)

(c)

Figure 3.18: LG modes with indices (a) $(\ell, p) = (0, 0)$, (b) $(\ell, p) = (1, 0)$ and (c) $(\ell, p) = (-1, 0)$.

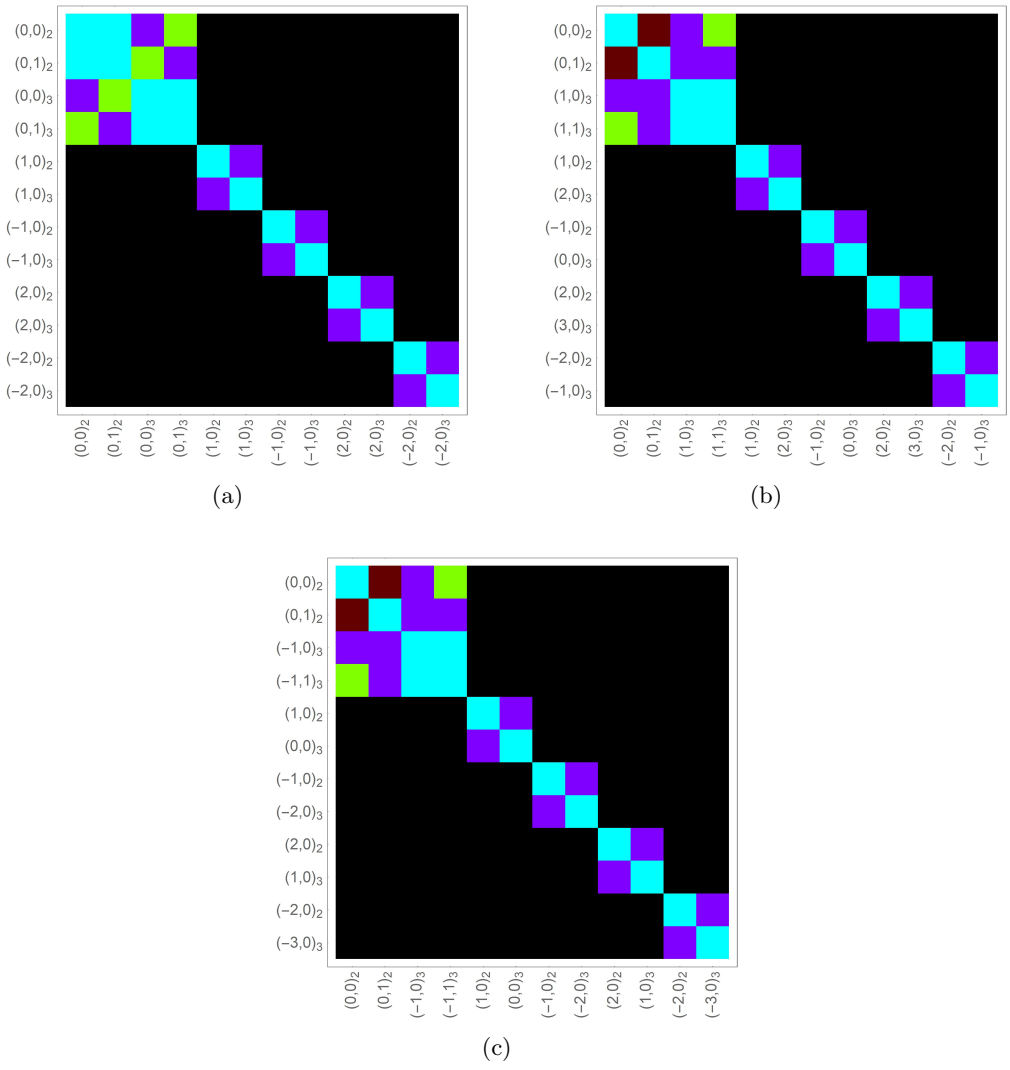

Figure 3.19: Scattering matrix, $\mathbf{S}$, for LG background fields shown in figure 3.18 represented on the false colour map in figure 3.13 (d) with indices $(\ell, p)_\tau = (\ell_\tau, p_\tau)$.

neglecting any constants of integration. The above integral shows that interactions between two perturbation fields and the background will only occur if the orbital angular momentum of the given interaction is conserved. The matrix elements of $v_{\tau,jk}$ can be shown to have similar behaviour where the dependence on the azimuthal angle is written

$$\int_0^{2\pi} e^{-i(\ell_{\tau,j}-\ell_{\tau,k})\phi}\,\mathrm{d}\phi = 2\pi\delta_{\ell_{\tau,j},\ell_{\tau,k}}, \tag{3.58}$$

which is non-zero if $\ell_{\tau,j} = \ell_{\tau,k}$. This is illustrated in figure 3.19, which shows the scattering matrix for multiple background fields which are displayed in figure 3.18.

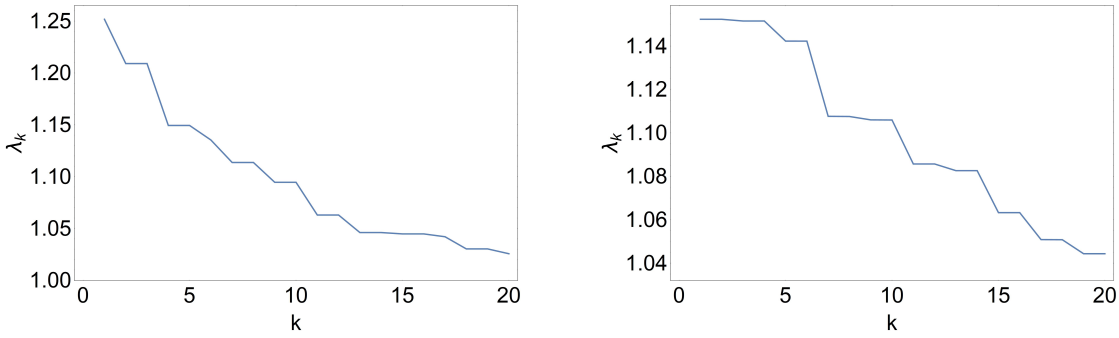

(a) (b)

Figure 3.20: Eigenvalues optical eigenmodes with (a) LG_{00} and (b) LG_{10} background field.

To calculate the optical eigenmodes, we consider the same probe space as chosen in section 3.3.3. Namely, a basis of 36 LG modes on each of the perturbation fields truncated with respect to $2p + |\ell| \leq 7$. As with previous examples, we show the first 20 intensity optical eigenmodes for the background fields in figure 3.18 (a) and (c). Again, similar to section 3.3.3, in the case of $\ell_b = +1$, we truncate the basis for each of the fields such that they are closed with respect to the interaction with the background, i.e., we take $\ell_2 = \{-7, \ldots, 7\}$ and $\ell_3 = \{-6, \ldots, 8\}$. As shown, from the interaction matrix, the only fields that interact are those that satisfy a selection rule which is reflected in the optical eigenmodes. Moreover, similar to the eigenmodes of bulk material shown in section 3.3.3, there are additional symmetries associated with the system that are not probed by the intensity operator. The degeneracy in this example arises from the same arguments made in section 3.3.3. Thus, we do not restate them here.

3.4.4 Propagation Eigenmodes

Hitherto, in this chapter, we have not yet discussed the propagation eigenmodes in a three-wave mixing scenario. We have already introduced the optical eigenmodes at the input and the output of a given optical system. However, we have said nothing about the behaviour of the eigenmodes as they evolve through the system. Using the coefficient form introduced in section 3.4.1, we define propagation eigenmodes that explicitly describe the evolution of the interacting fields through the nonlinear waveguide. One can develop some intuition for these propagation eigenmodes by assuming we have a single mode propagating in each of the wavelengths such that the matrices $\upsilon_{\tau,jk}$ and $g_{jk}(z)$ reduce to the coefficients υ_τ and $g(z)$. Similarly, the coefficient space in the single-mode case will consist of two elements, $a_2(z)$ and $a_3(z)$. The equations of propagation, in this case, reduce to the following form

$$-i\partial_z \begin{pmatrix} a_2(z) \\ a_3(z) \end{pmatrix} = \mathbf{P}(z) \begin{pmatrix} a_2(z) \\ a_3(z) \end{pmatrix} = \begin{pmatrix} \upsilon_2 & \chi_2 g(z) \\ \chi_3 g^*(z) & \upsilon_3 \end{pmatrix} \begin{pmatrix} a_2(z) \\ a_3(z) \end{pmatrix}. \tag{3.59}$$

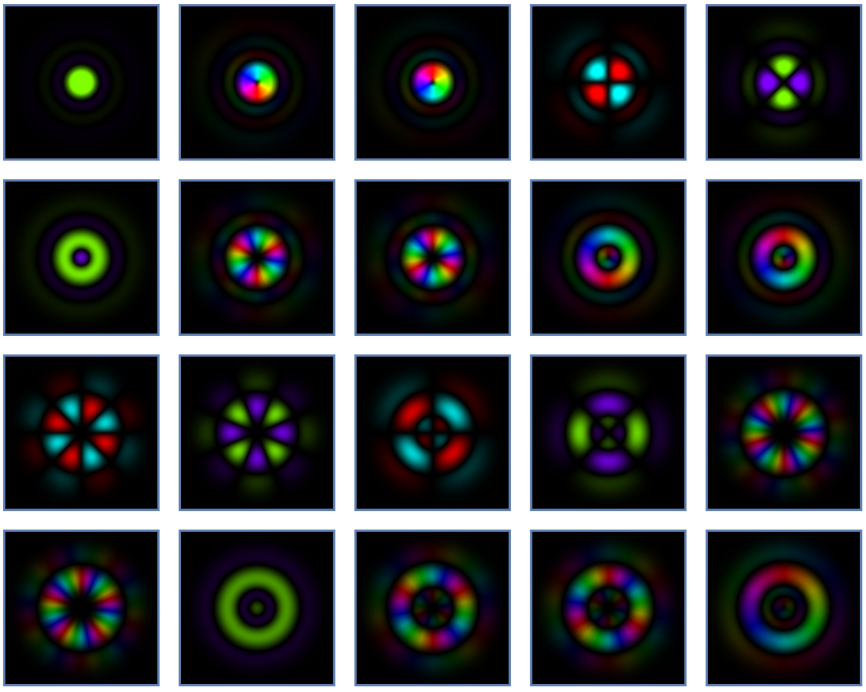

(a)

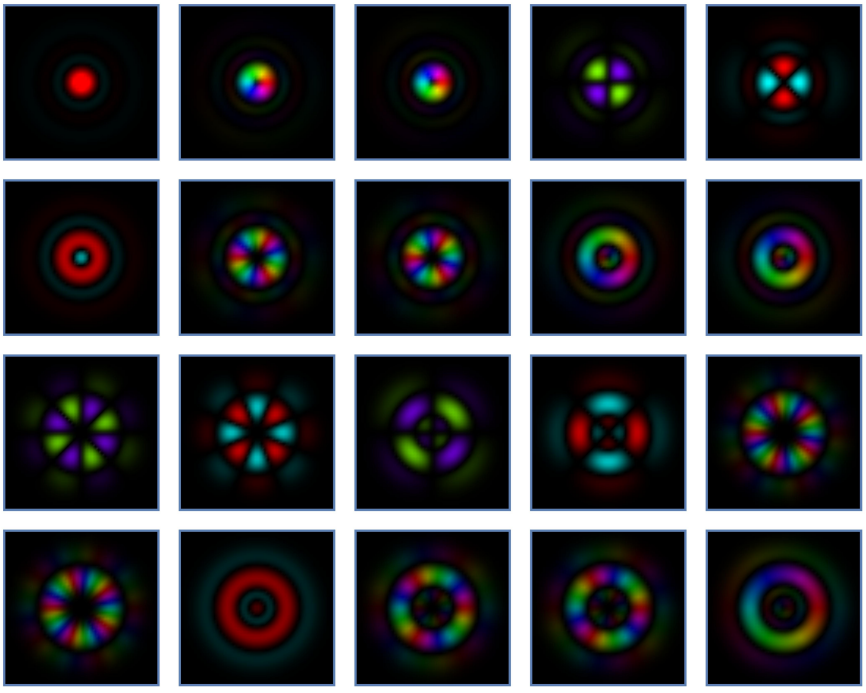

(b)

Figure 3.21: Intensity optical eigenmodes for a LG_{00} background with components (a) $\mathbb{F}_{2,k}(r_2)e^{-i\ell_{2,k}\phi}$ and (b) $\mathbb{F}_{3,k}(r_2)e^{-i\ell_{3,k}\phi}$ represented map in figure 3.13 (d).

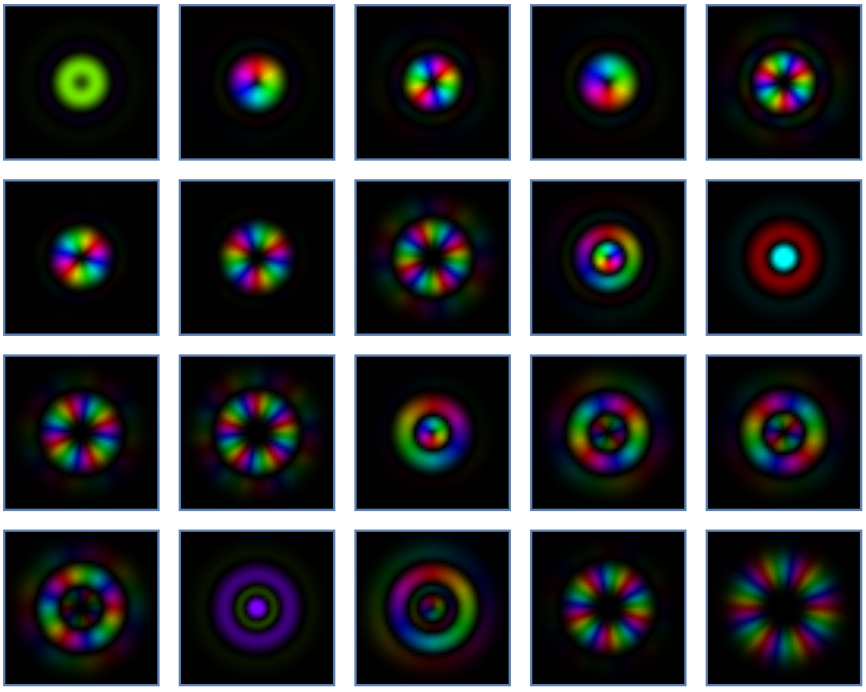

(a)

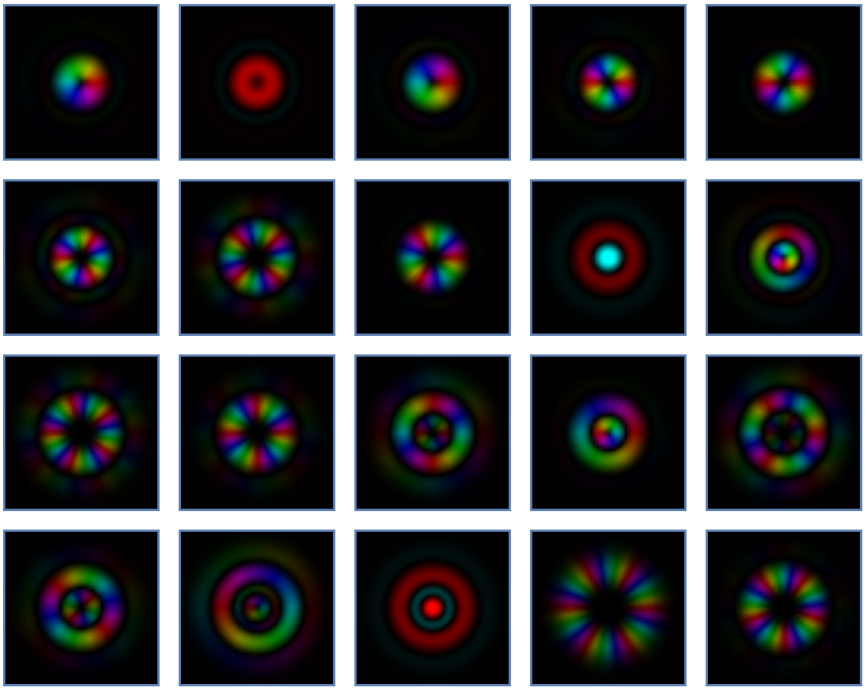

(b)

Figure 3.22: Intensity optical eigenmodes for a LG_{10} background with components (a) $\mathbb{F}_{2,k}(r_2)e^{-i\ell_{2,k}\phi}$ and (b) $\mathbb{F}_{3,k}(r_2)e^{-i\ell_{3,k}\phi}$ represented map in figure 3.13 (d).

Note, the matrix $\mathbf{P}(z)$ is not Hermitian due to the non-symmetric interaction strengths associated with the fields, that is, $\chi_2 \neq \chi_3$ with $\chi_\tau = \frac{\chi^{(2)}\omega_\tau}{n_\tau c}$. As the matrix is not Hermitian, the evolution of the field coefficients is not unitary, and the total energy density is not conserved. However, by transforming the fields, one can define a unitary matrix in the context of modified field variables - discussed in detail in section 4.3.1. Indeed, we make the transformations:

$$\alpha_2(z) = \frac{1}{\sqrt{\chi_3}} a_2(z), \tag{3.60}$$

$$\alpha_3(z) = \frac{1}{\sqrt{\chi_2}} a_3(z), \tag{3.61}$$

such that the evolution of the modified field coefficients is

$$-i\partial_z \begin{pmatrix} \alpha_2(z) \\ \alpha_3(z) \end{pmatrix} = \mathbf{P}'(z) \begin{pmatrix} \alpha_2(z) \\ \alpha_3(z) \end{pmatrix} = \begin{pmatrix} \upsilon_2 & g(z) \\ g^*(z) & \upsilon_3 \end{pmatrix} \begin{pmatrix} \alpha_2(z) \\ \alpha_3(z) \end{pmatrix}, \tag{3.62}$$

where the matrix $\mathbf{P}'(z)$ is Hermitian, and the evolution is, consequently, unitary. The transformations introduced in Eq. 3.60 and 3.61 normalise each of the coefficients with respect to the coupling strength of the other field such that the energy density which we define as $\sum_\tau \alpha_\tau(z)^* \alpha_\tau(z)$ is conserved. This conservation follows directly from the unitarity of the scattering matrix $\mathbf{S} = \exp\left(\int i\mathbf{P}'(z)\, dz\right)$. Indeed, for a Hermitian matrix with the property $\mathbf{P}'(z) = \mathbf{P}'^{\dagger}(z)$ we have

$$\begin{aligned} \mathbf{S}^\dagger \mathbf{S} &= \exp\left(\int_z i\mathbf{P}'(z)\mathrm{d}z\right) \exp\left(\int_z -i\mathbf{P}'^{\dagger}(z)\mathrm{d}z\right) \\ &= \exp\left(\int_z i\mathbf{P}'(z)\mathrm{d}z\right) \exp\left(\int_z -i\mathbf{P}'(z)\mathrm{d}z\right) = \mathbf{I}, \end{aligned} \tag{3.63}$$

where $\mathbf{I}$ is the identity matrix of the same dimensions as $\mathbf{S}$.

To illustrate the coupling between the fields, we consider stationary solutions of the matrix $\mathbf{P}'(z)$. That is eigenfunctions of the operator $-i\partial_z$ whose transverse structure is invariant with respect to the direction of propagation. Note, these solutions only exist in systems with translation invariance where $\partial_z \mathbf{P}'(z) = 0$ which is what we observe when the background field is z-independent, that is, $\partial_z g(z) = 0$. As a consequence of this translation invariance, field profiles that are eigenfunctions of the operator $-i\partial_z$ are found by diagonalising the following matrix

$$\mathbf{P}' = \begin{pmatrix} \upsilon_2 & g \\ g^* & \upsilon_3 \end{pmatrix}, \tag{3.64}$$

where

$$-i\partial_z \begin{pmatrix} a_2(z) \\ a_3(z) \end{pmatrix} = \mathbf{P}' \begin{pmatrix} a_2(z) \\ a_3(z) \end{pmatrix}. \tag{3.65}$$

The full solution of Eq. 3.65 is found to be of the form

$$\begin{pmatrix}\alpha_2(z)\\ \alpha_3(z)\end{pmatrix} = e^{i\delta z}\mathbf{W}(z)\begin{pmatrix}\alpha_2(0)\\ \alpha_3(0)\end{pmatrix} \tag{3.66}$$

where the matrix $\mathbf{W}(z)$ is

$$\mathbf{W}(z) = \begin{pmatrix}\mu\cos(\mu z) + i\upsilon\sin(\mu z) & ig\sin(\mu z)\\ ig\sin(\mu z) & \mu\cos(\mu z) - i\upsilon\sin(\mu z)\end{pmatrix} \tag{3.67}$$

and, for a crystal of length L, is related to the scattering matrix as $\mathbf{S} = e^{i\delta z}\mathbf{W}(z)|_{z=L}$. Note, in the matrix $\mathbf{W}(z)$ we have made use of the following substitutions:

$$\upsilon = \frac{(\upsilon_2 - \upsilon_3)}{2}, \tag{3.68}$$

$$\delta = \frac{(\upsilon_2 + \upsilon_3)}{2}, \tag{3.69}$$

and

$$\mu = \sqrt{|g|^2 + \upsilon^2}. \tag{3.70}$$

The argument μ in the trigonometric functions in the solution is always real regardless of the gain associated with the background field, g. Therefore, the solutions always exhibit oscillatory behaviour while interacting with one another. This is unsurprising as it is the same behaviour of the solutions found in section 2.3.2, where we considered sum-frequency generation in 1D. In this simplified case, where we have a single mode on each field, the eigenvalues of the matrix $\mathbf{P'}$ are of the form

$$\lambda_k = \delta \pm \mu \tag{3.71}$$

with corresponding eigenvectors given by $v_k = (\upsilon \pm \mu, g^*)^\top$. As discussed in section 3.2.1, the components of these eigenmodes will interact with one another due to the off-diagonal interaction terms in the scattering matrix. This interaction is dependent on the overlap with the background field given by the coefficient g which, for a stationary background field, is given by

$$g = \iint E_b^*(x,y) f_2^*(x,y) f_3(x,y)\ \mathrm{d}x\ \mathrm{d}y. \tag{3.72}$$

Thus, we observe from the above expression that the coupling strength of any two modes will be dependent on their overlap with the background field: a property that we observed in all of the intensity eigenmodes introduced in previous sections. Note, the operator $-i\partial_z$ acts to generate linear translations in the positive z-direction corresponding to momentum or energy transfer. The Hermiticity of this momentum operator follows from the Hermiticity of the matrix $\mathbf{P'}$, and by summing the eigenvalues of the matrix, $\sum_k \lambda_k = 2\delta = \upsilon_2 + \upsilon_3$, we

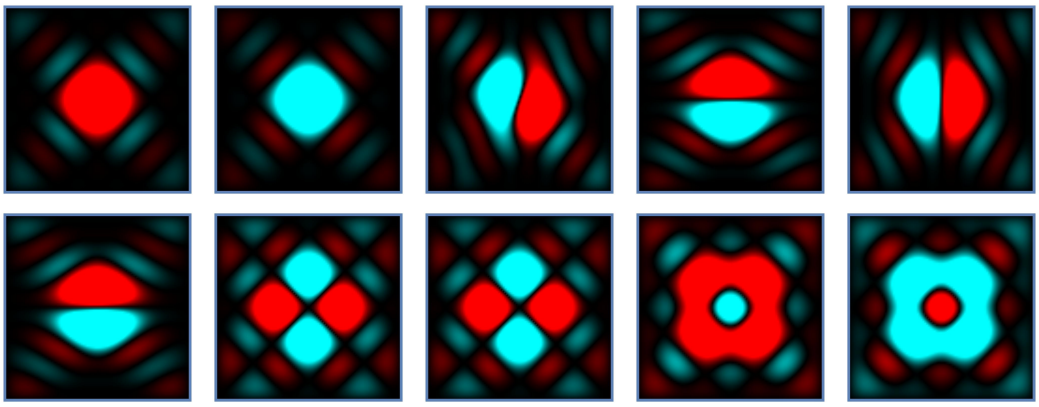

(a)

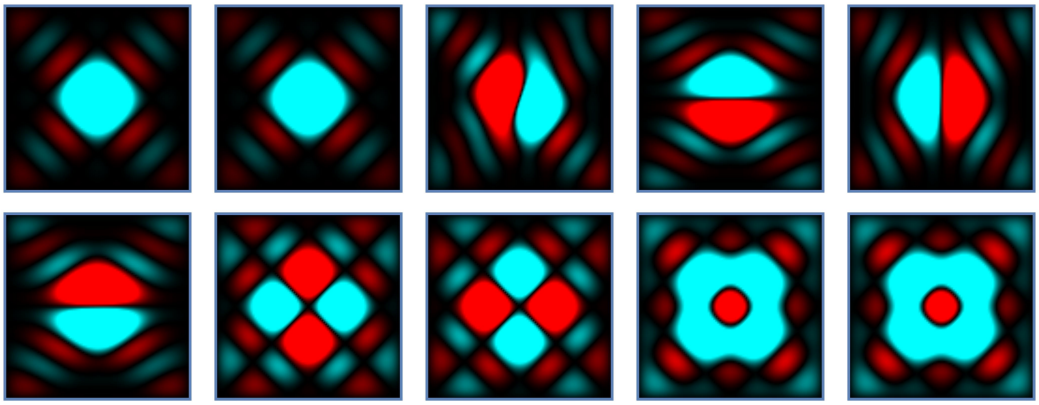

(b)

Figure 3.23: Propagation eigenmodes for a TM_{11} background with components (a) $\mathbb{F}_{2,k}(\mathbf{r}_2)$ and (b) $\mathbb{F}_{3,k}(\mathbf{r}_2)$.

find that the total linear momentum or energy density is conserved. Indeed, at the input of the thin slice of nonlinear material, we have no interaction between the fields. Therefore, if we set $g = 0$ in the matrix $\mathbf{P}'$, we find that the sum of the eigenvalues is also equal to $\upsilon_2 + \upsilon_3$. This result is unsurprising as we are in a lossless system in which the energy density is conserved.

This intuition can be extended to the multimode case in which we have more than one element in the decomposition for the interacting fields where Eq. 3.65 is now

$$-i\partial_z \begin{pmatrix} a_{2,j}(z) \\ a_{3,j}(z) \end{pmatrix} = \begin{pmatrix} \upsilon_{2,jk} & g_{jk} \\ g^*_{kj} & \upsilon_{3,jk} \end{pmatrix} \begin{pmatrix} a_{2,k}(z) \\ a_{3,k}(z) \end{pmatrix} = \mathbf{Q} \begin{pmatrix} a_{2,k}(z) \\ a_{3,k}(z) \end{pmatrix}. \tag{3.73}$$

Although one cannot derive a precise analytical form of the eigenvalues and eigenvectors in this context, the behaviour of the eigenmodes in a multimode system is equivalent to the single-mode case. Indeed, the eigenmodes are orthogonal to one another and have

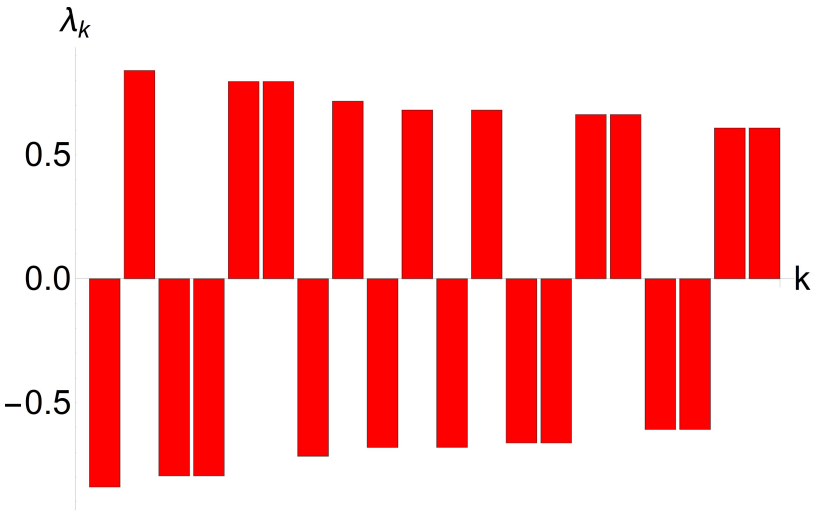

Figure 3.24: Eigenvalues λ_k for the propagation eigenmodes shown in figure 3.23.

some propagating term and coupling with the background field that is characteristic of that particular combination of fields. Indeed, we can make the transformation:

$$\beta_k(z) = \mathbf{U}^\dagger \left(\alpha_{2,k}(z), \alpha_{3,k}(z)\right)^\top,$$

where $\mathbf{U}^\dagger$ is made up of the eigenvectors of the matrix $\mathbf{Q} = \mathbf{U}\mathbf{\Lambda}\mathbf{U}^\dagger$, such that the equations of propagation are

$$\beta_k(z) = e^{i\lambda_k z}\beta_k(0), \tag{3.74}$$

where the eigenvalues λ_k correspond to the non-zero elements of the diagonal matrix $\mathbf{\Lambda}$. If we take, for example, a rectangular waveguide with the same basis set as used in section 3.4.2 then the first 10 propagation modes for a TM_{11} background field are as shown in figure 3.23. The corresponding eigenvalues are illustrated in the bar chart in figure 3.24. As expected, the eigenvalues behave like that of the single-mode case, that is, of the form of Eq. 3.71 with the sum $\sum_k \lambda_k \approx 0$.

Although we do not have a precise analytical form for the eigenmodes in the multimode case; one can, from the full solution given by Eq. 3.67, find the following single-mode eigenvalues for a nonlinear crystal of length L

$$\lambda_k = e^{i\delta L}\left(\mu\,\cos(\mu L) \pm \sqrt{-\left(\upsilon^2 + |g|^2\right)\,\sin(\mu L)^2}\right), \tag{3.75}$$

with corresponding eigenvectors

$$v_k = \left(-\upsilon\sin(\mu L) \pm i\sqrt{-\left(\upsilon^2 + |g|^2\right)\,\sin(\mu L)^2}, g^*\sin(\mu L)\right)^\top. \tag{3.76}$$

The eigenvalues, much like those for the non-diffracting fields described above, have a phase term independent of the background and an interaction term that depends on $E_b(x, y)$ with the coefficient g^*. These eigenmodes are sinusoidal like functions that interact with a background field and oscillate between some minimum value at the input and some maximum value at the interaction length of the nonlinear crystal [8, 9]. If the argument $\mu L = n\pi$ then $\sin(\mu L) = 0$ and the low-intensity fields will be decoupled, resulting in degenerate eigenmodes. Similarly, when $\mu L = n\pi/2$, the eigenvalues are complex, and the background field has a maximal coupling with the perturbation fields. This interaction is similar to that described above in which the fields are eigenfunctions of the operator $-i\partial_z$. Certainly, if we consider the fields propagating through a thin slice of nonlinear material, they will behave approximately like the stationary eigenmodes. Indeed, if the thin slice is of length $\epsilon \ll L$ the eigenvectors given in Eq. 3.76 reduce to the eigenvectors associated with the eigenvalues in Eq. 3.71. Moreover, for a crystal of length L, one can calculate the evolution of the fields by concatenating $n = \epsilon L$ thin slices of nonlinear material in which the fields are approximately invariant with respect to the direction of propagation.

3.5 Parametric Down-Conversion

Parametric down-conversion, much like sum-frequency generation discussed in the previous section, has proved a useful effect in the physical sciences. In this section, we are concerned with introducing optical eigenmodes to this effect in the same manner as done for sum-frequency generation in section 3.2.1. Note, although the introduction of optical eigenmodes in this context is formally very similar to that of sum-frequency generation, we begin the section by defining the optical eigenmodes for parametric down-conversion. Following this, we take some examples of optical eigenmodes in waveguides, where the distinction between down-conversion and sum-frequency generation is most apparent. Finally, at the end of the section, we discuss the propagation eigenmodes.

3.5.1 Optical Eigenmodes in Parametric Down-Conversion

We begin with the equations:

$$-i\frac{\partial}{\partial z}E_1(\mathbf{r}) = \frac{1}{2k_1}\nabla_T^2 E_1(\mathbf{r}) + \chi_1 E_2^*(\mathbf{r})E_b(\mathbf{r})e^{-i\Delta kz}, \tag{3.77}$$

$$-i\frac{\partial}{\partial z}E_2(\mathbf{r}) = \frac{1}{2k_2}\nabla_T^2 E_2(\mathbf{r}) + \chi_2 E_1^*(\mathbf{r})E_b(\mathbf{r})e^{-i\Delta kz}, \tag{3.78}$$

$$-i\frac{\partial}{\partial z}E_b(\mathbf{r}) = \frac{1}{2k_3}\nabla_T^2 E_b(\mathbf{r}), \tag{3.79}$$

where $E_{3,b}(\mathbf{r}) = E_b(\mathbf{r})$ corresponds to the high-intensity pump field oscillating at ω_3. Notice, unlike the equations for sum-frequency generation the above are conjugate linear. That is, the field $E_1(\mathbf{r})$ is dependent on $E_2^*(\mathbf{r})$ and similarly, $E_2(\mathbf{r})$ is dependent on $E_1^*(\mathbf{r})$. Again, we decompose the fields in the input plane as

$$E_\tau(\mathbf{r}_1) = \sum_{j=1}^{N} a_{\tau,j} E_{\tau,j}(\mathbf{r}_1). \tag{3.80}$$

The fields $E_{\tau,j}(\mathbf{r}_1)$ form an orthogonal basis at the input of the nonlinear material,

$$\iiint E^*_{\tau,j}(\mathbf{r}_1) E_{\sigma,k}(\mathbf{r}_1) e^{-i(\omega_\sigma - \omega_\tau)t}\,\mathrm{d}x_1\,\mathrm{d}y_1\,\mathrm{d}t = 2\pi\delta(\omega_\tau - \omega_\sigma)\delta_{jk}, \tag{3.81}$$

and evolve according to the equations:

$$-i\frac{\partial}{\partial z}E_{1,j}(\mathbf{r}) = \frac{1}{2k_1}\nabla_T^2 E_{1,j}(\mathbf{r}) + \sum_{k=1}^{N} \chi_1 E^*_{2,k}(\mathbf{r}) E_b(\mathbf{r}) e^{-i\Delta k z}, \tag{3.82}$$

$$-i\frac{\partial}{\partial z}E_{2,j}(\mathbf{r}) = \frac{1}{2k_2}\nabla_T^2 E_{2,j}(\mathbf{r}) + \sum_{k=1}^{N} \chi_2 E^*_{1,k}(\mathbf{r}) E_b(\mathbf{r}) e^{-i\Delta k z}, \tag{3.83}$$

resulting in the following decomposition at the output plane

$$F_\tau(\mathbf{r}_2) = \sum_{j=1}^{N} a_{\tau,j} F_{\tau,j}(\mathbf{r}_2). \tag{3.84}$$

As a proof of concept, we introduce the intensity of the small perturbation fields at the output as

$$I = \sum_{\tau}\sum_{j,k}^{N} a^*_{\tau,j} a_{\tau,k} \left(\int_\Omega \frac{1}{2} n_\tau \epsilon_0 c\; F^*_{\tau,j}(\mathbf{r}_2) F_{\tau,k}(\mathbf{r}_2) \mathrm{d}\Omega \right) = \mathbf{a}^\dagger \mathbf{M} \mathbf{a}, \tag{3.85}$$

where Ω is some region of interest in the output plane and the vectors $\mathbf{a}$ contain complex coefficients and their conjugates

$$\mathbf{a} = (a_{\tau,1}, \ldots, a_{\tau,N}, a_{\sigma,1}, \ldots, a_{\sigma,N})^T \tag{3.86}$$

and

$$\mathbf{a}^\dagger = \left(a^*_{\tau,1}, \ldots, a^*_{\tau,N}, a^*_{\sigma,1}, \ldots, a^*_{\sigma,N}\right) \tag{3.87}$$

and N is the number of independent basis elements in Eq. 3.80. We can write the total intensity as the sum of two distinct components as

$$\begin{aligned} I &= \sum_{j,k}^{N} \int_\Omega \left(\frac{1}{2} n_1 \epsilon_0 c\; a^*_{1,j} a_{1,k} F^*_{1,j}(\mathbf{r}_2) F_{1,k}(\mathbf{r}_2) + \frac{1}{2} n_2 \epsilon_0 c\; a^*_{2,j} a_{2,k} F^*_{2,j}(\mathbf{r}_2) F_{2,k}(\mathbf{r}_2) \right) \mathrm{d}\Omega \\ &= \mathbf{a}_1^\dagger \mathbf{M}_1 \mathbf{a}_1 + \mathbf{a}_2^\dagger \mathbf{M}_2 \mathbf{a}_2 \\ &= \mathbf{a}^\dagger \mathbf{M} \mathbf{a}. \end{aligned} \tag{3.88}$$

By diagonalising the cross-interaction matrix we define the optical eigenmodes at the output and input as:

$$\mathbb{F}_{\tau,k}(\mathbf{r}_2) = \sum_{j=1}^{N} v_{kj} F_{\tau,j}(\mathbf{r}_2), \tag{3.89}$$

$$\mathbb{E}_{\tau,k}(\mathbf{r}_1) = \sum_{j=1}^{N} v_{kj} E_{\tau,j}(\mathbf{r}_1), \tag{3.90}$$

where v_{kj} are the elements of the k^{th} eigenvector of $\mathbf{M}$ associated with the eigenvalue λ_k.

Although mathematically similar to the formalism outlined in section 3.2.1, there is a distinction between the optical eigenmodes of sum-frequency generation and parametric down-conversion. The most notable distinction is the conjugate linearity of Eq. 3.77 and 3.78. However, when we consider an optical measure, this conjugate linearity is not apparent due to the Hermicity of the related operators. This does, however, have interesting implications when considering the propagation modes of the system and can be problematic when we go towards the single-photon level - discussed in more detail in section 4.4.1.

3.6 Optical Eigenmodes in Waveguides

In the context of an optical waveguide, the system is best solved in terms of the 1D coefficients as done in section 3.4.1. If we assume, as in section 3.4.1, that the propagation modes defined in section 1.3.4 and 1.3.3 form our basis, the link between the coefficients and the fields is given by

$$E_\tau(\mathbf{r}) = \sum_{j=1}^{N} a_{\tau,j}(z) f_{\tau,j}(x,y), \tag{3.91}$$

where $f_{\tau,j}(x,y)$ describe a Hilbert space with orthogonal basis elements,

$$\iiint f^*_{\tau,j}(x,y) f_{\sigma,k}(x,y) e^{-i(\omega_\sigma - \omega_\tau)t} \,\mathrm{d}x\,\mathrm{d}y\,\mathrm{d}t = 2\pi\delta(\omega_\tau - \omega_\sigma)\delta_{jk}. \tag{3.92}$$

If we input this field expansion into the equations for parametric down-conversion we have:

$$-i\partial_z a_{1,j}(z) = \sum_{k=1}^{N} \upsilon_{1,jk} a_{1,k}(z) + \chi_2 g_{jk}(z) a^*_{2,k}(z), \tag{3.93}$$

$$-i\partial_z a_{2,j}(z) = \sum_{k=1}^{N} \upsilon_{2,jk} a_{2,k}(z) + \chi_3 g_{kj}(z) a^*_{1,k}(z), \tag{3.94}$$

with the matrices

$$\upsilon_{\tau,jk} = \iint \frac{1}{2k_\tau} \, f^*_{\tau,j}(x,y) \nabla^2_T f_{\tau,k}(x,y) \,\mathrm{d}x\,\mathrm{d}y, \tag{3.95}$$

and

$$g_{jk}(z) = \iint f^*_{1,j}(x,y) f^*_{2,k}(x,y) E_b(x,y,z) e^{-i\Delta k z}\,\mathrm{d}x\,\mathrm{d}y, \tag{3.96}$$

where $\Delta k = k_b + k_2 - k_3$ is the phase mismatch. Due to the conjugate linearity of the equations, the scattering matrix mixes the coefficients and their conjugates. Consequently, we have

$$\begin{pmatrix} a'_{1,k} \\ a'_{2,k} \\ a^{*'}_{1,k} \\ a^{*'}_{2,k} \end{pmatrix} = \mathbf{S} \begin{pmatrix} a_{1,k} \\ a_{2,k} \\ a^*_{1,k} \\ a^*_{2,k} \end{pmatrix} \tag{3.97}$$

where $a_{\tau,k}$ are the field amplitudes of the modes at the input and $a'_{\tau,k}$ are the amplitudes of the corresponding output modes and $\mathbf{S} = \exp\left(\int_z i\mathbf{P}(z)\mathrm{d}z\right)$ with

$$\mathbf{P}(z) = \begin{pmatrix} \upsilon_{1,jk} & 0 & 0 & \chi_1 g_{jk}(z) \\ 0 & \upsilon_{2,jk} & \chi_2 g_{kj}(z) & 0 \\ 0 & -\chi_1 g^*_{jk}(z) & -\upsilon_{1,jk} & 0 \\ -\chi_2 g^*_{kj}(z) & 0 & 0 & -\upsilon_{2,jk} \end{pmatrix}. \tag{3.98}$$

The above matrix can be reordered and made block-diagonal with respect to the pairs $\left(a_{1,k}, a^*_{2,k}\right)$ and $\left(a^*_{1,k}, a_{2,k}\right)$ with

$$-i\partial_z \begin{pmatrix} a'_{1,k} \\ a^{*'}_{2,k} \end{pmatrix} = \begin{pmatrix} \upsilon_{1,jk} & \chi_1 g_{jk}(z) \\ -\chi_2 g^*_{kj}(z) & -\upsilon_{2,jk} \end{pmatrix} \begin{pmatrix} a_{1,k} \\ a^*_{2,k} \end{pmatrix} \tag{3.99}$$

and

$$-i\partial_z \begin{pmatrix} a^{*'}_{1,k} \\ a'_{2,k} \end{pmatrix} = \begin{pmatrix} -\upsilon_{1,jk} & -\chi_1 g^*_{kj}(z) \\ \chi_2 g_{kj}(z) & \upsilon_{2,jk} \end{pmatrix} \begin{pmatrix} a^*_{1,k} \\ a_{2,k} \end{pmatrix}, \tag{3.100}$$

where one of the above gives the full solution of the system as $\left(a_{1,k}, a^*_{2,k}\right)^* = \left(a^*_{1,k}, a_{2,k}\right)$. The eigenmodes, in this case, are defined at the output and input planes as in Eq. 3.49 and 3.50, respectively.

3.7 Numerical Examples

In this section, we show some examples of optical eigenmodes in the context of parametric down-conversion using the same set up as in section 3.3.1. As the symmetry associated with the optical eigenmodes follows the arguments of section 3.3.2 and 3.3.3, we do not include examples of eigenmodes in a bulk material. Indeed, in order to highlight the distinction between the two effects, we consider the case of optical waveguides in which the differences between the two sets of equations can be analysed from a theoretical perspective.

3.7.1 Rectangular Waveguide

In this section, we consider some numerical examples of the intensity optical eigenmodes in waveguides for parametric down-conversion. In the first instance, we consider a rectangular waveguide with perfectly reflecting walls, as described in section 1.3.4. Our fields are decomposed in Hilbert space with basis elements of the following form

$$f_{nm}(x,y) = \sin\left(\frac{n\pi}{2b}x - n\frac{\pi}{2}\right)\ \sin\left(\frac{m\pi}{2c}y - m\frac{\pi}{2}\right), \tag{3.101}$$

where b and c correspond to the transverse dimensions of the waveguide. Due to the reality of the basis fields at the input, the matrix elements $\upsilon_{\tau,ij}$ are identical to that of section 3.4.2, i.e.,

$$\upsilon_{\tau,jk} = -\frac{(bm_j + cn_j)^2\pi^2}{4bc}\ \delta_{n_j,n_k}\delta_{m_j,m_k}. \tag{3.102}$$

Similarly, the interaction terms, $g_{jk}(z)$, will also be the same as derived for the sum-frequency generation case,

$$g_{jk}(z) = \frac{\zeta_n\left(1 \pm \cos\left(n_j\pi\right)\cos\left(n_k\pi\right)\right)}{(n_j^4 + (n_k^2 - n_b^2)^2 - 2n_j^2(n_k^2 + n_b^2))\pi^2}\frac{\zeta_m\left(1 \pm \cos\left(m_j\pi\right)\cos\left(m_k\pi\right)\right)}{(m_j^4 + (m_k^2 - m_b^2)^2 - 2m_j^2(m_k^2 + m_b^2))}e^{-i\Delta kz}, \tag{3.103}$$

with $\zeta_n = 4bn_bn_jn_k$ and $\zeta_m = 4cm_bm_jm_k$. Again, the numbers n_b and m_b correspond to the background field indices, which determines the sign of the matrix element. Although the interaction and phase term matrices are the same as in section 3.4.2, the scattering matrices couple different modes due to the conjugate linearity of the system. Indeed, this feature of the effect is what leads to an overall gain in the intensity of the perturbation fields as they propagate through the material. The symmetry of the intensity eigenmodes, therefore, can be easily understood with respect to the overall gain of their components. This gain is determined by the exchange of energy from the background field, and the eigenmodes that overlap most with the background will interfere more than those with only a small overlap. This is observed in the eigenmodes presented in figure 3.25, where we consider a TM mode basis truncated at $n+m \leq 7$ with a TM_{11} background field. The corresponding eigenvalues are shown in figure 3.26.

3.7.2 Circular Waveguide

As illustrated in section 3.4.3, systems with circular symmetry are best solved with the Laguerre-Gaussian modes introduced in section 1.3.3. Much like the rectangular waveguide, the results for the equations for parametric down-conversion are similar to those presented for sum-frequency generation in the previous section. Indeed, given the same set of basis elements the matrix $\upsilon_{\tau,jk}$ is identical for both sets of equations. The integral for the matrix

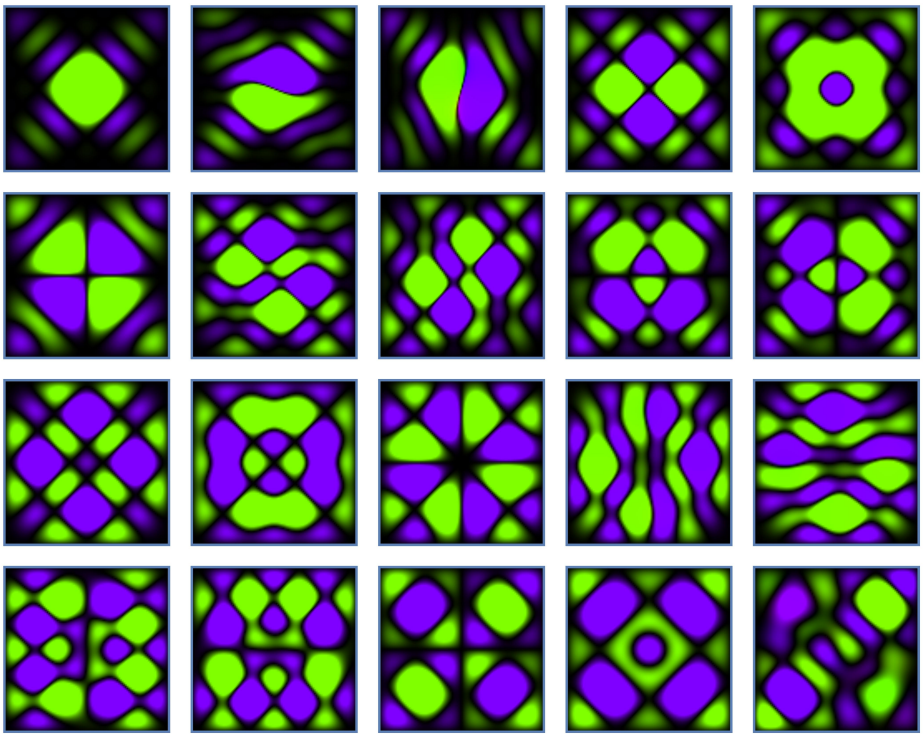

(a)

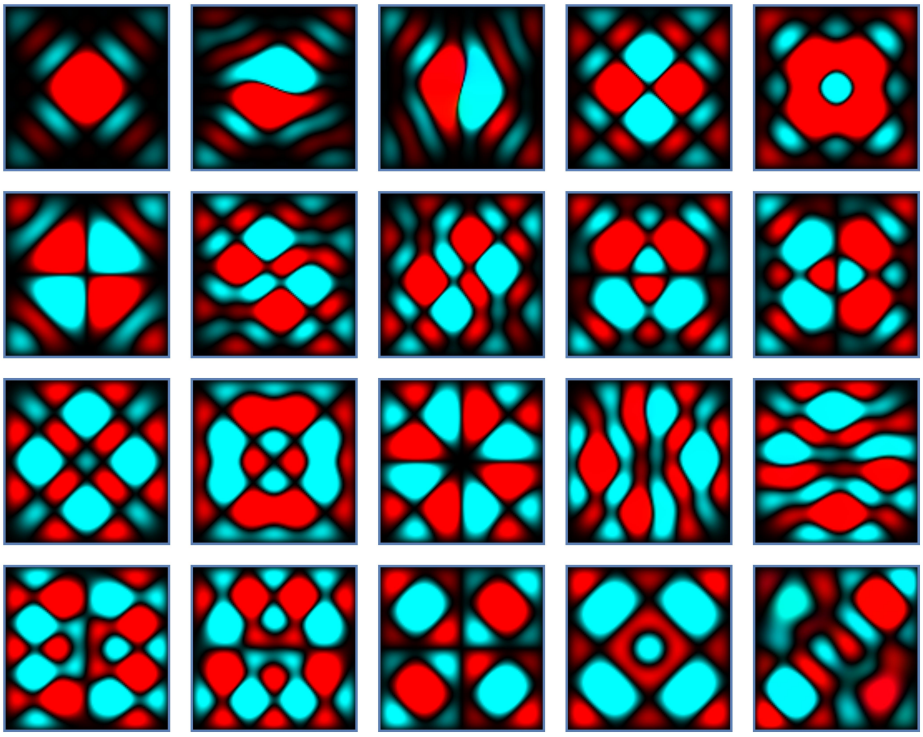

(b)

Figure 3.25: SPDC intensity optical eigenmodes for a TM_{11} background with components (a) $\mathbb{F}_{1,k}(\mathbf{r}_2)$ and (b) $\mathbb{F}_{2,k}(\mathbf{r}_2)$ represented map in figure 3.13 (d).

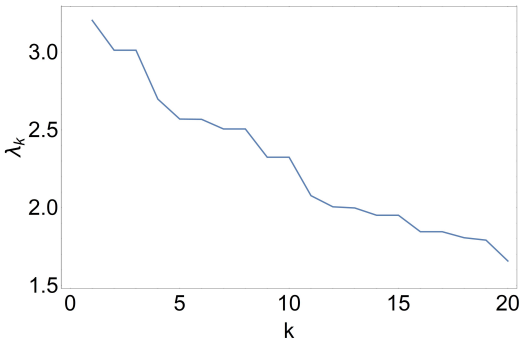

Figure 3.26: Eigenvalues for the intensity optical eigenmodes shown in figure 3.25.

$g_{jk}(z)$ is slightly different, however, resulting in different selection rules for interactions. This is unsurprising as the background field is oscillating at a different frequency. For $g_{jk}(z)$ in a Laguerre-Gaussian basis with fields of the form of Eq. 1.16 we have

$$g_{jk}(z) = \iint f^*_{1,j}(r) f^*_{2,k}(r) E_b(r,z) e^{-i\left(\ell_b - \ell_{2,k} - \ell_{1,j}\right)\phi} e^{-i\Delta k z} \, \mathrm{d}r\mathrm{d}\phi. \tag{3.104}$$

If we consider the interaction of two of the basis elements, we can evaluate the integral along the azimuthal angle, ϕ, as,

$$\int_0^{2\pi} e^{-i(\ell_b - \ell_2 - \ell_1)\phi} \, \mathrm{d}\phi = 2\pi\delta_{\ell_b, \ell_2 + \ell_1}, \tag{3.105}$$

neglecting any constants of integration. Therefore, interactions of fields that obey the selection rule $\ell_b = \ell_2 + \ell_1$ will exchange energy between one another. Similar to section 3.4.3, the selection rules for the OAM of the fields are observed in the field profiles of the intensity optical eigenmodes. To illustrate this, we consider a finite basis of Laguerre-Gaussian modes truncated with respect to the maximal index $2p + |\ell| \leq 7$. In this section, we consider a single example in which the background field has vortex charge $\ell_b = +1$. Therefore, to ensure the basis for the two perturbation fields is closed with respect to interaction with the background, we choose the basis to be $\ell_2 = \{-6, \ldots, 8\}$ such that we can have $\ell_1 = \{-7, \ldots, 7\}$ and satisfy the relation $\ell_1 + \ell_2 = \ell_b$ for all the elements. A more detailed discussion of this basis shift is outlined in section 3.3.3. The first 20 intensity optical eigenmodes for a background field with $\ell_b = +1$ are shown in figure 3.27. In all cases, we observe the selection rules for the orbital angular momentum.

3.7.3 Propagation Eigenmodes

Similar to section 3.4.4, we can develop some intuition with respect to the propagation eigenmodes of parametric down-conversion by considering the case where we have a single

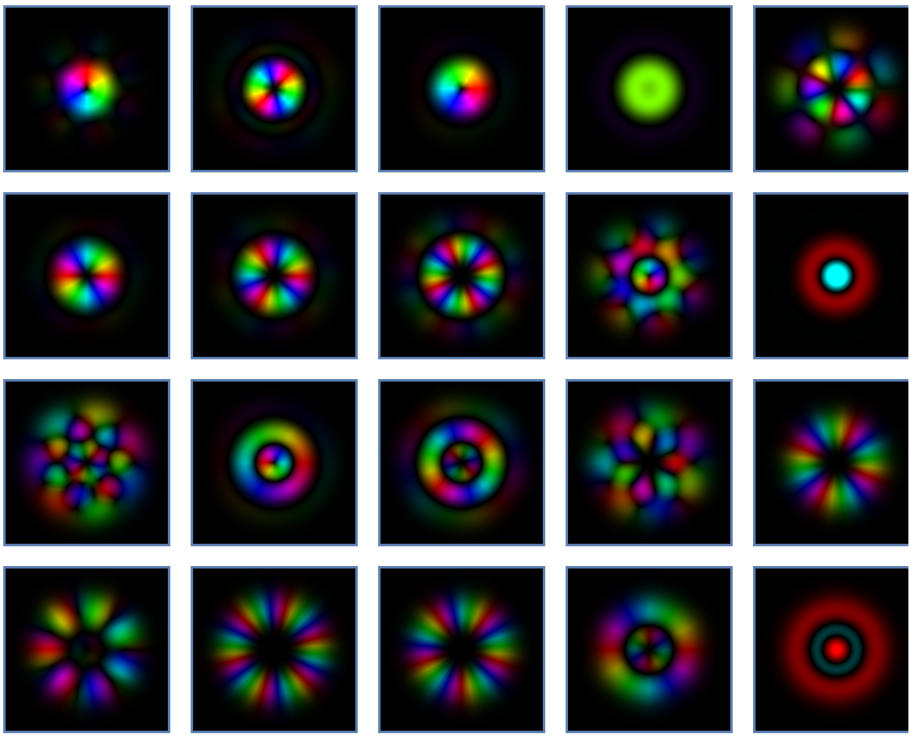

(a)

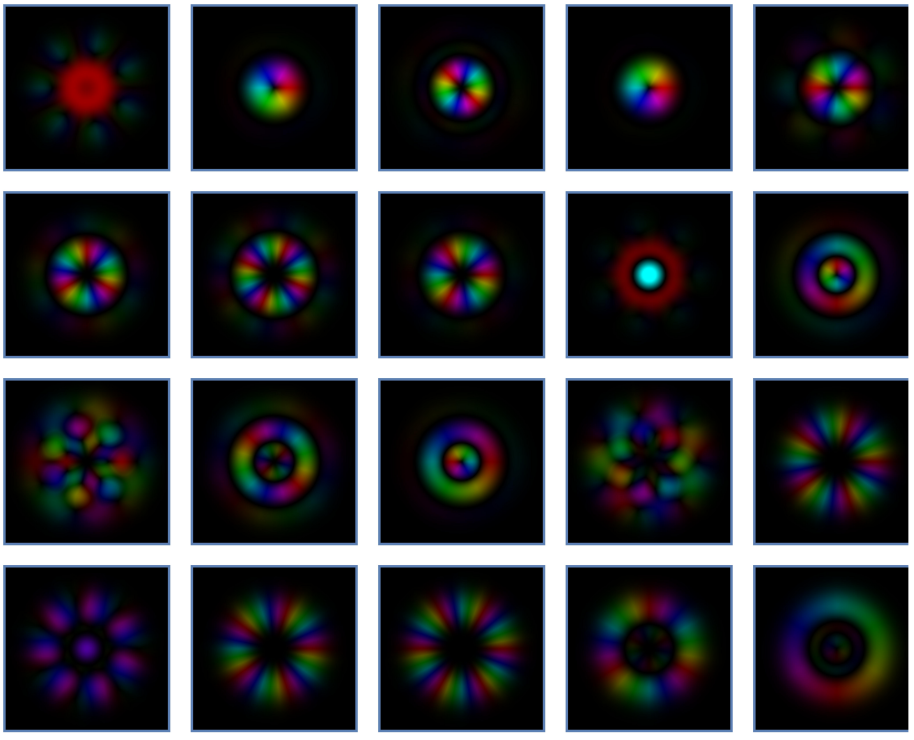

(b)

Figure 3.27: SPDC intensity optical eigenmodes for a LG_{10} background field with components (a) $\mathbb{F}_{1,k}(r_2)e^{-i\ell_{1,k}\phi}$ and (b) $\mathbb{F}_{2,k}(r_2)e^{-i\ell_{2,k}\phi}$.

mode propagating on each of the fields. In this simplified case the matrices $\upsilon_{\tau,jk}$ and $g_{jk}(z)$ reduce to single coefficients υ_τ and $g(z)$ such that

$$-i\partial_z \begin{pmatrix} a_1(z) \\ a_2^*(z) \end{pmatrix} = \begin{pmatrix} \upsilon_1 & \chi_1 g(z) \\ -\chi_2 g^*(z) & -\upsilon_2 \end{pmatrix} \begin{pmatrix} a_1(z) \\ a_2^*(z) \end{pmatrix}. \tag{3.106}$$

In general, the above matrix is not Hermitian, as was the case in section 3.4.4, however, with the following transformations:

$$\alpha_1(z) = \frac{1}{\sqrt{\chi_2}} a_1(z) \tag{3.107}$$

and

$$\alpha_2(z) = \frac{1}{\sqrt{\chi_1}} a_2(z) \tag{3.108}$$

the matrix is pseudo or quasi-Hermitian [97, 98, 99, 100]. The evolution of the coefficients $\alpha_\tau(z)$ is

$$-i\partial_z \begin{pmatrix} \alpha_1(z) \\ \alpha_2^*(z) \end{pmatrix} = \mathbf{P}(z) \begin{pmatrix} \alpha_1(z) \\ \alpha_2^*(z) \end{pmatrix} = \begin{pmatrix} \upsilon_1 & g(z) \\ -g^*(z) & -\upsilon_2 \end{pmatrix} \begin{pmatrix} \alpha_1(z) \\ \alpha_2^*(z) \end{pmatrix}, \tag{3.109}$$

which for a translation-invariant system where $\partial_z g(z) = 0$, has the solution $(\alpha_1(z), \alpha_2^*(z))^\top = e^{i\delta z}\mathbf{W}(z)\,(\alpha_1(0), \alpha_2^*(0))^\top$, where the matrix

$$\mathbf{W}(z) = \begin{pmatrix} \mu\cos(\mu z) + i\upsilon\sin(\mu z) & ig\sin(\mu z) \\ -ig^*\sin(\mu z) & \mu\cos(\mu z) - i\upsilon\sin(\mu z) \end{pmatrix} \tag{3.110}$$

is related to the scattering matrix as $\mathbf{S} = e^{i\delta z}\mathbf{W}(z)|_{z=L}$. The solution with respect to the variables $(a_1^*(z), a_2(z))^\top$ is found by taking the complex conjugate of the above solution, i.e., $(a_1^*(z), a_2(z))^\top = e^{-i\delta z}\mathbf{W}^*(z)\,(a_1^*(0), a_2(0))^\top$. Note, we have simplified the form of these solutions by making use of the following substitutions:

$$\upsilon = \frac{(\upsilon_1 + \upsilon_2)}{2}, \tag{3.111}$$

$$\delta = \frac{(\upsilon_1 - \upsilon_2)}{2}, \tag{3.112}$$

and

$$\mu = \sqrt{\upsilon^2 - |g|^2}. \tag{3.113}$$

The last of these substitutions describes two distinct regions in which the behaviour of the solution is different. Indeed, if $\upsilon > |g|$, then the argument in the sinusoidal functions is real, and the fields will behave in an oscillatory manner like that of sum-frequency generation as discussed in section 3.4.4. If, however, $\upsilon < |g|$ then μ will be complex and the sinusoidal functions become hyperbolic, leading to exponential growth. This is the same behaviour

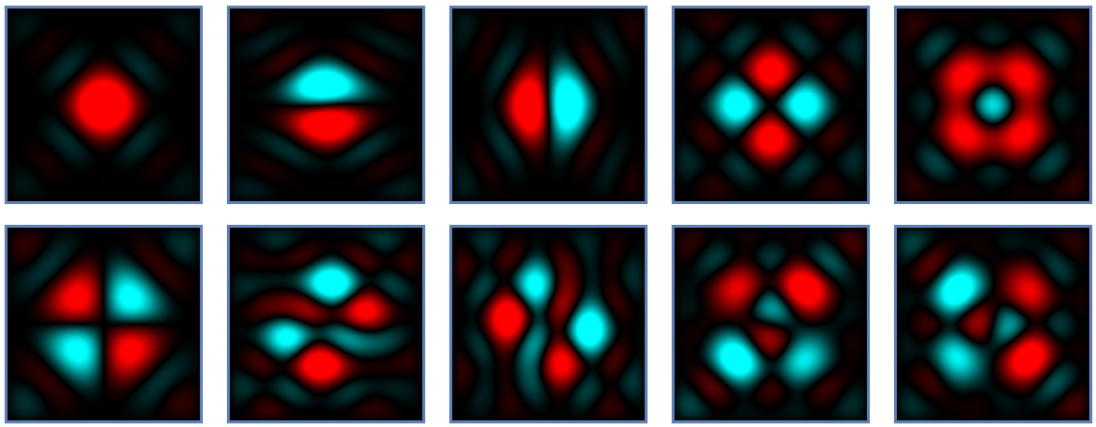

(a)

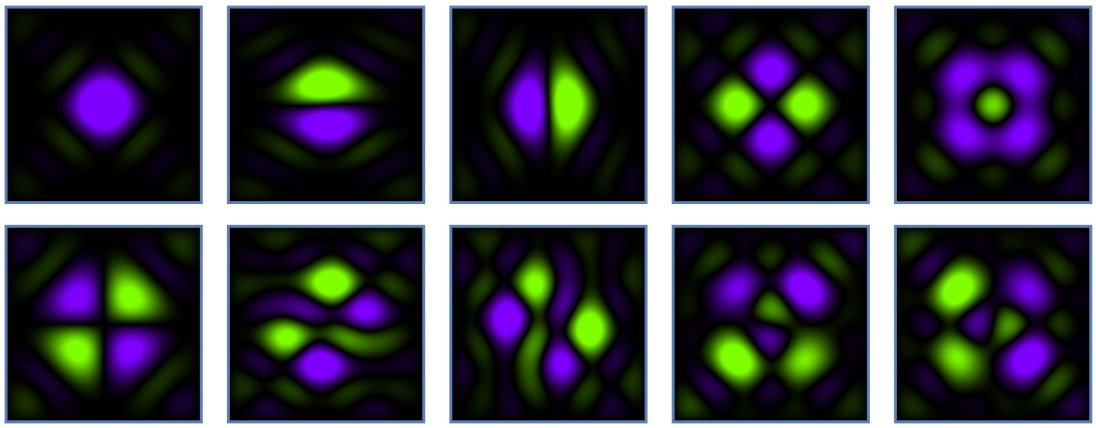

(b)

Figure 3.28: Propagation eigenmodes for a TM_{11} background with components (a) $\mathbb{F}_{2,k}(\mathbf{r}_2)$ and (b) $\mathbb{F}_{3,k}(\mathbf{r}_2)$.

observed in section 2.3.3 and is due to the pump or background field continuously transferring energy to the perturbation fields without depleting. This exponential behaviour is also manifest in the eigenvalues, which for the single-mode case with a stationary background field, take the form

$$\lambda_k = \delta \pm \mu, \tag{3.114}$$

with associated eigenvectors $v_k = (-\upsilon \pm \mu, g^*)^\top$ which evolve as $e^{i\lambda_k z}$. Observing the form of the eigenvalues, we note that as $|g|$ increases $\mu \to 0$, and the eigenvalues become degenerate. Furthermore, if $\upsilon < |g|$, μ is imaginary and one of the eigenvalues acquires a positive imaginary part - leading to exponential decay - while the other acquires a negative imaginary part - leading to exponential growth.

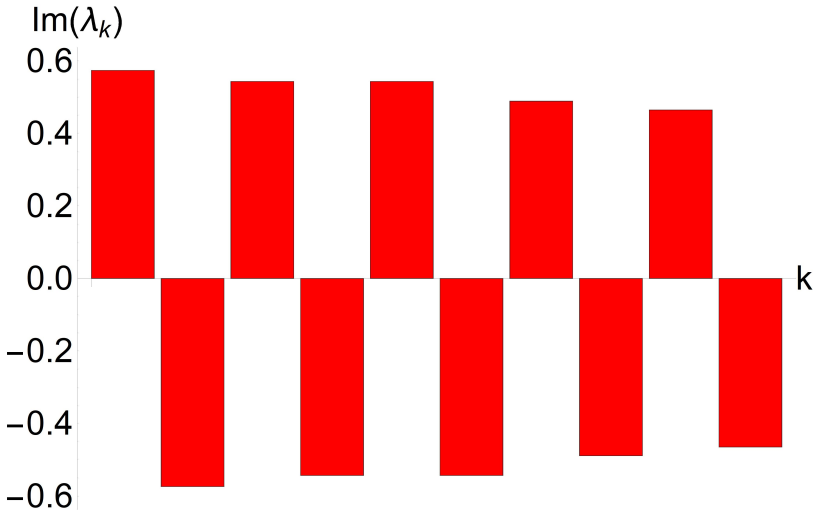

Figure 3.29: Eigenvalues λ_k for the propagation eigenmodes shown in figure 3.28

Again, the multimode case exhibits the same behaviour as the single-mode case. However, in general, these eigenmodes are not orthogonal to one another as $\mathbf{P}(z)$ is only symmetric if $g(z) \gg \upsilon$. Thus, for a system with translation invariance, we have the matrix

$$\mathbf{P} = \begin{pmatrix} 0 & g_{jk} \\ -g_{kj}^* & 0 \end{pmatrix}, \tag{3.115}$$

which is skew or anti-Hermitian with $\mathbf{P}^\dagger = -\mathbf{P}$. In this approximation, the matrix does have a set of orthogonal eigenvectors with purely imaginary eigenvalues. For example, if we take the basis used in section 3.7.1, we find the eigenmodes illustrated in figure 3.28 with their corresponding imaginary eigenvalues shown in figure 3.29. Note, these are for a TM_{00} background field.

The definition of the eigenvalues in Eq. 3.114 suggests that, for large μ, the gain of one of the eigenmodes will be large. As μ is dependent on the coefficient g, a high degree of overlap with the background field will result in large gain for the eigenmode. Similarly, the eigenmodes that overlap to a lesser extent with the background field will have a smaller g value and lower gain. We observe this behaviour with the eigenmodes presented here where the magnitude of the imaginary part of the eigenvalue is directly related to the gain of the eigenmode. This can be observed explicit when we consider the z-dependent eigenmodes. Indeed, using Eq. 3.110, we find, for a crystal of length L, eigenvalues of the form

$$\lambda_k = e^{i\delta L}\left(\mu\,\cos(\mu L) \pm \sqrt{(-\upsilon^2 + |g|^2)\sin(\mu L)^2}\right), \tag{3.116}$$

with corresponding eigenvectors

$$v_k = \left(\upsilon \sin(\mu L) \pm i\sqrt{(-\upsilon^2 + |g|^2)\ \sin(\mu L)^2}, g\sin(\mu L)\right)^\top. \tag{3.117}$$

Again we see a change in behaviour where if $\upsilon > |g|$ then μ is real and the evolution is periodic and when $\upsilon < |g|$ the coefficient μ is imaginary, and the trigonometric functions become hyperbolic. Similar to the non-diffracting case, these eigenmodes will not be orthogonal to one another unless we have the condition that $|g| \gg \upsilon$. In this case, the matrix $\mathbf{W}(z)$ reduces to the following form

$$\mathbf{W}(z) = e^{-i\delta z} \begin{pmatrix} \cosh\left(\sqrt{g^*}\sqrt{g}z\right) & i\frac{\sqrt{g}}{\sqrt{g^*}}\sinh\left(\sqrt{g^*}\sqrt{g}z\right) \\ -i\frac{\sqrt{g^*}}{\sqrt{g}}\sinh\left(\sqrt{g^*}\sqrt{g}z\right) & \cosh\left(\sqrt{g^*}\sqrt{g}z\right) \end{pmatrix} \tag{3.118}$$

such that the full solution is Hermitian,

$$\begin{pmatrix} \alpha_1(z) \\ \alpha_2^*(z) \end{pmatrix} = \begin{pmatrix} \cosh\left(\sqrt{g^*}\sqrt{g}z\right) & i\frac{\sqrt{g}}{\sqrt{g^*}}\sinh\left(\sqrt{g^*}\sqrt{g}z\right) \\ -i\frac{\sqrt{g^*}}{\sqrt{g}}\sinh\left(\sqrt{g^*}\sqrt{g}z\right) & \cosh\left(\sqrt{g^*}\sqrt{g}z\right) \end{pmatrix} \begin{pmatrix} \alpha_1(0) \\ \alpha_2^*(0) \end{pmatrix}, \tag{3.119}$$

and, for a crystal of length L, has real eigenvalues

$$\lambda_k = \cosh\Big(\sqrt{g^*}\sqrt{g}L\Big) \pm \sinh\Big(\sqrt{g^*}\sqrt{g}L\Big) = \exp\left(\pm\sqrt{g^*}\sqrt{g}L\right) \tag{3.120}$$

with corresponding orthogonal eigenvectors $v_k = \left(\pm i\sqrt{g}, \sqrt{g^*}\right)^\top$.

Note, the approximation that $|g| \gg \upsilon$ is compatible with our perturbation fields and high-intensity background. Indeed, the term υ corresponds to a propagating phase term of the perturbation fields and is dependent on the field strength of these fields: which for fields of low intensity is small. The term g, however, is dependent on the field strength of the perturbation fields and the background. If the background field is sufficiently intense, it will overcome the propagation term of the perturbation fields, and the approximation $|g| \gg \upsilon$ will be valid. If the approximation is valid, then this section will clearly define the propagation properties of the optical eigenmodes shown in the previous sections. That is, the fields will propagate independent of one another and, depending on their overlap and phase with respect to the background field, will exhibit gain or loss as they evolve. It is noteworthy, that this approximation is also true for the propagation eigenmodes outlined in section 3.4.4, however, as we did not require it to define orthogonal propagating eigenvectors it is left as a special case of the general theory outlined therein.

3.8 Degeneracy and Commuting Operators

In section 1.4.1, we introduced the operators corresponding to physical observables in the context of classical electromagnetic fields. The eigenvectors of these operators define the eigenmodes of the associated measure and are an orthogonal set of fields characteristic of a given optical system. Depending on the symmetry of the system, however, the eigenmodes

may not be unique with respect to a particular observable. Indeed, the eigenvectors may share eigenvalues as observed in the intensity eigenmodes introduced throughout this chapter. To deal with the degeneracy associated with these eigenmodes, one must break some intrinsic symmetry of the system. This symmetry breaking can be achieved through the use of a secondary observable. For example, one may have eigenmodes that are degenerate in intensity but have distinct orbital angular momentum. To label the intensity eigenmodes with respect to their orbital angular momentum, or indeed any other observable, they must also be eigenvectors of the associated operator. That is, the operators must commute with one another. More generally, to fully characterise the eigenmodes of a system in this manner requires a complete set of pair-wise commuting operators. In this work, we have observed a two-fold degeneracy and, therefore, the complete set of commuting operators consists of two elements. This set of operators highlight the symmetry of the equations of evolution of both sum-frequency generation and parametric down-conversion and allow us to lift the degeneracy found in the intensity eigenmodes.

3.8.1 Pairwise Commutation of Operators

Consider two operators, $\mathscr{O}_1$ and $\mathscr{O}_2$, that correspond to two distinct physical observables. Each of the operators has a set of eigenfunctions or eigenmodes which satisfy the property

$$\mathscr{O}_\tau \mathbb{F}_j = O_j \mathbb{F}_j, \tag{3.121}$$

where $\mathbb{F}_j$ is an eigenmode of the operator $\mathscr{O}_\tau$ and O_j is the associated eigenvalue. If the eigenmode on which we project happens to exist in a degenerate subspace, then more information is required to uniquely determine the measured state of the system. If we first consider a measurement with respect to $\mathscr{O}_1$, we are projecting onto some Hilbert space characteristic of the operator. In order for the eigenmodes in this Hilbert space to be additive for $\mathscr{O}_2$, we require

$$\mathscr{O}_2 \mathscr{O}_1 \mathbb{F}_1 = \mathscr{O}_2 \left(O_1 \mathbb{F}_1\right) = O_1 \mathscr{O}_2 \mathbb{F}_1 = O_1 O_2 \mathbb{F}_1, \tag{3.122}$$

which states that the field $\mathbb{F}_1$ is an eigenmode of both $\mathscr{O}_1$ and $\mathscr{O}_2$. If we consider instead that we have projected onto the basis associated with $\mathscr{O}_2$, then we have a similar relation,

$$\mathscr{O}_1 \mathscr{O}_2 \mathbb{F}_2 = \mathscr{O}_1 \left(O_2 \mathbb{F}_2\right) = O_2 \mathscr{O}_1 \mathbb{F}_2 = O_2 O_1 \mathbb{F}_2, \tag{3.123}$$

that is only true if $\mathbb{F}_2$ is an eigenmode of both of the operators. Satisfying one of the above conditions will automatically fulfil the other which suggests that $\mathbb{F}_1 = \mathbb{F}_2 = \mathbb{F}$. Subtracting Eq. 3.123 from Eq. 3.122 we find

$$\left(\mathscr{O}_1 \mathscr{O}_2 - \mathscr{O}_2 \mathscr{O}_1\right) \mathbb{F} = \left(O_1 O_2 - O_2 O_1\right) \mathbb{F} = 0, \tag{3.124}$$

from which we can define the commutator

$$[\mathscr{O}_1, \mathscr{O}_2] = \mathscr{O}_1\mathscr{O}_2 - \mathscr{O}_2\mathscr{O}_1. \tag{3.125}$$

If the above commutator is zero, then it is clear that the operators will share an eigenspace and the physical observables can be used to uniquely label the optical eigenmodes of a given system. In the context of the optical eigenmodes introduced in the previous sections of this chapter, we observed a number of degenerate eigenspaces. Moreover, we noted that this degeneracy was due to some symmetry of the system that was not broken by the intensity operator. In the next section, we discuss the symmetry that causes this degeneracy in rectangular and circular waveguides and how the introduction of a second commuting operator allows us to uniquely label these degenerate eigenmodes.

3.8.2 Discrete Symmetries

As already discussed, when introducing the intensity eigenmodes, any degeneracy can be attributed to some symmetry or invariance that has not been probed by the intensity operator. In the example of the rectangular waveguide in section 3.4.2 and the Hermite-Gaussian modes in section 3.3.2, we observed degenerate eigenmodes which have even or odd field profiles with respect to reflections in the transverse plane, i.e., $V_x : x \to -x$ and $V_y : y \to -y$.

3.8.2.1 Example

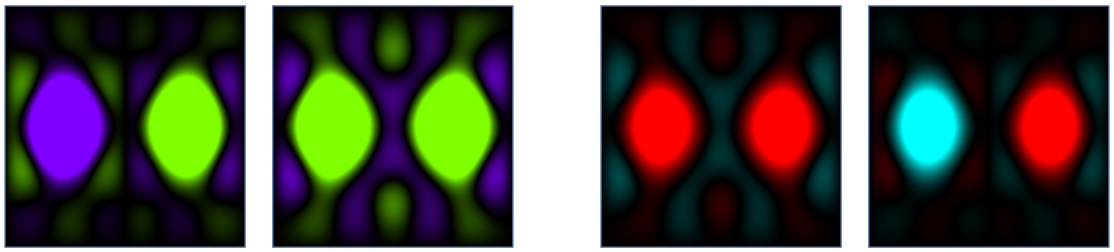

(a) (b)

Figure 3.30: Degenerate eigenmodes for a TM_{12} background with components (a) $\mathbb{F}_{2,k}(\mathbf{r}_2)$ and (b) $\mathbb{F}_{3,k}(\mathbf{r}_2)$ in the output plane where $k = 1, 2$ from left to right.

If we take, for example, a TM_{12} background field, as in section 3.4.3, we find eigenmodes that exist in a two-fold degenerate subspace, as shown in figure 3.30. Each of these eigenmodes is made up of two distinct field components as $\mathbb{F}_{2,k}(\mathbf{r}_2)$ and $\mathbb{F}_{3,k}(\mathbf{r}_2)$ where the total

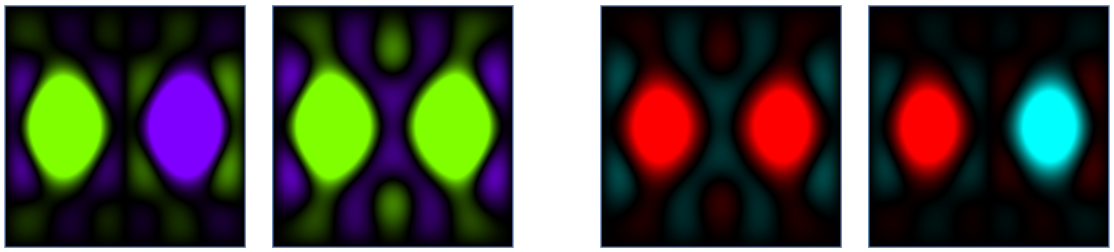

(a) (b)

Figure 3.31: Degenerate eigenmodes in figure 3.30 after transformation by V_x.

intensity eigenvalue in the output plane is the sum of the intensity of these components as

$$\lambda_k = \lambda_{2,k} + \lambda_{3,k} = \iint \frac{1}{2} n_2 \varepsilon_0 c \, \mathbb{F}^*_{2,k}(\mathbf{r}_2) \mathbb{F}_{2,k}(\mathbf{r}_2) \, \mathrm{d}x_2 \, \mathrm{d}y_2 + \iint \frac{1}{2} n_3 \varepsilon_0 c \, \mathbb{F}^*_{3,k}(\mathbf{r}_2) \mathbb{F}_{3,k}(\mathbf{r}_2) \, \mathrm{d}x_2 \, \mathrm{d}y_2, \tag{3.126}$$

where for two degenerate eigenmodes $\lambda_1 = \lambda_2$, $\lambda_{2,1} = \lambda_{2,2}$ and $\lambda_{3,1} = \lambda_{3,2}$. In this example, the TM_{12} background field is odd with respect to the operator V_x and even with respect to V_y. Consequently, the eigenmodes themselves are invariant for V_y but not invariant for a reflection about the x-axis. Indeed, the eigenmodes transform as:

$$V_x \mathbb{F}_{2,1}(\mathbf{r}_2) = -\mathbb{F}_{2,1}(\mathbf{r}_2), \quad V_x \mathbb{F}_{3,1}(\mathbf{r}_2) = \mathbb{F}_{3,1}(\mathbf{r}_2) \tag{3.127}$$

$$V_x \mathbb{F}_{2,2}(\mathbf{r}_2) = \mathbb{F}_{2,2}(\mathbf{r}_2), \quad V_x \mathbb{F}_{3,2}(\mathbf{r}_2) = -\mathbb{F}_{3,2}(\mathbf{r}_2), \tag{3.128}$$

as illustrated in figure 3.31. As the intensity operator commutes with V_x and V_y, the operators share an eigenspace. Indeed, the eigenvalues for V_x are found by projecting onto the initial eigenmodes and integrating over the output plane as

$$\xi_j = \iint \left(\mathbb{F}^*_{2,k}(\mathbf{r}_2) V_x \mathbb{F}_{2,k}(\mathbf{r}_2) + \mathbb{F}^*_{3,k}(\mathbf{r}_2) V_x \mathbb{F}_{3,k}(\mathbf{r}_2) \right) \mathrm{d}x_2 \, \mathrm{d}y_2, \tag{3.129}$$

which for the two eigenmodes in figure 3.30 is evaluated using the properties given in Eqs. 3.127 and 3.128 giving

$$\xi_1 = \iint \left(-\mathbb{F}^*_{2,1}(\mathbf{r}_2) \mathbb{F}_{2,1}(\mathbf{r}_2) + \mathbb{F}^*_{3,1}(\mathbf{r}_2) \mathbb{F}_{3,1}(\mathbf{r}_2) \right) \mathrm{d}x_2 \, \mathrm{d}y_2 = \frac{2\lambda_{3,1}}{n_3 \varepsilon_0 c} - \frac{2\lambda_{2,1}}{n_2 \varepsilon_0 c}, \tag{3.130}$$

and

$$\xi_2 = \iint \left(\mathbb{F}^*_{2,2}(\mathbf{r}_2) \mathbb{F}_{2,2}(\mathbf{r}_2) - \mathbb{F}^*_{3,2}(\mathbf{r}_2) \mathbb{F}_{3,2}(\mathbf{r}_2) \right) \mathrm{d}x_2 \, \mathrm{d}y_2 = \frac{2\lambda_{2,2}}{n_2 \varepsilon_0 c} - \frac{2\lambda_{3,2}}{n_3 \varepsilon_0 c}, \tag{3.131}$$

where, as $\lambda_{2,1} = \lambda_{2,2}$ and $\lambda_{3,1} = \lambda_{3,2}$, we have $\xi_1 = -\xi_2$. Consequently, the eigenmodes are not degenerate when acted on by the operator V_x. This process can be repeated with all of the degenerate subspaces in section 3.3.2 and 3.4.3. Assuming the degenerate subspace consists only of two eigenmodes the result given by Eq. 3.130 and 3.131 is the same regardless of the background field where the spatial translation breaks the symmetry of the background field.

3.8.3 Optical Angular Momentum

In sections 3.3.3, 3.4.3 and 3.7.2, we introduced the optical eigenmodes of the intensity operator in a basis whose elements exhibited circular symmetry. For these eigenmodes, we observed a two-fold degeneracy that was attributed to the orbital angular momentum, ℓ_τ, of the fields. As discussed in section 3.8.2, we can lift this system degeneracy by probing or breaking the symmetry that causes it. For this section, we drop the notation ℓ_b, used in sections 3.3.3, 3.4.3 and 3.7.2, to denote the background field as we discuss both sum-frequency generation and parametric down-conversion. Instead, we maintain the numerical indices to distinguish between the fields and their orbital angular momentum.

In section 1.4.1, we introduced the orbital angular momentum operator in the context of classical fields where the transformed field, $i\partial_\phi E_\tau(r,\phi,z)$, is itself a solution of Maxwell's equations. Given we have some fields $E_\tau(r,z)e^{-i\ell_\tau\phi}$ that are solutions of our equations for sum-frequency generation, we can check if the transformed field is itself a solution. Assuming the fields are of the form of the Laguerre-Gaussian modes used in both sections 3.3.3 and 3.4.3 the equations for sum-frequency generation, with a single mode on each field, are:

$$-i\partial_z E_2(r,z)e^{-i\ell_2\phi} = \frac{1}{2k_2}\nabla^2_{(r,\phi)}E_2(r,z)e^{-i\ell_2\phi} + \chi_2 E_1(r,z)^* E_3(r,z)\ e^{-i(\ell_3-\ell_1)\phi}e^{-i\Delta kz}, \tag{3.132}$$

$$-i\partial_z E_3(r,z)e^{-i\ell_3\phi} = \frac{1}{2k_3}\nabla^2_{(r,\phi)}E_3(r,z)e^{-i\ell_3\phi} + \chi_3 E_1(r,z)E_2(r,z)\ e^{-i(\ell_1+\ell_2)\phi}e^{i\Delta kz}, \tag{3.133}$$

where $\nabla^2_{(r,\phi)} = \left(\nabla^2_r + \frac{1}{r}\nabla_r + \frac{1}{r^2}\nabla^2_\phi\right)$ is the transverse Laplacian operator in cylindrical coordinates. If we now input the transformed fields $i\partial_\phi E_\tau(r,z)e^{-i\ell_\tau\phi}$ into the equations we find:

$$-i\partial_z E_2(r,z)e^{-i\ell_2\phi} = \frac{1}{2k_2}\nabla^2_{(r,\phi)}E_2(r,z)e^{-i\ell_2\phi} + \frac{\ell_3}{\ell_2}\chi_2 E_1(r,z)^* E_3(r,z)\ e^{-i(\ell_3-\ell_1)\phi}e^{-i\Delta kz}, \tag{3.134}$$

$$-i\partial_z E_3(r,z)e^{-i\ell_3\phi} = \frac{1}{2k_3}\nabla^2_{(r,\phi)}E_3(r,z)e^{-i\ell_3\phi} + \frac{\ell_2}{\ell_3}\chi_3 E_1(r,z)E_2(r,z)\ e^{-i(\ell_1+\ell_2)\phi}e^{i\Delta kz}, \tag{3.135}$$

which are only the same as the original equations when $\ell_3 = \ell_2$, that is when $\ell_1 = 0$. However, if we do not have $\ell_1 = 0$ the orbital angular momentum satisfies the relation $\ell_3 = \ell_2 + \ell_1$. In section 3.4.3, we showed that fields interact if and only if the OAM is conserved. Therefore, we can rewrite the equations as:

$$-i\partial_z E_2(r,z)e^{-i\ell_2\phi} = \frac{1}{2k_2}\nabla^2_{(r,\phi)}E_2(r,z)e^{-i\ell_2\phi} + \frac{\ell_2+\ell_1}{\ell_2}\chi_2 E_1(r,z)^* E_3(r,z)\ e^{-i(\ell_3-\ell_1)\phi}e^{-i\Delta kz} \tag{3.136}$$

$$-i\partial_z E_3(r,z)e^{-i\ell_3\phi} = \frac{1}{2k_3}\nabla^2_{(r,\phi)}E_3(r,z)e^{-i\ell_3\phi} + \frac{\ell_3-\ell_1}{\ell_3}\chi_3 E_1(r,z)E_2(r,z)\ e^{-i(\ell_1+\ell_2)\phi}e^{i\Delta kz} \tag{3.137}$$

From the interaction term in the above equations, we note that the OAM operator needs to be corrected for the background field in the instances when $\ell_1 \neq 0$. In sections 3.3.3 and 3.4.3, when we considered a non-zero background OAM, we shifted the basis for $E_3(r,z)e^{-i\ell_3\phi}$ such that all of the interactions were closed with respect to the selection rule $\ell_3 = \ell_2 + \ell_1$. Therefore, the interaction of any of the elements will not excite higher-order outwith the considered basis. We can write the conserved quantities in the form of the following set of operators:

$$E_2(r,z)e^{-i\ell_2\phi} \rightarrow (i\partial_\phi + \gamma)\, E_2(r,z)e^{-i\ell_2\phi}, \tag{3.138}$$

$$E_3(r,z)e^{-i\ell_3\phi} \rightarrow (i\partial_\phi + (\gamma - \ell_1))\, E_3(r,z)e^{-i\ell_3\phi}, \tag{3.139}$$

where γ is a free parameter which reflects the multiple ways in which the asymmetry between the two basis sets can be introduced. In both section 3.3.3 and 3.4.3, when we considered a background field with $\ell_1 = +1$, we shifted the ℓ_3 basis elements by $+1$. However, we could have just as easily shifted the ℓ_2 elements by -1 and achieve a closed set. More generally, one could shift the ℓ_3 or ℓ_2 basis elements by an arbitrary amount as long as there is a one to one correspondence between the two basis sets after interacting with the background. Following the same arguments presented above for the equations describing parametric down-conversion, we can derive a similar set of transformations:

$$E_1(r,z)e^{-i\ell_1\phi} \rightarrow (i\partial_\phi + \gamma)\, E_1(r,z)e^{-i\ell_1\phi}, \tag{3.140}$$

$$E_2^*(r,z)e^{i\ell_2\phi} \rightarrow (i\partial_\phi + (\gamma - \ell_3))\, E_2^*(r,z)e^{i\ell_2\phi}. \tag{3.141}$$

These transformations are the same as those for the sum-frequency generation equation as they are derived from the same selection rule, i.e., $\ell_3 = \ell_2 + \ell_1$. Certainly, as we are transforming the conjugate fields $E_2^*(r,z)e^{i\ell_2\phi}$ where $\ell_2 \rightarrow -\ell_2$ we observe that under this transformation, the OAM selection rule is similar to that of sum-frequency generation. Similar to the operators in Eq. 3.138 and 3.139 when we have a non-zero background OAM, we have two choices to ensure the basis set is closed with respect to all possible interactions. If for example, we have $\ell_3 = +1$, then we can shift the ℓ_2 basis elements by $+1$ or, alternatively, shift the ℓ_1 elements by -1. Consequently, if we choose the appropriate set of basis elements for the two interacting fields the orbital angular momentum will be conserved and with the OAM operator, we can uniquely label the optical eigenmodes.

(a) (b)

Figure 3.32: Degenerate eigenmodes for a LG_{00} background with components (a) $\mathbb{F}_{2,k}(r_2)e^{-i\ell_{2,k}\phi}$ and (b) $\mathbb{F}_{3,k}(r_2)e^{-i\ell_{3,k}\phi}$ in the output plane where $k = 1, 2$ from left to right.

3.8.3.1 Example

If we take, for example, the simple case for sum-frequency generation where the background OAM is $\ell_1 = 0$ we observed degeneracy in the eigenmodes shown in figure 3.32 where $\ell_{3,k} = \ell_{2,k} = \pm 1$. In this case the orbital angular momentum of the eigenmodes is

$$\begin{aligned}\mathscr{L}_k &= \iint \mathbb{F}^*_{2,k}(r_2)e^{i\ell_{2,k}\phi}i\partial_\phi\mathbb{F}_{2,k}(r_2)e^{-i\ell_{2,k}\phi} + \mathbb{F}^*_{3,k}(r_2)e^{i\ell_{3,k}\phi}i\partial_\phi\mathbb{F}_{3,k}(r_2)e^{-i\ell_{3,k}\phi}\,\mathrm{d}\phi\,\mathrm{d}r_2 \\ &= \iint \ell_{2,k}\mathbb{F}^*_{2,k}(r_2)\mathbb{F}_{2,k}(r_2) + \ell_{3,j}\mathbb{F}^*_{3,k}(r_2)\mathbb{F}_{3,k}(r_2)\,\mathrm{d}\phi\,\mathrm{d}r_2, \end{aligned} \tag{3.142}$$

where $\ell_{\tau,k}$ is the OAM of the k^{th} eigenmode component oscillating at ω_τ and the free parameter is chosen to be $\gamma = \ell_1 = 0$. In the eigenmodes in figure 3.32 we have $\ell_{2,1} = \ell_{3,1} = 1$ and $\ell_{2,2} = \ell_{3,2} = -1$ such that we have:

$$\mathscr{L}_1 = \iint \left(\mathbb{F}^*_{2,1}(r_2)\mathbb{F}_{2,1}(r_2) + \mathbb{F}^*_{3,1}(r_2)\mathbb{F}_{3,1}(r_2)\right)\,\mathrm{d}\phi\,\mathrm{d}r_2 = \frac{2\lambda_{2,1}}{n_2\varepsilon_0 c} + \frac{2\lambda_{3,1}}{n_3\varepsilon_0 c}, \tag{3.143}$$

$$\mathscr{L}_2 = \iint \left(-\mathbb{F}^*_{2,2}(r_2)\mathbb{F}_{2,2}(r_2) - \mathbb{F}^*_{3,2}(r_2)\mathbb{F}_{3,2}(r_2)\right)\,\mathrm{d}\phi\,\mathrm{d}r_2 = -\frac{2\lambda_{2,2}}{n_2\varepsilon_0 c} - \frac{2\lambda_{3,2}}{n_3\varepsilon_0 c}, \tag{3.144}$$

where as $\lambda_{2,1} = \lambda_{2,2}$ and $\lambda_{3,1} = \lambda_{3,2}$ we have $\mathscr{L}_1 = -\mathscr{L}_2$. This result is true in general for all of the degenerate subspaces in section 3.3.2 and 3.4.3 for $\ell_1 = 0$ where the eigenvalues λ_k are scaled by the total angular momentum of the fields. This kind of behaviour is also true for examples where $\ell_1 \neq 0$. Indeed, if we consider the eigenmodes of sum-frequency generation with $\ell_1 = +1$ as presented in section 3.4.3 we found degenerate eigenmodes with orbital angular momentum $\ell_2 = 0$, $\ell_2 = -1$ and $\ell_3 = 1$, $\ell_3 = 0$. Note, in each case we observe that $\ell_{3,k} = \ell_{2,k} + 1$. If we choose $\gamma = \ell_1$ we have the following operators:

$$\mathbb{F}_{2,k}(r_2)e^{-i\ell_{2,k}\phi} \to (i\partial_\phi + \ell_1)\,\mathbb{F}_{2,k}(r_2)e^{-i\ell_{2,k}\phi}, \tag{3.145}$$

$$\mathbb{F}_{3,k}(r_2)e^{-i\ell_{3,k}\phi} \to i\partial_\phi\mathbb{F}_{3,k}(r_2)e^{-i\ell_{3,k}\phi}, \tag{3.146}$$

acting on the optical eigenmodes. Indeed, the angular momentum of each of the eigenmodes is

$$\begin{aligned}\mathscr{L}_1 &= \iint \mathbb{F}^*_{2,1}(r_2)e^{i\ell_{2,1}\phi}\left(i\partial_\phi \mathbb{F}_{2,1}(r_2)e^{-i\ell_{2,1}\phi} + \mathbb{F}_{2,1}(r_2)e^{-i\ell_{2,1}\phi}\right) \\ &\quad + \mathbb{F}^*_{3,1}(r_2)e^{i\ell_{3,1}\phi} i\partial_\phi \mathbb{F}_{3,1}(r_2)e^{-i\ell_{3,1}\phi}\,\mathrm{d}\phi\,\mathrm{d}r_2 \\ &= \iint \mathbb{F}^*_{2,1}(r_2)\mathbb{F}_{2,1}(r_2) + \mathbb{F}^*_{3,1}(r_2)\mathbb{F}_{3,1}(r_2)\,\mathrm{d}\phi\,\mathrm{d}r_2 = \frac{2\lambda_{2,1}}{n_2\varepsilon_0 c} + \frac{2\lambda_{3,1}}{n_3\varepsilon_0 c},\end{aligned} \tag{3.147}$$

$$\begin{aligned}\mathscr{L}_2 &= \iint \mathbb{F}^*_{2,2}(r_2)e^{i\ell_{2,2}\phi}\left(i\partial_\phi \mathbb{F}_{2,2}(r_2)e^{-i\ell_{2,1}\phi} + \mathbb{F}_{2,2}(r_2)e^{-i\ell_{2,1}\phi}\right) \\ &\quad + \mathbb{F}^*_{3,2}(r_2)e^{i\ell_{3,2}\phi} i\partial_\phi \mathbb{F}_{3,2}(r_2)e^{-i\ell_{3,2}\phi}\,\mathrm{d}\phi\,\mathrm{d}r_2 \\ &= \iint -\mathbb{F}^*_{2,2}(r_2)\mathbb{F}_{2,2}(r_2) + \mathbb{F}^*_{2,2}(r_2)\mathbb{F}_{2,2}(r_2)\,\mathrm{d}\phi\,\mathrm{d}r_2 = 0.\end{aligned} \tag{3.148}$$

Note, in the second of the two examples, the total angular momentum is zero. This is because, for a non-zero OAM background field, the operator acting on the fields $\mathbb{F}_{2,k}(r_2)e^{-i\ell_{2,k}\phi}$ behaves like a conventional orbital angular momentum operator, $i\partial_\phi$, in a frame of reference rotating with $\ell_1 = +1$. Therefore, if we have $\ell_{2,k} = -1$, as we do in the example presented above, the total angular momentum with respect to the operator Eq. 3.145 is zero. In both examples, we observe that by accounting for the orbital angular momentum of the eigenmodes, they are no longer degenerate and can be uniquely labelled with respect to their angular momentum. This can be repeated for any degenerate subspaces in the intensity eigenmodes shown in the previous sections, for the sake of brevity; however, we only consider the two examples presented above.

3.9 Conclusion

In this chapter, we have introduced optical eigenmodes in the context of three-wave mixing within the non-depleting pump approximation. In linear optical systems, the optical eigenmodes define a set of orthogonal, non-interacting fields characteristic of the measure of a physical observable in some region of detection. The eigenmodes we define here, however, although orthogonal to one another, have components that interact due to the presence of a second-order nonlinear crystal. Indeed, although we are within the non-depleting pump approximation, the equations of evolution have an intensity dependence that leads to non-trivial eigenmodes distributed across multiple frequencies. The interaction of these low-intensity perturbation fields is determined by a high-intensity pump field and, therefore, the eigenmodes themselves are characteristic of that particular background.

In the context of three-wave mixing, we described two distinct effects in the form of sum-frequency generation and parametric down-conversion and their associated symmetries. In particular, we highlight the symmetry of the eigenmodes with respect to the choice of background field and how they are linked to the initial field decomposition considered. Indeed, through several numerical examples, we highlighted the distributed nature of the eigenmodes in bulk nonlinear material and optical waveguides. In the case of optical waveguides, we also discussed the propagation eigenmodes for sum-frequency generation and parametric down-conversion and highlighted the symmetries of the interactions between the low-intensity fields from an analytical perspective. We concluded the chapter by discussing degeneracy in the eigenvalue spectrum of the intensity optical eigenmodes and break the symmetry with the use of another operator that commutes with the intensity measure.

Chapter 4

Multiphoton Propagation Eigenmodes in Three-Wave Mixing

4.1 Introduction

In general, the asymptotic propagation of light through a linear optical system is fully characterised by a scattering matrix [11]. The same is true for sum-frequency generation and parametric down-conversion in the non-depleting pump approximation introduced in section 2.3. In the context of quantum optics, this scattering matrix also characterises the input-output relation of bosonic creation and annihilation operators of the corresponding classical fields where the field amplitudes are interpreted as probability amplitudes [12]. The quantum description of these optical systems has been studied extensively in recent years owing to their close link to the study of quantum computing, information and communication [101, 102, 103]. Further, the effective Hamiltonian describing the evolution of quantum states in optical networks can be derived directly from the classical scattering matrix that characterises the system [104, 105]. In this chapter, we study three-wave mixing in the context of a linear optical network in which two low-intensity perturbation fields interact as they propagate. This interaction is mediated through the high-intensity pump field and a second-order nonlinear material. By quantising the perturbation fields, we introduce a unitary scattering operator that describes the evolution of single-photon or Fock states, introduced in section 4.2.3, as they propagate: establishing a link between the classical fields discussed in previous chapters and single-photon states. With this link, we study the influence of the propagation eigenmodes on the quantum behaviour of sum-frequency generation and parametric down-conversion.

4.2 Quantum Description of Light

In this section, we introduce the theoretical considerations that we require for describing electromagnetic fields in the context of quantum mechanics. In particular, in section 4.2.1, we briefly discuss the Schrödinger picture of quantum mechanics and the evolution of states before introducing Heisenberg's time-dependent operator picture. We then introduce the operator solution of the quantum harmonic oscillator that gives rise to the raising and lowering or creation and annihilation operators. After this, we briefly outline how the creation and annihilation operator representation is applied to quantise the electromagnetic field. Using this quantisation procedure, we are in a position to describe not just the state of the system - described by the Heisenberg and Schrödinger pictures - but the number of quanta in a particular state. To conclude this section, we briefly outline the method of optical eigenmodes in the context of quantum operators.

4.2.1 The Wavefunction and the Schrödinger & Heisenberg Pictures

Like electromagnetic fields in optics, the fundamental object of quantum mechanics is the wavefunction, commonly denoted $\Psi(\mathbf{r}, t)$. This wavefunction is a mathematical description of the physical state, at time t, of some quantum particle or system and encodes knowledge of the particle or system that can be accessed via a measurement. If the position-space wavefunction is interpreted in this way, then it is often normalised to satisfy the following condition

$$\int_V \Psi^*(\mathbf{r}, t)\Psi(\mathbf{r}, t)\ \mathrm{d}V = 1, \tag{4.1}$$

where $\mathrm{d}V$ is some three-dimensional region of space. If the above condition is satisfied, then the sum of all probabilities distributed across space is equal to one. Note, in momentum-space, the inner product is defined for the functions $\Psi(\mathbf{p}, t)$ in a similar manner [106, 107]. The position-space normalisation condition was historically introduced to make sense of the so-called statistical interpretation of the wavefunction [108, 109]. The equation that defines the time evolution of the wavefunction was first proposed by Schrödinger and is a partial differential equation of the form

$$i\hbar\frac{\partial}{\partial t}\Psi(\mathbf{r}, t) = \hat{H}\Psi(\mathbf{r}, t), \tag{4.2}$$

where the notation $\hat{}$ denotes a quantum operator and $\hat{H}$ is the Hamiltonian that, when independent of time, evolves the wavefunction as

$$\Psi(\mathbf{r}, t) = e^{-\frac{i}{\hbar}\hat{H}t}\Psi(\mathbf{r}, 0). \tag{4.3}$$

For a single particle with linear momentum $\hat{p} = -i\hbar\nabla$ the Hamiltonian can be written in the form

$$\hat{H} = \frac{\hat{p}^2}{2m} + \hat{V}(\mathbf{r}) = -\frac{\hbar^2}{2m}\nabla^2 + \hat{V}(\mathbf{r}), \tag{4.4}$$

where m is the mass of the particle and $\hat{V}(\mathbf{r})$ is a potential function. Similar to the solution for the evolution of classical fields, introduced in section 1.2, we can separate the wavefunction as $\Psi(\mathbf{r}, t) = \psi(\mathbf{r})\Theta(t)$ such that

$$\Theta(t) = \exp\left(-i\frac{\hat{H}t}{\hbar}\right) \tag{4.5}$$

and we are left with the time-independent Schrödinger equation

$$\hat{H}\psi(\mathbf{r}) = -\frac{\hbar^2}{2m}\nabla^2\psi(\mathbf{r}) + \hat{V}(\mathbf{r})\psi(\mathbf{r}) = E\psi(\mathbf{r}), \tag{4.6}$$

where the separation variable E corresponds to the energy of the state $\psi(\mathbf{r})$. Note, the time-independent Schrödinger equation is linear and so if given two solutions $\psi_1(\mathbf{r})$ and $\psi_2(\mathbf{r})$ their superposition, $\psi_1(\mathbf{r}) + \psi_2(\mathbf{r})$, is itself a solution. Thus, the solutions of the time-independent Schrödinger equation are the eigenfunctions of the Hamiltonian operator where the associated eigenvalue is the energy of that state. As the Hamiltonian $\hat{H}$ is Hermitian, these eigenfunctions are orthogonal to one another with the inner product

$$\int \psi_\tau^*(\mathbf{r})\psi_\sigma(\mathbf{r})\,\mathrm{d}^3\mathbf{r} = \delta(\tau - \sigma) \tag{4.7}$$

where $\delta(\tau - \sigma)$ is the Dirac delta function. These properties are shared with the optical eigenmodes discussed in section 1.4.1 and 1.4.2, which are themselves orthogonal with eigenvalues associated with some physical observable. Indeed, the optical eigenmodes correspond to a classical analogue of the eigenfunctions discussed here, where the classical fields obey Maxwell's equations and the evolution of the wavefunction is determined by Schrödinger's equation.

In the Schrödinger picture, discussed above, the wavefunctions take on an explicit time dependence and evolve according to Eq. 4.2. According to the Heisenberg picture, however, one can instead describe the dynamics of a system by endowing the operators with explicit time dependence, i.e. $\hat{\mathscr{O}}(t)$. The Heisenberg picture is therefore distinct from the Schrödinger picture where the operators are fixed in time, and the wavefunctions evolve. Indeed, consider some observable $\hat{\mathscr{O}}$, the measurement of this observable is expressed in Dirac notation as

$$\mathscr{O} = \langle\Psi(\mathbf{r}, t)|\,\hat{\mathscr{O}}\,|\Psi(\mathbf{r}, t)\rangle\,, \tag{4.8}$$

where $\langle\Psi(\mathbf{r},t)|\,\hat{\mathscr{O}}\,|\Psi(\mathbf{r},t)\rangle = \int \Psi^*(\mathbf{r},t)\hat{\mathscr{O}}\Psi(\mathbf{r},t)\,\mathrm{d}\mathbf{r}$, which is formally similar to the Hermitian operators discussed in section 1.4.1 except here we have quantum wavefunctions in place of classical fields. Using the evolution of the states given by Eq. 4.3, the above relation can be written with respect to the input state $|\Psi(\mathbf{r},0)\rangle$ as

$$\mathscr{O} = \langle\Psi(\mathbf{r},0)|\left(e^{\frac{i}{\hbar}\hat{H}t}\hat{\mathscr{O}}e^{-\frac{i}{\hbar}\hat{H}t}\right)|\Psi(\mathbf{r},0)\rangle = \langle\Psi(\mathbf{r},0)|\,\hat{\mathscr{O}}(t)\,|\Psi(\mathbf{r},0)\rangle\,, \tag{4.9}$$

where the operators take on the time dependence and the wavefunctions are stationary states: this is analogous to the coefficient form introduced in section 3.4.1. Taking the time derivative of the operator $\hat{\mathscr{O}}(t)$ returns the following differential equation

$$\frac{d\hat{\mathscr{O}}(t)}{dt} = \frac{i}{\hbar}[\hat{H},\hat{\mathscr{O}}(t)] + \frac{\partial\hat{\mathscr{O}}(t)}{\partial t}, \tag{4.10}$$

which is commonly known as Heisenberg's equation of motion. Given the system is quantised using the Born-Jordan rule [110, 111], the Heisenberg and Schrödinger pictures are equivalent to one another [112, 113]. Throughout the rest of this chapter, we will utilise both of these representations to derive an effective Hamiltonian and associated scattering operator that describes the quantum behaviour of both sum-frequency generation and parametric down-conversion. Note, there is an intermediate representation of the Heisenberg and Schrödinger pictures known as the interaction picture [22, 114]. However, in this work, we do not utilise the interaction picture as we make use of fixed basis states as described in sections 3.4.3 and 3.7.2.

4.2.2 Creation & Annihilation Operators

In this section, we discuss second quantisation in which the harmonic oscillator itself is described in terms of operators. In particular, we introduce the creation and annihilation operators which raise and lower the energy of the harmonic oscillator. As opposed to being concerned with which state a given bosonic particle occupies, i.e. first quantisation, we are concerned with how many bosons occupy a given state: known as second quantisation. With these operators and the photon number states, which we will introduce in section 4.2.3, one has a formalism to describe quantum systems in the context of a field decomposition. Indeed, although we introduce the creation and annihilation operators with respect to the harmonic oscillator one can show that these same operators arise when quantising electromagnetic fields [114, 115, 116].

The mathematical form of the creation and annihilation operators are found from the operator solution of the quantum harmonic oscillator. The total energy of a 1D harmonic oscillator is given by the Hamiltonian

$$\hat{H} = \hat{T} + \hat{V} = \frac{\hat{p}_x^2}{2m} + \frac{1}{2}m\omega^2\hat{x}^2, \tag{4.11}$$

where $\hat{T}$ corresponds to the kinetic energy, $\hat{V}$ to the potential energy and the mass is defined as the ratio between average velocity and average momentum as illustrated with Ehrenfest's theorem,

$$m\frac{d\langle\hat{x}\rangle}{dt} = \langle\hat{p}_x\rangle. \tag{4.12}$$

This Hamiltonian can be factorised with the use of the ladder operators defined with the canonical observables $\hat{x}$ and $\hat{p}_x$ as:

$$\hat{a} = \frac{1}{\sqrt{2m\hbar}}\left(m\omega\hat{x} + i\hat{p}_x\right), \tag{4.13}$$

$$\hat{a}^\dagger = \frac{1}{\sqrt{2m\hbar}}\left(m\omega\hat{x} - i\hat{p}_x\right), \tag{4.14}$$

where m is the same mass as above, and the position and momentum have commutation relation $[\hat{x}, \hat{p}_x] = i\hbar$ which gives $[\hat{a}, \hat{a}^\dagger] = \hat{a}\hat{a}^\dagger - \hat{a}^\dagger\hat{a} = 1$. Using the creation and annihilation operators and their commutator, the Hamiltonian can be expressed as

$$\hat{H} = \hbar\omega\left(\hat{a}^\dagger\hat{a} + \frac{1}{2}\right). \tag{4.15}$$

With this Hamiltonian, we can calculate the commutation relations $[\hat{H}, \hat{a}^\dagger] = \hbar\omega\hat{a}^\dagger$ and $[\hat{H}, \hat{a}] = -\hbar\omega\hat{a}$. Using these commutation relations and Heisenberg's equation, we write the time dependence of these operators as:

$$\hat{a}(t) = \hat{a}(0)e^{i\omega t}, \tag{4.16}$$

$$\hat{a}^\dagger(t) = \hat{a}^\dagger(0)e^{-i\omega t}. \tag{4.17}$$

Operating on a state, Ψ_n, with $\hat{H}\hat{a}^\dagger$ we find

$$\hat{H}\hat{a}^\dagger\Psi_n = \left(\hbar\omega + E_n\right)\hat{a}^\dagger\Psi_n. \tag{4.18}$$

Similarly, for $\hat{H}\hat{a}$, we have

$$\hat{H}\hat{a}\Psi_n = \left(-\hbar\omega + E_n\right)\hat{a}\Psi_n, \tag{4.19}$$

which shows that $\hat{a}\Psi_n$ and $\hat{a}^\dagger\Psi_n$ are eigenfunctions of the Hamiltonian of a harmonic oscillator with energy $E_n - \hbar\omega$ and $E_n + \hbar\omega$, respectively. So by applying the operator $\hat{a}$ to the wavefunction, the energy is lowered by $\hbar\omega$ and by applying $\hat{a}^\dagger$ the energy is raised by the same factor. Therefore, the operators $\hat{a}^\dagger$ and $\hat{a}$ are known as the raising and lowering or the creation and annihilation operators.

Given the wave nature of the electromagnetic field, it is perhaps unsurprising that one can quantise light with the harmonic oscillator. To show the equivalence between the harmonic oscillator and the electromagnetic field we start with the classical free field Hamiltonian

$$H_{\mathrm{EM}} = \int_V \frac{1}{2}\left(\varepsilon_0 \mathbf{E}^*\mathbf{E} + \frac{1}{\mu_0}\mathbf{B}^*\mathbf{B}\right)\,\mathrm{d}V, \tag{4.20}$$

where V corresponds to the volume of an empty cavity in which the field is enclosed. If we take the simple case of a monochromatic, linearly polarised electric field propagating along the z-axis we have

$$E_x(z,t) = E_0 \sin(kz)\sin(\omega t) \tag{4.21}$$

with the corresponding magnetic field

$$B_x(z,t) = \frac{E_0}{c}\cos(kz)\cos(\omega t). \tag{4.22}$$

Integrating these fields over the cavity volume, assuming we have a standing wave with nodes at $z = 0$ and $z = z_{max}$, the Hamiltonian is rewritten as

$$H_{\mathrm{EM}} = \frac{V}{4}\left(\varepsilon_0 |E_0|^2 \sin^2(\omega t) + \frac{|E_0|^2}{\mu_0 c^2}\cos^2(\omega t)\right) \tag{4.23}$$

whereby introducing the two operators

$$\hat{q} = \sqrt{\frac{\varepsilon_0 V}{2\omega^2}} E_0 \sin(\omega t) \tag{4.24}$$

and

$$\hat{p} = \sqrt{\frac{\varepsilon_0 V}{2}} E_0 \cos(\omega t) \tag{4.25}$$

can be written in a form reminiscent of the harmonic oscillator as

$$H_{\mathrm{EM}} = \frac{1}{2}\left(\hat{p}^2 + \omega^2 \hat{q}^2\right), \tag{4.26}$$

where $\hat{p}$ and $\hat{q}$ act like the position and momentum of the electromagnetic field. Indeed, the above Hamiltonian can be made identical to the harmonic oscillator with the following substitutions:

$$\hat{q} = \sqrt{m}\hat{x}, \tag{4.27}$$

$$\hat{p} = \frac{1}{\sqrt{m}}\hat{p}_x, \tag{4.28}$$

which gives the commutator $[\hat{q}, \hat{p}] = i\hbar$. We can recast our creation and annihilation operators in terms of the electromagnetic field operators $\hat{p}$ and $\hat{q}$ as:

$$\hat{a} = \frac{1}{\sqrt{2\hbar\omega}}\left(\omega\hat{q} + i\hat{p}\right), \tag{4.29}$$

$$\hat{a}^\dagger = \frac{1}{\sqrt{2\hbar\omega}} \left(\omega\hat{q} - i\hat{p}\right), \tag{4.30}$$

which allow us to write the Hamiltonian Eq. 4.26 in the operator form

$$\hat{H}_{\mathrm{EM}} = \frac{1}{2}\hbar\omega \left(\hat{a}^\dagger\hat{a} + \frac{1}{2}\right), \tag{4.31}$$

which is identical to Eq. 4.15. With this, we observe that the quantisation of the quantum harmonic oscillator can be directly applied to electromagnetic fields. Furthermore, the above demonstration represents a simple example of so-called canonical quantisation where a classical theory is quantised by defining field and conjugate momenta operators that have the same algebraic structure as Eqs. 4.13 and 4.14.

4.2.3 Number State Representation

If the states Ψ_n are defined as eigenstates of the number operator $\hat{n} = \hat{a}^\dagger\hat{a}$ we have

$$\hat{n}\Psi_n = n\Psi_n, \tag{4.32}$$

where n is the total number of quanta in the state. We denote these states as the Fock states and represent them in Dirac notation with the kets $|n\rangle$. The raising and lowering operators $\hat{a}^\dagger$ and $\hat{a}$ act to increase and decrease the total number of photons in terms of these kets as:

$$\hat{a}^\dagger |n\rangle = \sqrt{n+1}\,|n+1\rangle, \tag{4.33}$$

$$\hat{a}\,|n\rangle = \sqrt{n}\,|n-1\rangle, \tag{4.34}$$

and

$$\hat{a}\,|0\rangle = |0\rangle, \tag{4.35}$$

where the Fock states form an orthonormal basis with $\langle n'|n\rangle = \delta_{n',n}$. The first of the above properties suggests that the number states can be described as the successive application of the creation operator in the following manner

$$|n\rangle = \frac{1}{\sqrt{n!}}(\hat{a}^\dagger)^n\,|0\rangle, \tag{4.36}$$

where $n!$ represents the factorial of the number n and the state $|0\rangle$ corresponds to the ground state in which no quanta of light are in an excited state. The total number of photons in a system can be found by applying the operator $\hat{n} = \hat{a}^\dagger\hat{a}$,

$$\hat{a}^\dagger\hat{a}\,|n\rangle = \sqrt{n}\hat{a}^\dagger\,|n-1\rangle = \sqrt{n}\sqrt{(n-1)+1}\,|n\rangle = n\,|n\rangle, \tag{4.37}$$

showing that the number states are indeed eigenstates of the number operator. If we consider a system with more than one oscillator the operators $\hat{a}_{\tau,j}$ corresponds to the creation and

annihilation operators with properties described by Eq. 4.33 and 4.34. Indeed, for some basis decomposition, the number states become $|n_1\rangle \otimes \cdots \otimes |n_m\rangle = |n_1, \ldots, n_m\rangle$ where m is the total number of orthogonal basis elements. The commutation relations for these creation and annihilation operators are

$$\left[\hat{a}_j, \hat{a}_k^\dagger\right] = \delta_{jk}, \tag{4.38}$$

where the operators $\hat{a}_j$ and $\hat{a}_j^\dagger$ act to decrease or increase the number of photons in j^{th} mode within some basis decomposition with the following relations:

$$\begin{aligned} &\hat{a}_j \left|n_1, \ldots, n_j, \ldots, n_m\right\rangle \\ &= \sqrt{n_j} \left|n_1, \ldots, n_j - 1, \ldots, n_m\right\rangle, \end{aligned} \tag{4.39}$$

$$\begin{aligned} &\hat{a}_j^\dagger \left|n_1, \ldots, n_j, \ldots, n_m\right\rangle \\ &= \sqrt{n_j + 1} \left|n_1, \ldots, n_j + 1, \ldots, n_m\right\rangle, \end{aligned} \tag{4.40}$$

and

$$\hat{a}_j \left|0, \ldots, 0, \ldots, 0\right\rangle = \left|0, \ldots, 0, \ldots, 0\right\rangle.$$

The total number of photons in the j^{th} mode is found using the operator $\hat{n}_j = \hat{a}_j^\dagger \hat{a}_j$, and the total number of photons in the decomposition is given by the sum $\sum_j \hat{n}_j = \sum_j \hat{a}_j^\dagger \hat{a}_j$.

4.2.4 Optical Eigenmodes for Quantum Operators

With the creation and annihilation operators defined in the previous section, one can quantise the optical eigenmodes in which the coefficients in section 1.4.1 and 1.4.2 are considered quantum operators. In the context of classical systems, we have two pictures in which we can evolve the fields as in sections 3.3.2 and 3.3.3 or evolve the coefficients as described in section 3.4.1. These two representations can be thought of as classical analogues to the Schrödinger and Heisenberg pictures of quantum mechanics introduced in section 4.2.1. The link between these two representations is in the field decomposition

$$E_\tau(\mathbf{r}) = \sum_{j=1}^{N} a_{\tau,j}(z) f_{\tau,j}(x, y), \tag{4.41}$$

where N is the number of elements in the basis and the fields $f_{\tau,j}(x, y)$ describe an orthogonal Hilbert space satisfying

$$\iiint \frac{1}{2\pi} f_{\tau,j}^*(x, y) f_{\sigma,k}(x, y) e^{-i(\omega_\sigma - \omega_\tau)t} \,\mathrm{d}x \,\mathrm{d}y \,\mathrm{d}t = \delta(\omega_\tau - \omega_\sigma)\delta_{jk}. \tag{4.42}$$

To quantise this system, we promote the coefficients to operators as:

$$\begin{aligned} a_{\tau,j} &\rightarrow \hat{a}_{\tau,j}, \\ a^*_{\tau,j} &\rightarrow \hat{a}^\dagger_{\tau,j}, \end{aligned} \tag{4.43}$$

with the canonical commutation relations

$$\left[\hat{a}_{\tau,j}, \hat{a}^\dagger_{\sigma,k}\right] = \hat{a}_{\tau,j}\hat{a}^\dagger_{\sigma,k} - \hat{a}^\dagger_{\sigma,k}\hat{a}_{\tau,j} = \delta_{jk}\delta_{\tau\sigma}. \tag{4.44}$$

In analogy with the operators described in section 1.4 an observable in quantum mechanics is described by a Hermitian measure, $\hat{m}$, which, in a finite basis, corresponds to a Hermitian matrix. This measure can be written in the form $\hat{m} = \hat{a}^\dagger M \hat{a}$ where the coefficient vectors are promoted to creation and annihilation operators as described above. As M is Hermitian, it has a set of orthogonal eigenvectors each with a real eigenvalue associated with it - corresponding to the physical observable being measured. In the context of the statistical interpretation of quantum mechanics, however, these eigenvectors take on additional significance [117]. Indeed, the eigenvectors correspond to orthogonal states of the observable, $\hat{m}$, where the act of measurement projects the system onto one particular eigenstate. The probability of measuring each eigenstate is given by the associated eigenvalue. Within this formalism, it would be possible to describe the optical eigenmodes for three-wave mixing in a quantum context by quantising the system as described here. In the following sections, however, we restrict our discussion to the propagation eigenmodes for three-wave mixing and their influence on the Fock state representation of the system.

4.3 Multiphoton Sum-Frequency Generation

In this section, we introduce the effective Hamiltonian describing the quantum behaviour of sum-frequency generation at the multiphoton level. In going towards this multiphoton level, we introduce, in section 4.3.1, modified field variables that normalise the coupling between the low-intensity fields where the conserving quantity associated with the system is the photon flux. In section 4.3.2.2, we introduce the effective Hamiltonian method that allows one to describe the quantum behaviour of our system. In sections 4.3.3 and 4.3.4, we consider the effective Hamiltonian for the single-mode and multimode case of sum-frequency generation. In each of these cases, we study the influence of the eigenmode decomposition of the scattering matrix on the quantum behaviour of the system. We conclude this section with some numerical examples to illustrate the theory previously outlined.

4.3.1 Sum-Frequency Generation Modified Field Variables

In this section, we describe the equations for sum-frequency generation with respect to modified field variables. Indeed, when discussing quantum states, it is useful to describe the system in terms of photon number or photon flux, i.e. photons m^{-2} s^{-1}. In the context of the nonlinear equations introduced in Chapter 2, we can do this by normalising the mixing term in a manner similar to that shown in section 3.4.1. We start with the set of coupled equations:

$$-i\partial_z E_b(x,y,z) = \frac{1}{2k_1}\nabla^2 E_b(x,y,z), \tag{4.45}$$

$$-i\partial_z E_2(x,y,z) = \frac{1}{2k_2}\nabla^2\ E_2(x,y,z) + \chi_2 E_b^*(x,y,z)E_3(x,y,z)e^{-i\Delta kz}, \tag{4.46}$$

$$-i\partial_z E_3(x,y,z) = \frac{1}{2k_3}\nabla^2\ E_3(x,y,z) + \chi_3 E_b(x,y,z)E_2(x,y,z)e^{i\Delta kz}, \tag{4.47}$$

where $\Delta k = k_b + k_2 - k_3$ is the wave vector mismatch and $E_2(x,y,z)$ and $E_3(x,y,z)$ are monochromatic electric fields oscillating at ω_2 and ω_3, respectively. The field $E_b(x,y,z)$ is a high-intensity, non-depleting pump oscillating with frequency $\omega_1 = \omega_3 - \omega_2$ which evolves independently of the fields $E_\tau(x,y,z)$. The interaction strength is given by $\chi_\tau = \frac{\chi^{(2)}\omega_\tau}{n_\tau c}$ where $\chi^{(2)}$ is the second-order susceptibility of the system. We can expand the fields as

$$E_\tau(x,y,z) = \sum_{j=1}^{N}\sqrt{\frac{\omega_\tau}{n_\tau}}a_{\tau,j}(z)f_{\tau,j}(x,y), \tag{4.48}$$

where the functions $f_{\tau,j}(x,y)$ form an orthonormal basis with

$$\iiint \frac{1}{2\pi}e^{-i(\omega_\sigma-\omega_\tau)t}\sqrt{\frac{\omega_\tau}{n_\tau}}\sqrt{\frac{\omega_\sigma}{n_\sigma}}f_{\tau,j}^*(x,y)f_{\sigma,k}(x,y)\,\mathrm{d}x\,\mathrm{d}y\,\mathrm{d}t = \delta(\omega_\tau-\omega_\sigma)\delta_{jk}. \tag{4.49}$$

If we input our expansion into Eqs. 4.46 and 4.47 we derive our equations of evolution in a coefficient form:

$$\begin{aligned}\partial_z a_{2,j}(z) &= \sum_{k=1}^{N} i\upsilon_{2,jk}a_{2,k}(z) + ig_{jk}(z)a_{3,k}(z),\\ \partial_z a_{3,j}(z) &= \sum_{k=1}^{N} i\upsilon_{3,jk}a_{3,k}(z) + ig_{kj}^*(z)a_{2,k}(z),\end{aligned} \tag{4.50}$$

with the matrices:

$$\upsilon_{\tau,jk} = \iint \frac{1}{2k_\tau}\ f_{\tau,j}^*(x,y)\nabla_T^2 f_{\tau,k}(x,y)\,\mathrm{d}x\,\mathrm{d}y, \tag{4.51}$$

$$g_{jk}(z) = \chi \iint E_b^*(x,y,z) f_{2,j}^*(x,y) f_{3,k}(x,y) e^{-i\Delta k z}\,\mathrm{d}x\,\mathrm{d}y, \tag{4.52}$$

where $\chi = \frac{\chi^{(2)}}{c}\sqrt{\frac{\omega_2\omega_3}{n_2 n_3}}$. The matrix $\upsilon_{\tau,jk}$ is a Hermitian phase term with $\upsilon_{\tau,jk} = \upsilon_{\tau,kj}^*$ and $g_{jk}(z)$ describes the interaction of the modes mediated by the non-depleting background field, $E_b(x,y,z)$. The evolution of the coefficients given by Eqs. 4.50 are written in terms of a scattering matrix as

$$\begin{pmatrix} a'_{2,k} \\ a'_{3,k} \end{pmatrix} = \mathbf{S} \begin{pmatrix} a_{2,k} \\ a_{3,k} \end{pmatrix}, \tag{4.53}$$

where $a_{\tau,k}$ are the field amplitudes of the modes at the input plane and $a'_{\tau,k}$ are the amplitudes of the corresponding output modes with the scattering matrix defined as $\mathbf{S} = \exp\left(\int_z i\mathbf{P}(z)\mathrm{d}z\right)$ where

$$\mathbf{P}(z) = \begin{pmatrix} \upsilon_{2,jk} & g_{jk}(z) \\ g_{kj}^*(z) & \upsilon_{3,jk} \end{pmatrix}. \tag{4.54}$$

The matrix $g_{jk}(z)$ is not Hermitian in general; however, the matrix $\mathbf{P}(z)$ is Hermitian i.e. $\mathbf{P}(z) = \mathbf{P}(z)^\dagger$. As a consequence of this Hermiticity, the scattering matrix is unitary

$$\begin{aligned} \mathbf{S}^\dagger\mathbf{S} &= \exp\left(\int_z i\mathbf{P}(z)\mathrm{d}z\right)\exp\left(\int_z -i\mathbf{P}(z)^\dagger\mathrm{d}z\right) \\ &= \exp\left(\int_z i\mathbf{P}(z)\mathrm{d}z\right)\exp\left(\int_z -i\mathbf{P}(z)\mathrm{d}z\right) = \mathbf{I}, \end{aligned} \tag{4.55}$$

where $\mathbf{I}$ is the identity matrix of the same dimensions as $\mathbf{S}$. From a physical perspective, the unitarity of the scattering matrix is an expression of the conservation of the quantity

$$\begin{aligned} \Phi &= \sum_\tau \frac{\mathscr{I}_\tau}{\hbar\omega_\tau} = \sum_\tau \frac{n_\tau c\varepsilon_0}{2\hbar\omega_\tau} E_\tau^*(x,y,z) E_\tau(x,y,z) \\ &= \sum_{\tau,j} \frac{c\varepsilon_0}{2\hbar} a_{\tau,j}^*(z) a_{\tau,j}(z) f_{\tau,j}^*(x,y,z) f_{\tau,j}(x,y,z), \end{aligned} \tag{4.56}$$

where $\mathscr{I}_\tau = \frac{1}{2} n_\tau \varepsilon_0 c E_\tau^*(x,y,z) E_\tau(x,y,z)$ is the intensity of the field and Φ has units proportional to the photon flux - that is, photons per unit area per unit time. If we now quantise this system by promoting the coefficients to operators as

$$a_{\tau,j} \to \hat{a}_{\tau,j}$$

and

$$a_{\tau,j}^* \to \hat{a}_{\tau,j}^\dagger$$

the scattering matrix in terms of the annihilation operators introduced in section 4.2.3 is

$$\begin{pmatrix} \hat{a}'_{2,k} \\ \hat{a}'_{3,k} \end{pmatrix} = \mathbf{S} \begin{pmatrix} \hat{a}_{2,k} \\ \hat{a}_{3,k} \end{pmatrix}, \tag{4.57}$$

where the unitarity of the system leads to the interpretation that the photon number, $\sum_{\tau,j} \hat{a}_{\tau,j}^\dagger \hat{a}_{\tau,j}$, is conserved, where $\hat{a}_{\tau,j}$ is the annihilation operator of the j^{th} mode with frequency ω_τ.

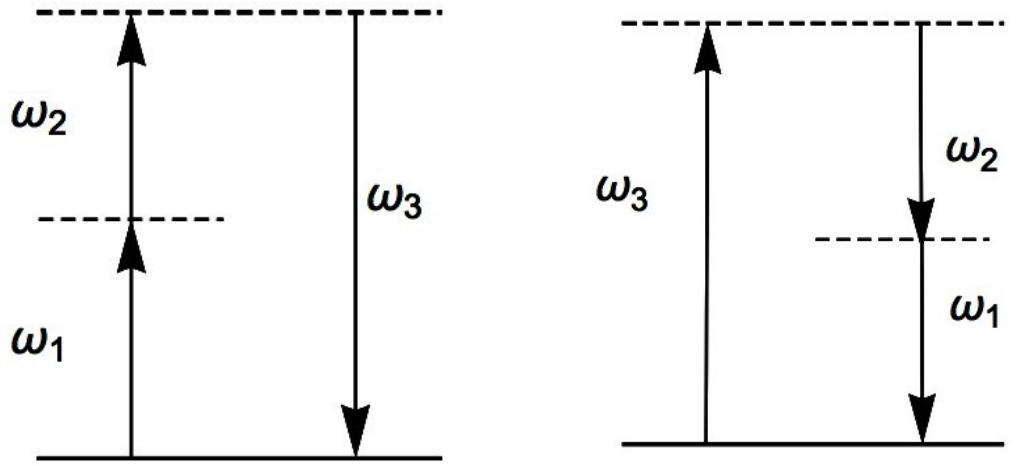

(a) (b)

Figure 4.1: Energy-level diagrams for (a) sum frequency and (b) parametric down-conversion. As we are off-resonance, the horizontal lines correspond to unobservable, short-lived, virtual states.

Consider the interaction depicted in figure 4.1, where a photon at ω_1 and ω_2 are annihilated or absorbed by a dipole, and the result is a photon at ω_3. From this interaction, we observe that the number of photons in the background field and perturbation field oscillating at ω_2 will decrease while increasing the number of photons in the field at ω_3. Similarly, to generate photons at ω_2 requires the annihilation of a photon at ω_3, which will also increase the number of photons in the background field. In the non-depleted pump approximation, however, we are not concerned with the photons transferred to and from the background field and the annihilation of a photon on one of the perturbation fields is always accompanied by the creation of photons in the other, conserving the number of photons.

4.3.2 Effective Hamiltonian Method

For linear systems made up of simple optical instruments, the transformation of input field amplitudes to output field amplitudes is fully described by a scattering matrix [118]. Of particular interest here, it has been shown that the effective Hamiltonian describing the evolution of quantum states in optical systems can be derived directly from the classical scattering matrix that characterises the system [104, 105]. The effective Hamiltonian method relies on well-known results from group theory which we discuss in section 4.3.2.1. We then introduce, in section 4.3.2.2, the effective Hamiltonian method for unitary scat-

tering matrices like that of sum-frequency generation shown in section 4.3.1. Indeed, we derive an effective Hamiltonian for sum-frequency generation in the single-mode case and introduce eigenmode operators in the context of the propagation eigenmodes introduced in the previous chapter. We also consider, in section 4.3.4, the multimode case and show that the description of multiphoton fields using the propagation eigenmodes simplifies the Fock state quantum behaviour of the system while remaining equivalent to the standard approach.

4.3.2.1 Group Theory

In section 3.3.2, we characterised the rotational symmetries of the field profiles of Hermite-Gaussian modes that lead to degenerate eigenmodes. Similarly, in section 3.8, we discussed how to lift the degeneracy of such eigenmodes by breaking these symmetries with discrete or continuous rotations. These discrete sets of symmetries are best understood in the context of group theory. Indeed, a group is a closed set of transformations that are composable and have an inverse [119]. Take, for example, the discrete spatial reflections, V_x and V_y, that we used to lift the degeneracy in the eigenmodes of section 3.4.2. These transformations are composable as taking the product, V_xV_y, defines a third transformation that acts as

$$V_xV_y : \begin{pmatrix} x \\ y \\ z \end{pmatrix} \rightarrow \begin{pmatrix} -x \\ -y \\ z \end{pmatrix}. \tag{4.58}$$

Also, by applying any of the spatial reflections V_x or V_y to the above relation, then we undo the initial transformation, which suggests that $V_x^{-1} = V_x$ and $V_y^{-1} = V_y$. This set of two spatial transformations describes a subgroup of the abelian or commutative group denoted $\mathbb{Z}_2$ [120]. For this group a function, ψ, is either even or odd under the spatial translations in the group such that $V_x\psi = \psi$ or $V_x\psi = -\psi$ and similarly for V_y. The group can consequently be described with the two-element set, $\mathbb{Z}_2 \equiv \{-1, +1\}$, which is used to define the parity and time-reversal symmetry of physical systems [121, 122, 123].

The group of spatial reflections or parity operators is an example of a discrete group. However, as outlined in section 3.4.3 systems can also be symmetric under continuous transformations of the x-y plane. If we consider a vector, $\mathbf{r} = (x, y)$, in the 2D plane, the matrix describing a counterclockwise rotation at an angle, ϕ, is

$$R(\phi) = \begin{pmatrix} \cos(\phi) & -\sin(\phi) \\ \sin(\phi) & \cos(\phi) \end{pmatrix}, \tag{4.59}$$

which for angles $\phi \in [0, 2\pi)$ defines the special orthogonal group SO(2). For all $R(\phi)$ the transformation is completely characterised by the angle ϕ. Groups that are characterised

by one or more continuous variables are known as Lie groups [124]: named after Norwegian mathematician Sophus Lie. The concept of Lie groups leads directly to another important idea in physics, namely, infinitesimal generators. The generators of elements in a Lie group correspond to the derivatives of the elements with respect to the parameters that characterise the group. Moreover, the generator of a Lie group is the simplest representation of the group from which all its elements can be derived [119, 120, 124]. For example, if we take the derivative of $R(\phi)$ with respect to ϕ evaluated at $\phi = 0$, we find

$$\frac{dR(\phi)}{d\phi}|_{\phi=0} = \begin{pmatrix} 0 & -1 \\ 1 & 0 \end{pmatrix}, \tag{4.60}$$

which generates infinitesimal rotations in the counterclockwise direction. One can see that, up to a factor of i, the orbital angular momentum operators introduced in section 3.8 are generators of infinitesimal rotations in 2D space.

In general, a group will have N elements whose infinitesimal generator(s) form a vector space that, if closed under commutation, is called the Lie algebra of the associated Lie group. So the generator given by Eq. 4.60 is a member of the Lie algebra associated with the group $R(\phi)$. An example of a group with more than one generator are rotations in 3D space which are defined by the three matrices:

$$R_x(\phi) = \begin{pmatrix} 1 & 0 & 0 \\ 0 & \cos(\phi) & -\sin(\phi) \\ 0 & \sin(\phi) & \cos(\phi) \end{pmatrix}, \tag{4.61}$$

$$R_y(\phi) = \begin{pmatrix} \cos(\phi) & 0 & \sin(\phi) \\ 0 & 1 & 0 \\ -\sin(\phi) & 0 & \cos(\phi) \end{pmatrix}, \tag{4.62}$$

and

$$R_z(\phi) = \begin{pmatrix} \cos(\phi) & -\sin(\phi) & 0 \\ \sin(\phi) & \cos(\phi) & 0 \\ 0 & 0 & 1 \end{pmatrix}, \tag{4.63}$$

with corresponding generators:

$$L_x = \begin{pmatrix} 0 & 0 & 0 \\ 0 & 0 & -1 \\ 0 & 1 & 0 \end{pmatrix}, \quad L_y = \begin{pmatrix} 0 & 0 & 1 \\ 0 & 0 & 0 \\ -1 & 0 & 0 \end{pmatrix}, \quad L_z = \begin{pmatrix} 0 & -1 & 0 \\ 1 & 0 & 0 \\ 0 & 0 & 0 \end{pmatrix}, \tag{4.64}$$

that describe rotations about the x, y and z axes, respectively. One can check the commutators of the three generators and find the relations:

$$[L_x, L_y] = L_z, \quad [L_y, L_z] = L_x, \quad [L_z, L_x] = L_y. \tag{4.65}$$

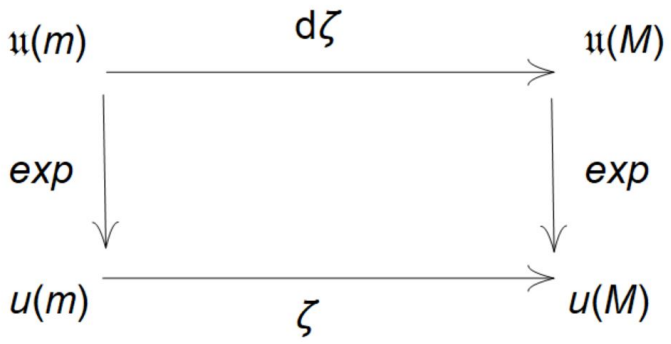

Figure 4.2: The commutative link between the Lie groups $U(m)$ and $U(M)$ and their associated Lie algebras.

These commutation relations show that the commutator of two of the generators gives another generator from the same group. Thus, this set of generators is closed under commutation and correspond to a Lie algebra. This algebra is often denoted $\mathfrak{so}(3)$ and is related to the special orthogonal group SO(3) which is a subgroup of the orthogonal group, O(3), with the additional constraint that the elements have a unit determinant. The link between a Lie algebra and its group can be made explicit by defining the exponential map $\exp : \mathfrak{g} \to G$. Consider a small rotation about the z-axis at an angle $\varepsilon \ll 1$. Given this angle is sufficiently small the matrix $R_z(\varepsilon)$ will be perturbed only a small amount from $R_z(0)$ and can be expanded as

$$R_z(\varepsilon) \approx R_z(0) + \varepsilon \frac{dR_z}{d\phi}|_{\phi=0} = I + \varepsilon L_z, \tag{4.66}$$

where I is the identity matrix. To describe a rotation of ϕ, we then iterate through the small angle ε a total of n times, where $n = \phi/\varepsilon$, as

$$R_z(\phi) = \lim_{n\to\infty} \left(I + \frac{\phi L_z}{n} \right)^n = e^{\phi L_z}, \tag{4.67}$$

where we have utilised

$$\lim_{n\to\infty} \left(I + \frac{X}{n} \right)^n = e^X$$

in which X is some generator [120]. This result allows one to recover the Lie group from its algebra and is central to the effective Hamiltonian method that will be introduced in the next section. One can check the group properties, i.e. that the elements are composable and have an inverse, using the properties of the exponential function. A mapping between a Lie group and its associated algebra while conserving the properties, e.g. commutator, of the group is a homomorphism [119].

4.3.2.2 Effective Hamiltonian

In the case of sum-frequency generation, we showed that the total number of photons is conserved and that the associated scattering matrix is unitary and belongs to the unitary group $U(n)$. In the context of quantum mechanics, the evolution of states is described by the Schrödinger equation

$$|\psi_{out}\rangle = \hat{S}\,|\psi_{in}\rangle\,, \tag{4.68}$$

where the matrix $\hat{S}$ also belongs to a unitary group which we denote $U(N)$. According to Heisenberg's picture as discussed in section 4.2.1, the output states can also be found by evolving time-dependent operators as $\hat{\mathbf{A}}' = \hat{S}^\dagger \hat{\mathbf{A}} \hat{S}$ where the operators $\hat{\mathbf{A}}$ are the annihilation operators of our quantised perturbation fields with $\hat{\mathbf{A}} = (\hat{a}_1, \ldots, \hat{a}_m)^\top$. Note, to simplify the notation in the labelling of these operators we have dropped the index τ that distinguishes between the two wavelengths such that

$$(\hat{a}_1, \ldots, \hat{a}_m) = (\hat{a}_{2,1}, \ldots, \hat{a}_{2,m_2}, \hat{a}_{3,1}, \ldots, \hat{a}_{3,m_3})\,, \tag{4.69}$$

where $m_2 + m_3 = m$ in which the numbers m_3 and m_2 are the number of modes in the decomposition, Eq. 4.109, for each field. Using the scattering matrix introduced in section 4.3.1, we can write the corresponding output operators as

$$\hat{\mathbf{A}}' = \mathbf{S}\hat{\mathbf{A}}. \tag{4.70}$$

The annihilation operators, as described in section 4.2.3, are associated with each of the modes that propagate through the system. From a physical perspective, if we were to consider a small number of photons that are coupled to particular perturbation fields, then the interaction of the photon states depends on the mixing of the fields to which they are coupled. Consequently, for the scattering operator $\hat{S}$ to describe the quantum behaviour of the system, it should agree with the classical mode transformation as

$$\mathbf{S}\hat{\mathbf{A}} = \hat{S}^\dagger \hat{\mathbf{A}} \hat{S}. \tag{4.71}$$

From the perspective of group theory, this suggests that one can define a homomorphism, which we denote ζ, between the groups $U(n)$ and $U(N)$. The derivative of ζ forms a map, $d\zeta$, that allows one to move to and from the associated Lie algebras, $\mathfrak{u}(n)$ and $\mathfrak{u}(N)$ [101]. As briefly outlined in section 4.3.2.1, the Lie algebra is - for an abelian group - a vector space of generators of a given Lie group that is closed under commutation. Moreover, we noted that the Lie group could be recovered from its associated algebra via the exponential map. In the context of the scattering operator, the exponential map is written $\hat{S} = \exp\Big(i\hat{H}_{\text{eff}}\varrho\Big)$.

Note, as the scattering operator characterises the link between the input and output, the variable ϱ corresponds to the fractional depth of the optical system. As we are not interested in fractional depths, ϱ is set to unity such that the scattering operator is defined as $\hat{S} = \exp\left(i\hat{H}_{\text{eff}}\right)$. Similarly, the scattering matrix, $\mathbf{S}$ can be expressed with the exponential map as $\mathbf{S} = \exp(i\mathbf{H})$ where the differential map, $d\zeta$, allows one to write an effective Hamiltonian, $\hat{H}_{\text{eff}}$, in terms of the matrix $\mathbf{H}$ as illustrated in figure 4.2. The differential map, $d\zeta$, between $\mathfrak{u}(N)$ and $\mathfrak{u}(n)$ can be expressed with the so-called Jordan-Schwinger map [125]

$$\hat{H}_{\text{eff}} = \left(\hat{a}_1^\dagger, \ldots, \hat{a}_m^\dagger\right) \mathbf{H} \begin{pmatrix} \hat{a}_1 \\ \vdots \\ \hat{a}_m \end{pmatrix} = \hat{\mathbf{A}}^\dagger \mathbf{H} \hat{\mathbf{A}}, \tag{4.72}$$

where the Hermiticity of $\hat{H}_{\text{eff}}$ follows from the Hermiticity of $\mathbf{H}$. Within the nonlinear crystal, there is an intermediate interaction in which the atoms in the material are excited before decaying back to their initial state by the emission of photons. As a result, $\hat{H}_{\text{eff}}$ is not a true Hamiltonian but an effective Hamiltonian [126]. This approach is equivalent to the one presented for photon conserving systems described by unitary scattering matrices as described in [105]. However, this method can be expanded to more general optical systems that include mechanisms for gain and loss [104, 127].

4.3.3 Single-Mode Case

If we take the case where we have a single mode propagating in each of the perturbation fields, described by Eqs. 4.50, with a stationary background field $\partial_z g(z) = 0$. Then the scattering matrix, $\mathbf{S}$, for an optical device of unit length can be written

$$\mathbf{S} = e^{i\delta} \begin{pmatrix} \mu\cos(\mu) + i\upsilon\sin(\mu) & ig\sin(\mu) \\ ig^*\sin(\mu) & \mu\cos(\mu) - i\upsilon\sin(\mu) \end{pmatrix}, \tag{4.73}$$

where the coefficients υ and δ are the same as those defined in section 3.4.4 with

$$\mu = \sqrt{|g|^2 + \upsilon^2}.$$

The scattering matrix is related to the Hermitian matrix $\mathbf{H}$ by the exponential map $\mathbf{S} = \exp(i\mathbf{H})$ with

$$\mathbf{H} = \begin{pmatrix} \upsilon_2 & g \\ g^* & \upsilon_3 \end{pmatrix}, \tag{4.74}$$

from which we can derive the effective Hamiltonian,

$$\hat{H}_{\text{eff}} = \upsilon_2 \hat{a}_2^\dagger \hat{a}_2 + \upsilon_3 \hat{a}_3^\dagger \hat{a}_3 + g^* \hat{a}_2^\dagger \hat{a}_3 + g \hat{a}_3^\dagger \hat{a}_2, \tag{4.75}$$

that describes the quantum behaviour of the operators associated with the quantised perturbation fields with $\hat{S} = e^{i\hat{H}_{\text{eff}}}$ satisfying Eq. 4.68. Moreover, using the Hamiltonian in

Heisenberg's equation will, up to a factor of $\hbar$, return the equations of evolution described by Eq. 4.50 for the single-mode case. This Hamiltonian, much like the equations of evolution, is made up of phase terms and mixing terms between the mode operators. Of particular note, the mixing terms in the Hamiltonian show that the creation or annihilation of a photon in one perturbation field is always accompanied by the annihilation or creation of a photon in the other - conserving the number of photons.

If we take, for example, a system with a single photon then we have three possible Fock states including the vacuum as $|n_2, n_3\rangle \in \{|0,0\rangle, |1,0\rangle, |0,1\rangle\}$. The creation and annihilation operators are consequently 3×3 matrices of the form:

$$\hat{a}_2 = \begin{pmatrix} 0 & 1 & 0 \\ 0 & 0 & 0 \\ 0 & 0 & 0 \end{pmatrix}, \quad \hat{a}_3 = \begin{pmatrix} 0 & 0 & 1 \\ 0 & 0 & 0 \\ 0 & 0 & 0 \end{pmatrix} \tag{4.76}$$

and

$$\hat{a}_2^\dagger = \begin{pmatrix} 0 & 0 & 0 \\ 1 & 0 & 0 \\ 0 & 0 & 0 \end{pmatrix}, \quad \hat{a}_3^\dagger = \begin{pmatrix} 0 & 0 & 0 \\ 0 & 0 & 0 \\ 1 & 0 & 0 \end{pmatrix}, \tag{4.77}$$

with the usual raising and lowering properties discussed in section 4.2.3 acting on the states $|n_2, n_3\rangle$. The Hamiltonian Eq. 4.75 in its matrix form is then

$$\hat{H}_{\text{eff}} = \begin{pmatrix} 0 & 0 & 0 \\ 0 & \upsilon_2 & g \\ 0 & g^* & \upsilon_3 \end{pmatrix}, \tag{4.78}$$

such that the scattering operator, $\hat{S}$, is written

$$\hat{S} = \begin{pmatrix} 1 & 0 & 0 \\ 0 & e^{i\delta}\left(\mu\cos(\mu) + i\upsilon\sin(\mu)\right) & ie^{i\delta}g\sin(\mu) \\ 0 & ie^{i\delta}g^*\sin(\mu) & e^{i\delta}\left(\mu\cos(\mu) - i\upsilon\sin(\mu)\right) \end{pmatrix}, \tag{4.79}$$

in which the 2×2 block in the bottom right of the matrix operator is equal to the initial scattering matrix, $\mathbf{S}$. We thus observe, that in the case of unitary systems consisting of a single photon, the scattering operator $\hat{S}$ reduces to the classical scattering matrix. This result indicates the significance of the fields to which the single-photon states are coupled. Indeed, if one was to prepare a photon in the state $|1,0\rangle$ which we can represent as the vector $(0,1,0)^\top$ then the state at the output is

$$|\psi_{out}\rangle = e^{i\delta}\left(\mu\cos(\mu) + i\upsilon\sin(\mu)\right)|1,0\rangle + ie^{i\delta}g^*\sin(\mu)\,|0,1\rangle, \tag{4.80}$$

which is made up of two components: one that gives the probability of the photon remaining in the first mode and the other the probability of being measured in the second mode. From a classical perspective, the terms in front of the kets are amplitudes and determine how much

energy the mode at ω_2 transfers to the mode at ω_3. At the single-photon level, however, the terms preceding the states, $|n_2, n_3\rangle$, correspond to probability amplitudes for a single photon to remain in the initial mode or to interact with the material and the background field and create a photon in the other mode. The distinction between these two perspectives comes from the fact one can predict the amount of energy transferred between the modes as the classical limit of the probability amplitude, but one cannot say with certainty how a single photon will behave as it propagates. Indeed, if we prepare a photon in the state $|1,0\rangle$ we can only predict with a certain probability if that photon will be measured in $|1,0\rangle$ or $|0,1\rangle$ at the output, as described by Eq. 4.80. Note, this behaviour is an effect of second quantisation and not sum-frequency generation. The values of the amplitudes are, however, dependent on the interaction of the fields in the nonlinear crystal.

In section 3.4.4, we introduced the eigenmodes of propagation for the scattering matrix similar to that of Eq. 4.73. These eigenmodes correspond to a distributed set of fields with components oscillating in both of the perturbation fields and are orthogonal to one another as they propagate. As shown in Eq. 4.55, the scattering matrix is unitary and therefore can be represented using an eigendecomposition of the form

$$\mathbf{S} = \mathbf{U}\mathbf{D}\mathbf{U}^{\dagger}, \tag{4.81}$$

where $\mathbf{U}$ corresponds to a unitary eigenvector matrix whose columns are the eigenvectors of the scattering matrix. For the single-mode case, this eigenvector matrix is

$$\mathbf{U} = \begin{pmatrix} \upsilon + i\csc(\mu)\sqrt{-\left(|g|^2+\upsilon^2\right)\sin(\mu)^2} & g^* \\ g^* & \upsilon - i\csc(\mu)\sqrt{-\left(|g|^2+\upsilon^2\right)\sin(\mu)^2} \end{pmatrix}, \tag{4.82}$$

with $\csc(\mu) = \sin(\mu)^{-1}$, $\mathbf{U}^{\dagger}\mathbf{U} = \mathbf{U}\mathbf{U}^{\dagger} = \mathbf{I}$ and $\mathbf{I}$ is a 2×2 identity matrix. The matrix $\mathbf{D}$ contains the eigenvalues associated with the eigenvectors in $\mathbf{U}$ and has the form

$$\mathbf{D} = \begin{pmatrix} \mu\cos(\mu) - \sqrt{-\left(|g|^2+\upsilon^2\right)\sin(\mu)^2} & 0 \\ 0 & \mu\cos(\mu) + \sqrt{-\left(|g|^2+\upsilon^2\right)\sin(\mu)^2} \end{pmatrix}. \tag{4.83}$$

Using this eigendecomposition, we can introduce a scattering matrix for the eigenmodes. Indeed, if we consider the transformation of the annihilation modes defined by Eq. 4.81 which we now write as

$$\begin{pmatrix} \hat{a}_2' \\ \hat{a}_3' \end{pmatrix} = \mathbf{U}\mathbf{D}\mathbf{U}^{\dagger} \begin{pmatrix} \hat{a}_2 \\ \hat{a}_3 \end{pmatrix}, \tag{4.84}$$

then we can define a scattering matrix for the eigenmode operators which we define at the input as:

$$\hat{b}_2 = \upsilon\hat{a}_2 - i\csc(\mu)\sqrt{-\left(|g|^2+\upsilon^2\right)\sin(\mu)^2}\hat{a}_2 + g\hat{a}_3, \tag{4.85}$$

$$\hat{b}_3 = \upsilon\hat{a}_3 + i\csc(\mu)\sqrt{-\left(|g|^2+\upsilon^2\right)\sin(\mu)^2}\hat{a}_3 + g\hat{a}_2, \tag{4.86}$$

and similarly for the output where $\hat{a}_\tau$ is replaced with $\hat{a}'_\tau$ in the above expressions. Like the original operators, $\hat{a}_\tau$, the eigenmode operators, $\hat{b}_\tau$, have bosonic commutation relations, $[\hat{b}_\tau, \hat{b}^\dagger_\sigma] = \delta_{\tau\sigma}$. By rearranging Eq. 4.84 as

$$\mathbf{U}^\dagger \begin{pmatrix} \hat{a}'_2 \\ \hat{a}'_3 \end{pmatrix} = \mathbf{D}\mathbf{U}^\dagger \begin{pmatrix} \hat{a}_2 \\ \hat{a}_3 \end{pmatrix}, \tag{4.87}$$

it becomes clear that the scattering matrix that maps the eigenmode operators from the input to the output is

$$\begin{pmatrix} \hat{b}'_2 \\ \hat{b}'_3 \end{pmatrix} = \mathbf{D} \begin{pmatrix} \hat{b}_2 \\ \hat{b}_3 \end{pmatrix}, \tag{4.88}$$

where the eigenvalue matrix $\mathbf{D}$, which now acts as a scattering matrix for the eigenmode operators, is diagonal as there is no mixing between the fields associated with the operators. With this new scattering matrix, we can derive an effective Hamiltonian that describes the behaviour of single photons coupled to the propagation eigenmodes. Following the method outlined in section 4.3.2.2, where the scattering matrix for the eigenmode operators is replaced by the eigenvalue matrix $\mathbf{D}$, we find the following effective Hamiltonian

$$\hat{H}_{b,\text{eff}} = -i\ln\left(\mu\cos(\mu) + \sqrt{-\left(|g|^2+\upsilon^2\right)\sin(\mu)^2}\right)\hat{b}^\dagger_2\hat{b}_2 \tag{4.89}$$

$$-i\ln\left(\mu\cos(\mu) - \sqrt{-\left(|g|^2+\upsilon^2\right)\sin(\mu)^2}\right)\hat{b}^\dagger_3\hat{b}_3, \tag{4.90}$$

in which there is no mixing between the eigenmode operators $\hat{b}_\tau$ and the system is therefore decoupled. If we consider a system with a single photon, then the creation and annihilation operators $\hat{b}_\tau$ and $\hat{b}^\dagger_\tau$ are the same as those defined in Eq. 4.77 and 4.76. The scattering matrix in this case is

$$\hat{S}_b = \begin{pmatrix} 1 & 0 & 0 \\ 0 & \mu\cos(\mu) - \sqrt{-\left(|g|^2+\upsilon^2\right)\sin(\mu)^2} & 0 \\ 0 & 0 & \mu\cos(\mu) + \sqrt{-\left(|g|^2+\upsilon^2\right)\sin(\mu)^2} \end{pmatrix}, \tag{4.91}$$

where we have introduced the subscript b to describe the transformation associated with the $\hat{b}$ operators. If we consider the state $|m_1, m_2\rangle = |1, 0\rangle$ at the input - where m_k denotes the number of photons in the k^{th} eigenmode - then the output state will also be measured as $|1, 0\rangle$ with probability 1. The same is true for any eigenmode Fock state, $|m_1, m_2\rangle$. Therefore, by transforming the classical fields into an eigenmodes basis, the evolution of the Fock states is decoupled such that the states $|m_1, m_2\rangle$ are eigenstates of the system. As with the scattering matrix $\hat{S}$ the 2×2 block in the bottom right of $\hat{S}_b$ is equal to the scattering

matrix which, in the context of the eigenmode operators, is $\mathbf{D}$. This simple single-mode case illustrates how the eigenmode representation of the classical scattering matrix simplifies the evolution of the Fock states. This can be extended to the case where we have multiple modes propagating on each of the fields.

4.3.4 Multimode Case

If we have multiple independent modes propagating on each of the wavelengths, then the scattering matrix linking the annihilation operators of the output modes $\hat{\mathbf{A}}'$ to the annihilation operators of the input modes $\hat{\mathbf{A}}$ as

$$\hat{\mathbf{A}}' = \mathbf{S}\hat{\mathbf{A}}, \tag{4.92}$$

with $\hat{\mathbf{A}}$ and $\hat{\mathbf{A}}'$ defined as $\hat{\mathbf{A}} = (\hat{a}_1, \ldots, \hat{a}_m)^\top$ and $\hat{\mathbf{A}}' = (\hat{a}'_1, \ldots, \hat{a}'_m)^\top$, where the symbol $\top$ denotes the transpose of the vectors and $m = m_2 + m_3$ is the total number of modes in the decomposition. The Fock states, in this case, are written

$$|\psi\rangle = |n_{2,1}, \ldots, n_{2,m_2}, n_{3,1}, \ldots, n_{3,m_3}\rangle = |n_1, \ldots, n_m\rangle\,,$$

where n_j is the total number of photons in the j^{th} mode. The states, $|n_1, \ldots, n_m\rangle$, written in terms of the creation operators are

$$|n_1, \ldots, n_m\rangle = \prod_{k=1}^{m} \left(\frac{\hat{a}_k^{\dagger n_k}}{\sqrt{n_k!}} \right) |0, \ldots, 0\rangle\,, \tag{4.93}$$

which evolve to the output plane as

$$\hat{S}\,|n_1, \ldots, n_m\rangle = \prod_{k=1}^{m} \frac{1}{\sqrt{n_k!}} \left(\sum_{j=1}^{m} \mathbf{S}^*_{kj} \hat{a}_j^\dagger \right)^{n_k} |0, \ldots, 0\rangle\,, \tag{4.94}$$

highlighting the link between the evolution of the photon states, $|n_1, \ldots, n_m\rangle$, and the evolution of the classical fields to which the photons are coupled. This is most apparent when the system consists of a single photon such that Eq. 4.94 is now written

$$\hat{S}\,|0, \ldots, n_k = 1, \ldots, 0\rangle = \left(\sum_{j=1}^{m} \mathbf{S}^*_{kj} \hat{a}_j^\dagger \right) |0, \ldots, 0\rangle\,, \tag{4.95}$$

where the input states on the left-hand side will have zero photons on all of the modes except the k^{th} mode. Regardless of the number of independent modes in the system, the scattering matrix is still unitary and the decomposition Eq. 4.81 is still valid. Indeed, the eigenmode operators in this instance are at the input and output defined as

$$\hat{\mathbf{B}} = \mathbf{U}^\dagger \hat{\mathbf{A}}, \tag{4.96}$$

$$\hat{\mathbf{B}}' = \mathbf{U}^\dagger \hat{\mathbf{A}}', \tag{4.97}$$

where $\mathbf{U}$ is the $m \times m$ eigenvector matrix. As with the vector $\hat{\mathbf{A}}$, we define

$$\hat{\mathbf{B}} = \left(\hat{b}_1, \ldots, \hat{b}_m\right)^\top,$$

as the annihilation operator for the eigenmodes at the input with elements

$$\hat{b}_k = \sum_{j=1}^{m} \mathbf{U}_{jk}^* \hat{a}_j. \tag{4.98}$$

Similarly, we define $\hat{\mathbf{B}}' = \left(\hat{b}'_1, \ldots, \hat{b}'_m\right)^\top$ as the operator associated with the output eigenmodes. Using this, we can introduce a new scattering matrix for the eigenmode operators starting with Eq. 4.92 which we rewrite as

$$\hat{\mathbf{A}}' = \left(\mathbf{U}\mathbf{D}\mathbf{U}^\dagger\right) \hat{\mathbf{A}}, \tag{4.99}$$

which can then be rearranged to give

$$\mathbf{U}^\dagger \hat{\mathbf{A}}' = \left(\mathbf{D}\mathbf{U}^\dagger\right) \hat{\mathbf{A}} \tag{4.100}$$

and using the transformation defined in Eqs. 4.96 and 4.97 the input-output relationship is simplified in the same way as the single-mode case as

$$\hat{\mathbf{B}}' = \mathbf{D}\hat{\mathbf{B}}. \tag{4.101}$$

The eigenmodes operators introduced in Eq. 4.98 have bosonic commutation relations

$$\left[\hat{b}_j, \hat{b}_k^\dagger\right] = \hat{b}_j \hat{b}_k^\dagger - \hat{b}_k^\dagger \hat{b}_j = \delta_{jk}.$$

These operators decouple the state evolution as described in Eq. 4.101 as $\mathbf{D}$ is a diagonal matrix with elements $|D_{jj}| = 1$. Therefore, by transforming the classical fields into an eigenmode representation, the Fock states associated with the eigenmodes correspond eigenstates of the quantum system unlike the states given by Eq. 4.94, which are distributed across the Fock state basis. In short, using the eigenmode decomposition, we replace the Fock state coupling by classical field coupling. Indeed, if we make use of the transformations described in Eq. 4.96 the evolution of the Fock states in the eigenmode basis is written

$$\begin{aligned}
\hat{S}_b \left|n_1, \ldots, n_m\right\rangle_b^{in} &= \prod_{k=1}^{m} \frac{1}{\sqrt{n_k!}} \left(\sum_{j=1}^{m} D_{jk} \hat{b}_k^\dagger\right)^{n_k} |0, .., 0\rangle \\
&= \prod_{k=1}^{m} D_{kk}^{n_k} \frac{1}{\sqrt{n_k!}} \hat{b}_k^{\dagger n_k} |0, .., 0\rangle ,
\end{aligned} \tag{4.102}$$

where the subscript $|\,\rangle_b$ is introduced for states in the eigenmode basis, and $\hat{S}_b$ is the scattering operator derived from the diagonal scattering matrix $\mathbf{D}$. This scattering operator $\hat{S}_b$ is diagonal, which we can show explicitly by substituting the input states,

$$|n_1,\ldots,n_m\rangle_b^{\text{in}} = \prod_{k=1}^{m} \frac{1}{\sqrt{n_k!}} \hat{b}_k^{\dagger n_k} |0,\ldots,0\rangle\,, \tag{4.103}$$

into Eq. 4.102 such that the matrix elements of the scattering operator become

$$\left\langle n_1',\ldots,n_m'\right|_b^{in} \hat{S}_b\, |n_1,\ldots,n_m\rangle_b^{in} = \prod_{k=1}^{m} D_{kk}^{n_k}. \tag{4.104}$$

Given the link between $\hat{\mathbf{A}}$ and $\hat{\mathbf{B}}$, we can write the states with respect to either of the operators in either of the associated Fock spaces

$$\begin{aligned} |n_1,\ldots,n_m\rangle_b^{\text{in}} &= \prod_{k=1}^{m} \frac{1}{\sqrt{n_k!}} \hat{b}_k^{\dagger n_k} |0,\ldots,0\rangle \\ &= \prod_{k=1}^{m} \frac{1}{\sqrt{n_k!}} \left(\sum_{j=1}^{m} U_{kj}\hat{a}_j^{\dagger}\right)^{n_k} |0,\ldots,0\rangle\,, \end{aligned} \tag{4.105}$$

where the vacuum state is the same for both representations. This expression gives us a direct way to transform between both representations in the context of Fock states and ensures the photon states correspond to the same physical states regardless of how they are represented. However, the propagation eigenmodes greatly simplify the evolution of Fock states. From the perspective of quantum field theory [22, 114] one can imagine the perturbation fields with their transverse structure as states that the single photons can occupy. Indeed, the same can be said for the propagation eigenmodes. However, in the case of the eigenmodes, the photons will remain coupled to the same state as it evolves through the system. It is, therefore, useful to consider not only the evolution of single or multiphoton states and how they evolve but also the fields to which they are coupled.

4.3.4.1 Numerical Examples

As a numerical example, we consider the set-up described in section 3.3.1. Namely, we have a KDP nonlinear crystal with $\chi_{\text{eff}}^{(2)} = 0.558$ pm/V for perturbation fields of wavelength $\lambda_2 = 740$ and $\lambda_3 = 436.5$ nm with the background field at wavelength $\lambda_b = 1064$ nm. Further, to simplify the model, we consider the case of type I perfect phase matching, $\Delta k = 0$, in which the fields at λ_b and λ_2 are polarised along the ordinary axis of the crystal, and the field at λ_3 is polarised along the extraordinary axis. For the example shown here, the background field considered, $E_b(x, y, z)$, has a beam waist $w_b = 20\lambda_b$, and average power of 10 nW which is equivalent to 10^{10} photons s^{-1}. Therefore, the background field will not

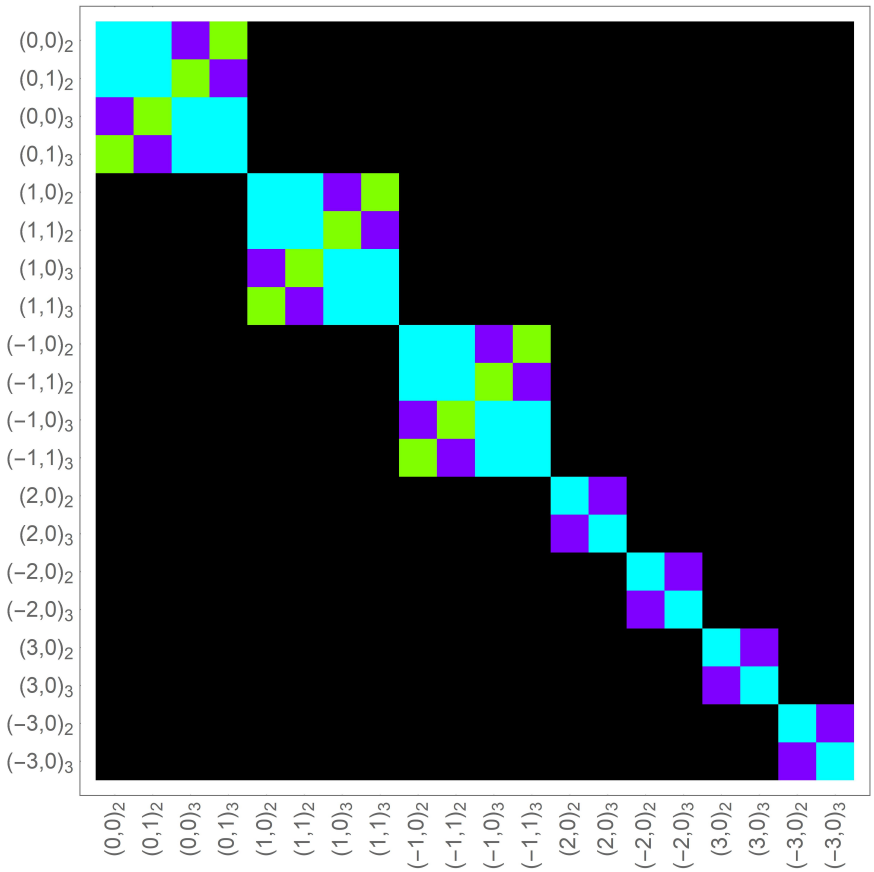

Figure 4.3: Scattering matrix for LG_{00} background field represented with the false colour map shown in figure 1.3 with indices $(\ell, p)_\tau = (\ell_\tau, p_\tau)$.

be perturbed by the presence of the other two fields. From an experimental context, one could detect single photons by using suitable notch filters allowing one to investigate each frequency component of the mode by attenuating the other component and the background.

For example, we can choose a finite basis set of Laguerre-Gaussian modes on which to decompose the low-intensity perturbation fields. To visualise the results, we truncate the Hilbert space defined by the Laguerre-Gaussian modes to a maximal index of $2p + |\ell| \leq 3$ and, in this case, we consider a background field with $\ell_b = 0$. The classical scattering matrix in this basis is illustrated in figure 4.3, which we observe to have a block-diagonal structure. This is due to the selection rules associated with the OAM of the fields, $\ell_3 - \ell_2 = \ell_b$, which for a background field with $\ell_b = 0$ reduces to $\ell_2 = \ell_3$. This selection rule remains true for all radial indices, illustrated in the 4×4 blocks in figure 4.3. This scattering matrix defines a scattering operator, as outlined in section 4.3.4, shown in figure 4.4. The scattering operator is shown up to a maximum total photon number of $N_{\max} = 2$ where the

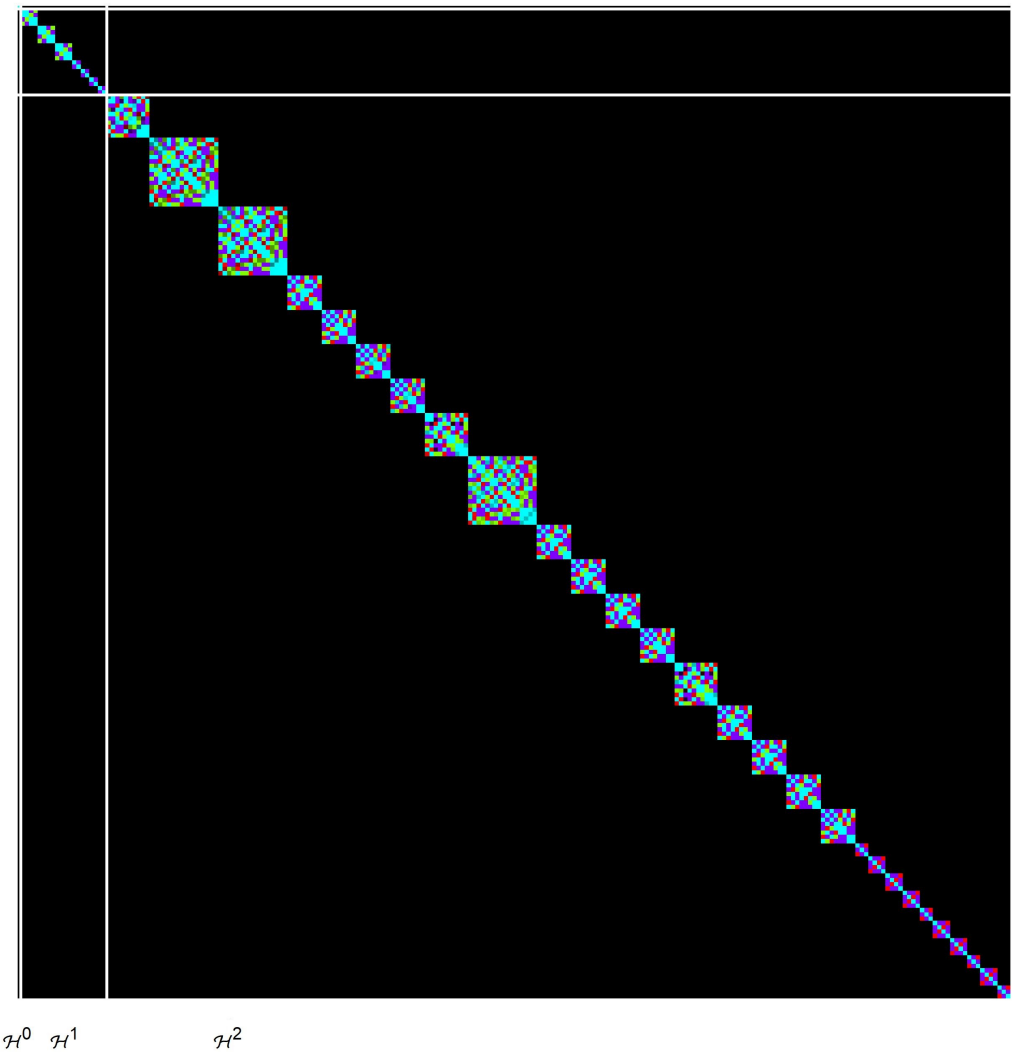

Figure 4.4: Unitary scattering operator $\hat{S}$ for LG_{00} background represented with the false colour map shown in figure 1.3. The labels $\mathcal{H}^n$ correspond to the n-photon number Hilbert space.

matrix blocks highlighted with the grid lines correspond to the n-photon Hilbert spaces. As shown in Eq. 4.55 and 4.56, the number of photons is conserved, and therefore there are no amplification or loss mechanisms in the optical system. Consequently, the n-photon Hilbert spaces do not interact with one another, hence their block structure. Each of these total photon number blocks is further block-diagonal due to the symmetries associated with the OAM, as illustrated in figure 4.3. Additionally, due to the non-interacting nature of the photon Hilbert spaces, a scattering operator calculated to higher photon number, $N_{\max}$, will leave the matrix shown in figure 4.4 unchanged. The truncation of the Fock state basis requires one to use truncated creation and annihilation operators and the details on how we construct these operators is described in Appendix B.

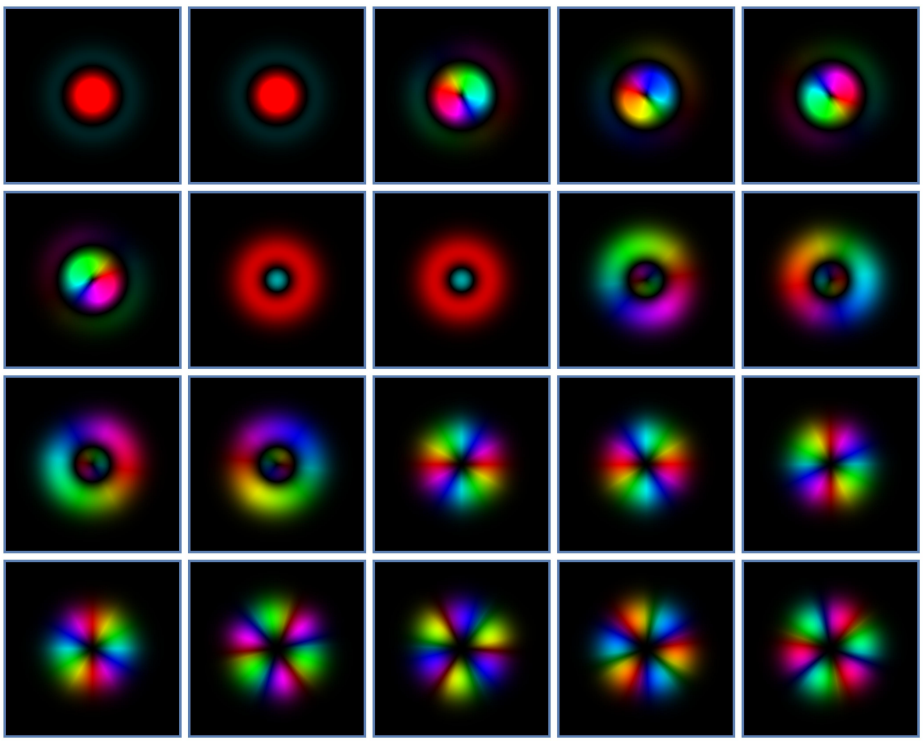

(a)

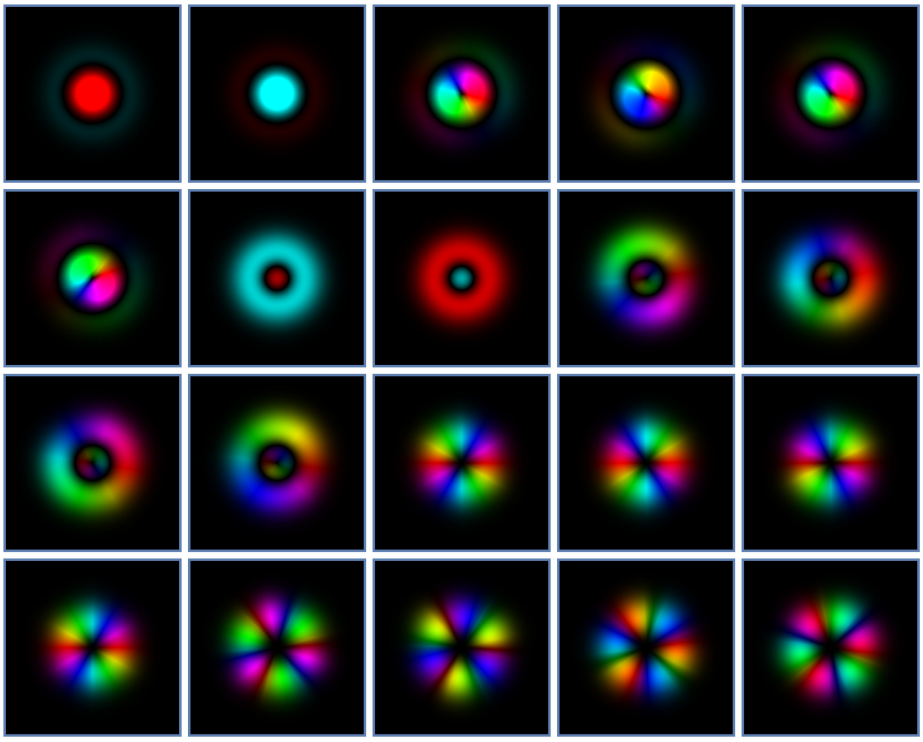

(b)

Figure 4.5: Propagation eigenmodes in the output plane for a LG_{00} background field with components (a) $\mathbb{F}_{2,k}(r_2)e^{-i\ell_{2,k}\phi}$ and (b) $\mathbb{F}_{3,k}(r_2)e^{-i\ell_{3,k}\phi}$.

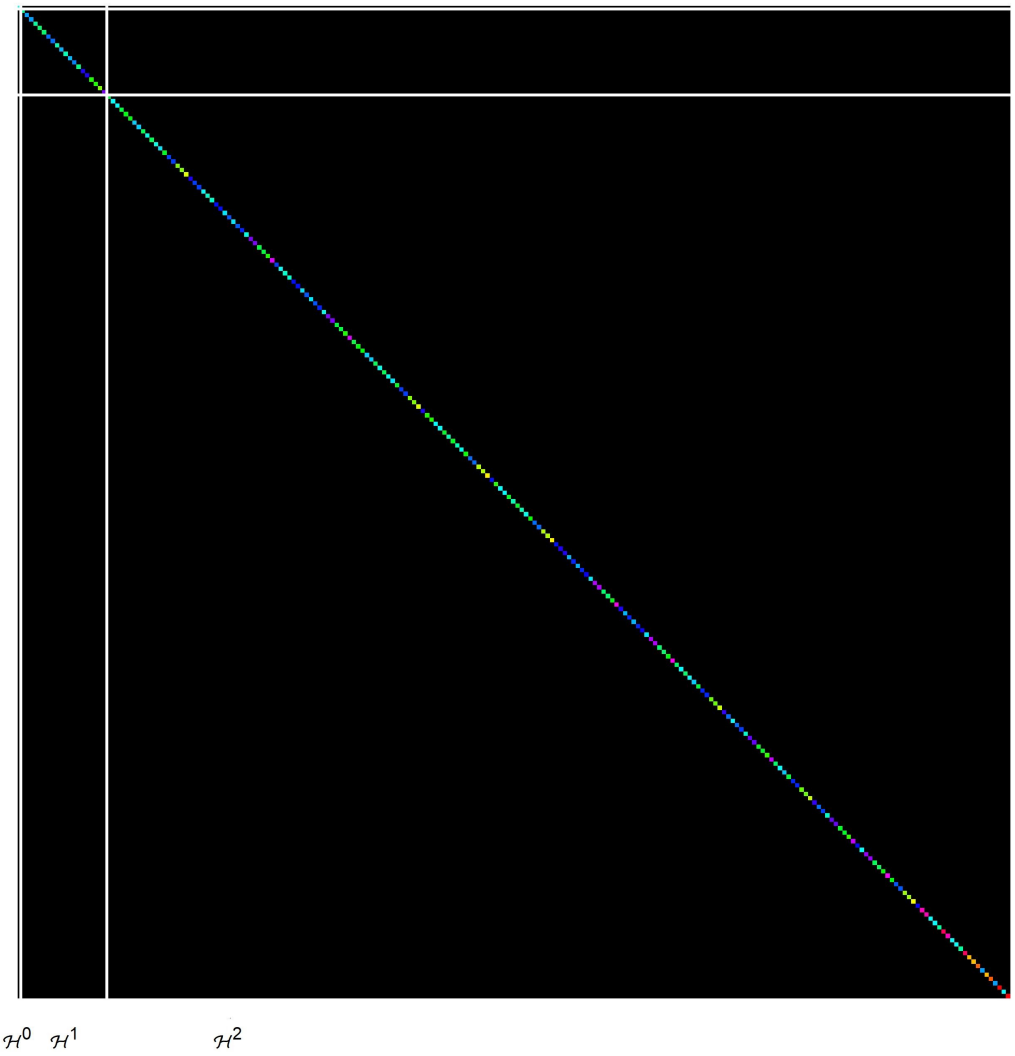

Figure 4.6: Unitary scattering operator $\hat{S}_b$ for LG_{00} background represented with the false colour map shown in figure 1.3. The labels $\mathcal{H}^n$ correspond to the n-photon number Hilbert space.

Utilising the decomposition of the scattering matrix, as described in section 4.3.4, we can introduce the propagation eigenmodes of the scattering matrix, shown in figure 4.5. The scattering matrix transforming these eigenmodes from the input to the output is the diagonal eigenvalue matrix $\mathbf{D}$. From this scattering matrix, we can derive a scattering operator, $\hat{S}_b$, describing the evolution of the Fock states with respect to the propagation eigenmodes. This is represented in figure 4.6, and like the scattering matrix from which it is derived, is diagonal. Therefore, by utilising the eigenmode transformation defined in, Eq. 4.96, the Fock states associated with the eigenmodes of $\mathbf{S}$ will evolve as eigenstates of the quantum system. Consequently, in this eigenmode basis, a single photon coupled to one of the eigenmodes will remain coupled to that eigenmode as it evolves through the nonlinear

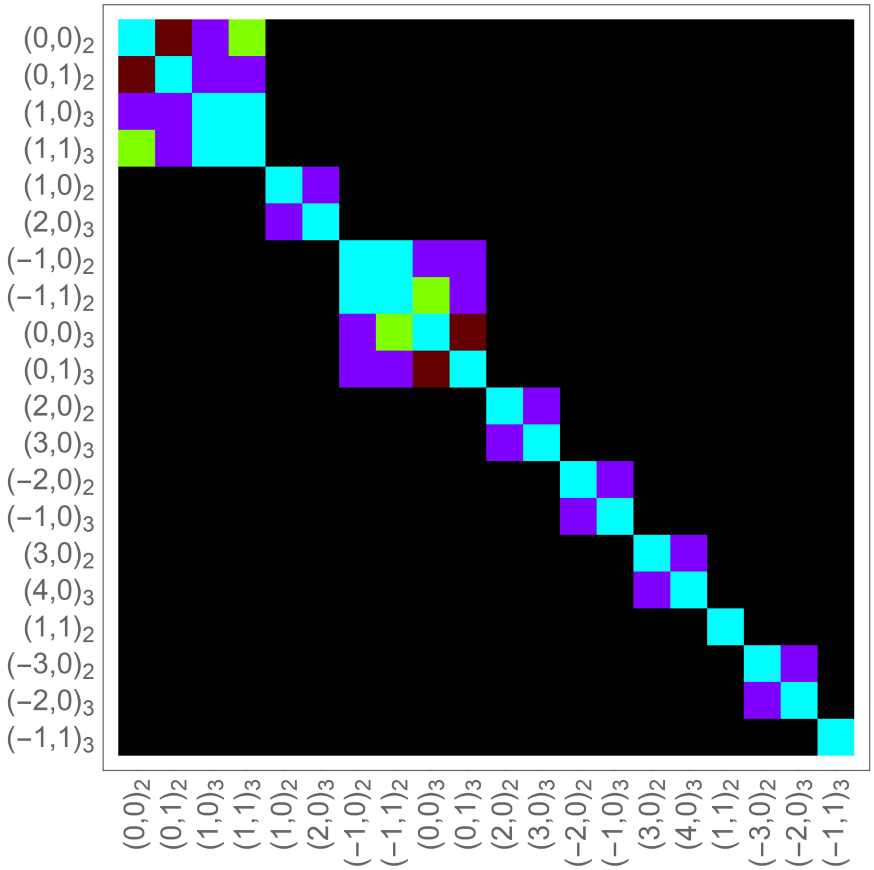

Figure 4.7: Scattering matrix for LG_{10} background field represented with the false colour map shown in figure 1.3 with indices $(\ell, p)_\tau = (\ell_\tau, p_\tau)$.

material.

As a secondary example, we consider a background field with OAM $\ell_b = +1$ with a basis of Laguerre-Gaussian modes truncated to some maximal index. However, as highlighted in section 3.3.3, choosing the same basis as used in the example for $\ell_b = 0$ will not be complete with respect to the conservation rule $\ell_3 = \ell_2 + \ell_b$. Indeed, if we consider the field with OAM $\ell_2 = 3$ interacting with a background which has $\ell_b = +1$ then the field resulting from this interaction would have OAM $\ell_3 = +4$: which is out with the truncated basis for the previous example. Therefore, in order to keep all possible interactions closed with respect to the basis, we truncate the basis elements as described in section 3.3.3.

The scattering matrix for this example is shown in figure 4.7. Again, the matrix is block-diagonal due to the conservation associated with the orbital angular momentum of the fields, i.e. $\ell_3 - \ell_2 = \ell_b$. Similar to the example presented above the scattering matrix

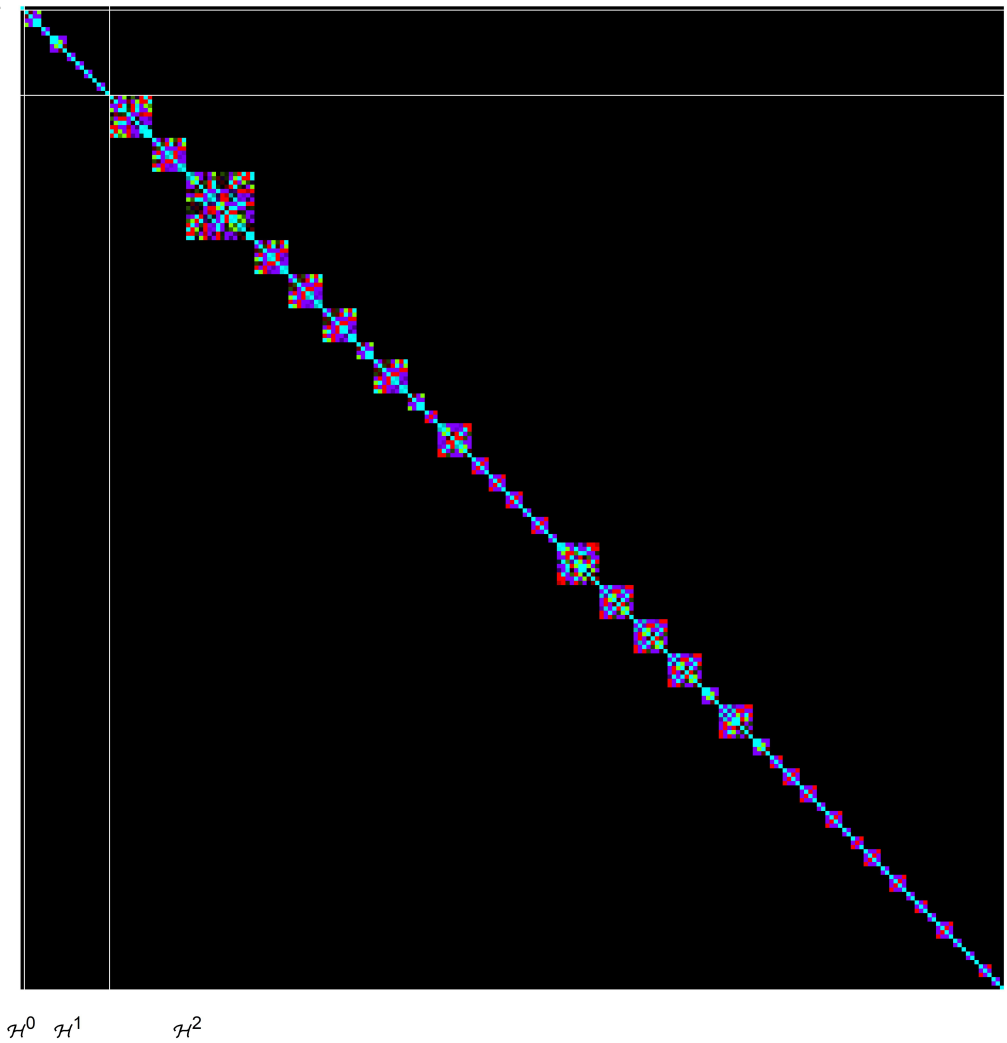

Figure 4.8: Unitary scattering operator $\hat{S}$ for LG_{10} background represented with the false colour map shown in figure 1.3. The labels $\mathcal{H}^n$ correspond to the n-photon number Hilbert space.

contains all of the symmetry associated with the system and is the same as the associated scattering operator if the system consists only of a single photon, i.e. when $N_{max} = 1$. This is indeed observed in the scattering operator for this example, which is depicted in figure 4.8. By changing the OAM of the background and truncating the basis fields appropriately, the eigenmodes of the scattering matrix encode all of the symmetry in the system. Consequently, if we diagonalise the scattering matrix as described in section 4.3.4, we find a diagonal, unitary scattering operator, $\hat{S}_b$, that acts on the Fock states, as shown in figure 4.9. Thus, the eigenmode Fock states are eigenstates of the system in the context of the classical propagation eigenmodes of the scattering matrix, which are shown in figure 4.10.

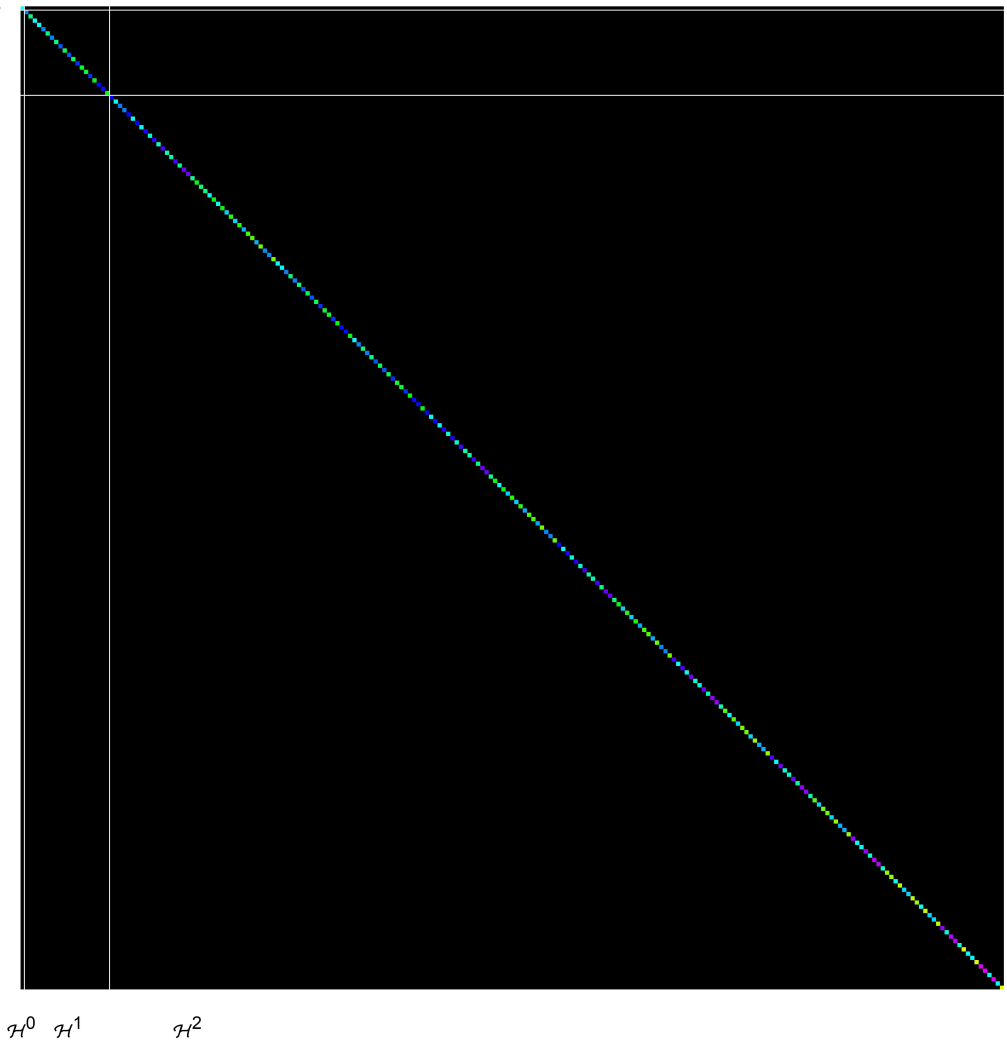

Figure 4.9: Unitary scattering operator $\hat{S}_b$ for LG_{10} background represented with the false colour map shown in figure 1.3. The labels $\mathcal{H}^n$ correspond to the n-photon number Hilbert space.

4.4 Multiphoton Parametric Down-Conversion

In this section, we turn our attention to the quantum behaviour of Fock states in the context of parametric down-conversion. As shown in Chapter 2, the effects of parametric down-conversion and sum-frequency generation are closely related. In the approximation where the pump field is non-depleting, these effects describe, as discussed in section 2.3, two interacting fields with rather different behaviour. Indeed, in the case of sum-frequency generation, the interacting fields transfer energy between one another in an oscillatory manner. In contrast, parametric down-conversion shows the fields to be exponentially increasing in energy density. Consequently, the scattering matrix defined for sum-frequency

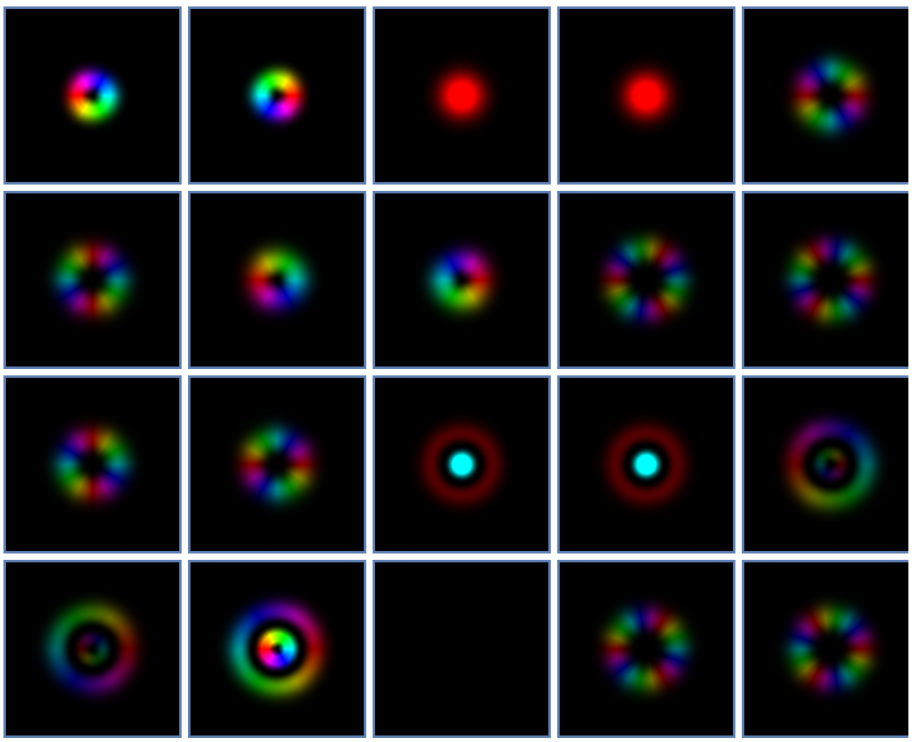

(a)

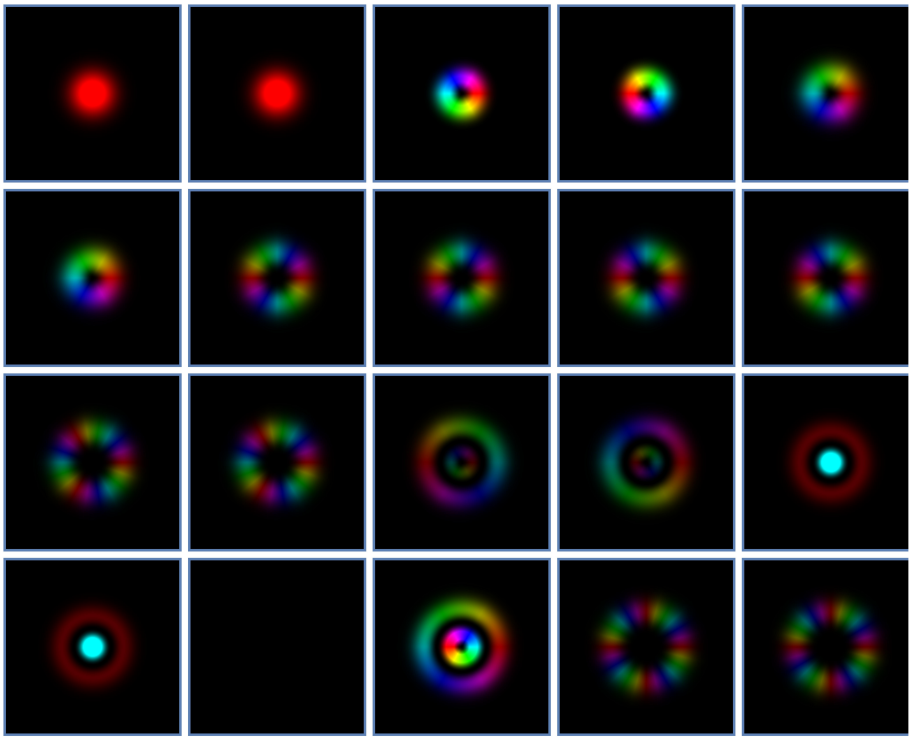

(b)

Figure 4.10: Propagation eigenmodes in the output plane for a LG_{10} background field with components (a) $\mathbb{F}_{2,k}(r_2)e^{-i\ell_{2,k}\phi}$ and (b) $\mathbb{F}_{3,k}(r_2)e^{-i\ell_{3,k}\phi}$.

generation, in section 3.4.4, is unitary and that which describes down-conversion, defined in section 3.7.3, is not. Therefore, the method for deriving an effective Hamiltonian as outlined in section 4.3.2.2 is not valid for the case of parametric down-conversion. In this section, we outline how to introduce an effective Hamiltonian in the context of parametric down-conversion. As in section 4.3.1, we first describe the system with modified field variables that have units of photon flux and quantise the system by promoting field amplitudes to creation and annihilation operators. As an example, we consider the single-mode case introduced in section 3.7.3 and use it to highlight the incompatibility of the conditions required to define orthogonal eigenmodes of the scattering matrix and those required to preserve the canonical commutation relations of bosonic operators.

4.4.1 Parametric Down-Conversion Modified Field Variables

Following the same procedure outlined in section 4.3.1, we find the following closed set of equations in the context of modified field variables:

$$\begin{aligned} -i\partial_z a_{1,j}(z) &= \sum_{k=1}^{N} \upsilon_{1,jk} a_{1,k}(z) + g_{jk}(z) a^*_{2,k}(z), \\ i\partial_z a^*_{2,j}(z) &= \sum_{k=1}^{N} \upsilon_{2,jk} a^*_{2,k}(z) + g^*_{kj}(z) a_{1,k}(z), \end{aligned} \tag{4.106}$$

with the matrices

$$\upsilon_{\tau,jk} = \iint \frac{1}{2k_\tau}\, f^*_{\tau,j}(x,y) \nabla_T^2 f_{\tau,k}(x,y)\, \mathrm{d}x\, \mathrm{d}y, \tag{4.107}$$

and

$$g_{jk}(z) = \chi \iint f^*_{1,j}(x,y) f^*_{2,k}(x,y) E_b(x,y,z) e^{-i\Delta k z}\, \mathrm{d}x\, \mathrm{d}y, \tag{4.108}$$

where again we have $\chi = \frac{\chi^{(2)}}{c}\sqrt{\frac{\omega_1 \omega_2}{n_1 n_2}}$ as the interaction strength and $\chi^{(2)}$ is the second-order nonlinear susceptibility of the propagating material. The coefficients in Eqs. 4.106 are related to the transverse field profiles via the expansion

$$E_\tau(x,y,z) = \sum_{j=1}^{N} \sqrt{\frac{\omega_\tau}{n_\tau}} a_{\tau,j}(z) f_{\tau,j}(x,y). \tag{4.109}$$

where again the functions $\sqrt{\omega_\tau/n_\tau} f_{\tau,j}(x,y)$ form an orthonormal basis satisfying the following condition

$$\iiint \frac{1}{2\pi} e^{-i(\omega_\sigma - \omega_\tau)t} \sqrt{\frac{\omega_\tau}{n_\tau}} \sqrt{\frac{\omega_\sigma}{n_\sigma}} f^*_{\tau,j}(x,y) f_{\sigma,k}(x,y)\, \mathrm{d}x\, \mathrm{d}y\, \mathrm{d}t = \delta(\omega_\tau - \omega_\sigma)\delta_{jk}. \tag{4.110}$$

The evolution of the coefficients given by Eqs. 4.106 are written in terms of a scattering matrix as

$$\begin{pmatrix} a'_{1,k} \\ a^{*\prime}_{2,k} \end{pmatrix} = \mathbf{S} \begin{pmatrix} a_{1,k} \\ a^{*}_{2,k} \end{pmatrix}, \tag{4.111}$$

where $a_{\tau,k}$ are the field amplitudes of the modes at the input plane and $a'_{\tau,k}$ are the amplitudes of the corresponding output modes and $\mathbf{S} = \exp\left(\int_z i\mathbf{P}(z)\mathrm{d}z\right)$ with

$$\mathbf{P}(z) = \begin{pmatrix} \upsilon_{1,jk} & g_{jk}(z) \\ -g^{*}_{kj}(z) & -\upsilon_{2,jk} \end{pmatrix}. \tag{4.112}$$

If we now quantise this system by promoting the coefficients to operators as, $a_{\tau,j} \rightarrow \hat{a}_{\tau,j}$ and $a^{*}_{\tau,j} \rightarrow \hat{a}^{\dagger}_{\tau,j}$ the scattering matrix in terms of the creation and annihilation operators is

$$\begin{pmatrix} \hat{a}'_{1,k} \\ \hat{a}^{\prime\dagger}_{2,k} \end{pmatrix} = \mathbf{S} \begin{pmatrix} \hat{a}_{1,k} \\ \hat{a}^{\dagger}_{2,k} \end{pmatrix}, \tag{4.113}$$

wherein the case of parametric down-conversion, there is mixing between creation and annihilation operators not observed for sum-frequency generation.

4.4.2 Effective Hamiltonian for Parametric Down-Conversion

As the matrix $\mathbf{P}(z)$ is not Hermitian, the scattering matrix $\mathbf{S}$ is not unitary but quasi-unitary [100]. As shown in [104], scattering matrices that are quasi-unitary can be transformed into a unitary space by introducing an appropriate metric [128, 129]. Indeed, if we transform $\mathbf{P}(z)$ into a Hermitian form, then the unitarity of the scattering matrix will follow. As shown in the previous section the $\mathbf{P}(z)$ matrix for parametric down-conversion is of the form

$$\mathbf{P}(z) = \begin{pmatrix} \upsilon_{1,jk} & g_{jk}(z) \\ -g^{*}_{kj}(z) & -\upsilon_{2,jk} \end{pmatrix}, \tag{4.114}$$

where $\mathbf{P}(z) \neq \mathbf{P}(z)^{\dagger}$. If we simplify this and assume that the gain is sufficiently high such that $\upsilon_{\tau,jk} \ll g_{jk}(z)$ then we are left with a skew-Hermitian or anti-Hermitian matrix of the form

$$\mathbf{Q}(z) = \begin{pmatrix} 0 & g_{jk}(z) \\ -g^{*}_{kj}(z) & 0 \end{pmatrix}, \tag{4.115}$$

in which $\mathbf{Q}(z) = -\mathbf{Q}(z)^{\dagger}$. As discussed in sections 3.6, this system does not conserve energy density due to exponential gain of the low-intensity perturbation fields. Therefore, the photon number is not conserved such that a suitable quantum description of the effect cannot follow from the method in section 4.3.2.2, which is valid for unitary scattering matrices.

In order to find the quantum behaviour of this system, we require a transformation that modifies the inner product space such that the matrix $\eta\mathbf{Q}(z)$ defines an exponential map that is unitary with respect to the metric operator η, which we assume to be real. In particular, we require

$$e^{(i\eta\mathbf{Q}(z))^\dagger}e^{(i\eta\mathbf{Q}(z))} = e^{\left(-i\mathbf{Q}(z)^\dagger\eta+i\eta\mathbf{Q}(z)\right)} = \mathbf{I}$$

which is satisfied if $\mathbf{Q}(z)^\dagger\eta - \eta\mathbf{Q}(z) = 0$. We can re-write this condition as the following

$$\mathbf{Q}(z)^\dagger = \eta\mathbf{Q}(z)\eta^{-1}, \tag{4.116}$$

where to map the matrix $\mathbf{Q}(z)$ to a Hermitian form we need to find the metric operator η. In general, finding this metric can be a difficult problem to solve, as highlighted in [130, 131, 132, 133]. However, in this instance, using $\mathbf{Q}(z)$ we have the relation

$$\mathbf{Q}(z)^\dagger \begin{pmatrix} \eta_{11} & \eta_{12} \\ \eta_{21} & \eta_{22} \end{pmatrix} = \begin{pmatrix} \eta_{11} & \eta_{12} \\ \eta_{21} & \eta_{22} \end{pmatrix} \mathbf{Q}(z), \tag{4.117}$$

that, upon inputting Eq. 4.115, we find the following set of matrix equations:

$$g_{jk}(z)\eta_{21} - g^*_{jk}(z)\eta_{12} = 0 \tag{4.118}$$

$$g_{jk}(z)\eta_{11} + g_{jk}(z)\eta_{22} = 0 \tag{4.119}$$

$$g^*_{jk}(z)\eta_{11} + g^*_{jk}(z)\eta_{22} = 0 \tag{4.120}$$

$$g_{jk}(z)\eta_{12} - g^*_{jk}(z)\eta_{21} = 0 \tag{4.121}$$

which gives $\eta_{12} = \eta_{21} = 0$ and $\eta_{11} = -\eta_{22}$. Although we have not yet chosen the form of η, using the Hermitian matrix

$$\mathbf{H} = \eta\mathbf{Q}(z)$$

we can find an effective Hamiltonian in the same manner as shown in section 4.3.2.2 that describes the quantum behaviour of the system.

4.4.3 Single-Mode Case

If we consider, as a first example, the case in which we have a single mode propagating on each of the wavelengths with a stationary background field then the matrices $g_{jk}(z)$ and η_{11} reduce to single coefficients which we denote g and ϑ, respectively. Consequently, the matrix $\mathbf{H}$ in the previous section, where $\upsilon_{\tau,jk} \ll g_{jk}(z)$, reduces to a 2×2 form. With this single-mode Hermitian matrix, we can use the Jordan-Schwinger map introduced in section 4.3.2.2 to find an effective Hamiltonian of the form

$$\hat{H}_{\text{eff}} = \vartheta\left(g\hat{a}_1^\dagger\hat{a}_2^\dagger + g^*\hat{a}_1\hat{a}_2\right). \tag{4.122}$$

Notice, the term inside the bracket is Hermitian so ϑ must be real; for the purposes of this section, we choose $\vartheta = 1$. The above Hamiltonian can be checked by inputting it into the Heisenberg equation introduced in section 4.2.1 where one will derive the original scattering matrix relation Eq. 4.113 where $\mathbf{S} = \exp\left(\int_z i\mathbf{Q}(z)\mathrm{d}z\right)$. Therefore, the following equality

$$\mathbf{S}\begin{pmatrix}\hat{a}_1\\ \hat{a}_2^\dagger\end{pmatrix} = \hat{S}^\dagger\begin{pmatrix}\hat{a}_1\\ \hat{a}_2^\dagger\end{pmatrix}\hat{S}, \tag{4.123}$$

where $\hat{S} = \exp\left(i\hat{H}_{\text{eff}}\right)$, is satisfied. Consequently, the effective Hamiltonian does indeed describe the quantum behaviour of parametric down-conversion in the context of the effective Hamiltonian method. From a physical perspective, the metric η is related to symmetries of the equations of evolution via the matrix $\mathbf{Q}(z)$. In particular, if the eigenvalues of the quasi-Hermitian matrix are real or come in conjugate pairs, the metric can be attributed to the parity-time symmetry of the system [134, 135, 136, 137]. For the purposes of this work, we are only concerned with the result that the Hamiltonian describes the quantum behaviour of the system in a manner that links it to the initially defined scattering matrix. The same can also be done when the approximation $\upsilon_{\tau,jk} \ll g_{jk}(z)$ is not valid. However, as outlined in section 3.7.3, this simplification allows us to define orthogonal propagation eigenmodes.

4.4.4 Eigenmode Operators and Bogoliubov Transformation

In section 4.3.3, we showed that in the single-mode case for sum-frequency generation, we can diagonalise the scattering matrix to define eigenmode operators that subsequently diagonalise the quantum operator. The scattering matrix associated with the single-mode case here, as shown in section 3.6, is of the form

$$\mathbf{S} = \begin{pmatrix}\cosh\left(\sqrt{g^*}\sqrt{g}z\right) & i\frac{\sqrt{g}}{\sqrt{g^*}}\sinh\left(\sqrt{g^*}\sqrt{g}z\right)\\ -i\frac{\sqrt{g^*}}{\sqrt{g}}\sinh\left(\sqrt{g^*}\sqrt{g}z\right) & \cosh\left(\sqrt{g^*}\sqrt{g}z\right)\end{pmatrix}, \tag{4.124}$$

and is Hermitian with $\mathbf{S} = \mathbf{S}^\dagger$. As the scattering matrix is Hermitian, it is unitary diagonalisable as

$$\mathbf{S} = \mathbf{U}\mathbf{D}\mathbf{U}^\dagger, \tag{4.125}$$

where $\mathbf{U}$ is a unitary matrix made up of the eigenvectors of $\mathbf{S}$ and the matrix $\mathbf{D}$ is diagonal and consists of real, positive eigenvalues. In section 4.3.3, we found that the unitary eigenvector matrix defined a set of eigenmode operators subject to bosonic commutation relations. In the most general case, the unitary matrix $\mathbf{U}$ can be written

$$\mathbf{U} = \begin{pmatrix}A & B\\ -e^{i\theta}B^* & e^{i\theta}A^*\end{pmatrix}, \tag{4.126}$$

where $|A|^2 + |B|^2 = 1$ and the determinant is $\det(\mathbf{U}) = e^{i\theta}$. This matrix gives rise to the following eigenmode operators:

$$\hat{b}_1 = A^* \hat{a}_2 - e^{-i\theta} B \hat{a}_3, \tag{4.127}$$

$$\hat{b}_2 = B^* \hat{a}_2 + e^{-i\theta} A \hat{a}_3, \tag{4.128}$$

$$\hat{d}_1 = A^* \hat{a}_1 - e^{-i\theta} B \hat{a}_2^\dagger, \tag{4.129}$$

$$\hat{d}_2 = B^* \hat{a}_1 + e^{-i\theta} A \hat{a}_2^\dagger, \tag{4.130}$$

where the operators $\hat{b}_\tau$ are for sum-frequency generation and $\hat{d}_\tau$ describe parametric down-conversion. The above are related to the $\hat{a}_\tau$ operators as

$$\begin{pmatrix} \hat{b}_1 \\ \hat{b}_2 \end{pmatrix} = \mathbf{U}^\dagger \begin{pmatrix} \hat{a}_2 \\ \hat{a}_3 \end{pmatrix} \tag{4.131}$$

and

$$\begin{pmatrix} \hat{d}_1 \\ \hat{d}_2^\dagger \end{pmatrix} = \mathbf{U}^\dagger \begin{pmatrix} \hat{a}_1 \\ \hat{a}_2^\dagger \end{pmatrix}. \tag{4.132}$$

In order for the eigenmode operators to be interpreted as bosonic creation and annihilation operators, they should have the same canonical commutation relations as defined in section 4.2.2. Indeed, here we find for the operators $\hat{b}_\tau$

$$\left[\hat{b}_\tau, \hat{b}_\sigma^\dagger\right] = \delta_{\tau,\sigma}, \tag{4.133}$$

and for the $\hat{d}_\tau$ operators

$$\left[\hat{d}_\tau, \hat{d}_\sigma^\dagger\right] = \left(|A|^2 - |B|^2\right) \left[\hat{a}_\tau, \hat{a}_\sigma^\dagger\right]. \tag{4.134}$$

As already discussed in section 4.3.3, the eigenmode operators for sum-frequency generation have bosonic commutation relations. Therefore, they can be interpreted as creation and annihilation operators acting on underlying, orthogonal, classical fields: this was the result of the previous section. As for the case of parametric down-conversion, we observe that we cannot define orthogonal eigenmodes of the scattering matrix while conserving the algebraic relations. Certainly, the condition for the commutation relations Eq. 4.134 to be bosonic contradict the conditions imposed on the unitary eigenvector matrix. Indeed, one can define eigenmode operators, for our two-mode system, that satisfy the commutation relations in the form of a Bogoliubov transformation [138]:

$$\hat{q}_1 = u\hat{a}_1 + v\hat{a}_2^\dagger, \tag{4.135}$$

$$\hat{q}_2^\dagger = u\hat{a}_2^\dagger + v\hat{a}_1, \tag{4.136}$$

where $|u|^2 - |v|^2 = 1$. With these eigenmode operators, we can interpret them as a set of creation and annihilation operators. However, the Bogoliubov transformation is not unitary but is instead symplectic [139, 140, 141]. The defining property of a symplectic transformation is the following

$$\mathbf{M}^\dagger \mathbf{\Omega} \mathbf{M} = \mathbf{\Omega} \tag{4.137}$$

where $\mathbf{\Omega}$ is of the form

$$\mathbf{\Omega} = \begin{pmatrix} 0 & 1 \\ -1 & 0 \end{pmatrix}.$$

If we write $\mathbf{M}$ in terms of the Bogoliubov operator coefficients in Eq. 4.135 and 4.136

$$\mathbf{M} = \begin{pmatrix} u & v \\ v & u \end{pmatrix} \tag{4.138}$$

then we have the following conditions for $\mathbf{M}$ to be complex symplectic:

$$u^* v - u v^* = 0, \tag{4.139}$$

$$v u^* - v^* u = 0, \tag{4.140}$$

$$u^* u - v v^* = 1. \tag{4.141}$$

These conditions are required for the operators to have bosonic commutation relations. Thus, in order to have appropriate commutation relations and orthogonal fields, one needs to find a decomposition of the scattering matrix, as done in section 4.3.1, that is simultaneously unitary and symplectic. Indeed, the symplectic matrix $\mathbf{M}$ is only unitary if the inverse $\mathbf{M}^{-1}$ is identical to the Hermitian conjugate $\mathbf{M}^\dagger$ such that $\mathbf{M}^{-1}\mathbf{M} = \mathbf{M}^\dagger \mathbf{M} = \mathbf{I}$. Which is only true if we have u and v satisfying:

$$u^* v + u v^* = 0, \tag{4.142}$$

$$v u^* + v^* u = 0, \tag{4.143}$$

$$u^* u + v^* v = 1, \tag{4.144}$$

which is in contradiction with the conditions required to preserve the commutation algebra in Eq. 4.139 to 4.141. So, we find that by simply decomposing the scattering matrix for parametric down-conversion we do not preserve the canonical commutation algebra of bosonic creation and annihilation operators. If we choose suitable operators that do perverse the commutation relations, we observe that the classical fields that these eigenmode operators act on are not orthogonal to one another. Therefore, we cannot, in terms of a unitary decomposition, define a set of bosonic operators corresponding to the propagation eigenmodes in the context of parametric down-conversion.

To conclude this section, we remark that the link between the classical field representation and the quantum states in the context of parametric down-conversion is not as elegant as observed for sum-frequency generation. Indeed, we have shown that it is not trivial to maintain the canonical commutation relation algebra and the orthogonality of the underlying classical fields and that this cannot be achieved with a unitary eigendecomposition of the scattering matrix. It is possible that this issue can be remedied by modifying the inner product space with a different metric [100, 130, 131]. However, this metric is required to map to a Hermitian effective Hamiltonian from our classical scattering matrix to constitute a valid quantum description of the system. Therefore, to progress, one would need to define an inner product space with the symplectic symmetry that renders the bosonic operators orthogonal in a classical context and also allow for unitary evolution in a quantum picture.

4.5 Conclusion

In this chapter, we have considered the quantum behaviour of sum-frequency generation by the introduction of an effective Hamiltonian. Indeed, using a high-intensity, non-depleting background field, we linearise the equations describing three-wave mixing in nonlinear materials. In this linearised system, the transformation of input mode amplitudes to the output amplitudes is fully characterised by a scattering matrix. In the context of quantum optics, this scattering matrix also describes the input-output relation of the creation and annihilation operators. Using the Jordan-Schwinger map, we define a unitary operator that describes the quantum behaviour of the system that is dependent on the initial classical scattering matrix. In the non-depleting pump approximation, we have restored the principle of linear superposition to the nonlinear system allowing us to define a set of orthogonal propagation eigenmodes. These eigenmodes differ from the general modes used in linear optics as they describe a set of orthogonal fields that are distributed across multiple wavelengths. Utilising these eigenmodes as a representation for our low-intensity perturbation fields allows us to define a scattering matrix that decouples the evolution of the associated quantum states. Initially, we consider the case where we have a single mode propagating on each of the wavelengths before generalising to the multimode case and showing some numerical examples.

In addition, we consider the quantum description associated with parametric down-conversion. Unlike sum-frequency generation, the scattering matrix for down conversion mixes the creation and annihilation operators. Therefore, in order to derive a suitable effective Hamiltonian that is Hermitian and preserves the canonical commutation relation

algebra, we introduced the metric operator η. We then considered the effective Hamiltonian for the single-mode case for parametric down-conversion and introduced the eigenmode operators using the eigenmode decomposition of the scattering matrix. However, we observed that a unitary decomposition could not preserve the canonical commutation relations required to interpret the eigenmodes as bosonic creation and annihilation operators. Moreover, given a decomposition that does preserve the commutation algebra, we find that the underlying classical fields are not orthogonal to one another. Future work exploring the fundamental physical and mathematical link between classical fields and quantum states for parametric down-conversion would provide further insight into the work presented herein.

Chapter 5

Concluding Remarks

In this thesis, we have discussed the eigenmodes of three-wave mixing for classical low-intensity perturbation fields and in the context of multiphoton states. Here we provide a summary of the work presented, set it in the context of other work in the field, and finally suggest potential future research.

Using a high-intensity background field, we reintroduce the principle of superposition to optical systems constructed with nonlinear materials. In particular, we consider systems with second-order, $\chi^{(2)}$, nonlinearities which include effects like sum-frequency generation and parametric down-conversion. In both of these effects, the background field mediates the interaction between two low-intensity fields that we denote perturbation fields. As the principle of superposition has been restored to the equations of propagation describing three-wave mixing, the eigenmode decomposition used for conventional linear optical systems is applicable. Unlike optical systems constructed by purely linear components, the perturbation fields interact with one another via the high-intensity background field, and therefore, the associated eigenmode decomposition is distributed across multiple wavelengths. These novel eigenmodes remain orthogonal to one another and propagate independent of each other, however, the components of which the eigenmodes are constructed interact throughout the nonlinear material. With these eigenmodes, we highlight the influence that the symmetry of the complex background field has on the Hilbert space at the output plane of different optical systems. Indeed, by decomposing the background field, we find a characteristic Hilbert space for each basis element, assuming they are non-depleting. The field profiles, and consequently the physical observables, associated with the eigenmodes are thus dependent on the choice of the background field. The propagation properties of these eigenmodes are also dependent on the choice of background field and are analysed for waveguide structures with circular and rectangular symmetry.

Future work associated with the classical eigenmode decomposition in terms of three-wave mixing could go beyond the approximations used here. Indeed, the non-depleting pump approximation allowed us to reintroduce the principle of superposition to our system and utilise the eigenmode decomposition. Lifting this approximation, however, is not so trivial. In the first instance, the mechanism for probing the system would no longer be linear but quadratic such that the interaction of two fields with a given wavelength would excite higher-order modes in the third wavelength. From a mathematical perspective, the vector product in the mixing term of the fields used in this work would become a tensor product with multilinear properties. Therefore, a multilinear probing mechanism should be implemented to define the components of a rank-3 tensor which would take the place of the scattering matrices used in this work. This is a non-trivial exercise given that the number of orthogonal modes is not conserved in nonlinear systems and as such a basis set cannot be appropriately truncated, i.e., we cannot choose a basis that is closed with respect to the interaction. From this perspective, the eigenmodes discussed in this work correspond to a first-order approximation of the full nonlinear eigendecomposition. Further research in this direction would provide insight not just into the concept of additive fields in the context of nonlinear systems but also offer new decomposition techniques for higher-order tensors. Moreover, the optical eigenmodes introduced in section 1.49 when defined for fully nonlinear systems would provide a method for optimising all-optical set-ups and offer insight into the representation of the fields when the number of degrees of freedom is not conserved.

In this thesis, we have also explored the eigenmode decomposition for sum-frequency generation at a single or multiphoton level. In our linearised system, the transformation of input mode amplitudes to the output amplitudes is fully characterised by a scattering matrix. In the context of quantum optics, this scattering matrix also describes the input-output relation of the creation and annihilation operators. For sum-frequency generation, using the unitary Hermitian homomorphism, we can define a unitary operator that satisfies Schrödinger's equation and hence describes the quantum behaviour of the system. Using the distributed eigenmodes as a basis for our fields, we define a new scattering matrix and observe that the evolution of the quantum photon states is decoupled. In particular, in a Fock state basis, the photon number states associated with these eigenmodes correspond to eigenstates of the quantum system. In addition, we briefly discuss the quantum description associated with parametric down-conversion and show that one cannot simultaneously preserve the canonical commutation relation algebra and the unitarity required to define orthogonal propagation eigenmodes. Indeed, we observe that defining a set of eigenmode operators with a Bogoliubov transformation is associated with a set of classical fields that

are not orthogonal and similarly, by decomposing the Hermitian scattering matrix we define a set of orthogonal eigenmodes that do not have bosonic relations. This is due to the symplectic nature of the commutation relations being at odds with the unitarity of the complex eigenvector matrix that allow us to define orthogonal propagation eigenmodes.

Future work on the quantum behaviour of the three-wave mixing effects could study the fundamental physical relationship between classical fields and quantum states in the context of parametric down-conversion. Indeed, in the last chapter of the thesis, we briefly outlined some of the stumbling blocks that make this link more complicated than sum-frequency generation. The difference between the two effects is, in the first instance, that the scattering matrix for down-conversion is quasi-unitary and not unitary. Therefore, the correspondence between classical field amplitude and probability amplitude is not as elegant as observed for sum-frequency generation. This is due to the fact that parametric down-conversion mixes the creation and annihilation operators, making the Fock state representation more complicated than that of sum-frequency generation. Given that parametric down-conversion is the most common source for generating entangled photons, the results of this work would be interesting. Further future work could also be concerned with the full treatment of optical eigenmodes in the context of quantum operators, as done in section 4.2.4, for three-wave mixing. Indeed, in the final chapter of the thesis, we limited our discussion to the propagation eigenmodes of three-wave mixing and did not discuss any optical measurement process. The propagation eigenmodes correspond to a set of mutually orthogonal solutions of the equations of evolution; however, unlike the optical eigenmodes, they are not associated with any physical observable or measure.

Appendix A

Split-Step Method

In calculating the optical eigenmodes in a given system, the more degrees of freedom one can excite, the better. If our basis is large, however, the computational intensity quickly becomes too large for the *Mathematica's* built-in numerical integration, *NDSolve*, to manage in a reasonable time with suitable accuracy. Consequently, for calculations in bulk material, we introduce the split-step method for solving the partial differential equations of three-wave mixing [8, 9, 10]. We start by considering the evolution of the perturbation fields in sum-frequency generation,

$$-i\partial_z E_2(\mathbf{r}) = \frac{1}{2k_2}\nabla_T^2 E_2(\mathbf{r}) + \chi_2 E_b^*(\mathbf{r}) E_3(\mathbf{r}), \tag{A.1}$$

$$-i\partial_z E_3(\mathbf{r}) = \frac{1}{2k_3}\nabla_T^2 E_3(\mathbf{r}) + \chi_3 E_b(\mathbf{r}) E_2(\mathbf{r}), \tag{A.2}$$

which we can rewrite in an operator form as

$$-i\partial_z \mathbf{E}(\mathbf{r}) = \mathbf{L}\cdot\mathbf{E}(\mathbf{r}) + \mathbf{C}\cdot\mathbf{E}(\mathbf{r}), \tag{A.3}$$

where $\mathbf{E}(\mathbf{r}) = (E_2(\mathbf{r}), E_3(\mathbf{r}))^\top$ and,

$$\mathbf{L} = \begin{pmatrix} \frac{1}{2k_2}\nabla_T^2 & 0 \\ 0 & \frac{1}{2k_3}\nabla_T^2 \end{pmatrix}, \tag{A.4}$$

and

$$\mathbf{C} = \begin{pmatrix} 0 & \chi_2 E_b^*(\mathbf{r}) \\ \chi_3 E_b(\mathbf{r}) & 0 \end{pmatrix}, \tag{A.5}$$

describe the diffraction of the fields and the nonlinear interaction. If we take a small step, Δz, along the direction of propagation, then we can consider the solution of each of the parts of Eq. A.3. In the linear term, there is no interaction between the two fields such that each field can be treated independently with

$$-i\partial_z E_\tau(\mathbf{r}) = \frac{1}{2k_\tau}\nabla_T^2 E_\tau(\mathbf{r}). \tag{A.6}$$

These equations are simplified greatly by utilising the fast Fourier transform [13] as

$$-i\partial_z \tilde{E}\tau(\mathbf{r}) = \frac{k_{\tau,x}^2 + k_{\tau,y}^2}{2k_1}\tilde{E}_\tau(\mathbf{r}), \tag{A.7}$$

where $\tilde{E}_\tau(\mathbf{r}) = \mathscr{F}[E_\tau(\mathbf{r})]$ is the field in Fourier space and $\mathscr{F}$ denotes the Fourier transform. In Fourier space, it is trivial to find the solution

$$\tilde{E}_\tau(x,y,z) = \tilde{E}_\tau(x,y,0)\,\exp\left(i\frac{k_{\tau,x}^2 + k_{\tau,y}^2}{2k_1}z\right), \tag{A.8}$$

which for each small discrete step, Δz, is written

$$\tilde{E}_\tau(x,y,z+\Delta z) = \tilde{E}_\tau(x,y,z)\,\exp\left(i\frac{k_{\tau,x}^2 + k_{\tau,y}^2}{2k_1}\Delta z\right). \tag{A.9}$$

The linear step is found in terms of the initial field by taking the inverse Fourier transform, $\mathscr{F}[\tilde{E}_\tau(x,y,z)]$, of the above solution. If we recombine these solutions, we can write the solution in terms of the vector $\mathbf{E}(\mathbf{r})$ as

$$\mathbf{E}(x,y,z+\Delta z) = \mathscr{F}^{-1}[\mathbf{R}\mathscr{F}[\mathbf{E}(x,y,z)]], \tag{A.10}$$

where $\mathbf{E}(x,y,z+\Delta z) = (E_2(x,y,z+\Delta z), E_3(x,y,z+\Delta z))^\top$ and the matrix $\mathbf{R}$ is a diagonal matrix with elements $\exp\left(i\frac{k_{\tau,x}^2+k_{\tau,y}^2}{2k_1}\Delta z\right)$. Although this derivation starts from the perturbation fields, this linear term is also used to propagate the background field.

We can now solve for the interaction terms associated with the perturbation fields. Unlike the linear term, the matrix $\mathbf{C}$, has off-diagonal elements such that we have to solve the full equation which, in our simplified vector form, is

$$-i\partial_z\mathbf{E}(\mathbf{r}) = \mathbf{C}\cdot\mathbf{E}(\mathbf{r}), \tag{A.11}$$

with the solution

$$\mathbf{E}(x,y,z) = \mathbf{E}(x,y,0)\,\exp\left(i\mathbf{C}z\right). \tag{A.12}$$

Again, if we are considering finite discrete steps, this solution is written

$$\mathbf{E}(x,y,z+\Delta z) = \mathbf{E}(x,y,z)\,\exp\left(i\mathbf{C}\Delta z\right). \tag{A.13}$$

With the solution to the linear part of the equation and the interaction part, we can propagate the fields one full step as

$$\mathbf{E}(x,y,z+\Delta z) = \mathscr{F}^{-1}[\mathbf{R}\mathscr{F}[\mathbf{E}(x,y,z)]]\ \cdot\exp\left(i\mathbf{C}\Delta z\right), \tag{A.14}$$

which describes an approximate solution to the initial partial differential equations. Here we have defined the solution such that the linear operator acts first followed by the interaction terms. This is noteworthy because, in general, the two operators do not commute with one another. However, if the step size is small enough, the error associated with treating them as commuting operators is $\propto \Delta z^2$.

Suppose we decompose our fields in the x-y plane onto a discrete grid of $N \times N$ pixels, then the operators acting on our fields in Eq. A.14 are finite matrix operators. This is apparent for the interaction term, $\mathbf{C}$, due to its dependence on the background field. For the linear term, the continuous Fourier transform now takes its discrete form, and the matrix $\mathbf{R}$ has wavevectors k_x and k_y specified for each point on the grid. Given all of the operators are matrices, we can write a discrete step, Δz, in terms of a single operator

$$\mathbf{E}(x, y, \Delta z) = [\left(\mathscr{F}_D \cdot \mathbf{R} \cdot \mathscr{F}_D^{-1}\right) .\exp(i\mathbf{C}\Delta z)] \cdot \mathbf{E}(x, y, 0) = \mathbf{P}(\Delta z) \cdot \mathbf{E}(x, y, 0), \tag{A.15}$$

where the operators $\mathscr{F}_D$ and $\mathscr{F}_D^{-1}$ are the 2D discrete Fourier and inverse Fourier transforms, respectively. To propagate through the whole optical system requires a number of small steps like that of Eq. A.15. If we have a total of N steps, then the length of the material is $z_{max} = N\Delta z$, and we have

$$\mathbf{E}(x, y, N\Delta z) = \mathbf{P}(N\Delta z) \cdot \mathbf{E}(x, y, (N-1)\Delta z). \tag{A.16}$$

Using Eq. A.15, we know how the fields evolve dependent on the previous step. Consequently, we can concatenate all of the matrices describing a discrete step such that the solution at the output can be explicitly written in terms of the input field

$$\mathbf{E}(x, y, z_{max}) = [\mathbf{P}(N\Delta z) \cdot \mathbf{P}((N-1)\Delta z) \ldots \mathbf{P}(\Delta z)] \cdot \mathbf{E}(x, y, 0) = \mathbf{\Omega} \cdot \mathbf{E}(x, y, 0). \tag{A.17}$$

Or more simply we have

$$\mathbf{E}_{out} = \mathbf{\Omega} \cdot \mathbf{E}_{in}. \tag{A.18}$$

So by using the split-step method, we can not only write an approximate analytical solution to the partial differential equations but also define a scattering matrix that characterises the whole optical system dependent on the background field, $E_b(\mathbf{r})$. Moreover, the input-output relation does not require one to choose a basis in order to define it. All that is required is for a background field to be defined across the whole domain of propagation.

Appendix B

Numerical Implementation of Creation and Annihilation Operators

In this section, we outline the numerical considerations not included in the main text. In section 4.3.4.1, we outlined an example of a truncated basis of OAM fields in a circular waveguide. In this example, the Fock state space was also truncated with respect to some maximum total photon number, N_{max}. As a consequence, we also truncate the creation and annihilation operators such that they are closed operations in our finite Fock state space. If we have an input state, $|n_2, n_3\rangle$, then the $\hat{a}_2$ and $\hat{a}_3$ operators should satisfy the following properties:

$$\begin{aligned} \hat{a}_2 |n_2, n_3\rangle &= \sqrt{n_2} |n_2 - 1, n_3\rangle , \\ \hat{a}_3 |n_2, n_3\rangle &= \sqrt{n_3} |n_2, n_3 - 1\rangle , \end{aligned} \tag{B.1}$$

If we write the output state as, $|n_2', n_3'\rangle$, then using the above properties, we can write the matrix elements of the annihilation operators as:

$$\begin{aligned} \langle n_2', n_3'| \hat{a}_2 |n_2, n_3\rangle &= \sqrt{n_2}\delta_{n_2-1,n_2'}\delta_{n_3,n_3'}, \\ \langle n_2', n_3'| \hat{a}_3 |n_2, n_3\rangle &= \sqrt{n_3}\delta_{n_3-1,n_3'}\delta_{n_2,n_2'}. \end{aligned} \tag{B.2}$$

If we take for example two modes with the maximum photon number, $N_{max} = 2$, we have the Fock state basis elements,

$$|n_2, n_3\rangle \in \{|0,0\rangle , |1,0\rangle , |0,1\rangle , |2,0\rangle , |1,1\rangle , |0,2\rangle\}. \tag{B.3}$$

In order to calculate the effective Hamiltonian, however, we use creation and annihilation operators calculated up to $N_{max} + 1$ with the following basis elements

$$|n_2, n_3\rangle_{\text{ext}} \in \{|0,0\rangle , |1,0\rangle , |0,1\rangle , |2,0\rangle , |1,1\rangle , |0,2\rangle , |3,0\rangle , |2,1\rangle , |1,2\rangle , |0,3\rangle\}. \tag{B.4}$$

In this case, the annihilation operators are of the form

$$\hat{a}_2 = \left(\begin{array}{c|cc|ccc|ccc|c} 0 & 1 & 0 & 0 & 0 & 0 & 0 & 0 & 0 & 0 \\ \hline 0 & 0 & 0 & \sqrt{2} & 0 & 0 & 0 & 0 & 0 & 0 \\ 0 & 0 & 0 & 0 & 1 & 0 & 0 & 0 & 0 & 0 \\ \hline 0 & 0 & 0 & 0 & 0 & 0 & \sqrt{3} & 0 & 0 & 0 \\ 0 & 0 & 0 & 0 & 0 & 0 & 0 & \sqrt{2} & 0 & 0 \\ 0 & 0 & 0 & 0 & 0 & 0 & 0 & 0 & 1 & 0 \\ \hline 0 & 0 & 0 & 0 & 0 & 0 & 0 & 0 & 0 & 0 \\ 0 & 0 & 0 & 0 & 0 & 0 & 0 & 0 & 0 & 0 \\ 0 & 0 & 0 & 0 & 0 & 0 & 0 & 0 & 0 & 0 \\ 0 & 0 & 0 & 0 & 0 & 0 & 0 & 0 & 0 & 0 \end{array}\right), \tag{B.5}$$

$$\hat{a}_3 = \left(\begin{array}{c|cc|ccc|ccc|c} 0 & 0 & 1 & 0 & 0 & 0 & 0 & 0 & 0 & 0 \\ \hline 0 & 0 & 0 & 0 & 1 & 0 & 0 & 0 & 0 & 0 \\ 0 & 0 & 0 & 0 & 0 & \sqrt{2} & 0 & 0 & 0 & 0 \\ \hline 0 & 0 & 0 & 0 & 0 & 0 & 0 & 1 & 0 & 0 \\ 0 & 0 & 0 & 0 & 0 & 0 & 0 & 0 & \sqrt{2} & 0 \\ 0 & 0 & 0 & 0 & 0 & 0 & 0 & 0 & 0 & \sqrt{3} \\ \hline 0 & 0 & 0 & 0 & 0 & 0 & 0 & 0 & 0 & 0 \\ 0 & 0 & 0 & 0 & 0 & 0 & 0 & 0 & 0 & 0 \\ 0 & 0 & 0 & 0 & 0 & 0 & 0 & 0 & 0 & 0 \\ 0 & 0 & 0 & 0 & 0 & 0 & 0 & 0 & 0 & 0 \end{array}\right). \tag{B.6}$$

We use these operators to calculate the effective Hamiltonian and scattering operator so to account for states with $N = 3$ that might contribute to states with $N = 2$. Indeed, take, for example, the state $|3, 0\rangle$ that is not in the truncated basis, however, $\hat{a}_2 |3, 0\rangle = \sqrt{2} |2, 0\rangle$, is an element of the basis. With the correct Hamiltonian calculated, we then truncate to the appropriate dimensions to agree with the basis at $N_{max} = 2$. We calculate all of these matrices and the numerical examples with *Mathematica* computer software [91].

Bibliography

[1] H. Kogelnik and T. Li. Laser beam and resonators. *Applied Optics*, 5(10):1550–1567, 1966.

[2] P Bienstman and R Baets. Optical modeling of photonic crystals and vcsels using eigenmode expansion and perfectly matched layers. *Optical and Quantum Electronics*, 33:327–341, 2001.

[3] Aasmund Sv Sudbo. Film mode matching: a versatile numerical method for vector mode field calculations in dielectric waveguides. *Pure Applied Optics*, 2:211–233, 1993.

[4] M Mazilu, J Baumgartl, S Kosmeier, and K Dholakia. Optical eigenmodes; exploiting the quadratic nature of the energy flux and of scattering interactions. *Optics Express*, 19:933–944, 2011.

[5] M. Mazilu. Density of optical degrees of freedom: Intensity, linear, and angular momentum. In *Proceedings of SPIE - The International Society for Optical Engineering*, volume 8999, 2014.

[6] Michael Mazilu. Optical eigenmodes; spin and angular momentum. *Journal of Optics*, 13(6):064009, 2011.

[7] Michael Mazilu. Spin and angular momentum operators and their conservation. *Journal of Optics A: Pure and Applied Optics*, 11(9):094005, 2009.

[8] Robert Boyd. *Nonlinear Optics*. Academic Press, London., 3rd edition, 2008.

[9] Y. R. Shen. *The Principles of Nonlinear Optics*. John Wiley & Sons, Hoboken, New Jersey, 2003.

[10] Geoffrey New. *Introduction to Nonlinear Optics*. Cambridge University Press, New York, 2011.

[11] A Wheeler, J. On the mathematical description of light nuclei by the method of resonating group structure. *Physical Review*, 52 (11):1107–1122, 1937.

[12] Johannes Skaar, Juan Carlos Garcia Escartin, and Harald Landro. Quantum mechanical description of linear optics. *American Journal of Physics*, 72:1385–1391, 2004.

[13] W. Goodman, Joseph. *Introduction to Fourier Optics*. McGraw-Hill, London, 1968.

[14] P. Vaveliuk and O. Martinez-Matos. Physical interpretation of the paraxial estimator. *Optics Communications*, 285(24):4816–4820, 2012.

[15] P. Vaveliuk, B. Ruiz, and A. Lencina. Limits of the paraxial approximation in laser beams. *Optics Letters*, 32(8):927–929, 2007.

[16] Max Born and Emil Wolf. *Principles of Optics*. Cambridge University Press, New York, 7th edition, 1999.

[17] E. Siegman, Anthony. *Lasers*. Science Books, Sausalitio, CA, 1986.

[18] Milton Abramowitz and Irene A. Stegun. *Handbook of Mathematical Functions with Formulas, Graphs, and Mathematical Tables*. Dover Publications, New York, 1964.

[19] L. Allen, M. Barnett S, and J. Padgett, M. *Optical Angular Momentum*. CRC Press LLC, Bristol, United Kingdom, 2016.

[20] G.P. Argawal. *Fiber-Optic Communication Systems*. Wiley & Sons, New York, 4th edition, 2010.

[21] J. Griffiths, David. *Introduction to Electrodynamics*. Pearson Education, Inc., New Jersey, 2013.

[22] Michio. Kaku. *Quantum Field Theory: A Modern Introduction*. Oxford University Press, New York, 1993.

[23] Jiří Petráček. A bidirectional eigenmode expansion and propagation technique for modeling Kerr-nonlinear photonic structures. *Microwave and Optical Technology Letters*, 55(11):2628–2631, 2013.

[24] Björn Maes, Peter Bienstman, and Roel Baets. Modeling of Kerr nonlinear photonic components with mode expansion. *Optical and Quantum Electronics*, 33:15–24, 2004.

[25] Björn Maes, Peter Bienstman, and Roel Baets. Modeling second-harmonic generation by use of mode expansion. *Journal of the Optical Society of America B*, 22(7):1378–1383, 2005.

[26] Benfeng Bai and Jari Turunen. Fourier modal method for the analysis of second-harmonic generation in two-dimensionally periodic structures containing anisotropic materials. *Journal of the Optical Society of America B*, 24(5):1105–1112, 2007.

[27] Subhajit Bej, Jani Tervo, Yuri P. Svirko, and Jari Turunen. Modeling the optical Kerr effect in periodic structures by the linear Fourier modal method. *Journal of the Optical Society of America B*, 31(10):2371, 2014.

[28] Jouni Makitalo, Saku Suuriniemi, and Martti Kauranen. Boundary element method for surface nonlinear optics of nanoparticles. *Optics Express*, 19(23):23386, 2011.

[29] J.P. Dewitz, W. Hubner, and K.H. Bennemann. Theory for nonlinear Mie-scattering from spherical metal clusters. *Zeitschrift Fur Physik D*, 37:75–84, 1996.

[30] David J. Richardson. Filling the light pipe. *Science*, 330:327–328, 2010.

[31] Partha P. Mitra and Jason B. Stark. Nonlinear limits to the information capacity of optical fibre communications. *Nature*, 411:1027–1030, 2001.

[32] René-Jean Essiambre, Gerhard Kramer, Peter J. Winzer, Gerard J. Foschini, and Bernhard Goebel. Capacity limits of optical fiber networks. *Journal of Lightwave Technology*, 28(4):662–701, 2010.

[33] Sergei K. Turitsyn, Jaroslaw E. Prilepsky, Son Thai Le, Sander Wahls, Leonid L. Frumin, Morteza Kamalian, and Stanialav A. Derevyanko. Nonlinear Fourier transform for optical data processing and transmission: advances and perspectives. *Optica*, 3(4):307–322, 2017.

[34] Y.S Kivshar and G.P. Agrawal. *Optical Solitons: From Fibers to Photonic Crystals*. Elsevier Inc., London, 2003.

[35] Akira Hasegawa. Eigenvalue communication. *Journal of Lightwave Technology*, 11(3):395–399, 1993.

[36] M. I. Yousefi and Kschischang F.R. Information transmission using the nonlinear Fourier transform. *IEEE Trans. Inform. Theory*, 60:4312–4369, 2014.

[37] Jaroslaw E. Prilepsky, Stanislav A. Derevyanko, Keith J. Blow, Ildar Gabitov, and Sergei K. Turitsyn. Nonlinear inverse synthesis and eigenvalue division multiplexing in optical fiber channels. *Physical Review Letters*, 113(1), 2014.

[38] Son Thai Le, Jaroslaw E. Prilepsky, and Sergei K. Turitsyn. Nonlinear inverse synthesis for high spectral efficiency transmission in optical fibers. *Optics Express*, 22(22):26720, 2014.

[39] T.H. Maiman. Optical and microwave-optical experiments in ruby. *Physical Review Letters*, 4(11):564–566, 1960.

[40] P. A. Franken, A. E. Hill, C. Peters, and G. Weinreich. Generation of optical harmonics. *Physical Review Letters*, 7(4):118–120, 1961.

[41] Richard L. Sutherland. *Handbook of Nonlinear Optics*. Marcel Dekker, Inc., New York, 2nd edition, 2003.

[42] J. A. Armstrong, N. Bloembergen, J. Ducuing, and P. S. Pershan. Interactions between light waves in a nonlinear dielectric. *Physical Review*, 127(6):1918–1939, 1692.

[43] Paul N. Butcher and David Cotter. *The Elements of Nonlinear Optics*. Cambridge University Press, New York, 1991.

[44] Mazza D. et al. *Non-Linear Microscopy*. Biophotonics. Biological and Medical Physics, Biomedical Engineering. Springer, Berlin, Heidelberg, 2008.

[45] W. R. Zipfel, R. M. Williams, and W. W. Webb. Nonlinear magic: Multiphoton microscopy in the biosciences. *Nature Biotechnology*, 21(11):1369–1377, 2003.

[46] F. Helmchen and W. Denk. Deep tissue two-photon microscopy. *Nature Methods*, 2(12):932–940, 2005.

[47] M. G. L. Gustafsson. Nonlinear structured-illumination microscopy: Wide-field fluorescence imaging with theoretically unlimited resolution. *Proceedings of the National Academy of Sciences of the United States of America*, 102(37):13081–13086, 2005.

[48] Winfried Denk, James H. Strickler, and Watt W. Webb. Two-photon laser scanning fluorescence microscopy. *Science*, 248, 1990.

[49] P. G. Kwiat, K. Mattle, H. Weinfurter, A. Zeilinger, A. V. Sergienko, and Y. Shih. New high-intensity source of polarization-entangled photon pairs. *Physical Review Letters*, 75(24):4337–4341, 1995.

[50] W. Ueno, F. Kaneda, H. Suzuki, S. Nagano, A. Syouji, R. Shimizu, K. Suizu, and K. Edamatsu. Entangled photon generation in two-period quasi-phase-matched parametric down-conversion. *Optics Express*, 20(5):5508–5517, 2012.

[51] J. Lee and Y. Kim. Spatial and spectral properties of entangled photons from spontaneous parametric down-conversion with a focused pump. *Optics Communications*, 366:442–450, 2016.

[52] Y. J. Yu, G. Y. Jin, C. Wang, X. Y. Chen, D. W. Hao, and J. X. Guo. All-solid-state continuous-wave doubly resonant all-intracavity cyan laser at 500.8 nm by sum-frequency-mixing in double-crystal RTP generation. *Laser Physics Letters*, 6(7):513–516, 2009.

[53] Y. Fujii, B. S. Kawasaki, K. O. Hill, and D. C. Johnson. Sum-frequency light generation in optical fibers. *Optics Letters*, 5(2):48–50, 1980.

[54] G. A. Massey and J. C. Johnson. Wavelength-tunable optical mixing experiments between 208 nm and 259 nm. *IEEE Journal of Quantum Electronics*, 12(11):721–727, 1976.

[55] J. C. Bienfang, C. A. Denman, B. W. Grime, P. D. Hillman, G. T. Moore, and J. M. Telle. 20 W of continuous-wave sodium D2 resonance radiation from sum-frequency generation with injection-locked lasers. *Optics Letters*, 28(22):2219–2221, 2003.

[56] A. P. Boughton and Z. Chen. *Surface Analysis and Techniques in Biology*. Springer, Berlin. 2014.

[57] S. Ye, F. Wei, H. Li, K. Tian, and Y. Luo. *Advances in Protein Chemistry and Structural Biology*. Academic Press Inc., Cambridge, Massachusetts. 2013.

[58] J.E House. *Physical Chemistry of Gas-Liquid Interfaces: a Volume in Developments in Physics & Theoretical Chemistry*. Elsevier Inc., Cambridge, MA. 2018.

[59] J. Lavoie, J. M. Donohue, L. G. Wright, A. Fedrizzi, and K. J. Resch. Spectral compression of single photons. *Nature Photonics*, 7(5):363–366, 2013.

[60] R. V. Roussev, C. Langrock, J. R. Kurz, and M. M. Fejer. Periodically poled lithium niobate waveguide sum-frequency generator for efficient single-photon detection at communication wavelengths. *Optics Letters*, 29(13):1518–1520, 2004.

[61] H. Takesue. Erasing distinguishability using quantum frequency up-conversion. *Physical Review Letters*, 101(17), 2008.

[62] R. Ghosh and L. Mandel. Observation of nonclassical effects in the interference of two photons. *Physical Review Letters*, 59(17):1903–1905, 1987.

[63] K. A. Forbes, J. S. Ford, and D. L. Andrews. Nonlocalized generation of correlated photon pairs in degenerate down-conversion. *Physical Review Letters*, 118(13), 2017.

[64] Y. H. Shih, A. V. Sergienko, M. H. Rubin, T. E. Kiess, and C. O. Alley. Two-photon entanglement in type-II parametric down-conversion. *Physical Review A*, 50(1):23–28, 1994.

[65] M. Bock, A. Lenhard, C. Chunnilall, and C. Becher. Highly efficient heralded single-photon source for telecom wavelengths based on a PPLN waveguide. *Optics Express*, 24(21):23992–24001, 2016.

[66] J. Chen, A. J. Pearlman, A. Ling, J. Fan, and A. Migdall. A versatile waveguide source of photon pairs for chip-scale quantum information processing. *Optics Express*, 17(8):6727–6740, 2009.

[67] A. Kuzmich, W. P. Bowen, A. D. Boozer, A. Boca, C. W. Chou, L. Duan, and H. J. Kimble. Generation of nonclassical photon pairs for scalable quantum communication with atomic ensembles. *Nature*, 423(6941):731–734, 2003.

[68] S. M. Spillane, M. Florentino, and R. G. Beausoleil. Spontaneous parametric down conversion in a nanophotonic waveguide. *Optics Express*, 15(14):8770–8780, 2007.

[69] M. A. M. Versteegh, M. E. Reimer, K. D. Jns, D. Dalacu, P. J. Poole, A. Gulinatti, A. Giudice, and V. Zwiller. Observation of strongly entangled photon pairs from a nanowire quantum dot. *Nature Communications*, 5, 2014.

[70] G. Brassard, N. Lütkenhaus, T. Mor, and B. C. Sanders. Limitations on practical quantum cryptography. *Physical Review Letters*, 85(6):1330–1333, 2000.

[71] T. E. Kiess, Y. H. Shih, A. V. Sergienko, and C. O. Alley. Tunable Bell-inequality violations by non-maximally-violating states in type-II parametric down-conversion. *Physical Review A*, 52(4):3344–3347, 1995.

[72] Z. Y. Ou and L. Mandel. Violation of Bell's inequality and classical probability in a two-photon correlation experiment. *Physical Review Letters*, 61(1):50–53, 1988.

[73] A. C. Dada, J. Leach, G. S. Buller, M. J. Padgett, and E. Andersson. Experimental high-dimensional two-photon entanglement and violations of generalized Bell inequalities. *Nature Physics*, 7(9):677–680, 2011.

[74] P. Zerom, K. W. C. Chan, J. C. Howell, and R. W. Boyd. Entangled-photon compressive ghost imaging. *Physical Review A - Atomic, Molecular, and Optical Physics*, 84(6), 2011.

[75] M. Gilaberte Basset, F. Setzpfandt, F. Steinlechner, E. Beckert, T. Pertsch, and M. Gräfe. Perspectives for applications of quantum imaging. *Laser and Photonics Reviews*, 13(10), 2019.

[76] J. Lamor. A dynamical theory of the electric and luminiferous medium. I. *Nature*, 49(1263):260–262, 1894.

[77] J. Lamor. A dynamical theory of the electric and luminiferous medium. II. *Nature*, 49(1264):280–283, 1894.

[78] C. K. Hong and L. Mandel. Theory of parametric frequency down conversion of light. *Physical Review A*, 31(4):2409–2418, 1985.

[79] C. K. Law and J. H. Eberly. Analysis and interpretation of high transverse entanglement in optical parametric down conversion. *Physical Review Letters*, 92(12):127903–1–127903–4, 2004.

[80] Y. Xue, A. Yoshizawa, and H. Tsuchida. Polarization-based entanglement swapping at the telecommunication wavelength using spontaneous parametric down-conversion photon-pair sources. *Physical Review A - Atomic, Molecular, and Optical Physics*, 85(3), 2012.

[81] M. F. Saleh, B. E. A. Saleh, and M. C. Teich. Modal, spectral, and polarization entanglement in guided-wave parametric down-conversion. *Physical Review A - Atomic, Molecular, and Optical Physics*, 79(5), 2009.

[82] J. E. Midwinter and J. Warner. The effects of phase matching method and of uniaxial crystal symmetry on the polar distribution of second-order non-linear optical polarization. *British Journal of Applied Physics*, 16(8):1135–1142, 1965.

[83] F. Zernike. Temperature-dependent phase matching for far-infrared difference-frequency generation in InSb. *Physical Review Letters*, 22(18):931–933, 1969.

[84] J. T. Lin, J. L. Montgomery, and K. Kato. Temperature-tuned noncritically phase-matched frequency conversion in LiB3O5 crystal. *Optics Communications*, 80(2):159–165, 1990.

[85] D. H. Jundt. Temperature-dependent sellmeier equation for the index of refraction, n_e, in congruent lithium niobate. *Optics Letters*, 22(20):1553–1555, 1997.

[86] M. Yamada, N. Nada, M. Saitoh, and K. Watanabe. First-order quasi-phase matched LiNbO3 waveguide periodically poled by applying an external field for efficient blue second-harmonic generation. *Applied Physics Letters*, 62(5):435–436, 1993.

[87] V. Berger. Nonlinear photonic crystals. *Physical Review Letters*, 81(19):4136–4139, 1998.

[88] M. M. Fejer, D. H. Jundt, R. L. Byer, and G. A. Magel. Quasi-phase-matched second harmonic generation: Tuning and tolerances. *IEEE Journal of Quantum Electronics*, 28(11):2631–2654, 1992.

[89] L. E. Myers, R. C. Eckardt, M. M. Fejer, R. L. Byer, W. R. Bosenberg, and J. W. Pierce. Quasi-phase-matched optical parametric oscillators in bulk periodically poled LiNbO3. *Journal of the Optical Society of America B: Optical Physics*, 12(11):2102–2116, 1995.

[90] G Docherty-Walthew and M Mazilu. Nonlinear optical eigenmodes; perturbative approach. *Proc. SPIE 10935, Complex Light and Optical Forces XIII*, 109351K, 2019.

[91] Wolfram Research Inc. *Mathematica*. Wolfram Research Inc., version 12.0 edition, 2019.

[92] A. V. Smith. *SNLO nonlinear optics code available from A. V. Smith, Albuquerque, NM.* AS-Photonics, snlo v71 edition, 2019.

[93] D. Eimerl. Electro-optic, linear, and nonlinear optical properties of KDP and its isomorphs. *Ferroelectrics*, 72(1):95–139, 1987.

[94] R. S. S. Kumar, S. S. Harsha, and D. N. Rao. Broadband supercontinuum generation in a single potassium di-hydrogen phosphate (KDP) crystal achieved in tandem with sum frequency generation. *Applied Physics B: Lasers and Optics*, 86(4):615–621, 2007.

[95] A. Stabinis, G. Valiulis, and E. A. Ibragimov. Effective sum frequency pulse compression in nonlinear crystals. *Optics Communications*, 86(3-4):301–306, 1991.

[96] D. W. Coutts, M. D. Ainsworth, and J. A. Piper. Sum frequency mixing of copper vapor laser output in KDP and (β-BBO. *IEEE Journal of Quantum Electronics*, 25(9):1985–1987, 1989.

[97] C. M. Bender and S. Boettcher. Real spectra in non-hermitian Hamiltonians having PT symmetry. *Physical Review Letters*, 80(24):5243–5246, 1998.

[98] A. Mostafazadeh and A. Batal. Physical aspects of pseudo-hermitian and PT-symmetric quantum mechanics. *Journal of Physics A: Mathematical and General*, 37(48):11645–11679, 2004.

[99] C. M. Bender, D. C. Brody, and H. F. Jones. Complex extension of quantum mechanics. *Physical Review Letters*, 89(27), 2002.

[100] A. Mostafazadeh. Metric operators for quasi-hermitian Hamiltonians and symmetries of equivalent hermitian Hamiltonians. *Journal of Physics A: Mathematical and Theoretical*, 41(24), 2008.

[101] S Aaronson and A Arkhipov. The computational complexity of linear optics. *Proceedings of the 43rd Annual ACM Symposium on Theory of Computing*, 11:333342, 2011.

[102] Si-Hui Tana and Peter P Rohded. The resurgence of the linear optics quantum interferometer recent advances & applications. *Reviews in Physics*, 4, 2019.

[103] M Suda, C Pacher, M Peev, M Duek, and F Hipp. Quantum interference of photons in simple networks. *Quantum Inf Process*, 12:1915–1945, 2013.

[104] U Leonhardt and V Neumaier. Explicit effective Hamiltonians for general linear quantum-optical networks. *Journal of Optics B: Quantum and Semiclassical Optics*, 6:L1–L4, 2004.

[105] C Garcia-Escartin, J, V Gimeno, and J Moyano-Fernndez. Multiple photon effective Hamiltonians in linear quantum optical networks. *Optics Communications*, 430:434–439, 2018.

[106] M Fox. *Quantum Optics; An Introduction.* Oxford University Press, Oxford. 2006.

[107] J. Griffiths, David. *Introduction to Quantum Mechanics.* Pearson Education, Inc., New Jersey, 2005.

[108] W. C. Schieve and L. P. Horwitz. *Quantum statistical mechanics.* Cambridge University Press, Cambridge. 2015.

[109] N. N. Bogoliubov and N. N. Bogoliubov. *Introduction to quantum statistical mechanics, 2nd edition.* World Scientific Publishing Co. Pte. Ltd., Hackensack, NJ. 2009.

[110] M. Born and P. Jordan. Zur Quantenmechanik. *Zeitschrift fr Physik*, 34(1):858–888, 1925.

[111] M. Born, W. Heisenberg, and P. Jordan. Zur Quantenmechanik. II. *Zeitschrift fr Physik*, 35(8-9):557–615, 1926.

[112] C Madrid Casado, M. A brief history of the mathematical equivalence between the two quantum mechanics. *Lat. Am. J. Phys. Educ.*, 2 (2):104–108, 2008.

[113] M. A. de Gosson. Born−Jordan quantization and the equivalence of the Schrödinger and Heisenberg pictures. *Foundations of Physics*, 44(10):1096–1106, 2014.

[114] F Mandl and G Shaw. *Quantum Field Theory.* John Wiley & Sons, New Jersey. 1984.

[115] A. Duncan. *The Conceptual Framework of Quantum Field Theory.* Oxford University Press, Oxford. 2013.

[116] J. Dimock. *Quantum mechanics and quantum field theory: A mathematical primer.* Cambridge University Press, New York. 2011.

[117] K. Ballantine and M. Mazilu. Optical eigenmode description of single-photon light-matter interactions. In *Proceedings of SPIE - The International Society for Optical Engineering 109351B*, volume 10935, 2019.

[118] Ulf Leonhardt. Quantum physics of simple optical instruments. *Reports on Progress in Physics*, 66:1207–1249, 2003.

[119] J.F Cornwell. *Group Theory in Physics.* Academic Press, London. 1997.

[120] Nadir Jeevanjee. *An Introduction to Tensors and Group Theory for Physicists.* Birkhäuser, Basel, 2nd edition, 2011.

[121] L. Fu and C. L. Kane. Time reversal polarization and a Z2 adiabatic spin pump. *Physical Review B - Condensed Matter and Materials Physics*, 74(19), 2006.

[122] T. Fukui and T. Fujiwara. A Z2 index of a dirac operator with time reversal symmetry. *Journal of Physics A: Mathematical and Theoretical*, 42(36), 2009.

[123] H. Katsura and T. Koma. The Z2 index of disordered topological insulators with time reversal symmetry. *Journal of Mathematical Physics*, 57(2), 2016.

[124] A. M. Bincer. *Lie Groups and Lie Algebras: A Physicist's Perspective.* Oxford University Press, Oxford, 2013.

[125] P Aniello and C Lupo. Exploring representation theory of unitary groups via linear optical passive devices. *Open Sys. & Information Dyn.*, 13:415426, 2006.

[126] K. Takayanagi. Unified theory of effective interaction. *Annals of Physics*, 372:12–56, 2016.

[127] L Braunstein, S. Squeezing as an irreducible resource. *Physical Review A.*, 71, 2005.

[128] A. Mostafazadeh. Metric operators for quasi-hermitian Hamiltonians and symmetries of equivalent hermitian Hamiltonians. *Journal of Physics A: Mathematical and Theoretical*, 41(24), 2008.

[129] A. Mostafazadeh. Time-dependent pseudo-hermitian Hamiltonians defining a unitary quantum system and uniqueness of the metric operator. *Physics Letters, Section B: Nuclear, Elementary Particle and High-Energy Physics*, 650(2-3):208–212, 2007.

[130] D. Krejcirik, H. Bila, and M. Znojil. Closed formula for the metric in the Hilbert space of a PT-symmetric model. *Journal of Physics A: Mathematical and General*, 39(32):10143–10153, 2006.

[131] D. Krejiik. Calculation of the metric in the Hilbert space of a PT-symmetric model via the spectral theorem. *Journal of Physics A: Mathematical and Theoretical*, 41(24), 2008.

[132] E. Ergun. A two-parameter family of non-hermitian Hamiltonians with real spectrum. *Journal of Physics A: Mathematical and Theoretical*, 43(45), 2010.

[133] E. Ergun and M. Saglam. On the metric of a non-hermitian model. *Reports on Mathematical Physics*, 65(3):367–378, 2010.

[134] A. Mostafazadeh. Pseudo-hermiticity versus PT-symmetry III: Equivalence of pseudo-hermiticity and the presence of antilinear symmetries. *Journal of Mathematical Physics*, 43(8):3944–3951, 2002.

[135] A. Mostafazadeh. Pseudo-hermiticity and generalized PT and CPT symmetries. *Journal of Mathematical Physics*, 44(3):974–989, 2003.

[136] A. Mostafazadeh and A. Batal. Physical aspects of pseudo-hermitian and PT-symmetric quantum mechanics. *Journal of Physics A: Mathematical and General*, 37(48):11645–11679, 2004.

[137] C. M. Bender, P. N. Meisinger, and Q. Wang. Calculation of the hidden symmetry operator in PT-symmetric quantum mechanics. *Journal of Physics A: Mathematical and General*, 36(7):1973–1983, 2003.

[138] N Bogoljubov, N. On a new method in the theory of superconductivity. *Il Nuovo Cimento*, 7:794–805, 1958.

[139] J. . Koszul and Y. M. Zou. *Introduction to Symplectic Geometry*. Springer, Singapore. 2019.

[140] D. McDuff and D. Salamon. *Introduction to symplectic topology, 3rd edition*. Oxford University Press, New York. 2017.

[141] G. Giachetta, L. Mangiarotti, and G. Sardanashvily. *Geometric formulation of classical and quantum mechanics*. World Scientific Publishing Co. Pte. Ltd., Hackensack, NJ. 2010.